UNIVERSITY OF LONDON THESIS

Degree PhD Year 2008 Name of Author VANHOESTENBERGHE, Anne

Implanted Devices: Improved Methods for Nerve Root Stimulation

Anne Vanhoestenberghe

A thesis submitted in fulfilment
of the requirements for the degree of
Doctor of Philosophy
of the
Department of Medical Physics and Bioengineering
University College London

Supervisor: Prof. N. de N. Donaldson
Second supervisor: Prof. D. N. Rushton

February 2008

ProQuest LLC
789 East Eisenhower Parkway
P.O. Box 1346
Ann Arbor, MI 48106-1346

Mes idées ont marché d'expérience en expérience, toujours très près du fait, et parfois, quand le fait l'a voulu, contrairement au sens que j'avais prévu.

My ideas walked from experience to experience, always close to the fact, and sometimes, when the fact required it, contrary to the direction I had foreseen.

Louis Lapicque, 1943

Official declaration

I, Anne Vanhoestenberghe, confirm that the work presented in this thesis is my own. Where information has been derived from other sources, I confirm that this has been indicated in the thesis.

Abstract

Nerve root stimulators for spinal cord injured patients were first developed in the 1970s in London and are now well established with the Sacral Anterior Root Stimulator Implant (SARSI) for bladder and bowel control. Experience with lumbar root stimulators (LARSI) led to a rethink of both the purpose of the device (through an improved understanding of patients' expectations) and of the stimulator's electronic design. Paraplegics willing to receive a SARSI would also benefit from leg exercise. Stimulating both sacral and lumbar roots with a single implant would combine both applications at little extra cost as placement would only require one operation.

Developing a new implant offered, via this thesis, an opportunity to advance the knowledge and refine the stimulation method. The primary hypothesis was that independent stimulation channels would improve the selectivity by eliminating cross-talk.

This thesis demonstrates and explains the occurrence of cross-talk (with patient's data and animal recordings) and its reduction with the new stimulation method. The design of both the experimental stimulator and the integrated-circuit developed as output stage of the new implant is detailed, complete with circuits schematics. Further, an analysis of the literature on nerve root compression supports an explanation of the mechanisms behind entrapment and compression damages. A study of electrode book impedance follows. It provides an insight into the respective influence of the electrode and mount dimensions and leads to a simple formula to estimate the overall impedance for the IC design.

While this work's contribution, as highlighted above, is mainly in the medical engineering domain, a short discussion setting it in a wider context has been added to insist on the human dimension of such a research project.

Acknowledgements

As this thesis is finally over, I am happy to thank those who have helped me throughout this long process, yet I fear that if I attempt to name everyone I will unavoidably forget a few. I wish therefore to thank you all at once, friends and colleagues who have become friends. This acknowledgement page will not become a list in which to search one's name.

Thank you all for your time, your patience, for the guidance, for actively listening to my doubts, suggestions and complaints, for the invaluable teaching, the persistent help, the countless reviews and advice. Thanks to the fantastic friends, family included of course, whom with seemingly endless compassion and resources have carried me further than I thought I could go. Thanks to the many scientists and occasional patients who shared their vision of electrical stimulation to widen my electronic engineer's perspective. Thanks to the "open source" programming community for providing and supporting such a variety of quality softwares. Thanks for your enthusiasm and for trusting me more than I sometimes did.

No one ever claimed "I did it on my own", but I wish to stress here how many of you contributed, directly or less obviously, to this project.

Merci a tous,

Anne
London, September 2007

Contents

List of Figures

List of Tables

Outline

Thesis statement: To advance the state of the art and demonstrate the pertinence of improved methods of electrical stimulation with a focus on implantable nerve root stimulators.

This thesis is divided in four parts. It is aimed at an audience with an interest in electrical stimulation, whether with an engineering or a medical background, and therefore starts with a substantial introduction to the subject of "functional electrical stimulation". The first chapter focuses on basic elements of neuroanatomy and spinal cord injury and is included for readers who may not all be familiar with the human nervous system and the consequences of the injury on nervous communication. The second chapter introduces basic electrical stimulation concepts including chronaxie, rheobase and virtual electrodes. The third, and last, introductory chapter presents a chronology of the key electro-medical developments that led to lower-body applications of FES with a focus on nerve root implanted stimulators. Major research centres and their respective contributions are also listed.

Part II covers some of the research tasks preliminary to the production of the SLARSI (Sacro Lumbar Anterior Root Stimulator Implant). As this new implant evolves from the combination of two previously separate devices (SARSI and LARSI), the first research action was to understand the drawbacks of the existing systems and identify knowledge gaps specific to implanted stimulators and electrodes. The most scientific aspect of this prospective step is developed in chapter 4 with an in-depth analysis of force measurements recorded during LARSI patient JH's training between 1995 and 2000. The analysis focuses on the lack of muscle selectivity and identifies a possible mechanism of co-stimulation: cross-talk activation. The following chapter (5) proposes a solution to avoid such unwanted co-activation. Performing simple, repeatable, nerve stimulation experiments, the theory behind cross-talk stimulation is developed and the validity of the proposed solution is assessed. The experimental results refute a common, yet so far unproven, electrical stimulation assumption. They also demonstrate the importance of anodal current imbalance for tripolar stimulation, anodal blocking, activation and propagation delays. Chapters 6 and 7 then tackle general issues related to electrodes and mounts, leading to applications beneficial not only for SLARSI but for any future implant. A question that has not so far been answered despite decades of implantable electrode development is that of the safe pressure that a peripheral nerve or nerve root may withstand during long term implantation. Chapter

6 opens the discussion with an extensive literature review gathering nerve compression data, with a focus on nerve roots; and proposes a maximum of 40mmHg, with short duration peaks limited to 100mmHg. The interest of such a pressure limit lies in the development by many research groups of tight-fitting electrode mounts, for both stimulation and recording, and the putative conclusion that widespread use of these performance enhancing mounts is mainly hindered by safety considerations. To close this section a "space limiting device", inspired by the trend for fitted mounts, is briefly presented. This design is currently being investigated and is not developed in this thesis. Chapter 7, the last of the research part, deals with the issue of stimulator output stage load: what is the impedance of an electrode book implanted in the cauda equina? The traditional answer, $1k\Omega$, is as good a "guesstimate" as any. Electrochemistry is a very complex subject and the many parameters intervening in this situation would render a complete answer too complicated to be of practical use. Rather, simplifications are applied and a formula to predict the maximum voltage drop across the electrodes of a book connected as a tripole is developed. Although it is too simple to be accurate, it will be useful as a design tool, to replace the classic $1k\Omega$ figure.

Part III, Technical Issues, has a more practical tone as it presents some of the SLARSI development steps. It begins with a chapter (8) on the versatile experimental stimulator used in chapter 5; followed by two chapters, 9 and 10, on SLARSI design. Chapter 9 shows some of the issues treated in this thesis in light of the SLARSI development. The following subjects are reviewed: electrodes and cables; stimulation parameters, including dynamic range; RF link and transmitter; external control box and user interface. Each requires a set of specific skills, making the design of a complete implantable electrical stimulator system a wide ranging, challenging, task for a team to tackle. Chapter 10 is more technical as it attempts to explain the design of the SLARSI purpose-built demultiplexor implementing the new "independent channels" concept developed in chapter 5.

Finally, part IV brings this thesis to a close with a brief summary highlighting the key developments and a discussion on FES applications and medical research to set this work in a wider social context.

Part I

Introduction

Chapter 1

Neurophysiology

1.1 The nervous system

1.1.1 The nervous system: CNS and PNS

The nervous system is commonly subdivided into the Central and the Peripheral Nervous Systems, see fig. 1.1:

- the *CNS* itself is composed of the brain (including the brainstem and the cerebellum), the spinal cord and the nerve roots, it is the "controlling" part;
- the *PNS* comprises all the nerves after they have exited the spinal cord, it is the "communication network", providing muscle activation and sensory information collection.

1.1.2 The spinal cord and the cauda equina

The spinal cord follows the brainstem, see fig. 1.1(a) and extends toward the lumbar region. Throughout its length, nerve fibres leave the spinal cord in bundles called *nerve roots* (fig. 1.3) which then become 31 pairs (left and right) of *spinal nerves*, each of which will split many times to innervate the whole body and form the complex network of the PNS (fig. 1.1(b)). Nerve roots are labeled according to their vertebral level of exit and direction, see fig. 1.2. Four roots leave the cord above each disc, two on each sides. Of the left and right pairs one root sprouts toward the back of the body, the other toward the front (posterior and anterior, or ventral and dorsal directions, see fig. 1.1(a)). For example, the posterior root L5R leaves the vertebral column in the lower lumbar area, above disc L5, on the right hand side, and toward the back.
The neural body of the spinal cord in itself ends as the *conus medullaris*, between the last thoracic (T12) and the first lumbar (L1) vertebra, where the *cauda equina* begins (fig. 1.2). There, the nerves roots are suspended in cerebrospinal fluid, protected by a thick membrane called the *dura* or *theca* [1], ending at the coccyx level. The top of the cauda equina thus contains most lumbar and sacral roots (L3 to S5): 32 roots very densely packed (fig. 1.4). The importance of the root density in the cauda equina will be further developed in chapter 6.

[1] The word theca is a more general term used in botanic and anatomy to refer to any case or sheath. In the context of this thesis it will be used as an equivalent to dura, as is often the case in scientific publications.

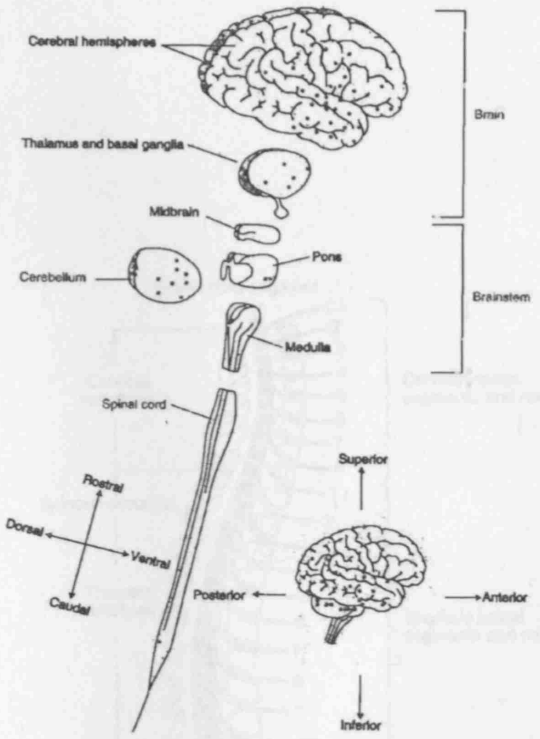

(a) Central Nervous System, reproduced from Kingsley [2000].

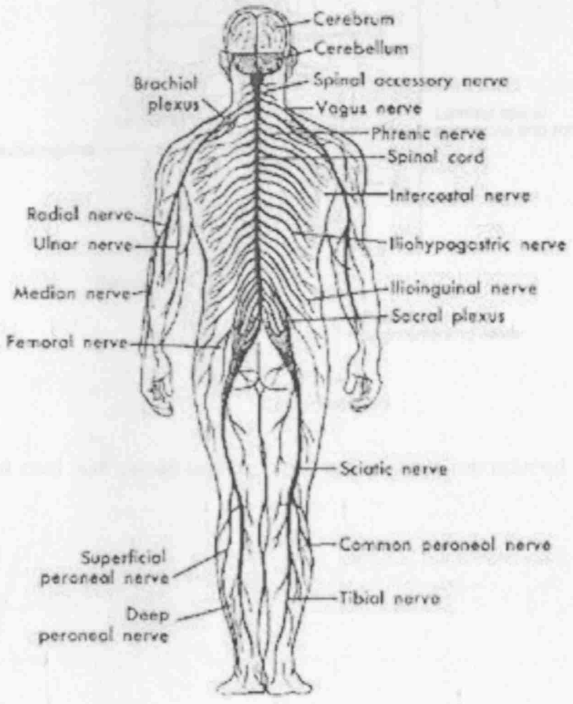

(b) Major nerves of the Peripheral Nervous System.

Figure 1.1: Human Nervous System.

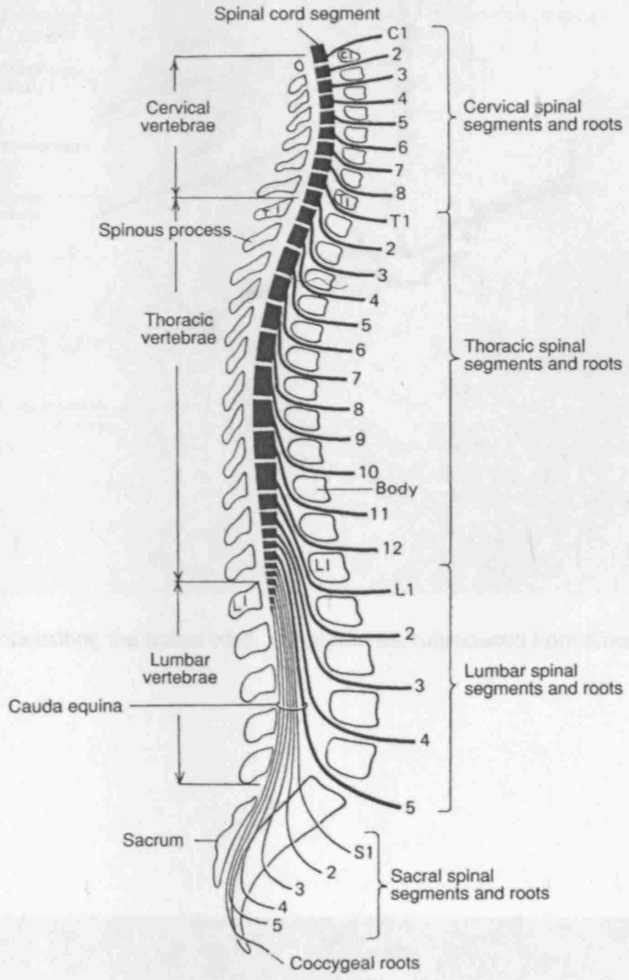

Figure 1.2: Spinal cord with cauda equina, right lateral view, reproduced from Noback et al. [2005].

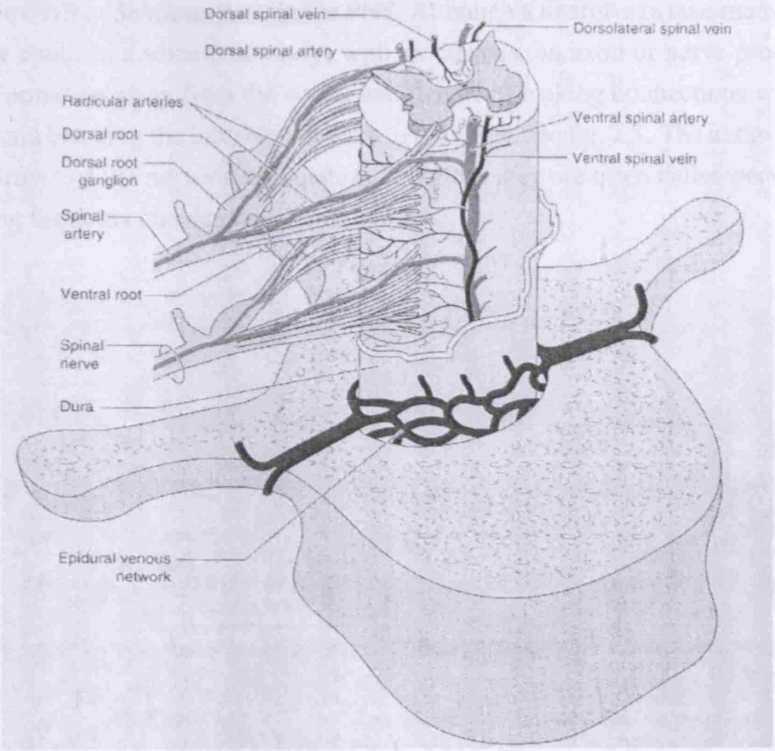

Figure 1.3: Roots exiting the spinal cord, spinal nerves, reproduced from Kingsley [2000].

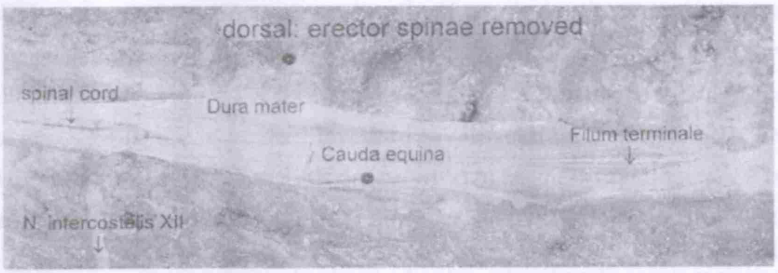

Figure 1.4: Nerve roots in cauda equina, reproduced from Schalow and Zach [1996].

1.1.3 Nerve anatomy

1.1.3.1 Nerve cells

Nervous structures are made of neurons, or nerve cells, surrounded by supportive cells: *glia* in the CNS or *Schwann cells* in the PNS. Although a neuron can take many shapes, it usually contains a soma (cell body) with its nucleus, an axon or nerve process carrying information away from the soma, and dendrites making connections with other neurons and bringing the information back to the soma, see fig. 1.5. The axons are seen as the carriers of the nervous information, therefore they are often called nerve fibres, neglecting the soma and dendrites.

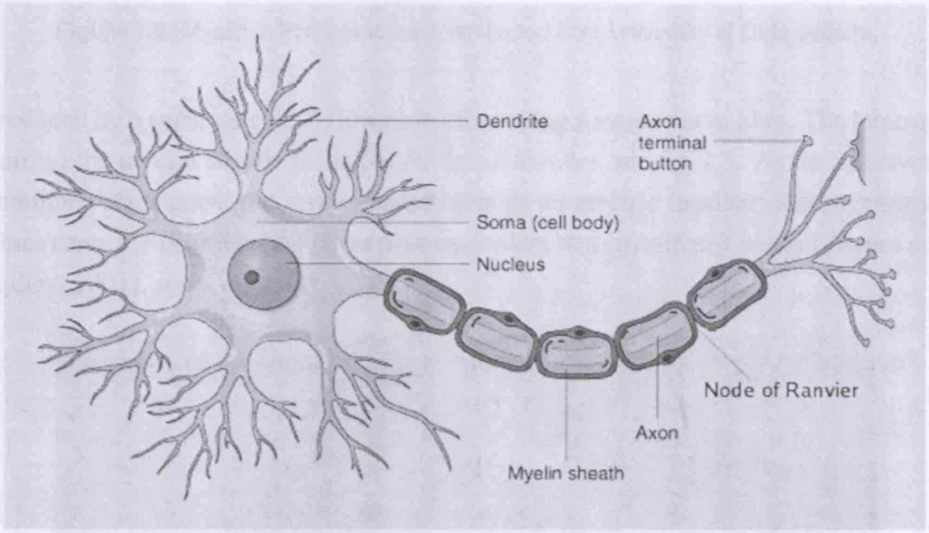

Figure 1.5: Motor neuron (soma, axon and dendrites).

1.1.3.2 Myelin

The supportive cells, glia or Schwann cells[2], wrap themselves around individual axons providing them protection and support[3]. If a cell forms many layers around an axon, it is said to be *myelinated*[4], the multiple folds of the supportive cell are known as the *myelin sheath*. Figure 1.6 shows a myelinated PNS axon, in the high magnification view (fig. 1.6(a)) the individual layers of myelin can be distinguished. Axons surrounded by only one or very few folds are referred to as "non-myelinated". The myelin is not normally continuous along one axon, rather, many short sections of myelin (each

[2]In the CNS, the myelinating glia are the oligodendrocytes, while the cells simply enclosing the axons (i.e. non-myelinating) are called astrocytes (for completeness, there is a third type of glia called microglia, which does not surround axons but has a macrophagic role). In the PNS, both myelin sheath and simple layers are formed by the Schwann cells.

[3]Not a one to one correspondence: there may be many supportive cells for one axon, or several axons may share one Schwann cell.

[4]*Myelinated* or *medullated* in older publications.

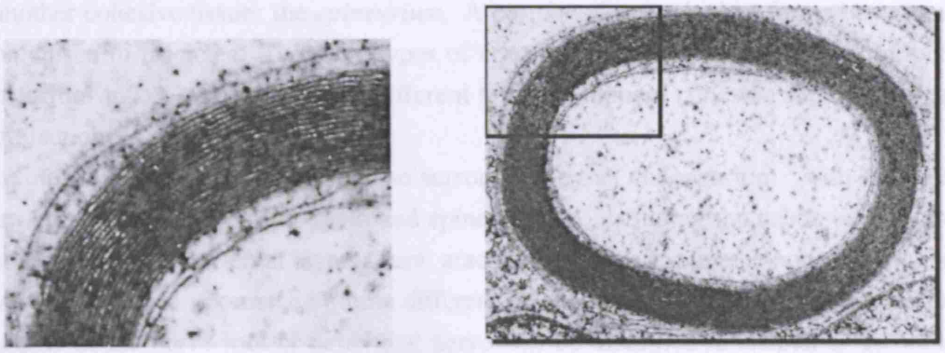

(a) Myelin layers at high magnification.

(b) Axon surrounded by myelin sheath, the square indicates the area shown in (a).

Figure 1.6: Myelin in PNS, pictures downloaded from University of Oulu website.

produced by a separate cell) follow each other along a single nerve fibre. The interruptions in the myelin sheath are called *Nodes of Ranvier*, see fig. 1.5. As far as nervous communication goes, the myelin sheath acts as an electric insulator and myelinated fibres carry the neural signal faster than equivalent non-myelinated axons [Keynes and Aidley, 2001], see section 1.3.

Figure 1.7: Peripheral nerve with large myelinated axons (in the corners) and a bundle of non-myelinated axons in the center, held together by one Schwann cell, picture downloaded from University of Oulu website.

1.1.3.3 Connective tissue

In the PNS, figure 1.9, axons and capillary blood vessels are surrounded by a loose connective tissue called the *endoneurium*. Groups of several axons with capillaries in endoneurium form fascicles, enclosed in a tough membrane: the *perineurium*, which offers a first degree of mechanical protection. The fascicles are bound together by

another cohesive tissue: the *epineurium*. A peripheral nerve is thus formed by axons organised in fascicles. The three types of connective tissues: the endoneurium, perineurium and epineurium provide different levels of support, cohesion and mechanical protection.

In the CNS, the neural cells are also surrounded by an endoneurium[5] with little extra protection, although the brain and spine at large, including the cauda equina, are shielded by three external layers (dura, arachnoid and pia)[6] plus the bones (skull and vertebrae). The importance of these different layers of protection for the structural integrity of the nerve root or peripheral nerve will be discussed in chapter 6. To some extent, an equivalence can be drawn between the PNS and CNS by associating the dura mater with the epineurium, the arachnoid and the pia mater with the perineurium as in Abbott et al. [1997], see fig. 1.8.

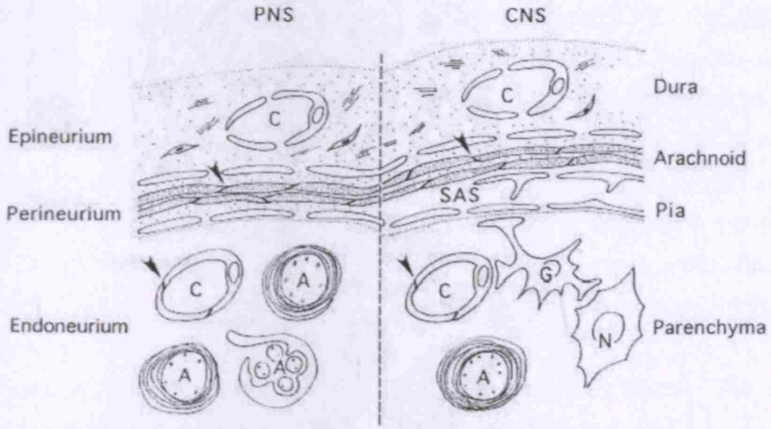

Fig. 1. Schematic diagram showing the relation between the sheathing layers of the peripheral nervous system (left, PNS) and the central nervous system (right, CNS), not to scale. Arrowheads mark sites of permeability barriers (zonulae occludentes). The epineurium corresponds to the dura and contains permeable capillaries. The perineurium corresponds to the arachnoid, and both these layers have a barrier function. In the CNS the cells bordering the neural tissue are identified as a distinct layer, the pia, with the subarachnoid space (SAS) containing cerebrospinal fluid. The endoneurium corresponds to the brain parenchyma. The endothelia of capillaries in both endoneurium and brain parenchyma form permeability barriers. A, axon; C, capillary; G, astrocytic glia; N, neuron.

Figure 1.8: Comparison between protective sheaths in PNS and CNS, reproduced from Abbott et al. [1997].

1.1.4 Vascularisation

As the aim of the first part of this thesis is to introduce all the concepts and elements of knowledge required to understand the following parts, a description of nerve roots vascularisation is needed. Although the focus for chapter 6 is on the blood supply to the cauda equina, an overview of the overall spinal cord supply is necessary.

The arterial network is divided in three zones: cervicothoracic, mid-thoracic and thoracolumbar. Running along the spine in the sub-arachnoidal space are one anterior spinal

[5] Sometimes referred to as brain parenchyma, also this definition is discussed [Macpherson, 1995]

[6] Of the three layers: the dura mater, the arachnoid and the pia mater, the dura is most often mentioned alone when talking about mechanical protection as it is the toughest. It is in the sub-arachnoid space, between the pia and the arachnoid, that the cerebro spinal fluid circulates.

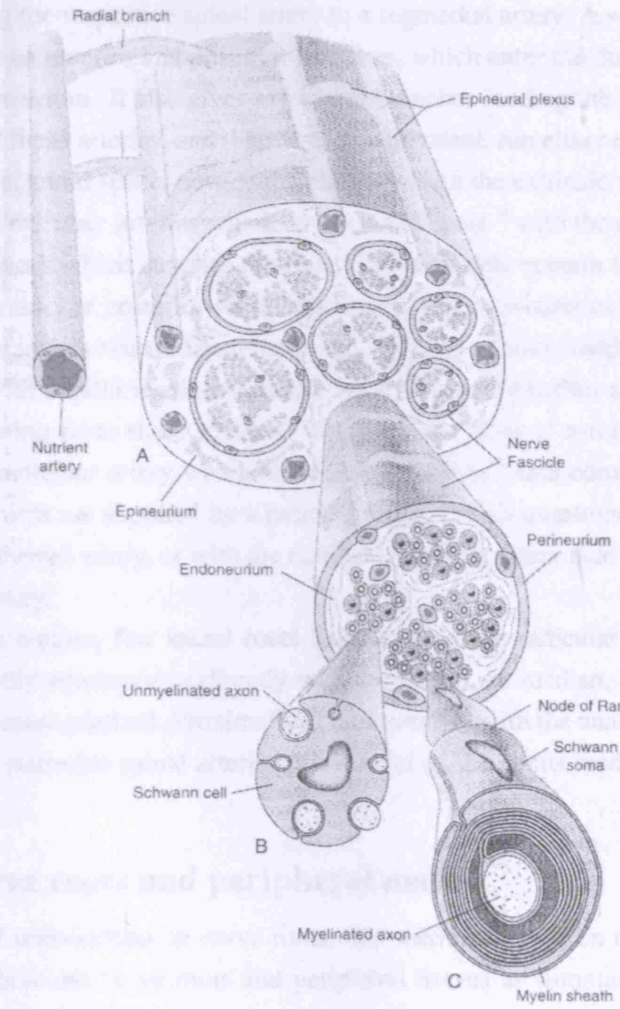

Figure 1.9: Endoneurium, perineurium, epineurium: the fascicular nature of a nerve, reproduced from Kingsley [2000].

artery and two posterior (or postero-lateral) spinal arteries. They appear continuous but the blood follows three separated circuits, flowing in both cranial and caudal directions in the arteries depending on the level of the nearest segmental artery which supplies blood to that section of the cord. The spinal arteries are branches from the vertebral artery while the segmental arteries derive from the aorta. Both anterior and posterior arteries produce a network of branches at the surface of the cord called the *vasa corona* or pial plexus. Along most roots runs an anterior or posterior radicular or medullary artery linking the respective spinal artery to a segmental artery. A segmental artery divides thus in an anterior and posterior branches, which enter the dura where it merges with the epineurium. It also gives extradural branches feeding the vertebral body and the dura. All these arteries, and their venous equivalent, run either outside the dura, or in the sub-arachnoid space, outside the pia, they form the extrinsic vascular network.
Beside these extrinsic arteries which do not anastomose [7] with the nerve roots runs an intrinsic network which supplies the roots. Most rootlets contain (inside the pia) one (or more for thicker posterior rootlets) intrinsic radicular arteries [8]. They form perpendicular branches which anastomose with thinner arteries inside the fascicles and eventually with capillaries deeper in the root. These T-branches are coiled, preventing them tearing from shear stresses. The proximal third of a rootlet is supplied by an intrinsic radicular artery which anastomoses with the vasa corona while the other, distal, two thirds are supplied by a radicular artery which anastomoses either directly with the segmental artery, or with the extrinsic radicular artery near its branch with the segmental artery.
In the cauda equina, few sacral roots have an extrinsic radicular artery. The roots intrinsic supply anastomoses directly with the lateral, or median, sacral arteries (the lowest segmental arteries). Proximally, it anastomoses with the anastomic loops of the anterior and posterior spinal arteries at the level of the conus medullaris Parke et al. [1999].

1.2 Nerve roots and peripheral nerves

After a brief introduction on nerve roots, this section focuses on the similarities and differences between nerve roots and peripheral nerves as summarised in table 1.1 [9]. Such a comparison is often necessary as there is little literature available on roots, and estimates have to be inferred from peripheral nerves behaviour, as in chapters 5 and 6. Within any nerve, the fibres are classified according to propagation direction (afferent or efferent) and conduction velocity or diameter. Because the motor and sensory fibres

[7] The anastomosis is the direct intercommunication of the branches of two or more veins or arteries without any intervening network of capillary vessels [Macpherson, 1995].

[8] These are sometimes called true radicular arteries to distinguish them from the extrinsic medullary arteries, commonly called radicular arteries too.

[9] The data do not specifically come from spinal cord injured patients. They are nonetheless relevant since the nerve fibres integrity (diameter, conduction velocity, organisation) is preserved after injury [Schalow et al., 1995].

were studied by different researchers, two naming conventions remain, one using greek letters (efferent fibres) and the other using roman numbers (afferent fibres.). There is no exact equivalence between these two marking systems probably introduced by Lloyd (sensory) and Erlanger (motor) in the 1940's and 1930's respectively [Whitwam, 1976]. The most common fibre classes and corresponding diameters and conduction velocities are given in table 1.1. For information, C fibres, or group IV fibres are unmyelinated. The $A-\gamma$ group is sometimes subdivided into $A-\gamma$ and $A-\delta$.

The nerve fibres leave the spinal cord as rootlets, which gather to form the roots, see fig. 1.3. The dorsal or posterior roots contain mainly *afferent*, or sensory, fibres; while the ventral or anterior roots consist mainly of *efferent*, or motor, fibres. This is known as the *Bell-Magendie* law [10]. Studies have long shown that the ventral roots are not exclusively efferent, and the dorsal not exclusively afferent [Phillips et al., 2000]. The posterior and anterior roots join as they leave the spine to form the spinal nerves, see fig. 1.3. In the spinal canal, the roots and spinal cord lie in cerebro spinal fluid (CSF). As mentioned before, the cord as a whole is surrounded by three protective membranes (the dura mater, the arachnoid and the pia mater) which constrain the CSF and offer some mechanical protection; and further shielded by the vertebrae. When the rootlets exit the spinal cord, they are floating in CSF, each surrounded by the thin pia mater. As they gather to become a root, the glial cells of the endoneurium give way to Schwann cells in a transition from CNS to PNS. The arachnoid becomes thinner as the dura ensheath the root more closely. Progressively, the subarachnoid space and CSF disappear and the arachnoid, together with the pia, form a sheath analogous to the perineurium. At the level of the dorsal root ganglion, the dura blends into the epineurium, and upon its exit from the intervertebral foramen the root has changed from CNS to PNS [FitzGerald and Folan-Curran, 2002].

In the cauda equina, the rootlets are often bound together in larger groups with arteries, surrounded only by the pia. They may stretch for several centimetres in CSF before their point of exit and are rather fragile. In comparison, peripheral nerves have no bony protection, but, as mentioned above, they are tougher per se, hence less susceptible to irreversible compression injuries. Both nerve roots and peripheral nerves can regenerate to some extent [Zhang and Yannas, 2005], as will be discussed in chapter 6.

1.3 Nervous communication

The transport of information within the brain, and between it and the rest of the body, is done via nervous signals of an electro-chemical nature. These impulses, called *action potentials* (APs), are carried through the body by the nerves. The communication between neurons, via the synapses, is a chemical process [11], while the transport of in-

[10] After Sir Charles Bell (1774-1842) and François Magendie (1783-1855).

[11] This falls beyond the scope of this introduction, for more information see any good neurology book, for example Carpenter [1996]; FitzGerald [1996]; Keynes and Aidley [2001]; Kingsley [2000]; Noback

Table 1.1: Nerve root versus peripheral nerve.

	Nerve Root		Peripheral Nerve	
	anterior	posterior	motor	sensory
Endoneurium	present[a] hardly any [Schalow, 1992; Schalow and Zach, 1996], 1 to 9 layers of cells [Matsui et al., 1997]		present 100 or more layers of cells [Keynes and Aidley, 2001]	
Perineurium				
Epineurium	absent		present	
Myelin [Carpenter, 1996] [Mathers, 1985]	$\leq \frac{1}{3}$ of all fibres unmyelinated[c]	$\frac{2}{3}$ of all fibres unmyelinated	mixed, thinner fibres (diameter $\geq 1\mu m$) are myelinated	
Fibre diameter[d]	3-13,	0.5-20	A-α 12-20	Ia 12-22
in μm	mostly	mostly	A-β 7-14	Ib 12-22
[Carpenter, 1996]	9-13	3-14	A-γ 2-10	II 5-15
[Mathers, 1985]			B 1-5	III 2-10
			C 0.2-0.5	IV 0.2-1.5
Conduction	15-60	5-120	A-α 65-210	Ia 65-130
speed[e]		mostly	A-β 40-80	Ib 65-130
in m/sec		10-70	A-γ 10-50	II 20-90
[Carpenter, 1996]			B 4-25	III 12-45
[Schalow et al., 1995]			C 0.2-2.0	IV 0.2-2.0
Stiffness (mice) [Beel et al., 1986]	ratio 1 to 6			
Strength (mice) [Beel et al., 1986]	ratio 1 to 6			
Elasticity (mice) [Beel et al., 1986]	ratio 1 to 1			

[a] Glial cells in the first mms, Schwann cells appearing distally [Parke et al., 1981].

[b] Formed by the pia matter.

[c] The unmyelinated fibres in the anterior nerve roots are mostly sensory [Carpenter, 1996; Coggeshall et al., 1975; Phillips et al., 2000].

[d] Includes the axon itself and the myelin sheath when present.

[e] At body temperature.

formation along the axon is of a simpler electro-chemical nature. This section is an introduction to the subject of nervous communication and action potential generation, focusing on two essential concepts: the "all or nothing" property of the nervous signal and the cable theory and associated saltatory conduction, it does not cover more complex phenomena like fatigue.

1.3.1 Action potential: all or nothing character and frequency modulation

Within a quiet axon, ions, mainly calcium, potassium and sodium, maintain the potential at a resting level (stable), negative relative to the external potential (around -70mV in human). The membrane at rest is thus negatively polarised. This is a stable situation, small disturbances of the transmembrane potential are damped by fast ion movements. When the transmembrane potential is reversed above a certain threshold level it reaches an unstable state and positive charges flow inwards causing the transmembrane potential to increase even more and become positive before falling back to, and temporarily below, its initial negative resting potential, see fig. 1.10. This process spreads along the membrane as an action potential [12]. It is possible to induce this excitation using electrodes passing a burst of current to lower the external potential below the axon's inner potential. Action potentials might then propagate along the axon, in both directions (called *antidromic* and *orthodromic*). Figure 1.11(a) illustrates the "all or nothing" character of action potential generation: the action potential of a single fibre is either present, or it is not, its amplitude is meaningless. Small potential variations do not disturb the resting fibre. When the transmembrane potential reaches the threshold value, an AP appears. A further increase of the potential will not change the shape of the axon's signal in a significant manner. Since the nerve fibre does not modulate the amplitude of the signal, the information to be transmitted is coded as a function of the frequency of the nervous impulses. A more intense stimulus does not give rise to a specifically larger or higher action potential but to a burst whose frequency is related to the stimulus intensity, see fig. 1.11(b).

For simplicity, the stimuli in figure 1.11 are represented as pulses of varying amplitude that depolarise the membrane. Action potentials may be triggered by sensory inputs like temperature, touch, sound; by upper nervous centres as part of a motor action or by an external intervention as explained in chapter 2.

This explanation, given at the axon level, can easily be extended to the whole nerve. The single action potentials add up to form a *compound action potential* (CAP) including all axon contributions. Every nerve fibre has its own activation threshold (this is the transmembrane voltage necessary to elicit an AP) and activation delay so the amplitude of the CAP will vary depending on how many fibres are firing together.

---

et al. [2005]; Parent [1995].

[12] The exact mechanism allowing for the charges exchange is unclear and two hypothesis exist: the classic "ion channels" view [Sabah, 2000] and the outsider "gel" option [Pollack, 2001].

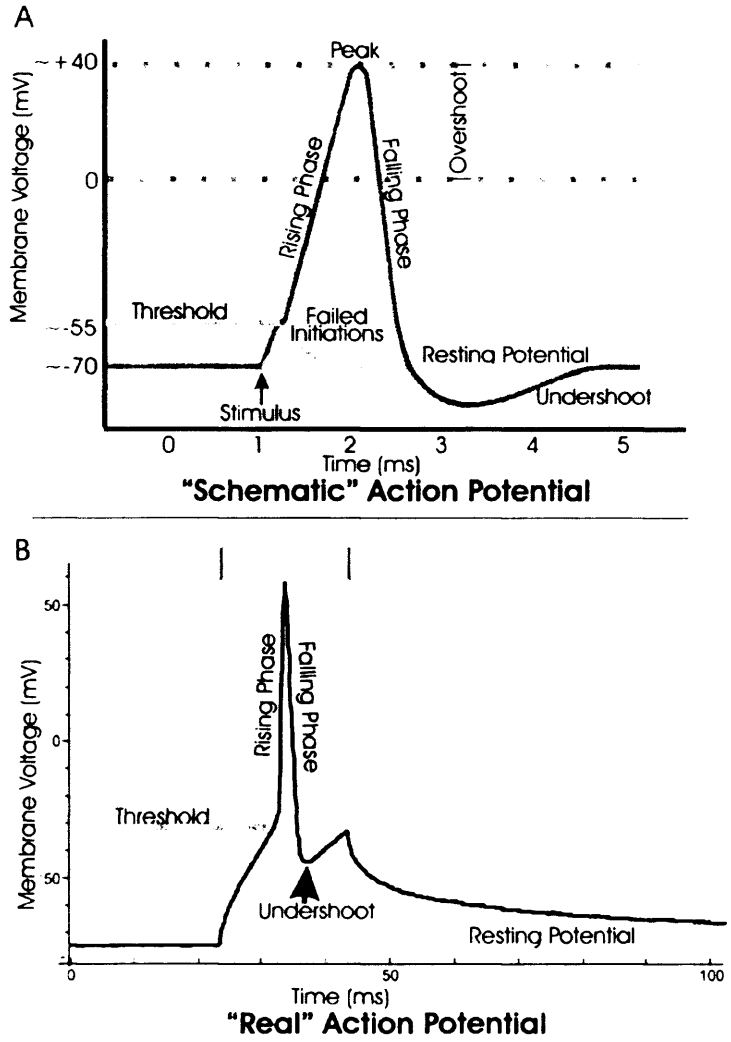

Figure 1.10: Action potential, reproduced from Wikipedia [last accessed in 2007] under the GNU Free Documentation License.

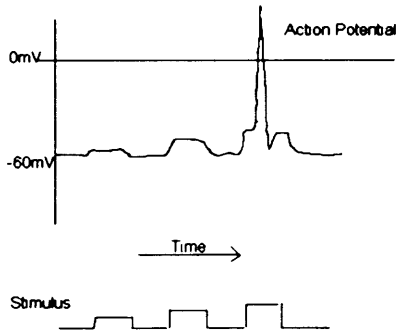

(a) "All or nothing" behaviour: the action potential is only triggered when the stimulus intensity reaches a certain threshold.

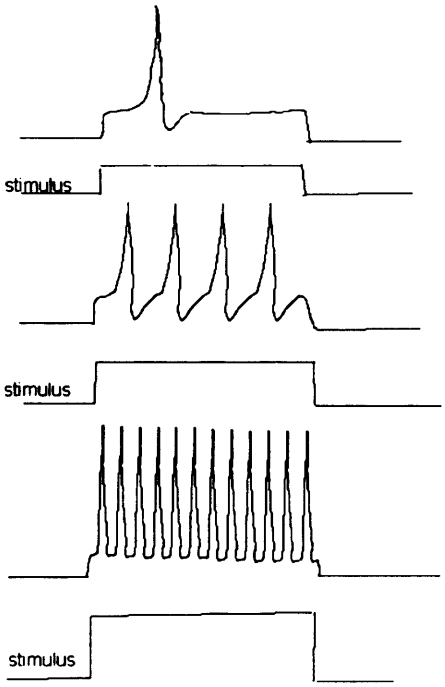

(b) Frequency modulation: the firing frequency of the action potentials increases with the stimulus intensity.

Figure 1.11: Action potentials.

1.3.2 Cable theory and saltatory conduction

Since axons carry electrical signals, they can be represented with an equivalent circuit: a poorly insulated cable model to schematise their electrical properties, see fig.1.12. The internal and external environments are mainly resistive, while the axon's membrane behaves as a leaky capacitor. In myelinated fibres the nodes of Ranvier are represented with discrete RC cells (a resistor in parallel with a capacitance). An axon potential is represented with a battery, travelling through the cable with the AP's peak [Hodgkin, 1971; Keynes and Aidley, 2001; Sabah, 2000]. Current will then flow in local circuits as shown by the arrows on fig.1.12(a). The conduction velocity is therefore limited by the time it takes to charge the RC cells one after the other.
The myelin, increasing the membrane resistance and decreasing its capacitance [13], accelerates the AP propagation [Altman and Plonsey, 1989; Holsheimer, 1998]. The term *saltatory conduction* [14] was apparently introduced by Lillie in 1925 to indicate that the current propagates in discrete steps, it seems to "leap" along the axon, from one node of Ranvier to the next [Stampfli, 1954]. Since the myelin has a large resistance, the current seems concentrated at the myelin gaps (the nodes of Ranvier) where it is easier to cross the membrane [Frankenhaeuser and Schneider, 1951]. Because of that current concentration, myelinated nerve fibres are easier to excite [Rattay, 1998].

1.4 Spinal Cord Injury and paraplegia

A spinal cord injury (SCI) may be caused by a trauma (traffic incident, violence, fall, recreational activities accident, etc) or be atraumatic (due to multiple sclerosis, transverse myelitis, etc). Although both kinds of injury exhibit many similarities of clinical signs and symptoms [McDonald and Sadowsky, 2002] and of rehabilitation methods and outcomes [McKinley et al., 2001], this section is limited to traumatic SCI only. The processes involved are complex as a secondary injury (due to blood flow disruption, chemical imbalance and nervous structure degeneration) follows the original mechanical trauma [Tator and Koyanagi, 2006]. Peripheral nerves may also get crushed, stretched or avulsed during the accident [Lundborg et al., 1983]. Eventually, often after some surgical and pharmaceutical intervention, the injury stabilises and the extent of the damages may be evaluated. The following data (North America, 2001), give an idea of the importance of traumatic spinal cord injury in the 21st century: there are around 10,000 new cases reported every year with a prevalence of more than 200,000 [McDonald et al., 2002; McDonald and Sadowsky, 2002; Pickett et al., 2003; Sadowsky et al., 2002]. In the UK the estimate in 2004 was of 1,200 new cases of traumatic SCI a year, and nearly four times more of atraumatic origin, with a prevalence

[13] Analogy with two parallel plates separated by a dielectric: increasing the distance between them allows for more charges to be stored, hence the capacitance decreases. Here the myelin acts as a dielectric between the outer and inner fluids. The potential across the charging transmembrane capacitor is proportional to $\frac{i \cdot dt}{C}$, decreasing C means V is reached faster.

[14] *Saltatory*, formed from the English *saltation*, comes from the Latin *saltare*: 'to keep leaping' [Encarta, 1999].

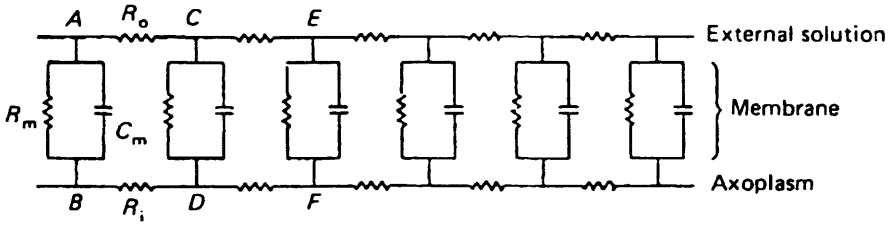

(a) Cable theory: poorly insulated cable model of a nerve.

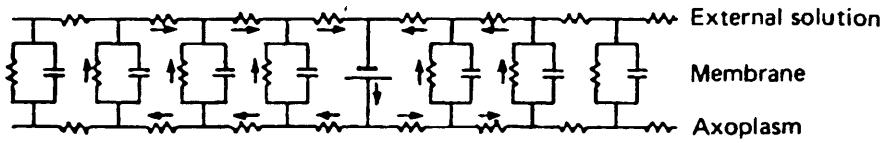

(b) Current flow propagating along the cable model.

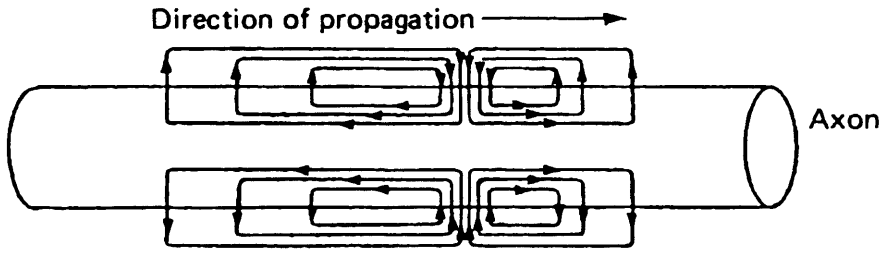

(c) Current flow propagating an action potential along an axon.

Figure 1.12: Cable theory, reproduced from Keynes and Aidley [2001].

of 40,000 [Aspire, online, last accessed in November 2006; RDS, online, last accessed in November 2006]. Finally worldwide estimates vary from 15 to 40 new cases (of traumatic SCI) per million people per year [Lim and Tow, 2007].

1.4.1 Level and completeness

An injury is complete if the cord has been fully transected and no sensation nor any motor control remains, it is incomplete otherwise. In the developed world, about one third of the new cases are complete, another third are incomplete, and the remaining are anatomically incomplete but show no signs of motor activities below the lesion, although some sensory function may remain [Verma and Fawcett, 2005]. For patients with an incomplete lesion [15] there is little relationship between the cross-sectional area of the section and the resulting incapacity. Severe but incomplete sections may sometimes cause only minor disabilities, a few axons of the spine can carry a great deal of information [Mettler and Liss, 1959]. Paraplegia results from a section of the cord at the level of the thoracic vertebrae or below while tetraplegia (also known as quadriplegia [16]) is caused by a cervical lesion. This is a gross separation, there are many degrees of impairment within paraplegic groups.

The level of injury is traditionally assessed on both a sensory and a motor scale as these may be different. The practitioners use pin-pricks to test skin feelings, and refer to a dermatome map like the one shown on fig. 1.13 to evaluate the sensory level of injury. The patient is then asked to move different body parts (10 muscle groups) to perform a similar motor assessment.

Patients with a complete lesion nearly all lose control of their bladder, bowel and sexual functions. Concerns with kidney infection, continence and other uro-genital aspects usually score the highest in quality of life assessments, or patients wish lists [McDonald and Sadowsky, 2002; Verma and Fawcett, 2005]. Paralysed muscles often shrink (muscle atrophy), bone density is also seen to decrease in disused limbs [Clasey et al., 2004]. As a consequence the patients are more at risks of bone fractures. The muscle atrophy also affects the blood flow in the area and, coupled with the typical seated position of wheelchair users and a lack of sensation, increases the risks of pressure sores and complications. Another issue that has gained increased attention in the last decade is that of cardio-vascular and respiratory illnesses. Even low level paraplegics may suffer from such ailments, and respiratory complications are now one of the major causes of death amongst SCI sufferers in developed countries (together with suicide and septicemia) [Garshick et al., 2005; O'Connor, 2005a,b].

[15] In the context of this thesis, the words complete and incomplete refer to the extent of the spinal cord lesion of a patient.

[16] The word quadriplegia is formed with a Latin prefix (quadri, four) followed by a Greek root (plegia, palsy). It is often abandoned in favour of the more etymologically correct tetraplegia (tetra being the Greek root for four) except in the US where it is still commonly used.

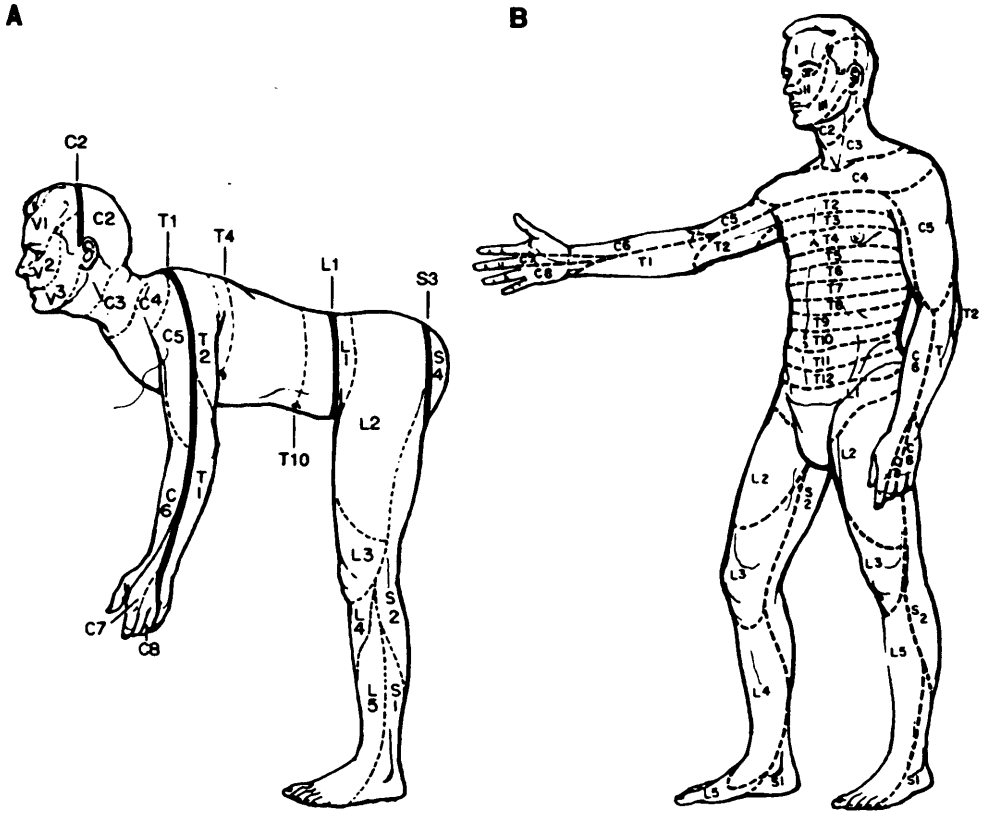

Figure 1.13: Dermatome map for SCI level assessment, there are 28 dermatomes, reproduced from Noback et al. [2005].

1.4.2 Paraplegic rehabilitation

Rehabilitation is the (long term) process by which a patient regains the ability to live in society, as comfortably, cost-efficiently and independently as possible. It is a broad form of disability management that includes: learning to perform everyday tasks (including those needed to return to work), adapting their environment and ways of life to, and accepting, the new situation; as well as education and training with a focus to prevent medical complications and repeated injuries. The role of the rehabilitation team extends far beyond that of physical therapists. Emotions and feelings cannot be disregarded in favour of purely physical outcomes and moral support and teaching are keys to a patient's successful return to an active, satisfying, social life. Although the goals of rehabilitation imply an early involvement of the team following the injury, patients are likely to require help and advice to deal with, prevent or overcome, the degenerative evolution of their disability at many stages of their life, hence the need for long-term follow-up. Yet, due mainly to financial pressure, patients are often discharged early from specialist SCI units (there are only 12 such units in the UK) and are thereafter cared for in local hospitals where practitioners may not be SCI specialists, and where the rehabilitation (in the larger, longer term, sense of the word) opportunities may not be optimum due to a lack of general information, funding and poor publicity of new or lesser known clinical applications and their potential benefits [Sadowsky et al., 2002; Teeter, 1999; Yarkony et al., 1987]. Here follows a list of the major physical rehabilitation options for traumatic SCI patients:

- Surgical restoration of upper extremity through tendon transfer, reimplantation of avulsed nerve or nerve anastomosis [Carlstedt et al., 1995; Livshits et al., 2004].
- Electrical stimulation (introduced in chapters 2 and 3): for functional movements to help perform a selected task (grasp, pinch, stand, transfer), to support organs (cardiac pacing, breathing and coughing, bladder and bowel management), to manage pain, to prevent pressure sores, to prevent osteoporosis by muscle strengthening, to provide cardio-vascular training and therapeutic benefits, to prevent contractures and spasticity [Adams and Hicks, 2005].
- Physical therapy to recover and maintain flexibility of the muscles and joints.
- Pharmacological intervention, not only acutely to minimise secondary injury, but also to help everyday life, for example: anticholinergic drugs, Botox, Viagra.

1.4.3 Recovery and regeneration

Spontaneous recovery often occurs after the first assessment (typically made 72 hours after the initial injury). During the first 6 months to one year, patients may regain one motor level, although their muscle strength does not always improve enough to become fully functional [Calancie et al., 2004; Lim and Tow, 2007; McDonald et al.,

2002]. Young patients are more likely to make a functional recovery, and this process may continue for years and be enhanced by sustained, dedicated, rehabilitation therapy. Incompleteness of the lesion is often associated with increased chances of improvements. Even a partial regeneration of the nervous system may lead to dramatic improvements [Hook et al., 2007; Mettler and Liss, 1959; Verma and Fawcett, 2005]. The signs of recovery, although not always obvious, can usually be clinically evaluated. Yet what triggers and promotes recovery is the subject of much debate [Balasubramaniam et al., 2005]. The following phenomena all contribute to motor and sensory improvements. Since they happen at the same time, and over a more or less extended period, it is difficult to qualify their respective importance in the overall return of function or sensibility [Barbeau et al., 1998; Steeves and Wolfram, 1998; Verma and Fawcett, 2005].

- Reduction of edema, lowering the pressure around the initial site of injury, accompanied with improved blood flow;
- Recovery from "collateral damages" like broken bones, muscles and tendon damage, etc which impaired functional movements;
- Peripheral nerve recovery following nerve crush or overstretching [Zhang and Yannas, 2005];
- Regeneration of motor axons at root level (late onset of recovery [Calancie et al., 2004]);
- Learning and adaptation of nervous structures enhancing spinal cord plasticity.

These various contributions can be helped by drugs and surgical interventions aiming to: compensate for demyelination, block inhibitors, promote axon regrowth (scaffolding structures, directive cells).
The above list shows that neural regeneration is not the only event contributing to the perceived recovery. Yet, ultimately, the damaged cord needs to be repaired if a full return of function is to be achieved. Peripheral nerves and nerve roots (especially anterior roots) have the ability to regrow [Brindley, 1990; Buti et al., 1996; Kingsley et al., 1983; McCouch, 1955; Ramon y Cajal, 1991 translation], but do not necessarily do so, or form functional connections when they do regenerate, as seen in humans by the return of spasms following extensive deafferentation [Angelov et al., 2007; Collado et al., 2006]. For the past 25 years, scientists in the fields of neural regeneration, cell therapy or spinal cord repair have been reporting promising animal results [Cowan, 2001; Kao et al., 1982; Navarro et al., 1994; Schwab, 2002; Seil, 1983]. Intense media attention [17] has artificially built up the hopes for an impending cure to SCI. Yet, the retractive and degenerative processes that accompany a spinal cord injury as well as the long term scaring process are serious complications to the medically transected

[17] Of broadsheets as well as scientific publishing houses like Nature group [Lindwall, 2006].

cords of laboratory animals. Lately, probably influenced by the demise of South Korean star scientist Dr. Hwang Woo Suk, the reports of neural regeneration have become more careful [Jones et al., 2003; Lindwall, 2006]. While it is clear that regrowth of the nervous structures of the spinal cord will at some point be achieved, the time line for such an achievement is questionable. Reviews of studies on stem cells, olfactory ensheathing cells (OEC) or other therapies, while optimistic, all highlight the need for more research [Edgerton and Roy, 2002; Lindwall, 2006; Schwab, 2002; Verma and Fawcett, 2005]. Essentially, the following points are raised by the reviewers:

- Danger of aberrant, maladaptive, axonal sprouting and anarchist overgrowth of non-injured axons;
- Risks of other side effects like tumour formation due to the lack of control over nervous system cell differentiation after cell transplant;
- Mitigated results interpretation: the species used as models in the studies (mice, rats, cats) have shown spontaneous recovery to similar functional levels without cell therapies, hence the question, also raised by Verma and Fawcett [2005], whether the return of function is due to sprouting of unlesioned axons and plasticity, or truly to axonal regeneration;
- Time between injury and treatment: the treatments are often applied acutely on neatly cut spinal cords, the physiological changes undergone over the years by the nervous structures following a traumatic tear and crush injury might have been overlooked.

In this light, the only realistic short to mid-term application of cell regeneration might be to aid remyelination.
Spontaneous recovery is also enhanced by less drastic therapies like physiotherapy, partial weight bearing stepping, functional electrical stimulation, robotic and more. These techniques were mostly developed as rehabilitation tools, to prevent contracture, decrease spasticity and provide functional movements. Yet, their effect sometimes extends beyond the immediate treatment [Baldi et al., 1998; Borgens, 1991; Buti et al., 1996; Edgerton and Roy, 2002; Navarro et al., 1994; Rushton, 2003; Steeves and Wolfram, 1998]. In some cases, the increase in muscle bulk may simply render visible the neural activity already present. However, retraining the body to perform a task or movement against a reasonable load enhances learning and spinal cord plasticity. Studies have shown not only an increase in the activation of spinal neurons, but also a better coordination between neural motor pools.

Chapter 2

Electrical stimulation

2.1 Principle

Artificial stimulation of nerve fibres may occur where current is made to flow out of the nerve membrane. Previously, the axon can be seen as resting in a stable, quiescent, state. The stimulation pulse tends to disturb this state. For a small amplitude the disruption dies out without much happening. A large surge of current will however push the nerve in an unstable state, characterised by a reversed transmembrane potential (*depolarisation*), and trigger the firing of an action potential. Afterwards, a refractory period follows (the axon is less excitable) before a return to the resting state. This notion of equilibrium and brisk disturbance helps explain why a slowly increasing current applied to the nerve membrane does not induce stimulation, an effect known as accommodation [Hill, 1936; Hodgkin and Huxley, 1952; Keynes and Aidley, 2001; Solandt, 1936; Stoney and Machne, 1969]. Likewise, unexpectedly long latencies [1] can be explained as the membrane can hang at the boundary between its stable and unstable (AP firing) states [Mortimer, 1990]. Since the firing of an impulse is the result of a "build up" that pushes the nerve out of its stable state, any event just before or after the stimulation pulse influences its capacity to trigger an action potential. This consideration is especially true with pre- and post-pulses, often used to balance the charges [Mortimer, 1990]. A small anodic current will hyperpolarise the membrane, making it "more difficult" to reverse the potential. An action potential entering an hyperpolarised zone will slow down, and might even be stopped if the anodic current is large enough. Practically, these observations have led to the development of *electrical stimulation devices* that, very basically, send controlled bursts of electricity to nervous structures to cause motor or sensory reactions. The blocking effect of larger anodic current is also exploited to interrupt action potential propagation, for selective stimulation or neuromodulation.

The simplified reasoning of this introduction shows the importance not only of the amount of charge delivered, but also of timing, frequency, pulse shape, amplitude and more in the study of electrical stimulation, hence in this thesis. While chapter 1 fo-

[1] The latency is time between the onset of the pulse and a pre-defined, repeatedly recognisable, instant in the AP.

cused on anatomical and medical considerations, this chapter introduces the key electrical concepts required to understand electrical stimulation and the research presented hereafter.

2.2 Theory of nerve stimulation

2.2.1 Chronaxie, rheobase, strength-duration curve

In their studies on nervous stimulation, Engelmann, the Lapicque couple, Weiss, Hoorweg and others in the late 19^{th} century, early 20^{th} noted that all nerves and muscles could be excited by an electrical stimulus [Blair, 1932a,b; Davis and Forbes, 1936; Fredericq, 1928; Gasser and Erlanger, 1930; Lapicque, 1926; Rushton, 1927, 1932]. They showed that with square or capacitive discharge pulses, an increase of the pulse width led to a decrease in the threshold intensity required to excite the tissue, until a minimal threshold was reached. Increasing the pulse width any longer did not lead to any further reduction of the threshold intensity[2]. Although different tissues required very different stimulus width and intensity, all followed a qualitatively similar *strength-duration* curve[3].

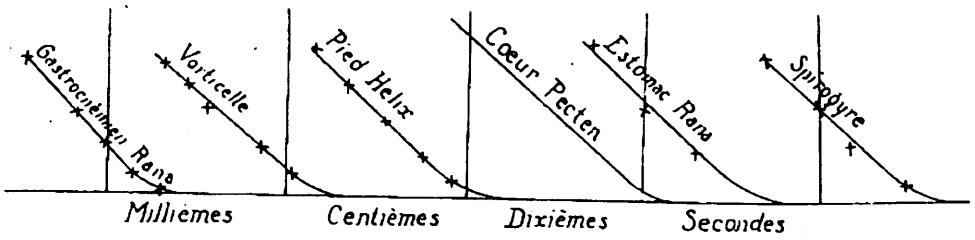

Figure 2.1: Strength-duration curves, normalised to the minimum threshold, for a selection of tissues, plotted on a log. scale in Lapicque [1926]

Many researcher attempted to describe the shape of the strength-duration curve with a formula whose parameters could be given a physiological meaning. The most commonly used nowadays are the hyperbola, attributed to Weiss and Hoorweg:

$$I_{thr} = r * (1 + \frac{c}{pw}) \tag{2.1}$$

and the exponential, attributed, perhaps incorrectly as discussed in appendix ??, to Lapicque:

$$I_{thr} = \frac{r}{1 - e^{\frac{-pw * ln2}{c}}}. \tag{2.2}$$

Another formula sometimes mentioned is Lapicque's canonical curve, developed as an attempt to provide a purely mathematical formula, i.e. a formula including adjustment

[2]Larger stimuli may even cause the disappearance of the compound action potential

[3]The strength-duration curve is obtained by plotting the stimulus amplitude, often expressed as a current, versus the stimulus pulse width.

parameters without physiological meaning, that would offer a better fit to the experimental data gathered by him and others [Lapicque, 1926]:

$$I_{thr} = r * \sqrt{\frac{pw + \theta + \sqrt{(pw - \theta)^2 + 0.16 * \theta^2}}{2 * pw}} \tag{2.3}$$

where $\theta \approx 3.8 * c$. In the three equations (2.1 to 2.3) pw is the pulse width, or duration. The two parameters introduced: r and c, the *rheobase* and the *chronaxie*, will be discussed below. None of these equations does quite predict the actual shape of the strength-duration curve and comments about which is more adequate are still expressed nowadays [Geddes, 2004; Irnich, 1980; Testerman, 2005]. Despite these, there is agreement on the fact that for a fresh nerve, there is a minimum stimulus amplitude below which no action potential may be elicited, no matter how long the pulse lasts. This minimum amplitude is the rheobase, r, seen as the asymptote of the strength-duration curve. The chronaxie, c, is then evaluated as the pulse width required for an amplitude twice the rheobase. Knowing r and c is sufficient to qualify the excitability of a stimulation system containing a nervous structure, some electrodes and a conductive environment[4]. A low rheobase is associated with high excitability, i.e. efficient electrodes placement [Geddes and Bourland, 1985], coupled with a low chronaxie, this indicates a highly excitable tissue.

[4]It is worth noting that these parameters are dependent of the stimulation setup. Moving the electrode(s) away from a nerve or increasing the impedance of the environment is likely to increase r [Fredericq, 1928; Lapicque, 1943, pages 106 and 516]. The chronaxie on the other hand is dependant on the physiological conditions (temperature, state of the nerve,...), and the electrode dimensions [Rushton, 1928a]. Irnich and Geddes say otherwise, to them, the chronaxie is dependent on: stimulus waveform, electrode characteristics, stimulator output impedance, tissue inhomogeneity and temperature [Geddes, 2004; Irnich, 1980]. The latter received comments in Testerman [2005]. The stimulator output impedance directly affects the stimulus waveform, therefore the two considerations can be reduced to that of the temporal aspect of the charge delivery. Lapicque defined the chronaxie, and strength-duration curve, for rapidly rising stimuli, discussing at length the influence of the stimulus waveform in [Lapicque, 1926, 1943]. Regarding the electrodes characteristics, Geddes writes

> "If the cathodal electrode is distant from the excitable tissue, the rheobase will be higher. Therefore the current strength-duration curve will have the same shape, but it will lie above that obtained with an electrode that is closer to the excitable tissue."

According to his text, the chronaxie would then be the same, only the rheobase will differ. Testerman however, quoting [Grill et al., 2000; McIntyre et al., 2002; West and Wolstencroft, 1983], insists that the chronaxie changes with distance from the electrode. The three previously quoted papers look at single fibre activation, either experimentally [West and Wolstencroft, 1983] or from modelling studies. The changes seem to be rather due to the type of fibres activated. As was already recognised by scientists in the early 1900, the chronaxie is somehow inversely related to conduction velocity and fibre diameter [Davis and Forbes, 1936; West and Wolstencroft, 1983]. This point is covered by Geddes under the heading "tissue inhomogeneity":

> "When the chronaxie of nerve is measured, it is important to recognize that most nerve trunks contain bundles of fibers having different diameters and, hence, different propagation velocities, with each fiber group having its own chronaxie."

This last comment is important. When working with whole nerve recordings where different fibres groups can be elicited over a large range of amplitudes and pulse widths, giving distinct CAPs, different strength-duration curves may be plotted. This will be further discussed in section 5.6.

2.2.2 Recruitment

The strength-duration curve qualifies the excitability of a nerve with regards to threshold values but it lacks information about the force output generated with a given stimuli. If electrical stimulation is to have functional outcomes, the effect of the stimuli need to be quantified in terms of force produced. This is the role of the *recruitment* curve. In a typical recruitment curve the force [5] is plotted as a function of either the pulse width or stimulus amplitude. Such plots often contain several curves as the stimulus parameter which is not used for the x-axis is varied in discrete steps. Other x-axis or parameters are commonly used depending on what criteria may be altered by the researcher or user, figure 2.2 shows two examples of recruitment curves.

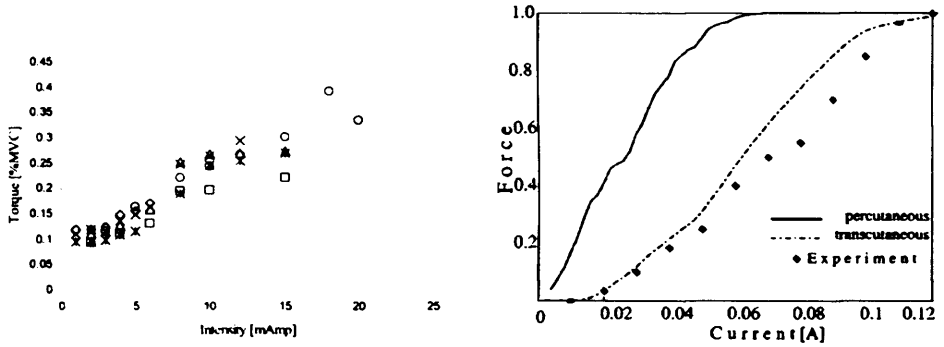

(a) Recruitment curve from Langzam et al. [2005]. (b) Recruitment curve from Livshitz et al. [2000].

Figure 2.2: Typical recruitment curves.

2.2.3 Monopolar, dipolar, tripolar stimulation

Usually, two electrodes are used, a *cathode* (most negative voltage), and an *anode* (most positive voltage) to form a circuit. When the pulse is biphasic, as is often the case for electrical stimulation, the cathode is by definition the electrode that has the most negative voltage during the "active" pulse, and the most positive voltage during the "balancing" pulse [6]. The anode is, by opposition, the most positive during the active phase and negative during the balancing phase. Cathodes and anodes are sometimes referred to as respectively *lag* and *lead* electrodes, especially in electrochemical reviews, see for example the series of papers: Brummer and McHardy [1977]; Brummer and Turner [1977a,c].

In many cases, one of the electrodes (usually the anode) is distant from the stimulation site, and common to all the cathodes. This is called *monopolar* stimulation with common anode. With *dipolar* stimulation, the two electrodes are physically present in the stimulation area. They form a pair, close together. Obviously, more electrodes can be introduced in the circuit. A typical setting is the *tripolar* situation when two

[5] The force in a typical recruitment curve may be expressed either directly (N or N.m), relatively as a percentage of maximum voluntary contraction or indirectly as with muscle activity (EMG).

[6] The meaning of the words active and balancing pulse will become clear in chapter 7.

anodes are used for a single cathode, though not distant [Peckham, 1999]. Compound action potentials [7] can also be generated by ways of magnetic stimulation. The activation mechanism is similar to the one described above, but the means of applying the stimulus are different [Hsu and Durand, 2000; Roth, 1994].

2.2.4 Activating function

As mentioned in section 2.1, the firing of an action potential depends on how and where the axon's transmembrane potential varies. At nerve level, the stimulus effect is related to the second derivative of the external voltage along the nerve axis, $\frac{\partial^2 V}{\partial z^2}$, the *activating function* [Rattay, 1986; Roth, 1994], see fig. 2.3. A positive value of the activating function indicates a depolarised membrane, where the likelihood of an action potential arising is increased [8]. A negative peak indicates a zone where CAPs are less likely to be triggered. When more than one electrode are involved, the inter-electrodes distance affects the depolarisation area. See figure 2.3(c) for example, bringing the two anodes closer together would cause the different peaks to influence each other [Rijkhoff et al., 1994a].

2.2.5 *Cathode-make* and *anode-break* stimulation

Four types of artificial activations are possible as summarised in table 2.1.

2.2.5.1 Direct activation

The name direct activation expresses the fact that the activation originates near the electrode. At the cathode, the current flows out of the axon, depolarising the membrane in the vicinity of the active electrode. This is seen as a positive peak in the activating function, as in fig. 2.3(a), where the stimulus threshold is lower [9]. Action potentials may thus be triggered by a small cathodic stimulus, this is called *cathode-make* stimulation, it is believed to be the most commonly used electrical stimulation method.
Hyperpolarisation (negative value of the activating function) may also result in an action potential, though at higher threshold (4 times higher in [McNeal and Apkarian, 1978; McNeal and Bowmann, 1985; Mortimer, 1990; Rattay, 1998]). This activation process is called *anode-break* stimulation because it is triggered at the anode by a rapidly falling edge of the stimulation pulse, leading to an instantaneous chemical imbalance inside the axon (for more details see [Grill and Mortimer, 1995a; Mortimer, 1990]). It can be avoided by using exponentially decaying pulses. Since the chemical equilibrium depends on the passive electrical properties of the connective tissue sheath [Keynes and Aidley, 2001], anode-break activation is more likely in peripheral nerves than in spinal roots [Brindley and Craggs, 1980]. It can be distinguished from

[7] Compound Action Potentials (CAP) are whole nerve signals. They are the sum of all single action potential fired at a given instant by the fibres active in the nerve (see chapter 1). Electrical stimulation (and recording) work most often with CAPs rather than single APs.

[8] The activation function would only be a true indicator for an ideal axon, for whole nerve it is a predictor, useful but not always accurate.

[9] The activating function introduced in the previous section indicates a disposition to fire an action potential, i.e. a lowered threshold.

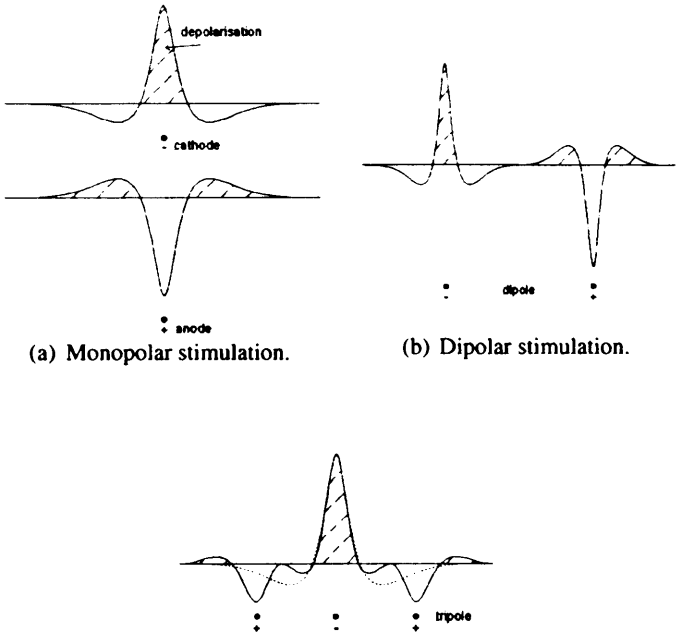

(a) Monopolar stimulation.

(b) Dipolar stimulation.

(c) Tripolar stimulation, the dotted line shows the equivalent monopolar cathodal activating function.

Figure 2.3: Activating function for most common stimulation.

cathode-make activation both because of the higher threshold required and the longer latency, mostly noticeable for long stimulus pulses.

Table 2.1: Artificial stimulation modes.

	direct	virtual
depolarisation	**cathode-make activation**: onset of CAP physically near the cathode, usually lowest threshold	**virtual cathode**: higher threshold (depends on the geometry of the electrodes) and onset of activation at some distance from the real electrodes
hyperpolarisation	**anode-break activation**: 4 times cathode-make stimulation threshold, longer latency and onset in the vicinity of the anode	**virtual anode**: as above, the virtual activation threshold depends on the electrodes position

2.2.5.2 Virtual electrodes

Activating functions often present more peaks than there are real electrodes. Any positive peak not physically related to a cathode is associated with a *virtual cathode*, similarly for negative peaks and *virtual anodes*. These electrodes are not real but the result of steep current gradient in these areas, causing extra peaks in the activating function. For example: when a cathode is placed inside an insulating cuff, current from a distant, external, anode will concentrate towards the cuff's ends, creating two virtual electrode zones. This concentration effect may occur with any un-balanced configuration. The influence of a virtual electrode on the nerve and its activation depends on the stimulation setup. The threshold for activation with a virtual electrode is often much higher than for direct activation but not always as discussed in chapter 5.
Activation can occur not only in the direct neighbourhood of an active electrode, but also away from it, in a *virtual* stimulation zone.

2.2.6 Fibre diameter, conduction velocity, stimulation and blocking

A fibre's conduction velocity (the speed of a propagating action potential) depends on the physical properties of the fibre (membrane resistivity, diameter,...) as mentioned in section 1.3.2. Keeping with the electrical analogy, a larger fibre has a lower inner resistance, hence a higher conduction velocity. Diameter and myelination also affect the excitability of a fibre. Faster (i.e. larger and\or myelinated) fibres have lower activation thresholds. As mentioned in section 2.1, higher intensity stimulus may slow or block the propagation of an action potential. As is the case with activation, larger

fibres also have lower blocking thresholds. These considerations are common knowledge that were already established experimentally in the 1950s [Kuffler and Williams, 1953] and have since been demonstrated analytically, with models as those referred to in the following section. Different physiological mechanisms have been thought of to explain action potential block. Amongst these, the most common are (for references see the papers cited above as well as the review by Bowman and McNeal [1986]): depletion of neurotransmitter at the neuromuscular junction, alteration of ion channels gates and pumps or alteration of ions mobility. The last two have for common consequence abnormal ions gradients. As more ions have to be shifted, and as it takes longer to displace them, the propagating action potential is either slowed down or completely stopped.

2.2.7 Analytical models

To extend their understanding of the phenomena underlying the firing of an action potential (threshold, quiescent period, all or nothing character, etc), researchers developed predictive analytical models. These were often limited to one animal, even one nerve, within a narrow temperature range. The best known early models are those of:

- Hodgkin-Huxley: squid giant axon (unmyelinated), intra-cellular current injection [Hodgkin, 1971];
- Frankenhaeuser-Huxley: frog sciatic nerve [Frankenhaeuser and Huxley, 1964].

Advances in this field owe much to these pioneers, and while their work has been many times re-appraised and improved [Allingham et al., 2004; Coburn, 1988; Frijns et al., 1994; Grill et al., 2000; Guckenheimer and Oliva, 2002; McNeal, 1976; Moffitt et al., 2004; Rattay, 1986; Rattay et al., 2000; Schwarz, 1995; Shen et al., 2001; Sweeney et al., 1987], the original equations still lie at the heart of most modern stimulation softwares. Despite their limitations, models offer insights into the mechanisms of action potential generation. They are often used to estimate relationships between activation or blocking thresholds and specific nerve fibre or stimulation setup parameters like fibre diameter, fibre-electrode distance, inter-electrode distance, influence of insulation layer, etc.

2.2.8 Selective activation

For various reasons, researchers have long tried to activate only some fibres of the nerve or muscle stimulated [Fang and Mortimer, 1991b; Grill and Mortimer, 1995b]. Most methods rely either on a specific electrode geometry or on the variation of activation and blocking thresholds with fibres diameter. The most common techniques are listed below with references for further information.

- AC blocking: Andrews and Kooi [1996]; Shaker et al. [1998]; Solomonow [1981]; Solomonow et al. [1978, 1984]; Williamson and Andrews [2005].

- DC blocking (aka anodal blocking): Brindley and Craggs [1980]; Petrofsky and Phillips [1981]; Rijkhoff and Sinkjaer [1998]; Solomonow et al. [1984]; Van Den Honert and Mortimer [1979].
- Collision block: Brindley [1978]; Van Den Honert and Mortimer [1981a,b].
- Pulse shape, it is based on hyperpolarisation, like the DC block [10]: Fang and Mortimer [1991b]; Grill and Mortimer [1995a]; Seif et al. [2002]; Shen et al. [2001]; Stieglitz et al. [1997]; Uranga and Rijkhoff [2001]; van Bolhuis et al. [2001]; Vuckovic and Rijkhoff [2001].
- Pre or post pulse: Grill and Mortimer [1997]; Sassen and Zimmermann [1973]; Zimmermann [1968].
- Special electrode design (essentially a very small contact area): Fang and Mortimer [1991a]; Tai and Jiang [1994]
- Multicontact surrounding electrodes: McNeal and Bowmann [1985]; Petrofsky [1979]; Rozman and Trlep [1992]; Veraart et al. [1999, 1993].
- Multicontact penetrative electrodes: Smit et al. [1999]; Veltink et al. [1988, 1989a].

2.2.9 Safety considerations

Electrical stimulation may cause damage in different ways [Grill and Mortimer, 1995b; McCreery et al., 1990]. For the stimulation of nerves or nerve roots in cuffs or books, the following must be considered.

- Placement of the electrode mount: this delicate operation requires direct handling of the nerve and may damage it by overstretching or squeezing. Implantation consideration influence electrodes and mount designs, see section 6.1.1.
- Mechanical considerations such as nerve compression, stretching due to tension of the wires, or friction due to the relative movement between the nerve and electrode mount, see chapter 6.
- Adverse physiological reactions due to the artificial nature of the recruitment sequence and the induced hyperactivity of a large number of axons at once [Agnew and McCreery, 1990; Agnew et al., 1990a; McCreery et al., 1992].
- Biocompatibility considerations limit the choice of implantable materials, see section 2.3.2.
- Thermal damage, loosely proportional to the energy of the stimulus pulse width, essentially seen for very short pulses of large amplitude [Lilly, 1961].

[10] Using special pulse shapes may induce anodal blocking with a lower charge per phase, hence making it safer than common square pulses.

- Charge imbalance: Lilly and coworkers [Lilly, 1961] established the need for balanced stimulation pulses to avoid adverse effects such as metal dissolution and other irreversible electrochemical reactions [Donaldson and Donaldson, 1986b,c]. Excessive charge transfer, or too long pulse widths, may lead to similar damage [Mortimer and Kaufman, 1980], see section 7.1.

Long term tests are needed to ascertain biocompatibility. The limit on charge transfer and the risks of physiological reactions mean that successful selective stimulation and blocking methods may not be applied to human implants. More longer term research is needed at this stage for the chronic use of selective activation methods. The relative fragility of peripheral nerves, even more of nerve roots, and the risks associated with handling, post-operative swelling, chronic irritation, and other mechanical considerations often limits the use of alternative electrode designs to animal experiments, or eventually acute, operating room, human applications. These safety considerations partly explain why, despite much research and development, few applications are commercialised for chronic implantation.

2.3 Electrical Stimulation System

While the previous sections reviewed the principles and key concepts of electrical stimulation, this one surveys the practical implementation of electrical stimulation devices. Any system conceived for artificial stimulation of nerves or muscles contains three logically separate entities: a stimulator, a controller and a set of electrodes, detailed in sections 2.3.3, 2.3.4 and 2.3.5 respectively. The stimulator and the controller may each physically consist of "several boxes", together fulfilling one logical function. The stimulator produces the electrical stimuli. The controller is the human interface, allowing the user to set the stimulation parameters (frequency, amplitude, timing, etc) and to control the stimulator (on/off, program selection, etc). It can also provide some feedback using an LCD display, a buzzer, etc. In systems where little external intervention is required the controller may be integrated with the stimulator (e.g. pacemakers). When both are separate, communication between the controller and the stimulator may be wired or via a radio frequency (RF) link as is the case with most implanted devices. Finally, the electrodes, most often wired to the stimulator, deliver the stimulus to the body.

There exists nowadays numerous applications of electrical stimulation, some of which will be discussed in chapter 3. Almost every application has its own dedicated stimulator, but the principles are common to all and will be discussed in section 2.3.3. Similarly, there are many electrodes, although they are all based on a limited choice of electrode designs, as presented in section 2.3.5. For a review of electrical stimulation devices, see Bhadra et al. [2001]; Grill et al. [2001a]; Jezernik et al. [2002]; Rushton [1997]. The following sections do not intend to form some sort of implanted device design manual. They merely highlight the "multi-disciplinarity" of the key concepts

developed in the domain. The stimulator, the controller and the electrodes are each presented briefly, as a global view of a complete electrical stimulation system is important to understand the challenges faced in many of the key areas of development.

2.3.1 External system, fully implantable or halfway?

The electrical stimulation system can be purely external, using electrodes stuck on the surface of the skin (hence its common name of *surface stimulation*). Part of the system may also be implanted. If the electrodes only are implanted, and the cables are routed under the skin to connectors maintained at the surface of the skin, the system is called a *percutaneous system*. In that case all the electronic components (stimulator, battery, controller) remain outside the body. Finally, the stimulator may be implanted together with the electrodes, then no cable needs to "penetrate" the skin, although there will often be some external (outside the body) controller. Communication between the external controller and the implanted stimulator requires a wireless link. The battery may be implanted (active implant) or remain with the external components (passive implant). The former may use any type of airborne transmission while for passive implants energy must be transferred together with the logic signals, and the preferred method is via a pair of tuned coils forming a *radio frequency (RF) link*. The dedicated circuits dealing with transmission and reception of signals and power are called *transmitter* (Tx) and *receiver* (Rx). They are associated with the controller and stimulator respectively and may be integrated with them or form separate units depending mainly on practical considerations.

The choice between surface, percutaneous or implanted electrodes is the result of a compromise influenced by various factors, the most technical of which are listed in table 2.2. Other factors like costs (device, surgery and direct hospital costs, support, technological or not, recurrent costs like medication, physiotherapy), user preferences, perceived user benefits, availability of components (rate of obsolescence) also play a role in the decision process [Creasey and Dahlberg, 2001; Dryden et al., 2005; Kilgore et al., 2001; Priebe et al., 2007]. Yet, as these factors vary from one country, or even hospital, to another or are more subjective, they have not been included in the table.

2.3.2 Implantable materials

It is important to study the bio-compatibility of any material to be implanted [Schuettler, 2002]. The two main concerns are: surface compatibility, i.e. physical, chemical and morphological compatibility; and, for any given shape, structural compatibility, i.e. good external design as well as inner-structure adaptation. The biocompatibility of at least two different kinds of material must be considered. On the one hand, a metallic conductor to form the lead and the electrode itself where it will come in direct contact with the nervous tissue, and on the other hand, an insulator for the electrode mount, the cable, and often to coat the stimulator. The electronic components of the stimulators should not come in contact with the surrounding tissues, their biocompat-

Table 2.2: Some factors influencing the choice of a surface, percutaneous or implanted system.

	Surface	Percutaneous	Implanted	
			Epimysial	Nerve or root
Surgery	none	medium	intensive	intensive[a]
Selectivity	poor [b]	good	good	good to medium [c]
Donning and doffing time	long	medium	short	short
Skin problems	medium [d]	high to medium [e]	none	none
Infection (excl. skin)	none	high [f]	medium	medium to low [g]
Repeatability (in session)	medium	medium to poor [h]	medium to good	good
Repeatability (day after day)	poor	good [i j]	good [j]	good [j]
Cosmetic appearance	poor	poor	medium to good[k]	good
Freedom of movements	low [l]	low [l]	medium to high [m]	medium to high [m]
Failure repair, replacement	easy	medium	difficult	medium to difficult [n]

[a] Compromise between selectivity and surgery. Dissecting nerve branches to single muscles improves the selectivity but complicates the operation.

[b] Difficult to activate deep muscles without contracting shallower ones.

[c] Dependent on the nerve and its ramifications.

[d] Risks of burns, may be lowered with patient education, good stimulator design and tuned usage protocol.

[e] Mainly at the exit point of the cable, although burns due to unconnected cable have been reported [Marsolais and Kobetic, 1988]. Can be reduced with patient education, good stimulator design and tuned usage protocol.

[f] Along the cable more often than at the electrode site.

[g] Dependant on the extend of surgery, concentrating all the cables in the cauda equina reduces the risks of infection.

[h] Improved electrode design is less prone to displacement during movement.

[i] Based on results with improved electrodes.

[j] Connective tissue growth alters the performance in the long term.

[k] Many scars if multi-channel system.

[l] Loose cables in the way.

[m] Necessity to maintain an RF link with external controller for passive implants.

[n] Concentrating all cable in the cauda equina means the cables are easier to access and repair but electrode replacements are too risky.

ibility is therefore less studied [11]. The choice of a biocompatible conductive material depends amongst other on its flexibility, workability, on the current density [12] or maximal charge before irreversible transformation occurs (the conductor must not dissolve in the adjacent tissue) [Ziaie et al., 1996]. The important characteristics are a high corrosion resistance, good resistance to fatigue (for the lead mainly) and a low electric resistance. Typical materials used are platinum and more often platinum-iridium (more charges per unit area [Lee et al., 2001]). As far as the insulator is concerned, its electric resistance must be much higher. Mechanically, it must be resistant (long-lasting), flexible and smooth to limit the damages to surrounding biological tissues. Good adherence to the chosen substrate, with low water absorption, are also a concern if the implant has long term applications [13] [Donaldson, 1982, 1991, 1994, 1996]. The most common insulator and coating materials nowadays are silicone polymers or PDMS (poly-dimethylsiloxane).

2.3.3 Stimulator

2.3.3.1 Logical concept

The stimulator is not concerned with the generation of trains of stimuli nor with patient specific data. It receives from the controller streams of logical information that it decodes systematically into stimulation pulse parameters. The stimulator delivers the charge, via pulses of a defined shape [14]. The output is either current-controlled or voltage-controlled (for transparency, the word "pulse amplitude" is often used to refer to either current or voltage). A typical stimulator contains a logic bloc, decoding the controller signals, and a charge delivery bloc, or output stage. As the latter will be under much scrutiny in Parts II and III of this thesis, a few key issues for the design of a charge delivery circuits are highlighted hereafter.

2.3.3.2 Practical application: the output stage

One of the main concerns when designing an output stage is: will there be enough charge available to deliver the requested pulse (width x amplitude)?

If the output current is controlled, the electronic circuit must be able to deliver the given current to the load within the limits of the voltage rail. Similarly, for voltage controlled output, the current capacity must be large enough for any conceivable load, see section 9.2. Biological systems present the added difficulty that the load is unknown and will vary over time, with tissue growth. It is therefore difficult to predict an "expected load"

[11] Current concerns with the use of lead (Pb) in electronic assemblies (RNoH) have raised the attention on this issue, especially with regards to ions and compounds migrating through the insulator.

[12] Edge effects on planar electrodes have lead to the development of alternative electrode structures [Ziaie et al., 1996].

[13] The issue here is not complete hermeticity but the absence of water in direct contact with metal as it may corrode or tracks may become shorted. A relatively low water absorption is advised as it will limit the swelling that could otherwise jeopardise the structural integrity of the assembly. Internal stresses and poor adherence may lead to the appearance of gaps where water vapour may condense. The same goes for voids, air bubbles and impurities left in the coating material. These increase the risks of adhesion loss, corrosion and short-circuits.

[14] Various pulse shapes have been developed to influence different factors, see for example section 2.2.8.

(see section 7.4) and this further complicates the design task, as explained in chapter 10.

The load will often be capacitive, intrinsically or due to an extra capacitor added to prevent direct current flow and help balancing the charges. The stimulator must care for the discharge phase, either actively, by producing a pulse of alternated sign, or passively, by providing a low impedance discharge path across the load, see sections 7.1.3 and 8.2.5.

Safety issues such as current leakages, high voltages fault conditions, over-heating (i.e. poor heat dissipation) [15] must also be investigated throughout the design stages.

Practically, the main issues are reliability, ease of fault assessment and repair, and physical size, especially for implantable devices.

2.3.4 Controller

2.3.4.1 Logical concept

The controller is the human interface to the stimulator. It receives and interprets users inputs to create the logical information required by the stimulator to produce the desired trains of stimuli (amplitude, pulse width, interpulse delay, frequency, etc). To do so, a limited set of patient-parameters can be memorised and recalled to adjust the stimuli to the user's need. In the simplest cases when no user interaction is required (typically with pacemakers), the controller is integrated with the stimulator. In most other systems, user commands will range from the basic on-off, to the selection of a specific program performing a set of actions, occasionally requiring proprioceptive feedback (from motion sensors, pressure sensors, etc) or neuro-feedback from recording electrodes [Loeb et al., 2001]. The term *closed-loop system* was introduced to identify a system that does not require active patient contribution. Once started, the system is supposed to "know the state it is in" and take the appropriate actions with little user involvement.

2.3.4.2 Practical implementation

The controller must be portable, therefore lightweight, small, robust to the environment (water, dust, heat), mechanically resistant (withstand low height falls, scratches,..). It interacts with the user via buttons, buzzers, LCD display, analog inputs and sensors, and pc connections for more complex operations. The interface must be user-friendly, so despite being small, the buttons and display, if present, must be of realistic size, the various actions must be easy to select and activate. The connection of cables, when required, must be simple, clear and unique, ideally standardised (to avoid the risks of plugging for example the battery charger in the pc input socket). The feedback to the user must be clear, unequivocal and happen in (near) real-time. Loading the patients parameters should be straight forward, either by using the display and buttons available, or via a dedicated pc program, depending on the system's complexity. The pc program, if provided, also has to show user-friendliness, and include special safety

[15] The local tissue temperature should not rise by more than 2°C [BS EN 45502-1, 1998]

steps to avoid the parameters from one patient being loaded in another patient's controller as inadequate stimulation levels may have dramatic consequences.

2.3.5 Electrodes

2.3.5.1 Charge transfer

Electrodes are needed both to stimulate living tissues and to record electrical activity within those tissues. A complete description of the electrochemistry of the electrode-electrolyte interface falls beyond the scope of this introduction [16], it will be discussed in section 7.1, on page 162. Electrodes are required to transduce the electron current (in the conductor) into ionic current (in the tissues), without disturbing the local pH [17]. Therefore, only a limited amount of charge per surface area can be delivered before harmful reactions occur [Craggs et al., 1986; Donaldson and Donaldson, 1986a]. One method to increase the maximum charge deliverable by an electrode of a given size is to "roughen" it, i.e. to increase its physical surface without altering the geometrical dimensions. Very rough platinum [18] has been investigated for use in electrodes design [Schuettler et al., 2001].

2.3.5.2 Electrode leads

The leads must provide a reliable, long-term and low impedance subcutaneous connection between the electrode and the stimulator, see fig. 2.4 for a few examples. The wires must be insulated and flexible enough to traverse the joints and resist multiple flexions. They can be grouped together in an insulating tubing to form a single lead of small diameter. A typical type of lead is the Cooper cable [19] (extreme left on fig. 2.4): three to five platinum-iridium insulated wires wound in a helical configuration, silastic tubing and Medical Adhesive are then used for insulation [Donaldson, 1983]. Cooper cables are usually terminated by a dedicated connector known as the Craggs connector [Donaldson, 1985] [20]. Another commercially available lead is the Cooner wire [21], made of multiple strands stainless steel coated in silicone rubber.

2.3.5.3 Electrode examples

The choice of electrode strongly depends on the application considered, hence the electrode's position inside the body. Although electrodes are usually purpose-built, there are only four main types of implantable electrode designs. They are briefly presented in the following sections. Muscle [22] and spinal cord stimulation are not the focus of this thesis but the electrodes are included for completeness.

[16] The purpose of this chapter is to introduce the concepts exploited in the other parts of this thesis to support the reader and place the work in context.

[17] Risks of electrolysis, formation of gas (oxygen and hydrogen) by the cathode and anode respectively [Donaldson and Donaldson, 1986a,b,c].

[18] Known as platinum black as its surface does not reflect much light, making it appear black.

[19] Commercially available from FineTech Medical Ltd.

[20] For reliability reasons, it is not advised to put more than 5 wires in one cable (in case of cable failure).

[21] Available from CoonerWire [Cooner Wire, online, last accessed in September 2007].

[22] Electrical stimulation of denervated muscle is possible but requires very high charge levels, muscle stimulation usually refers to the activation of nervous structures within the muscle bulk [Crago et al., 1974].

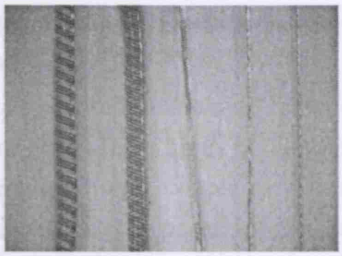

Figure 2.4: Subcutaneous electrode leads, from left to right: 3-wire Cooper cable with white core, 4-wire Cooper cable with transparent core, home-made copper cable (11 strands coated with medical grade silicone rubber) and 2 types of Cooner wires (AS634 and AS632). The diameter of the Cooper cable is 1.75mm while that of the AS632 is 0.3mm.

Muscles

Epimysial electrodes, see fig. 2.5, can be monopolar, or dipolar to reduce current spread. They are made of a central circular electrode, usually platinum, surrounded by a second ring of metal in the dipolar case. The electrodes are attached to an insulating structure of larger diameter which can be sutured to the muscle which is to be activated. Percutaneous and implanted *intramuscular electrodes* have also been developed. They are smaller, with dimensions close to the diameter of the cable, and are inserted in the muscle body, using small-gauge needles. The closer the electrode is to the motor end plate, the lower the activation threshold but the steeper the recruitment curve [Grandjean and Mortimer, 1986]. To improve the control of the contraction strength, the electrode can be moved further from the nerve ending. The threshold is then higher and the slope lower but high pulse amplitudes may activate other muscles. Hence, selectivity depends on appropriate placement.

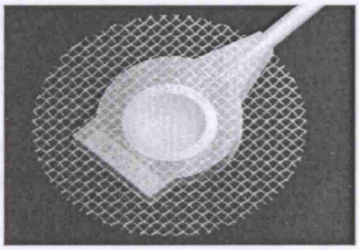

Figure 2.5: Computer representation of a monopolar epimysial electrode.

Spinal cord

During spinal cord stimulation (also known as dorsal column stimulation in the treatment of chronic pain) low voltage pulses are applied using percutaneous or surgically implanted leads. The percutaneous mounts with multiple electrodes are made by removing the insulation in various areas towards the end of the wire. They are placed with interlaminar needles. The permanent, implanted, electrodes have a flat flexible mount containing an array of small circular electrodes. They must be surgically introduced in the spine between two discs. After placement, both types of electrodes are tested to find the most effective combination of electrodes. The set giving the best

results is selected for stimulation and this can later be altered as the threshold changes [Holsheimer and Struijk, 1987].

Intraspinal microstimulation is another domain of spinal cord stimulation. Here, the aim is to selectively stimulate some nerve fibres in the spinal cord motor neuron pools or in the roots, targeting single muscles (whole root stimulation generally activates groups of muscles, see section 4.1). The penetrating electrodes used are often called *microwires* due to their smaller size [23].

Peripheral nerve

The three most common kinds of electrodes are: the cuff or helix electrode [Coggeshall et al., 1975; Fenik et al., 2001; Veraart et al., 1993], encircling the nerve; the penetrating electrode [Tyler and Durand, 1994] or endoneural wire multielectrode [Smit et al., 1999]; and the epineural electrodes [Gellman et al., 1990]. The latter were developed in the 1970s in Vienna [Thoma et al., 1988]. They are ring shaped, usually 1mm diameter and directly sutured onto the protective sheath of the peripheral nerve (epineurium). Each single circular electrode has its own helical wire connection to a main cable which contains up to four single wires, see fig. 2.6. Cuff-electrodes on the contrary require the epineurium to be dissected before placement of the electrode mount. The freed section is then wrapped in the so-called cuff. These are of a tubular shape, containing one, two, three or more electrodes, depending on the freed length available along the nerve and the application considered, see fig. 2.7(a) and 2.7(b). Cuff electrodes differ in the way they are closed. The cuff may be self-curling, making one or more turns around the nerve. Other types may require suture or glue. Another slightly different type of mount is the helical, or helix, electrode, see fig. 2.7(c) and 2.7(d). In any type of cuff, the electrodes can either be long enough to form a complete ring, or only touch sections of the nerve. The latter (multi-contact electrodes) is meant to improve the recruitment characteristics as different fibre fascicles may be selected separately [Veraart et al., 1993]. Finally, Durand *et al.* have developed a flattening cuff electrode which reshapes the nerve in an attempt to improve fascicle selectivity [Leventhal and Durand, 2004; Tyler and Durand, 2003].

Nerve roots

Nerve root stimulation can be achieved both with electrodes placed intrathecally or outside the dura, to avoid the laminectomy or when arachnoiditis [24] renders intradural placement difficult [Creasey, 1993]. While the latter requires a less complex surgical procedure, the intradural placement profits from the fact that the spine protects the electrode, and that the motor and sensory fibres can be easily segregated within the

[23] Mushawar, in Canada, has used intraspinal stimulation to elicit gait like motion in fully supported spinal cats [Mushawar and Horch, 2000] although these results have been criticised and she seems to have moved towards other techniques. McCreery and his group at the HMRI (Huntington Medical Research Institutes, Neural Engineering Program) have investigated the use of microwires for bladder management [McCreery et al., 2004].

[24] Arachnoiditis: inflammation of the arachnoid, one the membrane surrounding the spinal cord, see section 1.1.3.3

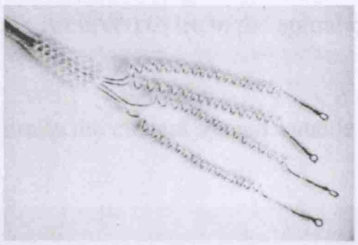

Figure 2.6: Four single epineural electrodes with individual helical wires and main cable.

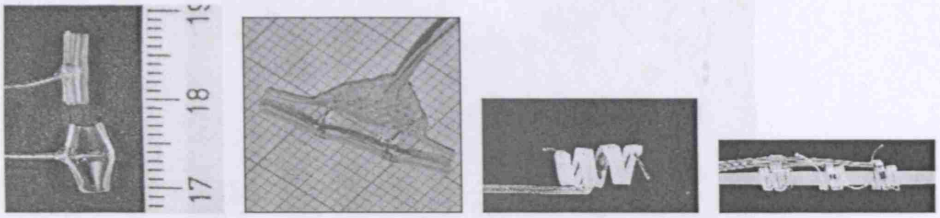

(a) Monopolar cuff electrode. (b) Dipolar cuff electrode. (c) Helical electrode. (d) Helical electrode.

Figure 2.7: Electrodes for peripheral nerve stimulation.

dura [Sauerwein et al., 1990]. The main interest of this type of stimulation is that all the sacral and lumbar roots can be accessed (in the cauda equina) during a single surgical operation. Although this operation is complex, the risks of infection are lower than for a peripheral stimulation system targeting more than a couple of muscles as, in the latter case, each stimulation site must be opened to access the nerve. The risks of cable failure are also lower with cauda equina implantation as they do not cross any joints [Grant, 1988]. Since the protective epineurium is not yet present, the activation threshold is lower than for peripheral nerve stimulation. The roots are also more fragile (see section 1.2) and demand a more delicate handling than a peripheral nerve. Further, the intrathecal space is rather limited, which increases the likelihood of damage. The high root density also presents a risk of unexpected activation of neighbouring roots as developed in chapters 4 and 5. These limitations have led to the development of the *electrode book*, see fig. 2.8. These are highly reliable, in a review of over 300 human implant-years, no electrode failures have been reported [Brindley and Rushton, 1990]. A single book counts one to four separate *slots*[25] and the surgeon may trap one or more rootlets in each depending on the implant (see section 9.1.1). Every slot contains one set of three electrodes symmetrically organised (usually connected as two external anodes and a central cathode). This design offers the three key advantages listed below.

- The slots naturally rest open as seen in fig. 2.8(a), minimising the risks of damage when inserting the rootlets.

[25] A slot is a division of an electrode book. It contains a set of three electrodes. The roots or rootlets are placed in slots as they are physical entities, see section 4.1.3.1.

- The bottom of the book is curved to lie in the spinal canal without damaging the dura, see fig. 2.8(b).
- Tripolar stimulation limits the current spread outside the slot, see chapter 5.

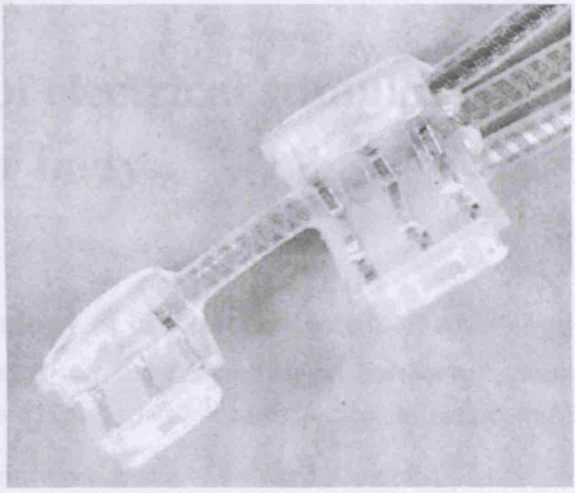

(a) SARSI electrode mount: a 3-slot book with the central slot wide open (top right) and a 1-slot book (bottom left).

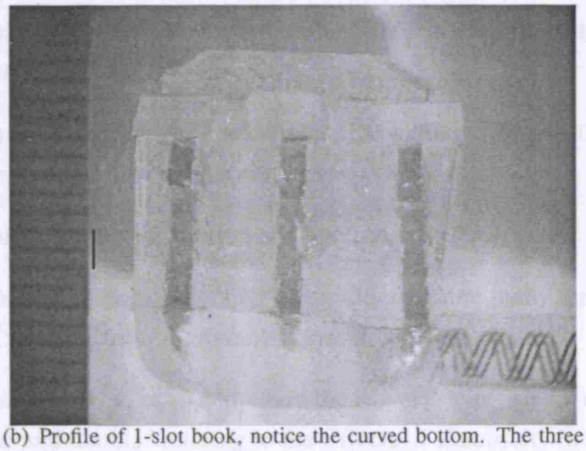

(b) Profile of 1-slot book, notice the curved bottom. The three electrodes are clearly visible; the scale bar is 1mm, each graduation on the ruler is 0.5mm.

Figure 2.8: Electrode book for spinal root stimulation.

Chapter 3

Review of electrical stimulation devices for the lower body

3.1 Chronology of electrical stimulation

Antiquity: Egypt, Greece and Roman Empire: bathing with electric eels or rays to treat various pain related diseases (*Scribonius Largus*, 46AD);

1646: First written occurrence of the word *electricity*;

1664: *Swammerdam:* dissected muscles occasionally twitch when touched by a silver wire, although he offers no explanation why;

1740s: Switzerland and Germany: first clinical use of electricity to treat paralysis and pain (*Jallabert, Kruger and Kratzenstein*);

1745: Leyden jar, 1st means of storing electricity (*Ewald Jurgen Georg von Kleist and Pieter van Musschenbroek*)

1746: *J.A. Nollet:* 1st demonstration of "electrotherapy";

1750s: New concept of electrotherapy: electricity can cure many (any?) illnesses (in the UK: *Patrick Brydon, Robert Whytt, John Wesley*);

1758: *Benjamin Franklin*, in an address to the Royal Society (UK), expresses his experience and doubts "relating to the Effects of Electricity in Paralytic Cases" (his words);

1769: *E. Bancroft:* states that fish bathing treats pain through electric shock;

1774: 1st attempt at electroshocks to resuscitate a drowned woman;

1780: *L. Galvani:* frog leg twitches when electro-stimulated;

1784: *Caldini* stimulates a frog's brain to cause leg twitches;

1793: Foundation of the *London Electrical Dispensary* "to administer electricity for all complaints in which its application may be useful";

1818: Mary Shelley's *Frankenstein*: epitome of miraculous electricity;

1838: *C. Matteucci:* observes cardiac electricity, and hypothesise the electric nature of nervous communication;

1843: *E. Dubois-Reymond:* action potential;

1870: *R. Caton:* study of dogs and apes "brain current";

1880: *Fritsch and Hitzig:* use of electrical stimulation for the study of the human cerebral cortex;

1893: *W. Einthoven:* 1st publication on ECG, based on prior work influenced by a demonstration by *Waller*;

1929: *H. Berger:* 1st publication on EEG;

1936: Hearing aids concept (*Gersuni and Volokhov*);

1948: Phrenic nerve implants concepts;

1952: 1st external percutaneous pacemaker for post-surgical shock;

1957: 1st cochlear implant by *Djourno and Eyries*;

1960: Implantable pacemakers (2 teams) by *W. Greatbatch* and Dr. *W.M. Chardack* and by *E. Bakken* and Dr. *C. Lillehei*;

1960s: Concept of Functional Electrical Stimulation (peroneal nerve, elbow, ankle);

1964: *Vudovnik and Reswick:* first practical tests of FES on a C5 patient;

1967: Drop-foot patent after *Liberson*'s "electronic personal stimulator";

1970: Cochlear implants;

1970: Peripheral nerve stimulation (surface and implanted) for standing and stepping, in Ljubljana, London, Rancho Los Amigo (California) and Vienna;

1977: Benefits of spinal cord stimulation for multiple sclerosis patients;

1978: Bladder controllers;

1990: Deep Brain Stimulation for Parkinson Disease (subthalamic nucleus stimulation);

1990s onward: Commercialisation: FreeHand stimulators, dropped-foot stimulators, pain treatment;

2000: Retinal stimulation.

The main sources for this review were: Beaudreau and Finger [2006]; Brazier [1961]; ECG library, online [last accessed in May 2006]; Finger [2006]; IEEE, online [last accessed in May 2006]; Kralj and Bajd [1989]; Kralj et al. [1980]; Kuhfeld [1995]; Lancet editorial [1990]; Maghribi et al. [2002]; Pacemaker Club, online [last accessed in 2007]; Rushton [1997]; Stanic [1998]; Vesper et al. [2002]. Most dates were cross checked between at least two of these references.

Besides its intrinsic interest in placing this work in its historical context, this list highlight a key factor in electrical stimulation, as in many other areas of science. The underlying concepts are simple and were thought of long before the first application was ever designed. Conceptual simplicity is key to both the development of medical devices and their acceptance by patients and the public in general. Once researchers have identified core phenomena and developed essential tools for their observation it still takes the life-long dedication of many researchers to turn a theoretical idea into a fully functional product. Following the success of the early applications, the rate of (and investments in) research and development picks up and more exploitation of the same principle are brought to the market. At this stage commercial interests may overshadow the more basic, more ethical, essence of scientific research: to improve people's quality of life in the largest possible sense of the term. It is essential to keep this in mind when assessing the long term potential and merits of any research project. Nowadays more than 250,000 new pacemakers are implanted each year in the United States only [Pacemaker Club, online, last accessed in 2007] and by 1990 more than 1000 phrenic nerve implants were in use [Lancet editorial, 1990]. Research and development of electrical stimulators cover a wide range of applications: phrenic stimulation, bladder and bowel management, upper limb stimulation (pinch, grasp), lower limb stimulation (standing, transfer, stepping), cardiac assistance, cochlear implants, vagus nerve stimulation, deep brain stimulation, treatment of pain (both for peripheral nerves and spinal cord stimulation).

3.2 Bladder and bowel controller

These devices have two related aims: to restore continence (action on the sphincters) and/or to provide voiding (action on the detrusor) [Rushton, 1997]. Often the detrusor reflex should be inhibited to restore continence and these two purposes are met by a single device. The most common implant of this type is the Sacral Anterior Root Stimulator Implant (SARSI). It was developed by G. Brindley and his group in London in the 1970s [Brindley, 1977; Perkins, 1986], and successfully implanted from 1978; nowadays, an estimated 2,500 are in use worldwide [Brindley, 1994; Jezernik et al., 2002]. The implant is known as the FineTech-Brindley stimulator, manufactured by FineTech-Medical Ltd. Other alternatives using electrical stimulation exist, as summarised in Johnston et al. [2005]; Peters et al. [2005]; van Balken et al. [2004] but they lack the success of SARSI. Many reviews of users expectations and satisfaction have been carried out [Brindley, 1994; Brindley and Rushton, 1990; Creasey, 1999; Creasey

et al., 2001; Kutzenberger et al., 2005; Vastenholt et al., 2003]. The main benefits of the implants, as summarised from these publications, are: continence, larger filling volume, decreased infection rate compared to previous methods used, decreased or interrupted use of medication, disappearance or reduction in frequency and severity of autonomic dysreflexia attacks, improved social life and improvement of overall quality of life [1]. Cost benefit studies have also shown the implant to score better than more traditional methods like drugs and catheters [Creasey and Dahlberg, 2001].

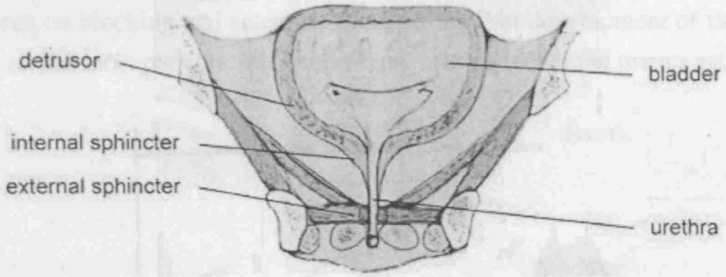

Figure 3.1: Simplified drawing of the bladder, showing the detrusor and the internal and external sphincters.

3.2.1 Principle

The sacral anterior roots carry the majority of the motor nerves leaving the spinal cord towards the detrusor muscle, rectum, colon and pelvic floor [2]. The posterior roots receive the majority of the sensory inputs from these organs and muscles. Electrode books (see section 2.3.5.3) are implanted in the cauda equina where all sacral roots are available in a single space [3]. Activation of the motor fibres innervating the detrusor muscle produces bladder contractions which can lead to micturition. However, it has proved difficult to increase intravesical pressure without causing reflex sphincter activation (detrusor-sphincter dyssynergia) hence obstructing the urethra. Poor timing between sphincter and bladder contraction may result in high intravesical pressure and noxious reflux that threatens the kidneys [Rijkhoff et al., 1994b]. In the case of the SARSI, this reflex sphincter activation is enhanced by the fact that the sacral nerve roots stimulated contain motor neurons innervating both the sphincters, and the detrusor. The latter being smaller, thus with a higher current threshold (see section 2.1), direct activation is likely to cause contractions of the sphincters before the bladder. Effective voiding is however possible because the striated sphincter muscle contracts and relaxes faster than the smooth detrusor muscle. By stimulating the roots intermittently, the peak in bladder pressure lasts longer than it takes to the sphincter to contract and

[1] This benefits list does not only represent the opinion of the medical workers, it also includes the results of patients surveys.

[2] Sacral anterior roots also innervate other muscles and organs such as the penis and some muscles of the lower limb.

[3] The electrodes are most often implanted intradurally although extradural electrodes (not books) are available [Sauerwein et al., 1990]

relax [Brindley et al., 1982; Chancellor and Chartier-Kastler, 2000; van Balken et al., 2004]. Micturition will then occur between the stimulation bursts, see fig. 3.2. Special stimulation techniques, like anodal-block [Brindley, 1978; Brindley and Craggs, 1980; Rijkhoff et al., 1994a,b], depolarising prepulse [Bhadra et al., 2005], special pulse shape [Bhadra et al., 2002], steering current have been proposed to improve selectivity and reverse the recruitment order. Magnetic stimulation too has been investigated [Bycroft et al., 2004]. Other methods to block the external urethral sphincter fibres exist (see for example Shaker et al. [1998], or refer to section 2.2.8 for a longer list of references on blocking and selective stimulation). Yet development of these methods is slow as, for most patients, the intermittent voiding technique proves satisfactory.

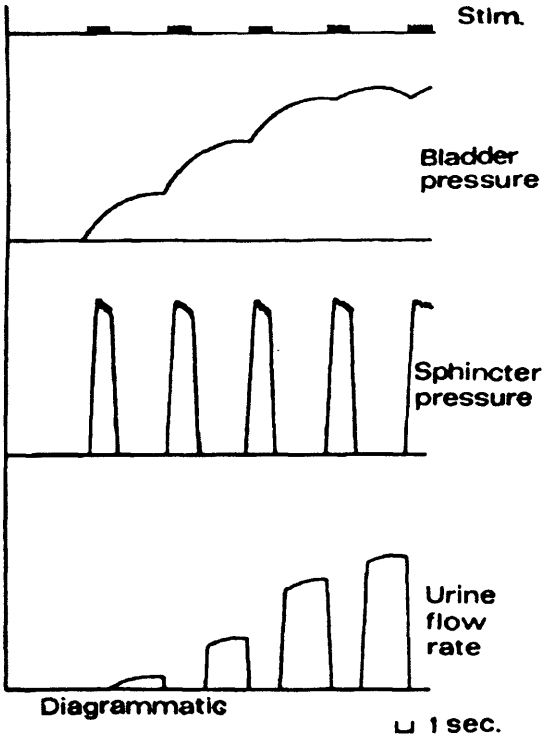

Figure 3.2: Sphincter relaxation and urine flow during intermittent sacral root stimulation, reproduced from Brindley et al. [1982].

3.2.2 Sacral root stimulation, detrusor hyperreflexia, detrusor-sphincter dyssynergia and rhizotomy

Detrusor hyperreflexia[4] is a common consequence of spinal cord injury. The hyperreflexia in itself may, although not always, cause incontinence. Often it occurs in combination with detrusor-sphincter dyssynergia and it may have more problematic consequences like vesicoureteric reflux which, if undetected and hence untreated, may lead to renal impairment. This condition may be treated with drugs or surgically by per-

[4]Hyperreflexia: overactive or overresponsive reflexes.

forming a sacral deafferentation [5], for S2 to S4, bilaterally. Sacral deafferentation, also known as sacral rhizotomy, requires a surgical intervention and may therefore be combined with other operations involving similar surgery. This is the case when a sacral root stimulator is implanted. The cauda equina is exposed, the motor fibres (anterior roots) separated from the sensory (posterior roots) and the latter can be cut. As the posterior roots carry nearly [6] all of the sensory fibres from the bladder, the rhizotomy reduces or eliminates reflex activity and hyperactivity, returning continence, improving compliance and preventing autonomic dysreflexia [7]. Detrusor-sphincter dyssynergia is not directly corrected (as posterior roots do not carry motor fibres) but as the bladder contractions are controlled by the implant, so is the dyssynergia. In other words, when rhizotomy is performed for a SARSI patient, detrusor-sphincter dyssynergia does only occur during stimulation and is dealt with using the intermittent voiding technique. As Brindley already reported in his review of the first 500 SARSI patients [Brindley, 1994], sacral deafferentation (or accidental damages to the posterior roots) helps decrease dyssynergia and improves voiding performance with intermittent anterior root stimulation.

3.2.3 Neuromodulation

Rhizotomy is seen by patients as a traumatic intervention due to its irreversibility. An alternative to limit reflex activity without cutting the posterior roots is *neuromodulation* [Craggs and McFarlane, 1999; van Kerrebroeck et al., 2005].

Mild stimulation of sacral afferent roots suppresses bladder activity [Previnaire et al., 1996]. Since the afferent fibres targeted for neuromodulation have a larger diameter than the motor fibres to the detrusor, neuromodulation can be achieved by low level stimulation of unseparated (i.e. anterior and posterior together) nerve roots. Working with the whole nerve root is safer as the stimulation can be achieved extra-durally, with only minimal root handling during electrode placement. It also has the added advantage that it recruits the afferent fibres present in the anterior roots [Coggeshall et al., 1975; Yuen et al., 1984]. Neuromodulation efficiently blocks unwanted bladder activity due to detrusor hyperreflexia. It can be triggered with the increase in bladder pressure (possibly detected by sacral roots recording) so that this conditional stimulation only occur when needed. An implant offering conditional sacral root neuromodulation could potentially increase bladder capacity and improve continence without rhizotomy. Detrusor-sphincter dyssynergia may however limit the voiding performances as neuromodulation of the sensory fibres will not happen during activation of the bladder

[5] Sacral deafferentation: to eliminate the afferent, i.e. sensory, contribution which triggers the motor reflex, the posterior sacral roots are cut.

[6] See discussion on the Bell-Magendie law, page 11.

[7] Autonomic dysreflexia: an autonomic reflex causing a sudden, severe, increase in blood pressure in response to pain stimuli or discomfort, usually originating below the level of paralysis. Commonly caused by an over-full bladder or bowel it is experienced by the patient as profuse sweating, flushing and a blinding headache. It may be a medical emergency in its most severe form and may cause death if untreated [Spinal Injuries Association, online, last accessed in April 2007].

autonomic fibres [Kirkham et al., 2002]. The intermittent voiding method would thus be used with such an implant as it is with traditional SARSI.

3.3 Lower limb controller

In 1963, Kantrowitz reported a paraplegic patient (T3) standing in a laboratory environment using surface stimulation of the quadriceps femoris and gluteus maximus (main knee and hip extensors) [Bijak et al., 2001]. As the technologies evolved diverse applications of electrical stimulation for paraplegic patients developed. Twenty years after this early success, peripheral nerve stimulators (fully or partially implanted or external) had been provided to patients in at least four centres: Ljubljana, London, Rancho Los Amigo and Vienna [Donaldson, 1986; Holle et al., 1984; Kralj et al., 1980; Marsolais and Kobetic, 1986].

Nowadays, applications of lower limb stimulation can be functional, or purely therapeutic when there is no intention of restoring useful movements. Simple muscle training aims to prevent or reverse strength loss, atrophy of the leg muscles, osteoporosis and to improve cardio-vascular fitness [Belanger et al., 2000; Bhadra and Peckham, 1997; Cikalo et al., 2000]. Rehabilitation centres may also offer lower limb surface stimulation in combination with partial weight-supported walking or for other defined actions like standing with a frame or crutches or cycling on a recumbent tricycle. This has proved especially successful for patients with incomplete lesions who may recover some walking ability [Barbeau et al., 2002]. Once at home, the patients may continue using surface stimulation to cause muscle contractions and include this in their daily activities. While not really functional for weaker muscles, even this simple use of electrical stimulation has been reported to improve the user's quality of life by reducing spasticity, improving digestion and decreasing pain [Benko et al., 2002]. Despite these benefits, few patients go on using surface stimulation after being discharged from the rehabilitation clinic. This drop out is unanimously blamed mainly on the long time necessary to adequately position the surface electrodes (donning) and to take them off (doffing) [Bajd et al., 1999b; Kralj et al., 1988; Moynahan et al., 1996]. Besides, the loose wires hanging from the electrodes and the intrinsic lack of selectivity of surface stimulation often impair the performances, and contribute to a poor user's perception of the device, see section 2.3.1 (page 33). A solution to these drawbacks is the implantation of electrodes, as a basis for further discussion, table 2.2 (page 34) compares briefly the pros and cons of surface, percutaneous and implanted systems. For the lower limbs, the stimulation sites are distant from each other, and not always easy to access. Placement of a typical 16 channel walking device requires long and delicate surgical operations [Sharma et al., 1998]. Another option is the use of spinal root stimulation, as in SARSI. Such a device, called Lumbar Anterior Root Stimulator Implant, LARSI, was developed in the 1980s in the Implanted Devices Group of University College London, and has been implanted in three patients. It is presented in section 3.3.2 and 4.1. All these options have been studied for the last 40 years in various research centres as

summarised in table 3.1. Finally, one everyday life application of lower-limb electrical stimulation which has encountered a recognised success and is mentioned here for completeness is the dropped-foot stimulator. It is a small single (sometimes dual) channel device used by walking patients who cannot lift their toes clear of the ground. It stimulates the common peroneal nerve to elicit ankle dorsi-flexion and eversion during the swing phase. The few electrodes can be fixed on the skin every day, or implanted for ease of operation, repetitivity and aesthetic considerations [Haugland et al., 2000].

3.3.1 Review of research applications

Over the world, many biomedical engineering centres are involved with FES. Table 3.1 presents the major research groups working, or which have worked, on lower limb stimulation. The list places nerve root stimulators amongst other applications and is not exhaustive. Many spinal cord injury centres use electrical stimulation as a rehabilitation and prognostic tool [Bajd et al., 1999a] and have not been included. Likewise, other groups have focused on the development of control algorithms for existing stimulation (Milan, Glasgow, Hong Kong) and are also excluded [Ferrante et al., 2004; Hu et al., 2004; Hunt et al., 1997].

3.3.2 LARSI: lumbar anterior root stimulator implant

3.3.2.1 Concept

The LARSI is an implant designed to stimulate anterior nerve roots for leg muscles contraction. It was conceived at the Medical Research Council (see table 3.1) after the success of the SARSI, and is based on similar technologies. Excluding technical development of the implant, the LARSI project ran from 1992 to 2001. It was set up to investigate the use of spinal root stimulation for the restoration of leg function in paraplegics with a complete lesion; mainly to permit standing up from the wheelchair during everyday life activities. Some outcomes of the project are detailed in section 4.1.

3.3.2.2 Patients

After an initial phase of surface electrical stimulation to improve muscle bulk and test individual recruitment characteristics, twelve selected patients were trained to stand with surface electrodes [Rushton et al., 1998]. Yet it was not known during the training and evaluation phase how the spinal root stimulation would relate to these results. Three patients were implanted (TF in 1990, JH in 1994 and CB in 1996) with two different versions: Mark III device for TF and Mark V for JH and CB.

Patient JH trained for standing with her implant for several years, but the results were never quite satisfying, see fig. 3.3(b). Her poor posture was due to extensive hip flexion and lumbar lordosis [8], leading her to support a large amount of her weight through her hands, hence rapidly suffering from fatigue [Norton et al., 2000]. This problem is difficult to understand, let alone to solve, considering the complexity of the muscle responses to single root stimulation. Besides, there is probably unexpected co-activation

[8] Lordosis is an abnormal increase in the normal curvature of the lumbar spine.

Table 3.1: Major research groups involved (at present or in the past) with lower limb FES systems.

Group or company name	suggested publication	type of electrodes	application
Cleveland Veteran Medical Centre Case Western Reserve University	Marsolais and Kobetic [1983, 1987] Kobetic et al. [1994, 1999] Sharma et al. [1998] Mortimer and Peckham [1990] Davis et al. [2001] Bhadra et al. [2001]; Bhadra and Peckham [1997]	epimysial intramuscular	standing sitting walking static exercise
Faculty of Electrical Engineering University of Ljubljana and Institute for Rehabilitation of the Republic of Slovenia	Kralj and Grobelnik [1973] Kralj et al. [1980, 1987] Bajd et al. [1998] Matjacic et al. [2003]	surface [a]	standing stepping
Pritzker Institute of Medical Engineering Illinois Institute of Technology, USA using the Parastep system from Sigmedics Inc Dayton, OH, USA	Troyk and Donaldson [2001] Graupe [2002] Guest et al. [1997] Jaeger et al. [1990, 1989] Yarkony et al. [1990] Gruner et al. [1983]	transcutaneus plus AFO	standing stepping exercise
Shriners Hospitals for Children[b] Philadelphia, PA, USA	Johnston et al. [2005, 2004] Davis et al. [2000]	epineural, epimysial and cuff	standing stepping urological

[a] Improved by the use of wireless communication between some actuators and the controller and stimulator.

[b] Using stimulators from either Neopraxis Pty. Ltd Lane Cove, NSW, Australia; or NeuroControl Corporation, Valley View, Ohio, USA. The latter having gone out of business in the late 1990s.

Implanted Devices Group University College London formerly the Medical Research Council London, UK	Donaldson [1986] Donaldson and Yu [1996, 1998] Donaldson et al. [1999, 1997a, 2000, 1997b,c] Perkins et al. [2002a, 2001] Brindley [1977, 1990] Donaldson [1987]	nerve roots cuffs surface	cycling standing stepping urological visual
Aalborg University, Denmark	Sinkjaer et al. [2003] Popovic et al. [2003, 1993]	surface	stepping
Twente Universiteit	Veltink and Donaldson [1998] van der Aa et al. [2002]	surface nerve root	standing urological
SUAW [b]: Montpelier Faculty of Medicine Medical University Munster	 Guiraud et al. [2001, 2000] von Wild et al. [2001]	 epimysial and neural	 standing stepping
Vienna	Mayr et al. [2001]	neural and muscular	phrenic nerve pacing, standing, stepping
Japan	Hatakeyama et al. [2000]	percutaneous	standing

[b] SUAW: Stand Up and Walk was a European project involving partners in Belgium, Denmark, Finland, France, Germany, Italy, Spain and United Kingdom.

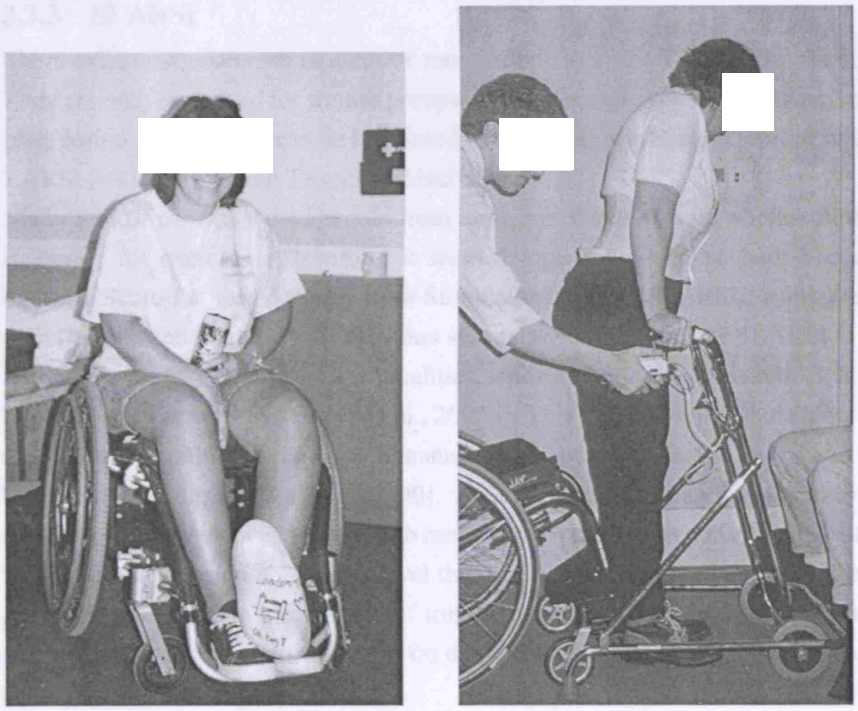

(a) JH after training, back in her wheelchair. (b) JH standing using her implant.

Figure 3.3: Patient JH.

of pairs of antagonist muscles that further reduces the selectivity. This can be explained partly by the occurrence of cross-talk stimulation between nerve roots in the spinal canal, see chapter 4.
Nevertheless, the stimulation responses proved suitable for FES-cycling using a recumbent tricycle. With a relatively simple apparatus, the patient can exercise daily which improves her general fitness [Donaldson et al., 1997c]. Figure 3.3(a) is a picture of JH, about 5 years after implantation (9 years after injury), thanks to the implant her legs have recovered muscle bulk and the blood flow has improved, they look healthier (stronger and pinker) than most paraplegics lower limbs. When well trained, she has been able to cycle over 1 km on several occasions [Perkins et al., 2002a].

3.3.3 SLARSI

There exist now two types of anterior roots stimulators: the SARSI, and the LARSI. They are both conceived for similar groups of patients, namely paraplegics with a complete lesion. The SARSI can be implanted in tetraplegics, while the level of injury for LARSI has to be between T3 and T12 inclusive[9].
Many SARSI patients would benefit from lumbar root stimulation, whether functional or purely for exercise. Therefore, it seemed logical to combine both implants in one: the Sacro-Lumbar Anterior Root Stimulator Implant (SLARSI), using the well-established technologies of the previous stimulators. The focus of SLARSI is to offer reliable bladder-emptying functionalities, while including the possibilities of lower limbs muscles activation [Perkins et al., 2002b]. This implant will stimulate the sacral roots S2 to S4 for bladder and bowel management, and stimulate the roots L3 to S1 for lower limb movements [Rushton, 1990]. As it is presented as an implant for bladder and bowel management and lower limb exercise, the patient group may include patients with a complete lesion at a higher level than LARSI patients who needed to be more independent and retain a minimum of trunk control as the implant was designed for standing and stepping. Further details on the stimulation system are given in chapter 9, starting page 206.

3.3.4 Benefits of FES of the lower body

To close this chapter, here is a brief list of the major benefits most regularly attributed to FES of the lower body.

- Increased blood flow in lower limb [Graupe, 2002]
- Improved cardiovascular fitness [Graupe, 2002; Nash et al., 1997].
- Improved resting arterial blood flow [Nash et al., 1997].
- Improved bone density [Triolo and Bogie, 1999].

[9]These limitations are not biological, they are rather based on consideration of patient independence. A tetraplegic would not be able to make much use of a device for lower limb stimulation, while all patients, no matter the level of their lesion, may benefit from continence, bladder control and improved bowel movements.

- Improved tissue oxygen level [Triolo and Bogie, 1999].
- Improved muscle bulk and self image [Graupe, 2002; Guest et al., 1997; Scremin et al., 1999; Triolo and Bogie, 1999].
- Improved resistance to pressure sores [Agarwal et al., 2003; Triolo and Bogie, 1999].
- Decreased spasticity [Stefanovska et al., 1989].
- Decreased cholesterol [Agarwal et al., 2003].
- Improved overall skin condition [Agarwal et al., 2003].
- Reduced spasm frequency [Agarwal et al., 2003].
- Mixed alteration in spasm intensity [Agarwal et al., 2003].
- Reduced urinary tract infection [Agarwal et al., 2003; Creasey, 1999].
- Reduced usage of medication and appliances [Creasey, 1999]

Part II

Scientific issues

Not only was it important to understand the LARSI situation, but our broader aim was to gain a more general understanding of the effect of virtual activation. As the virtual electrodes position will depend on the type of electrode, the geometry of the electrode mount used and the site of implantation, the focus is on the use of tripolar electrode books in the cauda equina.
This improved knowledge had to come from a better grasp of the theoretical concepts corroborated by pertinent experiment results. Therefore, the research developed in three directions:

1. *Analyses of the LARSI performances to highlight the strengths and needs for improvement;*
2. *A better understanding of virtual stimulation applied to the specific case of a tripolar electrode book;*
3. *The study of the electrode book itself, both from a mechanical and from an electrical points of view, i.e. nerve root compression, connective tissue growth, resistivity and geometrical imbalances hence current asymmetry.*

Chapter 4

Selectivity: the LARSI under scrutiny

4.1 LARSI

4.1.1 Concept (partly repeated from section 3.3.2)

The LARSI is an implant designed to stimulate anterior nerve roots to cause contractions of the leg muscles. It was conceived at the Medical Research Council Neuroprosthetics Unit (see table 3.1) after the success of the SARSI (section 3.2), and is based on similar technologies. Excluding technical development of the implant, the LARSI project ran from 1992 to 2001. The aim was to investigate the use of spinal root stimulation for the restoration of leg function in complete paraplegics; mainly to permit standing up from the wheelchair during everyday life activities.
The LARSI consists of the following units:

- a set of electrode books and cables;
- an internal receiver/stimulator, usually implanted above the hip;
- an external transmitter connected to the control box;
- a control box with patient-interface and producing all the required control signals; and
- a pack of rechargeable batteries including smoothing circuits.

To understand the problem of selectivity which is the focus of this chapter it is not necessary to present these individual parts in detail. Only the electrode book and its connections to the implant will be discussed in this chapter as they are directly relevant to the problem of *cross-talk*. Other parts such as the stimulator/receiver, the control box and the battery pack will be discussed in chapter 9 while in depth information on the LARSI design can be found in Donaldson [1990a].

4.1.2 Root selection, muscle innervation and lower limbs movements

As the LARSI is a nerve root stimulator, it was essential to find out which muscles are innervated by each sacral or lumbar root. The roots could then be chosen and stimulated in sequence to mimic natural gait movements. Unfortunately, the root innervation of lower limbs is not clearly established, see the different references summarised in table 4.1. The number of roots potentially innervating a specific muscle

reflects a strong inter-subject variability and, although this is not obvious from the table, left-right asymmetry in patients. A root may therefore contribute to a large range of movements as illustrated by table 4.2. From this last table it emerges that a single root may innervate antagonist muscles, for example L4 causing strong hip flexion, and possibly some hip extension. Regarding foot movements, each individual root from L4 to S2 may cause plantar and dorsiflexion, and inversion and eversion. In Dolenc et al. [1999], the torque obtained by stimulation of an L5 root was inverted from plantar flexion near threshold to dorsiflexion at higher stimulus amplitude.
It was with this vague information that the LARSI team had to decide which sacral and lumbar roots were most likely to contribute to the different phases of the standing and walking movements and select them for the implant. To minimise the likelihood of damages during the operation, the roots were to be trapped whole [1], although from experience with the SARSI, post-operative recovery is often seen within 6 to 12 months, therefore the risks of damages should not be over emphasized. The question was whether "the essential degrees of freedom would be attainable without splitting the roots" [Rushton, 1990]. Further, as the space in the cauda equina is limited, the number of books implanted, hence the number of roots selected, had to be kept low. The roots L2 to L5 plus S1 and S2 were suggested in Rushton [1990]. Six roots to be trapped, left and right separately. This gave a total of 12 channels.

4.1.3 Electrodes and mount

The root selection requires 12 channels as detailed in section 4.1.2. As the LARSI is based on SARSI technology, the electrode mounts used are similar to the SARSI electrode books (section 2.3.5.3). These are divided in slots, 2 to 4 slots depending on the type of book. Figure 4.1 shows for example a three-slot book.

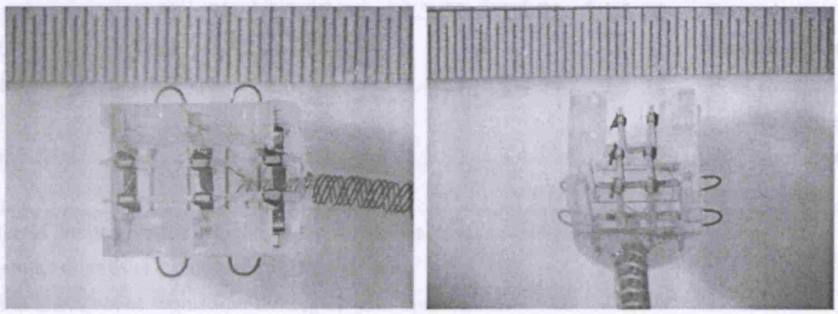

(a) LARSI 3-slots book, top view, with 4-wires Cooper cable on the right.

(b) LARSI 3-slots book, tilted, with three U-shaped electrodes per slot.

Figure 4.1: LARSI 3-slots book, graduation: 0.5mm.

[1] It is possible to separate a root into rootlets and identify those innervating the muscles of interest. Only the selected rootlets are then trapped in the slot. This is done by some surgeons during SARSI implantation to exclude the rootlets giving foot movements [van der Aa, 2002].

Table 4.1: Root innervation of leg muscles, based on a similar table in Rushton [1990] and on Stone and Stone [1990]. The roots between brackets were noted as providing only occasional innervation.

Muscles	MRC	Gray	Brain	Stone	Pala	Action
Psoas	L1, 2, (3)	L2, 3, (4)	L1-5	L(1), 2, 3, (4)	L2,3	Hip flexion
Iliacus	L1, 2, 3	L(2), 3	L1-5	L2, 3	L2, 3	Hip flexion
Gluteus maximus	L5, S1, (2)	L5-S2	L5-S2	L5-S2	L5-S2	Hip extension and thigh external rotation
Adductors	L2, 3, (4)	L2, 3, (4)	L2-4	L3, 4	L2-4	Thigh adduction (i.e. lateral leg flexion at the hip) and thigh rotation
Quadriceps femoris[a]	L(2), 3, 4	L(2), 3	L2-4	L2-4	L2-4	hip flexion and knee extension
Medium Hamstrings[b]	(L5), S1, (2)	L(4), 5, S1	L4-S1	L5-S2	L5-S2	hip extension and knee flexion
Biceps femoris	(L5), S1, (2)	L5-S3	L5-S2	L5-S3	L5-S2	knee flexion accompanied by slight hip extension
Gastrocnemius	S1, 2	S1, 2	L5-S2	S1, 2	S1, 2	knee flexion, foot plantar flexion
Soleus	S1,2	L5, S1, 2	L5-S2	S1, 2	S1, 2	Foot plantar flexion
Tibialis posterior	L4, 5	L4, (5)	L5-S1	L5-S1	L4, 5	Foot plantar flexion and inversion[c]
Tibialis anterior	L4, (5)	L4, 5	L4, 5	L4-S1	L4, 5	Foot dorsiflexion and inversion[c]
Peroneus	L5, S1	L5, S1	L5, S1	L4-S1	L5, S1	Foot dorsiflexion and eversion[d]
Toe flexors[e]	(L5), S1, (2)	L5-S2	L5-S2	L5-S2	L5-S2	Foot plantar flexion and inversion and toe flexion
Toe extensors[f]	L5, (S1)	L5, S1	L4-S1	L4-S1	L5-S1	Foot dorsiflexion and inversion and toe extension
Small mm[g] foot	S1, 2 (3)	L5-S2	L5-S2	L4-S2	L5-S2	Toe movements, phalange per phalange

[a] Rectus femoris, vastus lateralis, vastus medialis and vastus intermedius muscles.

[b] Semitendinosus and semimembranosus muscles.

[c] Foot inversion, or supination: turning the foot inwards.

[d] Foot eversion: turning the foot outwards.

[e] Flexor hallucis longus and flexor digitorum longus only, all muscles located solely in the foot are listed under "small mm foot".

[f] Extensor hallucis longus and extensor digitorum longus only, all muscles located solely in the foot are listed under "small mm foot".

[g] "mm" is a common abbreviation for "muscles".

Table 4.2: Movements associated with individual lumbar and sacral nerve roots, based on table 4.1. Not all references include S3, and none go as far as S4 and S5. The table is therefore limited to S1, S2 and S3. The S3 movements have been completed by data from SARSI patients, from Rushton [1990]

Nerve root	Movements
L1	Hip flexion
L2	Hip flexion, thigh adduction and rotation, knee extension
L3	Hip flexion, thigh adduction and rotation, knee extension
L4	Hip flexion and extension[a], thigh adduction and thigh rotation,
	knee extension and flexion[a]
	Foot plantar flexion and dorsiflexion[b] and inversion
	Toe extension and movements, phalange per phalange
L5	Hip extension, thigh rotation and knee flexion
	Foot plantar flexion and dorsiflexion[c] and inversion and eversion[d]
	Toe extension and movements, phalange per phalange
S1	Hip extension, thigh rotation, knee flexion
	Foot plantar flexion and dorsiflexion[c] and inversion and eversion[d]
	Toe extension and movements, phalange per phalange
S2	Hip extension, thigh rotation, knee flexion
	Foot plantar flexion and inversion
	Toe extension and movements, phalange per phalange
S3	Knee flexion accompanied by slight hip extension
	Foot plantar flexion
	Toe movements, phalange per phalange

[a] L4 potentially innervates antagonist muscles: quadriceps femoris (hip flexion and knee extension) and medium hamstrings (hip extension and knee flexion).

[b] L4 potentially innervates antagonist muscles: tibialis posterior (plantar flexion) and anterior (dorsiflexion). The toe extensors also contribute to the dorsiflexion.

[c] L5 and S1 potentially innervate antagonist muscles: soleus, tibialis posterior and toe flexors (plantar flexion) and tibialis anterior, peroneus and toe extensors (dorsiflexion).

[d] L5 and S1 potentially innervate antagonist muscles: tibialis anterior and posterior, toe flexors and extensors (inversion) and peroneus (eversion)

4.1.3.1 Of slots and channels

A slot is a division of an electrode book. It contains a set of three electrodes and has two side-walls as seen on fig. 4.1. The roots or rootlets are placed in slots.
A channel is a stimulation concept. The stimulator delivers current pulses to channels. This distinction is important since more than one slot may be connected to a single channel output stage. For example, the S2 roots are used for gluteal stimulation. Physically, in the cauda equina, the S2 left and S2 right are often trapped in two separate slots. However, if the stimulation protocol does not require the independent activation of the left or right muscle, the two slots may be connected together as a single channel. Stimulating this channel will cause non-side-specific gluteus contraction [2].

4.1.3.2 LARSI books and electrodes dimensions

The LARSI team decided that four three-slot books would give the needed 12 channels [3] without taking up too much volume in the cauda equina. Each book had a four-wire Cooper cable. The consequences of using only four wires for six electrodes connections (one anode and one cathode connection in a slot, three slots in a book book) will be investigated hereafter (section 4.1.3.3). Of the three LARSI patients (see section 3.3.2.2), TF was implanted with SARSI-size books. The slots turned out to be so much larger than the roots they trapped (see fig. 4.2) that JH and CB received smaller books. Unfortunately, CB's roots were much thicker than average, they fitted tightly in the new slots. This may have led to some damage as the surgeon had to "push" the roots in the slots, and the recruitment for some roots was poor if present (see in appendix table ??, page ??). Table 4.3 summarises the books and electrodes dimensions.

Table 4.3: LARSI books dimensions, TF has a SARSI-size book, the other two patients received books with smaller, narrower slots.

	TF	JH	CB
length	9mm	9mm	9mm
slot width	2mm	1.5mm	1.5mm
slot height	3.5mm	2.5mm	2.5mm
electrode shape	U	flat	flat
anode surface area	$9mm^2$	$0.94mm^2$	$0.94mm^2$
cathode surface area	$9mm^2$	$1.88mm^2$	$1.88mm^2$

[2] Stimulation programs to limit the occurrence of pressure sores typically stimulate both S2L and S2R together.
[3] In the LARSI each slot corresponds to a channel.

Figure 4.2: SARSI book electrode in the spinal canal during operation, notice how large the slots are with respect to the roots they trap.

The electrodes in TF's books are made of platinum foil, cut in strips 1mm wide. They are U-shaped to cover both walls and the floor of the slot. The surface area of each electrode is 9mm^2. The electrodes in JH and CB's books are made of platinum-iridium [4] wire, 0.1mm diameter, covering the floor of the slot only. Flat electrodes were used because it was expected that they would give a smoother strength-duration curve as fascicles further from the bottom of the book would be recruited with a slightly higher threshold. This hypothesis however still requires further investigations. For the anodes (the two external electrodes in a slot), the wire is threaded twice across the floor, while for the central cathode it is threaded four times. Assuming half of the wire circumference contributes to the electrode, the approximate surface areas are $4 \times \pi \times 0.05 \times 1.5 \approx 1.88mm^2$ for the cathode, and half of it for each anode.

4.1.3.3 LARSI connections

Four three-slot books are used. To reduce the size and number of cables leaving the spinal canal, only one four-wire Cooper cable is connected per book. The resulting 4 cables pass through the dura in one or two separate grommets [Brindley, 1981] (grommets are available for two, three or four cables, see figure 4.4).
Any slot in an electrode book contains three electrodes: one central cathode and two external anodes connected together. A three-slot book therefore has nine electrodes and six "logic terminals" (three cathodes and three anodes) but only four wires. To solve this inequality, all six anodes are connected together, requiring only one wire, leaving three wires for the three cathodes.

[4] 80% Pt, 20% Ir

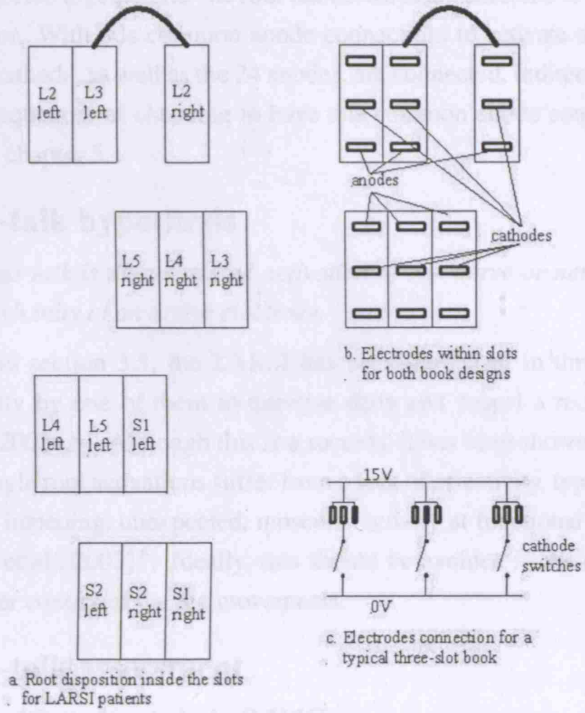

Figure 4.3: Electrodes connection and roots disposition in LARSI books for patients JH and CB.

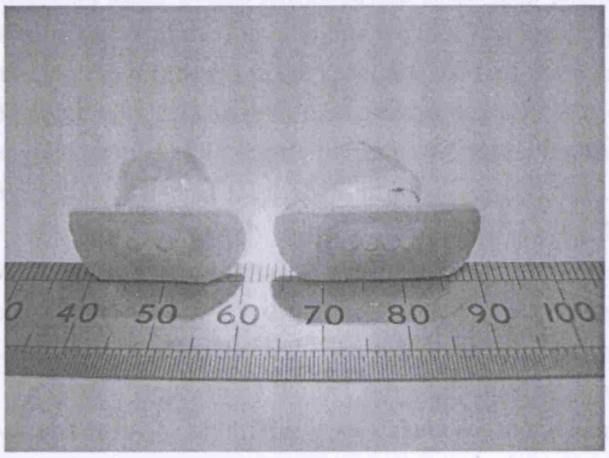

Figure 4.4: A two cables and a four cables grommets used with intra-thecal electrodes.

To simplify the stimulator circuit, improve reliability and save space [5], all anodes are physically connected together, i.e. the four anode-wires are soldered to a common node on the stimulator. With this common anode connection, to activate a single slot, the corresponding cathode, as well as the 24 anodes, are connected, indirectly, to the power rails. The consequences of choosing to have this common anode connection will become clearer in chapter 5.

4.2 Cross-talk hypothesis

Definition: *Cross-talk is the unwanted activation of one nerve or nerve root lying in the vicinity of an active electrode.*

As mentioned in section 3.3, the LARSI has been implanted in three patients, and used successfully by one of them to exercise daily and propel a recumbent tricycle [Perkins et al., 2002a,b]. Although this is a success, it has been shown that the muscle responses to single root activations suffer from a lack of selectivity, typically illustrated by the onset of impeding, unexpected, muscular activity at functional stimulation levels [Donaldson et al., 2003] [6]. Ideally, this should be avoided in the next implants to allow for a better control of the leg movements.

4.3 Cross-talk assessment

4.3.1 The multi-moment chair (MMC)

The responses to stimulation were evaluated using the *multi-moment chair* (MMC, see fig. 4.5): an apparatus developed by Donaldson, Wood and others to measure the joint moments of the leg [Donaldson et al., 1999; Wood et al., 1999]. The seven individual moments recorded are: hip joint flexion-extension (i.e. movement in the sagittal plane), leg abduction-adduction (i.e. movements in the coronal plane), leg rotation at the hip, knee flexion-extension, ankle flexion-extension aka ankle dorsi-plantar flexion, foot eversion-inversion (rotation of the foot pointing the toes outwards-inwards) and "leg rotation" (i.e. turning the leg, flexed at the knee, and the foot, inwards or outwards). The MMC is equipped with built-in sensors to measure those 7 moments on both left and right sides, giving a total of 14 curves for each stimulation sequence. For example, the first seven plots of figure 4.6 results from stimulation of root L4L alone. The stimulus pulse width was progressively increased from 0 to $57\mu s$ (fig. 4.6(h)).
It is difficult to guarantee free movements at the hip, knee and ankle joints of both legs and yet hold the patient's upper body perfectly still. The recordings may therefore be affected by the presence of mechanical cross-talk, essentially around the hip joint. See fig.4.6(a), the flexion response on the left is accompanied by a weaker, yet non negligible, hip extension on the right. This is very likely due to mechanical correlation

[5] On a circuit the size of the stimulator, the wire solder pads occupy an important part of the cross-sectional area, therefore limiting the number of wires required limits the overall volume of the implant.

[6] The tables published in Donaldson et al. [2003] are reproduced in appendix ??, see tables ??, ?? and ??.

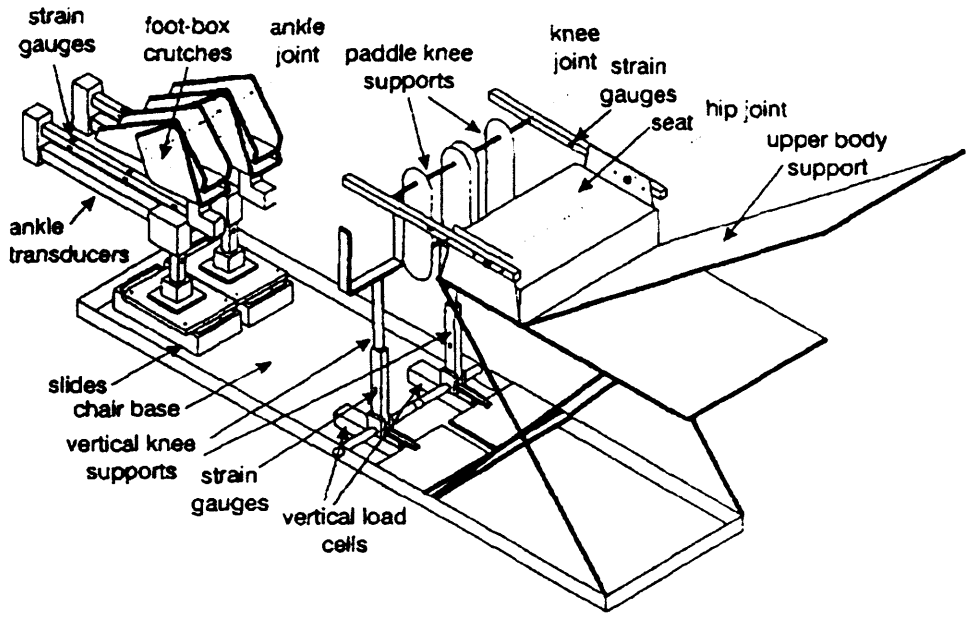

Figure 4.5: Drawing of the multi-moment chair, reproduced from Wood et al. [1999].

rather than cross-talk stimulation. A further complication comes from *reflex activity*[7]. Typically, manually moving the ankle of a patient may cause temporary yet strong hip extension. After a few movements, the reflex dies away and the hip relaxes. Reflex activity may be identified by the delay in its onset, and, more reliably, as it disappears when the stimulation pulse or initiating movement is repeated a few times. Knee extension is less subject to mechanical imprecision and reflex contractions and is therefore ideal for cross-talk assessment. Figure 4.7 shows the knee moment response to each of the 12 roots L2 to S2, left and right, as recorded in March 1999. As expected from table 4.2, the higher roots (L2 to L5R) give knee extension (quadriceps femoris) and the lower roots (L5L to S2) give knee flexion (medium hamstrings, biceps femoris, gastrocnemius). Note also the lack of in-patient symmetry as L5R gives strong knee extension while L5L causes flexion. All data presented and analysed in the following sections on cross-talk were recorded by the LARSI team using the MMC. It has not been previously published except for the tables of appendix ?? published in Donaldson et al. [2003].

4.3.2 Ipsilateral cross-talk

Due to the rather widespread innervation from each root, the co-activation is not obvious from observation of the ipsilateral[8] response to single root stimulation. Yet ipsilateral cross-talk can be highlighted in the two following cases: root L3R stimulation showing a sacral response and root L4R showing a step-like recruitment. All the data

[7] Action potentials spreading back up to the spinal cord (on either sensory or motor nerve fibres [Donaldson et al., 2003]), and being reflected down along another nerve root, causing delayed muscle contractions.

[8] *Ipsilateral*: on or relating to the same side (of the body).

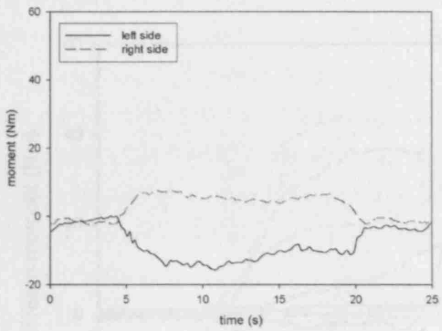

(a) L4L hip extension moment.

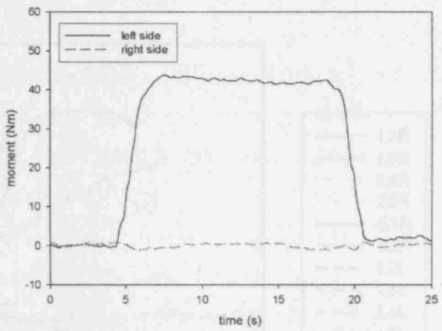

(b) L4L knee extension moment.

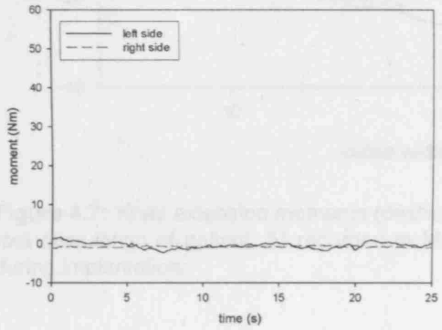

(c) L4L ankle extension moment.

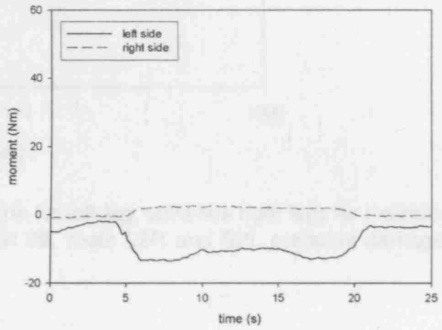

(d) L4L hip abduction moment.

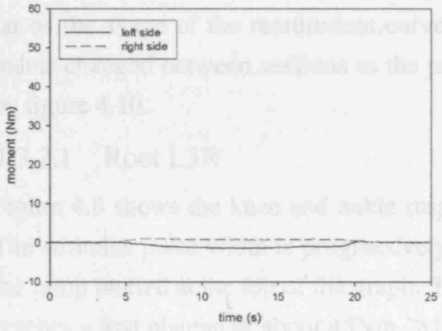

(e) L4L ankle abduction moment.

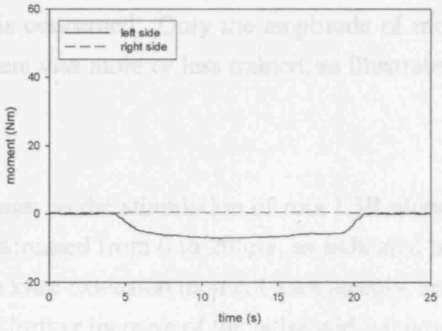

(f) L4L hip external rotation moment.

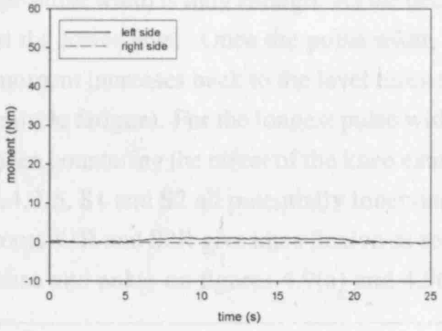

(g) L4L inversion moment.

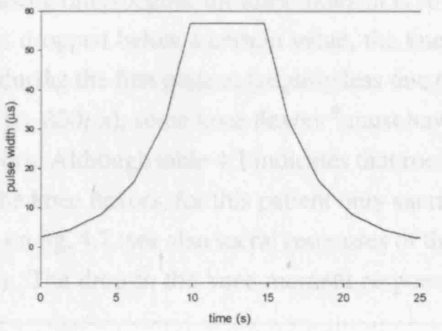

(h) L4L stimulus pulse width (μs).

Figure 4.6: Responses to single L4L root stimulation of patient JH, recorded in March 99.

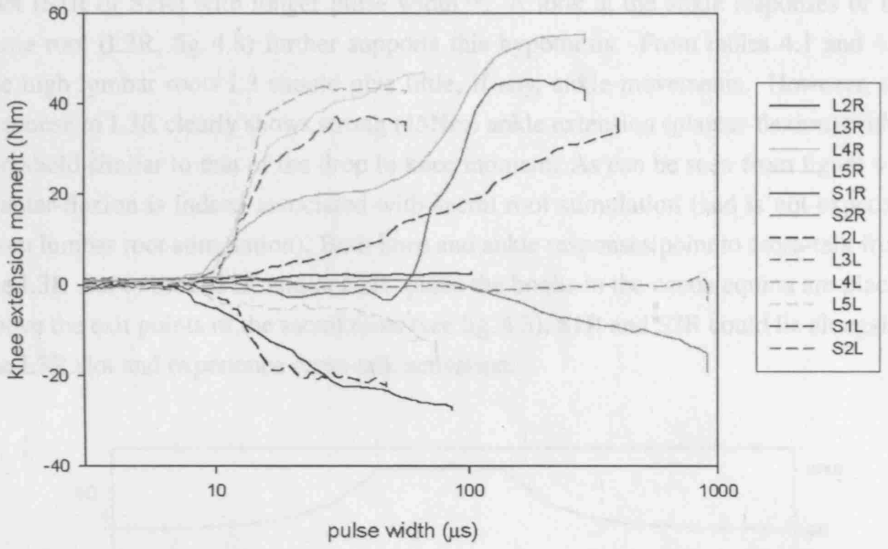

Figure 4.7: Knee extension moments (dashed line for left leg, solid line right leg) for individual root stimulation of patient JH recorded in March 99, roots L2R and S2L probably damaged during implantation.

presented here were recorded with patient JH, in March 1999 and May or September 2000 as indicated. Many other recording sessions took place, giving similar results as far as the shape of the recruitment curves is concerned. Only the amplitude of moments changed between sessions as the patient was more or less trained, as illustrated by figure 4.10.

4.3.2.1 Root L3R

Figure 4.8 shows the knee and ankle responses to the stimulation of root L3R alone. The stimulus pulse width is progressively increased from 0 to $295\mu s$, as indicated by the ramp plotted at the top of the graph. The knee extension moment rises steeply, and reaches a first plateau of about 45Nm. After further increase of the pulse width (above $295\mu s$), however, the moment drops to a lower level (40Nm), where it remains while the pulse width is long enough. As the decreasing ramp begins, the knee moment is still at the lower level. Once the pulse width has dropped below a certain value, the knee moment increases back to the level reached during the first plateau (slightly less due to muscle fatigue). For the longest pulse width ($> 300\mu s$), some knee flexors [9] must have been countering the effect of the knee extensors. Although table 4.1 indicates that roots L4, L5, S1 and S2 all potentially innervate the knee flexors, for this patient only sacral roots S1R and S2R give knee flexion as seen on fig. 4.7 (see also sacral responses of the knee and ankle on figures 4.9(a) and 4.9(b)). The drop in the knee moment response

[9] Due to the length and complexity of the recording procedure, no effort was made to identify which of the medium hamstrings, biceps femoris or gastrocnemius specifically was/were activated.

to root L3R stimulation (fig. 4.8) may be due to the unexpected recruitment of a sacral root (S1R or S2R) with longer pulse width [10]. A look at the ankle responses of the same root (L3R, fig. 4.8) further supports this hypothesis. From tables 4.1 and 4.2, the high lumbar roots L3 should give little, if any, ankle movements. However, the response to L3R clearly shows strong (15Nm) ankle extension (plantar-flexion) with a threshold similar to that of the drop in knee moment. As can be seen from figure 4.9, plantar-flexion is indeed associated with sacral root stimulation (and is not expected from lumbar root stimulation). Both knee and ankle responses point to cross-talk from the L3R slot to roots S1R and/or S2R. Since the books in the cauda equina are placed above the exit points of the sacral roots (see fig. 4.3), S1R and S2R could lie alongside the L3R slot and experience cross-talk activation.

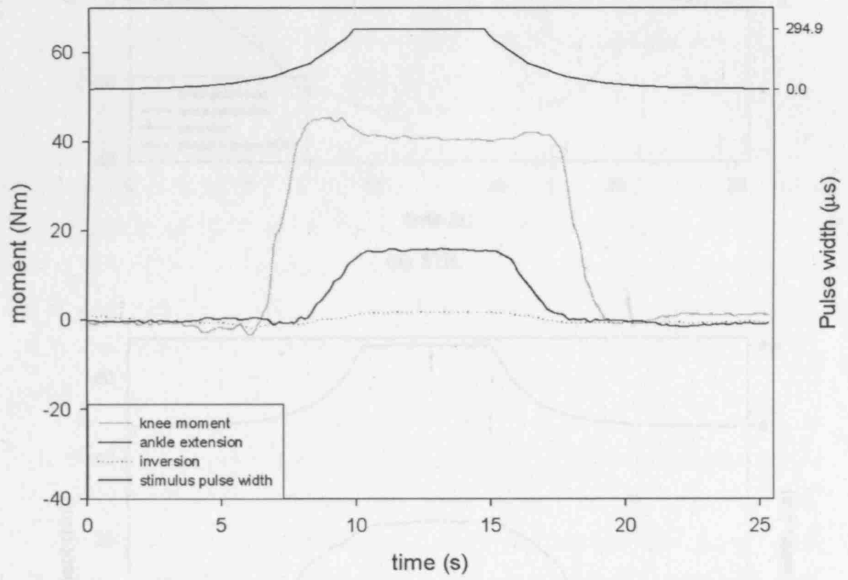

Figure 4.8: Knee and ankle responses to single root L3R stimulation of patient JH, recorded in March 99.

4.3.2.2 Root L4R

The knee moment generated by stimulation of root L4R has a particular shape, as seen on fig. 4.7 and 4.10, the latter compares the moments for L4R and L5R stimulation on two separate days. As training level varied, the amplitude had decreased before the second session but the shape is similar for both sessions. Although it reaches the highest maximum, it does so in two steps (as if there were two thresholds). Here are several possible explanations for this:

A. There are two groups of fibres in L4R with a considerable difference in diameter, both innervating knee extensors. The first group, with the larger diameter,

[10] The presence of smaller fibres (higher threshold) in L3 innervating the knee flexors is unlikely but may not be ruled out as a complementary explanation.

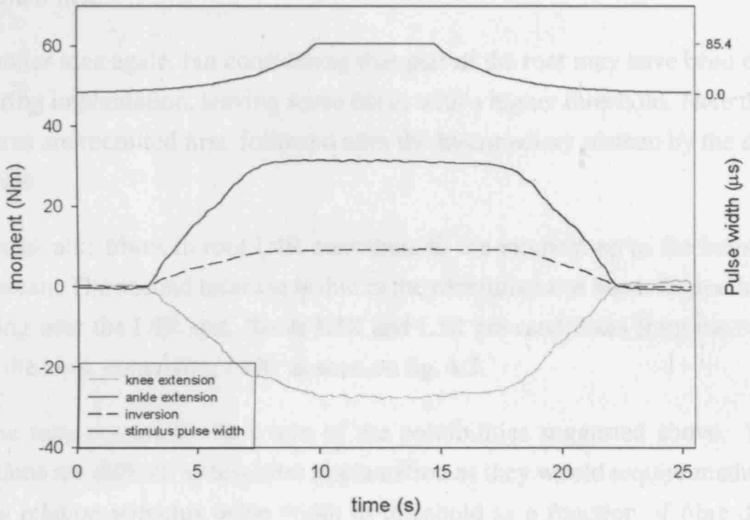

(a) S1R.

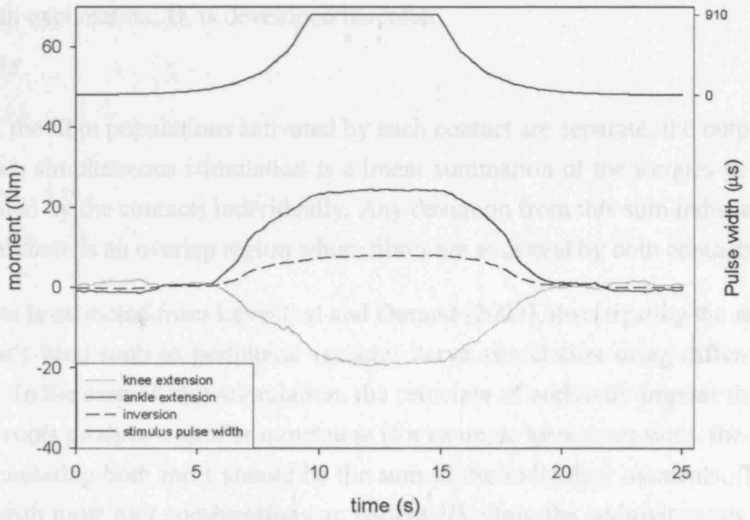

(b) S2R.

Figure 4.9: Knee and ankle responses to single sacral root stimulation of patient JH, recorded in March 99.

is fully recruited before contribution from the second group begins, hence the intermediary plateau.

B. Similar idea, but considering two groups of fibres lying at different distances from the flat electrodes. The fascicles closest to the bottom of the slot are recruited first.

C. Similar idea again, but considering that part of the root may have been damaged during implantation, leaving some fibres with a higher threshold. Here the intact fibres are recruited first, followed after the intermediary plateau by the damaged fibres.

D. Cross-talk: fibres in root L4R contribute to the moment up to the intermediary plateau. The second increase is due to the recruitment of fibres from other roots, lying near the L4R slot. Roots L3R and L5R are candidates from their position in the book containing L4R, as seen on fig. 4.3.

The cause may potentially be a mix of the possibilities suggested above. The first three options are difficult to test after implantation as they would require mathematical equations relating stimulus pulse width to threshold as a function of fibre diameter, distance to electrode and physical state of the fibres [11]. There were however no signs of L4R damages in the weeks following the operation, so alternative **C** is less likely. The fourth explanation, **D**, is developed hereafter.

Additivity

> "If the fibre populations activated by each contact are separate, the output from simultaneous stimulation is a linear summation of the torques generated by the contacts individually. Any deviation from this sum indicates that there is an overlap region where fibres are activated by both contacts."

This quote is extracted from Leventhal and Durand [2003], investigating the responses of the cat's hind limb to peripheral (sciatic) nerve stimulation using different electrodes [12]. In the case of root stimulation, the principle of additivity implies that if two different roots produce a similar movement (for example knee extension), the moment while stimulating both roots should be the sum of the individual moments. This was verified with most root combinations on patient JH. Only the additivity tests of roots L4R and L5R are presented here, as recorded in July 1999. Figure 4.11 shows four records, with different pulse widths for L4R and L5R. In each of them, the moment for L4R and L5R is close [13] to the sum of the single root moments (averaged over two

[11] A study of the M-waves latency might also help to qualify the activation pattern.

[12] This additivity principle has been used to demonstrate fascicular selectivity in [Leventhal and Durand, 2003; Tyler and Durand, 2002].

[13] The relative error is less than 10%, the reading for L4R & L5R being always smaller than the sum of individual moments.

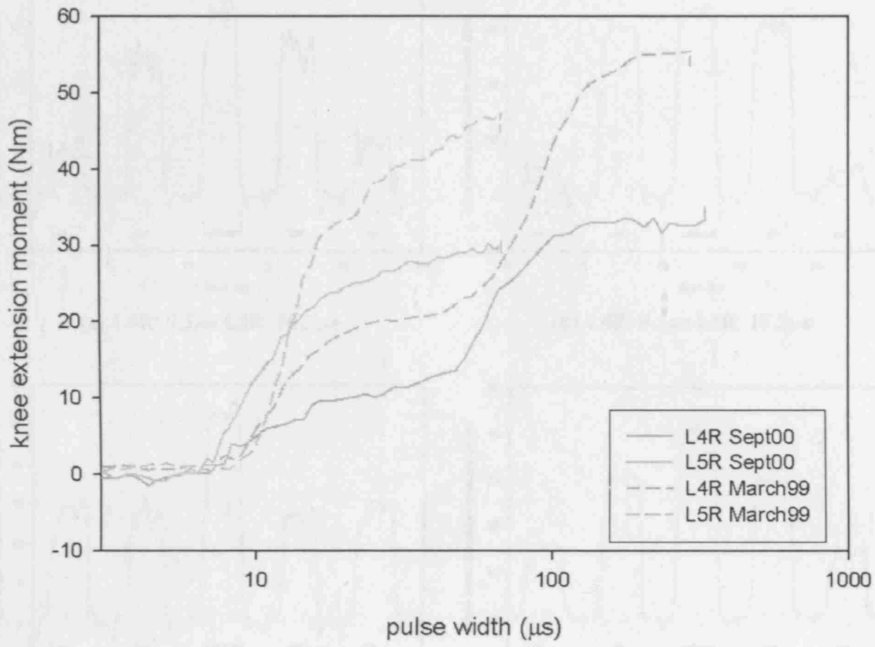

Figure 4.10: Knee extension moments for individual root (L4R and L5R) stimulation of patient JH recorded in March 99 and May 00.

measurements to account for fatigue). It must be emphasised that in all four tests, the pulse width for L4R is below the second threshold (with reference to the plateau seen on fig.4.10). Figure 4.12 on the other hand shows a longer test (May 2000, patient JH) where the pulse width for root L4R is above the second threshold. The contribution of root L5R, introduced progressively as indicated by the ramps at the top of the figure, has no noticeable effect.

So far, the data presented have shown that there is additivity of moments only for the first part of the recruitment curve of L4R (added with L5R). The lack of effect of L5R contribution when added to strong L4R root stimulation suggest that all fibres in L5R innervating the knee extensors are already recruited by the stimulation pulses of the L4R slot. And, since there is additivity for low pulse width, the activation of L5R fibres by L4R stimuli must happen during the second phase of the L4R recruitment curve.

For completeness another additivity test was performed, on the same day (May 00), looking at the contribution from root L4R to the contraction obtained with root L5R, see fig. 4.13. If the stimuli to the L5R slot do not cause cross-talk to root L4R then the knee moment should increase as L4R begins to be stimulated, and flatten when the pulse width reaches a value corresponding to the intermediary plateau of the L4R recruitment curve. There should be no further increase as the second rise of the L4R

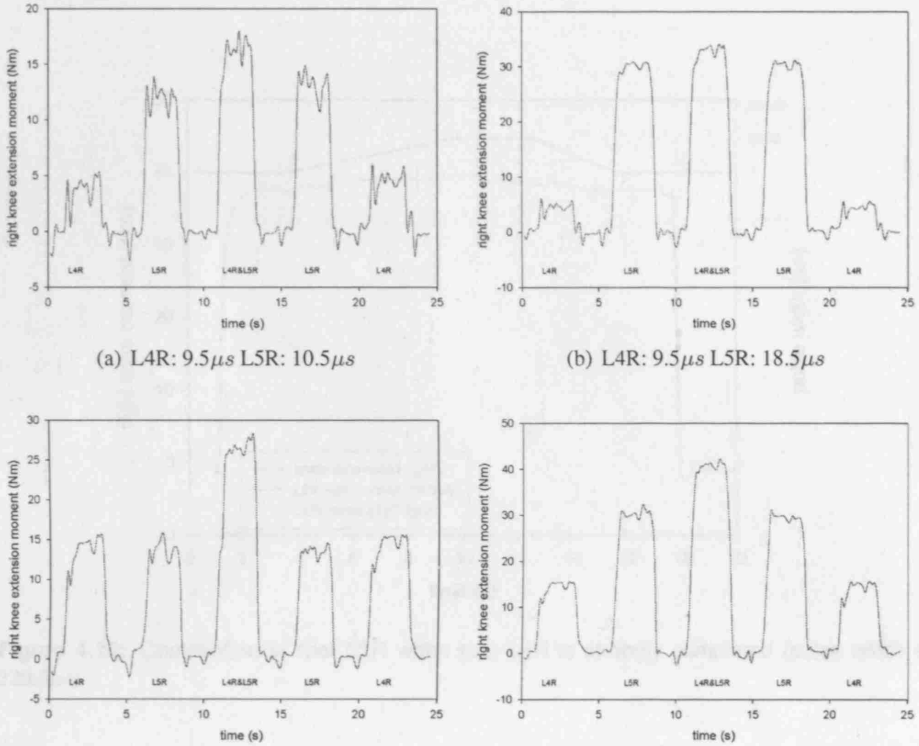

(a) L4R: 9.5μs L5R: 10.5μs

(b) L4R: 9.5μs L5R: 18.5μs

(c) L4R: 16μs L5R: 10.5μs

(d) L4R: 16μs L5R: 18.5μs

Figure 4.11: Additivity tests for roots L4R and L5R, in all four cases, the first and last peaks are for root L4R alone, the second and fourth peaks are for root L5R alone and the central peak is for both roots L4R and L5R together.

recruitment curve involves nerve fibres from root L5R that will already be active. From the trace of fig. 4.13, root L4R, strongly stimulated, adds a contribution to the knee moment. Root L5R alone gives a knee extension moment of about 30Nm for a pulse width of 29.5μs, in agreement with the recruitment curve recorded four months later (Sept 00) and plotted on fig.4.10. The pulse width for root L4R at which the knee moment starts to increase again is close to the threshold for L4R, the added moment is about 10Nm. The recruitment curve recorded in September 2000 does not exhibit as clear a plateau as that of March 1999 (fig.4.10). Yet 10Nm corresponds to a level at which the curve clearly flattens.

L4R to L5R cross-talk

The different additivity tests have shown the following:

1. At low level, there is additivity of the moments generated by stimulation of roots L4R and L5R, indicating that different populations of fibres are recruited.

2. Addition of L5R to L4R strongly stimulated has no effect, indicating that strong

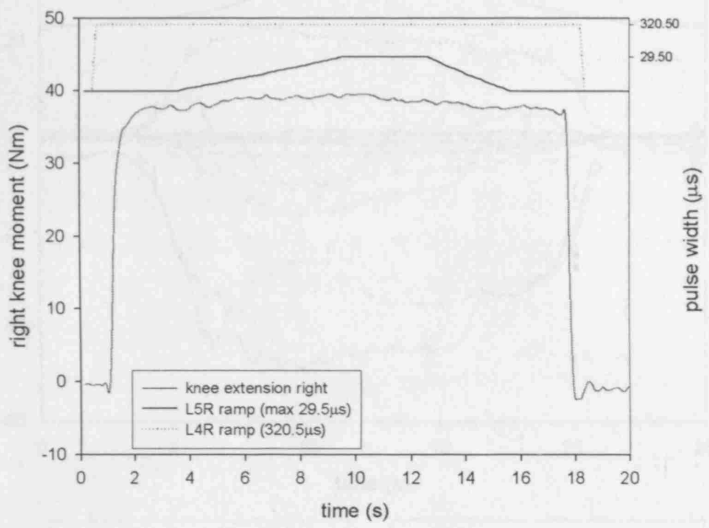

Figure 4.12: Contribution of root L5R when root L4R is strongly stimulated (pulse width of $320.5\mu s$)

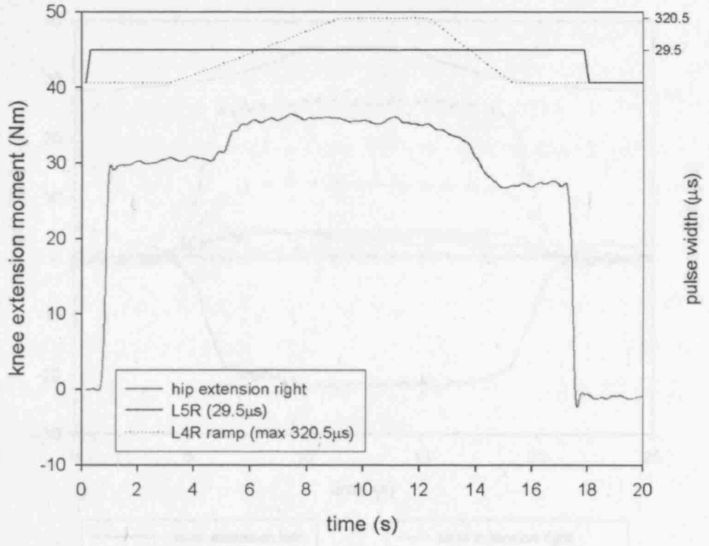

Figure 4.13: Contribution of root L4R when root L5R is stimulated (pulse width of $29.5\mu s$)

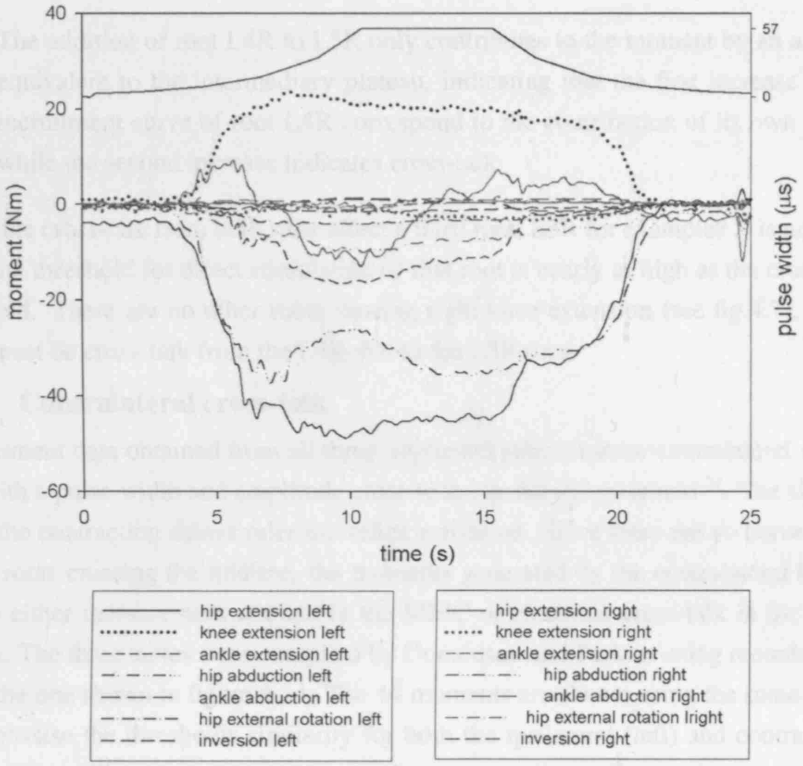

Figure 4.14: Responses to root L3L stimulation, as recorded with patient JH in September 2000

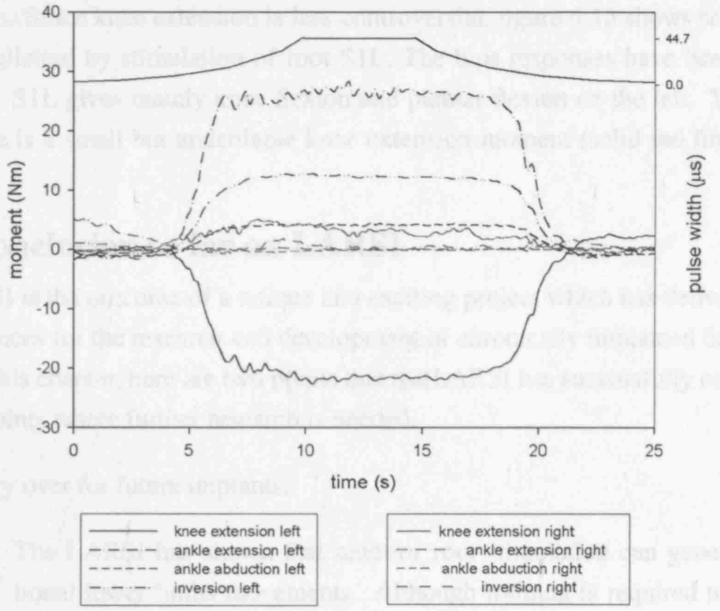

Figure 4.15: Responses to root S1L stimulation, as recorded with patient JH in March 1999

stimuli to root L4R recruit all fibres recruited by stimuli to root L5R.

3. The addition of root L4R to L5R only contributes to the moment by an amount equivalent to the intermediary plateau, indicating that the first increase in the recruitment curve of root L4R correspond to the contribution of its own fibres, while the second increase indicates cross-talk.

Could the cross-talk from both slots affect a third root, L3R for example? It is unlikely since the threshold for direct stimulation of that root is nearly as high as the cross-talk threshold. There are no other roots causing right knee extension (see fig.4.7), hence there must be cross-talk from the L4R slot to the L5R root.

4.3.3 Contralateral cross-talk

Recruitment data obtained from all three implanted patients show contralateral activation with a pulse width and amplitude close to the ipsilateral threshold [14]. The similarity of the contraction delays rules out reflex activation. Since there are no nerve fibres in the roots crossing the midline, the moments generated by the contralateral leg are due to either measurement artefact in the MMC or electrical cross-talk in the cauda equina. The three tables were compiled by Donaldson and Perkins using records similar to the one shown in figure 4.14. The 14 moments are shown using the same x axis to emphasise the thresholds similarity for both the ipsilateral (left) and contralateral (right) sides. The pulse width is increased progressively as illustrated by the ramp at the top of the graph (right time scale). As explained before, the hip extension moment may be subject to mechanical interferences, and it is up to the person present during the recording session to assess whether the moment is, or is not, due to cross-talk stimulation. Since knee extension is less controversial, figure 4.15 shows some of the moments elicited by stimulation of root S1L. The hips responses have been omitted for clarity. S1L gives mainly knee flexion and plantar-flexion on the left. Yet, on the right, there is a small but undeniable knee extension moment (solid red line), due to cross-talk.

4.4 Conclusion so far on LARSI

The LARSI is the outcome of a unique and exciting project which has delivered some solid advances for the research and development of chronically implanted devices. To conclude this chapter, here are two points that the LARSI has successfully established, and two points where further research is needed.

- Carry over for future implants:
  - The LARSI has shown that anterior root stimulation can generate functional lower limbs movements. Although training is required to build up

[14] These data have previously been published in Donaldson et al. [2003], and are reproduced in appendix ??, tables ??, ?? and ??.

some muscle mass, patient JH has repeatedly demonstrated her cycling skills in the past 10 years, even after many months away from her tricycle. This emphasizes the concept of "readiness". From a short term stance, readiness means that the implant is always "ready", the patient does not need hours of preparation and setting before and after the exercise, making the implant attractive to use at any time, even for a few minutes only. From a long term stance, readiness implies that, even after long quiescent periods, the implant can still generate the same movements, albeit less functional if the muscles are too weak, and the potential to retrain them always remains with the implant. This idea of readiness shows how LARSI has brought paraplegic exercise closer to able bodied exercise. It is always a matter of will, but now the potential for lower limb exercise and recreation is within reach of paraplegic patients.

- The implants have been implanted for a decade without any reported breaks or other failures. Any future implants should benefit from the reliable technology and the expertise developed by the team who designed and built the LARSI.

- Further research:

  - The issue of cross-talk, which hinders selectivity, has already been assessed. It requires further study and improved understanding if it is to be avoided for future implants, see chapter 5.

  - The book dimension is another issue that requires improvement, as highlighted in section 4.1.3.2, page 61. Chapter 6 explores a proposed amelioration of the existing electrode mounts.

Chapter 5

Cross-talk: understanding the causes and solving the problem

5.1 Concept

Nowadays, many computer models for single axons or peripheral nerve stimulation exist [Grill, 1996; Grill et al., 2000; McNeal, 1976; Mino and Grill, 2000; Moffitt et al., 2004; Oozeer et al., 2006; Rattay, 1998; Rattay and Aberham, 1993; Rattay and Resatz, 2004; Rijkhoff et al., 1994a; Struijk et al., 1993; Sweeney et al., 1989; Veltink et al., 1989b; Vuckovic et al., 2004; Williamson and Andrews, 2005]. While these are helpful to predict the potential along a single nerve fibre, they underestimate the complexity of real, whole nerve, stimulation [1]. With the prospect of developing new (nerve root) stimulator implants, a practical display of the performances and weaknesses of LARSI and the proposed improvements was sought. It was necessary to study a more physiological model of nerve roots stimulation with book electrodes. As, obviously, experiments on human nerve roots are rather difficult to justify and organise, a series of in vitro experiments on frog sciatic nerves were performed. The aims were as follows:

- to demonstrate the general occurrence of cross-talk stimulation, both in another slot of the active book and outside in its vicinity;
- to understand the LARSI situation;
- to test the alternative solution of independently switching each tripole (one switch for the pair of anodes and one switch for the cathode) which will be incorporated in future implants: Sacro-Lumbar Anterior Root Stimulator Implant (SLARSI), Healthy Aims implant;
- to illustrate the effect of hyperpolarisation (the presence of an anode, real or virtual) on whole nerve stimulation;

[1] Animal experiments performed to complement computer simulation often deliver mitigated, inconclusive, results [BeMent and J. B. Ranck, 1969a,b; Miller et al., 2003; Ooyama and Wright, 1961; Rozman and Trlep, 1992; Struijk et al., 1993, 1998].

- to assess the influence of various practical parameters like the position of the nerve inside the slot, the quality of the seal obtained with the lid or a kink in the nerve.

Pfluger's law

> "The action potentials always originate at or very near the cathode."

This is known as Pfluger's law, stated circa 1859 with the notion of electrotonus [Lapicque, 1926, page 28]. It is still nowadays considered to be true for direct stimulation with a true tripole [Wright and Ooyama, 1961]. According to Rushton [1928b, 1949], when the tripole is asymmetrical however, the CAP originates on the side of the weaker anode, Pfluger's law does not hold.
Cross-talk stimulation being a subject so far untreated in the literature, there are no hypotheses regarding the site of activation. It is assumed that here too the action potential will originate on the side of the weaker anode. It is one of the aims of these experiments to demonstrate this statement, as well as to confirm the assumptions for direct stimulation.

5.2 Preliminary experiment

5.2.1 Imperfect tripole

The books used for nerve root stimulation contain three electrodes. In use, the two external anodes are connected to a single wire, without any control on how the current is shared between them. There are unavoidable differences between books, the central cathode may not lie precisely in the middle of the anodes and the surface area of each electrode may not be equal. Furthermore, the connective tissue growth after implantation will not be symmetrical. All these asymmetries will introduce a certain imbalance between the two anodal currents. In theory it is assumed that in a tripole the current is equally shared between the two anodes. This will not be the case in practice, the tripolar arrangement is imperfect and the following work on book electrode stimulation needs to account for this imbalance. To evaluate the influence of the geometrical asymmetry on current division, some preliminary tests with three purpose built books were performed.

5.2.2 Special offset electrode books

The books used for nerve root stimulation are manufactured by Finetech Medical Ltd. Those used in this experiment were made specially by the company following the dimensions of fig. 5.1. They are three single-slot mounts, made with extra care to have three electrodes with equal surface area (this is difficult because the electrodes are made of thin platinum-iridium strips, cut to size, shaped and "pinched" in the book's silicone frame, and more or less silicone may cover the metal). The cathodes in the three books have a known offset with respect to the centre (0mm, 0.5mm and 1mm), see fig. 5.1. Any number of electrodes placed in saline forms an impedance with both a capacitive

and resistive parts. Although this will be the subject of chapter 7, it is necessary here to say that the capacitive part depends mainly on the surface area of the electrodes, while the resistive part is more influenced by the distance between electrodes and the resistivity of the solution or tissue. The books used in this experiment have a known offset, giving a controlled resistive imbalance, while the matched electrode areas should give nearly equal capacitive parts.

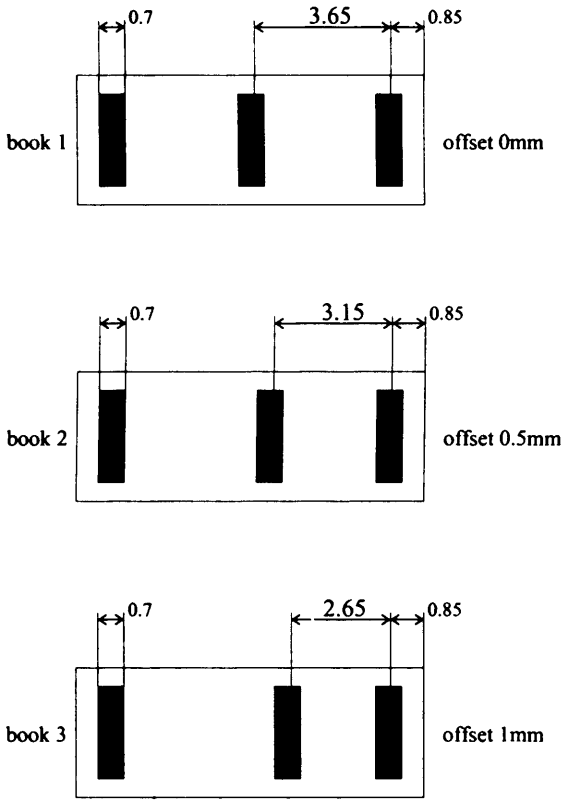

Figure 5.1: Cathode position in the three "offset" books (lateral views), dimensions in mm, book length 9mm.

5.2.3 Current imbalance due to geometrical asymmetry

5.2.3.1 Setup

Three books were used, with offset 0mm, 0.5mm and 1mm. Each was setup in a similar way, as shown in fig. 5.2. The cathode was plugged into the cathode connection of a stimulator (described in chapter 8), while each anode was connected to the anode connection of the stimulator via a virtual-earth ammeter[2]. This situation corresponds well to the real implants as the two anodal branches are connected together to the same stim-

[2]Virtual-earth ammeters: connection of the anode to the negative input of an operational amplifier with a resistor (R) as a negative feedback loop. The two positive inputs were plugged into one (the same) anode connection of the stimulator, thereby closing the current path. The amplifier's reference terminal was also connected to this common anodal point, making it a virtual ground with respect to the output of the amplifiers.

ulator's anodal output, albeit via two operational amplifiers, acting as null-impedance current meters. Constant current pulses were sent from the cathode and the current in each anodal branch was evaluated by displaying the output voltage of the amplifiers on an oscilloscope. The measurements were done with the books in physiological saline, and in two more resistive solutions to simulate the effect of connective tissue growth.

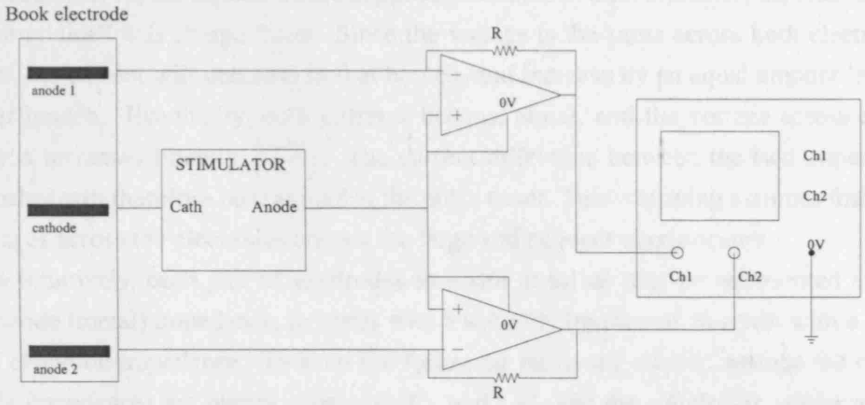

Figure 5.2: Setup for the book-electrode "offset" preliminary experiment.

5.2.3.2 Theory

Simple theory, current imbalance for very short pulses

Let i_1 be the current entering the slot by one anode (called $anode_1$ by association), and i_2 the current through $anode_2$. The current i at the cathode is the sum $i_1 + i_2$. If the effect of the capacitive accumulation of charges may be neglected as is the case with very short pulses, i_1 and i_2 may be regarded as constant since i is constant.

Let Z_1 be the impedance between $anode_1$ and the cathode, and Z_2 between $anode_2$ and that same cathode. The capacitive part of these impedances should be similar (as explained before), while the resistive part will depend on the distance d between the cathode and the anode as $R = \rho * \frac{d}{A}$ where ρ is the resistivity of the solution and A is the cross-sectional area of the slot.

The voltages displayed on the oscilloscope are $V_j = i_j * R$ (j is the branch index), where R is the same in the negative feedback loop of both amplifiers. The current imbalances can be evaluated in % as

$$I_j = \frac{i_j}{i_1 + i_2} = \frac{V_j}{V_1 + V_2}$$

while the relative current difference, with respect to the current in the branch of a pure tripole ($i_0 = \frac{i_1+i_2}{2}$ and $V_0 = \frac{V_1+V_2}{2}$) is given by

$$\frac{|i_0 - i_j|}{i_0} = \frac{|V_0 - V_j|}{V_0}.$$

Taking the capacitance into consideration

Since the anodes are connected together, their potential differences to the cathode are equal: $i_1 * Z_1 = i_2 * Z_2$ at all time. Intuitively, at the onset of the current pulse, the capacitors are discharged and the current i_j is proportional to $\frac{1}{R_j}$, j being 1 or 2 depending on the anode. Therefore the shorter branch, being less resistive, passes more current. As the capacitors are supposed identical in both branches, the one on the "shorter side" will charge faster. Since the voltage is the same across both electrode pairs, the current will decrease in that branch, and increase by an equal amount in the other branch. Eventually, both currents become equal, and the voltage across each branch increases linearly $\left(\frac{i_j * t}{C}\right)$. The current difference between the two imperfect branches will therefore be maximal at the pulse onset. This reasoning assumes that the voltages across the electrodes are not too large and no electrolysis occurs.

Less intuitively, each pair of electrodes in a slot in saline may be represented as an electrode (metal) impedance, in series with a solution impedance, in series with a second electrode impedance. To keep the following reasoning simple, assume the electrode impedances are purely capacitive(C_1 and C_2), and the solution is purely resistive(impedance taken from either anode to the central cathode, R_1 and R_2). As previously, a current pulse i at the cathode (of width T) divides into i_1 and i_2, creating a potential difference between the cathode and either of the anodes (connected together) called V.

$$V = i_1 R_1 + \frac{1}{C_1}\int_0^T i_1 dt \tag{5.1}$$

$$= i_2 R_2 + \frac{1}{C_2}\int_0^T i_2 dt \tag{5.2}$$

Hence

$$i_1 R_1 - i_2 R_2 = \int_0^T (\frac{1}{C_2}(i - i_1) - \frac{i_1}{C_1})dt \tag{5.3}$$

$$= \frac{iT}{C_2} - (\frac{1}{C_2} + \frac{1}{C_1})\int_0^T i_1 dt \tag{5.4}$$

Due to the capacitance, the current in each branch will vary exponentially as

$$i_j = K + K' e^{-\frac{t}{\tau}} \tag{5.5}$$

Solving for *anode*1 gives

$$\int_0^T i_1 dt = \left\{Kt - \tau K' e^{-\frac{t}{\tau}}\right\}_0^T \tag{5.6}$$

$$= KT - \tau K' e^{-\frac{T}{\tau}} + \tau K' \tag{5.7}$$

Using $i = i_1 + i_2$, the left-hand side of (5.4) can be rearranged as

$$i_1 R_1 - i_2 R_2 = i_1 R_1 - (i - i_1) R_2 = i_1 (R_1 + R_2) - i R_2 \tag{5.8}$$

Introducing (5.5) and (5.7) in (5.8) and making $t = T$ in the rearranged (5.4) gives

$$(K + K' e^{-\frac{T}{\tau}})(R_1 + R_2) - i R_2 - \frac{iT}{C_2} = -(\frac{1}{C_1} + \frac{1}{C_2})(KT - \tau K' e^{-\frac{T}{\tau}} + \tau K') \tag{5.9}$$

Equating the T terms of (5.9) and posing $(\frac{1}{C_1} + \frac{1}{C_2}) = \frac{C_1 + C_2}{C_1 C_2} = \frac{1}{C}$:

$$-\frac{i}{C2} = -(\frac{1}{C_1} + \frac{1}{C_2})K \tag{5.10}$$

$$i\frac{1}{C_2} = \frac{1}{C}K \tag{5.11}$$

$$\frac{C}{C_2} = \frac{K}{i} \tag{5.12}$$

$$\longrightarrow \frac{K}{i} = \frac{C_1}{C1 + C2} \tag{5.13}$$

Equating the exponential terms of (5.9) and posing $(R_1 + R_2) = R$:

$$K' e^{-\frac{T}{\tau}} (R_1 + R_2) = (\frac{1}{C_1} + \frac{1}{C_2}) \tau K' e^{-\frac{T}{\tau}} \tag{5.14}$$

$$K' R e^{-\frac{T}{\tau}} = \frac{1}{C} \tau K' e^{-\frac{T}{\tau}} \tag{5.15}$$

$$R = \frac{\tau}{C} \tag{5.16}$$

$$\longrightarrow \tau = RC \tag{5.17}$$

Equating the constant terms of (5.9):

$$K(R_1 + R_2) - i R_2 = -(\frac{1}{C_1} + \frac{1}{C_2}) \tau K' \tag{5.18}$$

$$KR - i R_2 = \frac{\tau K'}{C} \tag{5.19}$$

$$\longrightarrow \frac{K'}{i} = \frac{R_2}{R} - \frac{C}{C_2} \tag{5.20}$$

From (5.5) with $j = 1$,

$$\frac{i_1}{i} = \frac{K}{i} + \frac{K'}{i} e^{-\frac{t}{\tau}} \tag{5.21}$$

$$\frac{i_1}{i} = \frac{C_1}{C1 + C2} + \left\{ \frac{R_2}{R_1 + R_2} - \frac{C_1}{C_1 + C_2} \right\} e^{-\frac{t}{RC}} \tag{5.22}$$

$$\text{For } t = 0 \Rightarrow \frac{i_1}{i} = \frac{R_2}{R_1 + R_2}$$

$$\text{For } t \rightarrow \infty \Rightarrow \frac{i_1}{i} = \frac{C_1}{C_1 + C_2}$$

Figure 5.3 is a plot of typical curves [3] of the branch currents, normalised with the total current, for $C_1 = C_2$ and $R_1 = 2R_2$. It shows that the resistances are dominant at the onset of the pulse, at $t = 0$, $\frac{i_2}{i} = 2\frac{i_1}{i}$. For $t \rightarrow \infty$, the capacitors dominates, and as they are supposed equal in this experiment, $i_1 - i_2 \rightarrow 0$. This is surprising as it shows that currents through two unequal resistors are eventually equalised by the capacitors provided these are equal. If the capacitors are different, the currents will become proportional to $\frac{C_i}{C_1+C_2}$ as $t \rightarrow \infty$, eliminating the influence of the resistors.

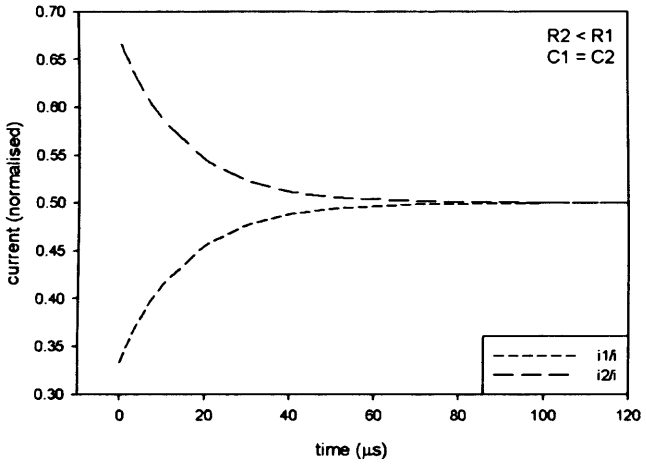

Figure 5.3: Branch current, normalised with the total current, as a function of time, calculations based on the theory developed in section 5.2.3.2, not on actual measurements.

5.2.3.3 Results of preliminary imbalance experiment

In the presentation of the following results, it is assumed that the resistance difference is exclusively due to the distance inequality of the two anodal branches. The resistive imbalance is defined as the difference between R_0, the anode-cathode impedance for a perfectly centered electrode, and R_j, the resistance of the offset branch. Dividing this by R_0 gives the relative resistance imbalance $\left(\frac{R_j - R_0}{R_0}\right)$, which, expressed in %, gives an idea of how far from ideal the tripole is. Based on $R_j = \rho * \frac{d_j}{A}$, with ρ, the resistivity, and A, the cross-section area, equal for the two branches [4], the relative difference becomes that of the anode-cathode distance $\frac{d_j - d_0}{d_0}$. Figure 5.4(a) shows the relationship between this relative indicator and the offset. Although the relationship $\left(\frac{d_j - d_0}{d_0} = f(d_0)\right)$ is obviously linear, it is plotted here to highlight how, due to the small overall dimensions of the book, a small absolute offset (as can easily happen) can cause a large relative variation.

[3] Although the curves were plotted from a formula and are not based on experimental measurements, the shape of the curves observed during the experiments were similar to those shown on fig. 5.3.

[4] The assumption that A and ρ are constant is verified if the books are handled with care so as not to pinch them, and no air bubbles or other heterogeneities disturbs the saline inside the slots.

Figure 5.4(b) is a plot of the relative current difference, defined as $\frac{|i_j - i_0|}{i_0}$, where the current are measured at the pulse onset, when they are proportional to the resistors, as a function of the relative resistance difference. This notion of relative current variation may be confusing. Practically: a variation of 20% means that if $100mA$ are fed through the cathode, $40mA$ will come out of one anode, and $60mA$ out of the other.

5.2.3.4 Conclusion of preliminary imbalance experiment

The theoretical development of section 5.2.3.2 led to the unexpected conclusion that for long enough pulse widths the current in each branch become proportional to a ratio of capacitors without influence of the resistors. This was verified qualitatively during the experiment. The relative current imbalance ($\frac{|i_1 - i_2|}{i_1 + i_2}$) is dominated by the relative resistance difference at the pulse onset, then the influence of the relative capacitance difference becomes progressively dominant. The other outcome of these offset measurements is the demonstration of the importance of the offset, and resistance imbalance in general, on the current difference between the two branches of a tripole. The cathode offset may be limited by controlled production of the electrode books and is not expected to cause such large impedance variation. However, other factors, both geometrical (electrode surface irregularities or electrode surface area inequalities) and physiological (connective tissue growth and heterogeneity in the slot) will contribute to the overall imbalance. Assuming little capacitive imbalance, the anodal currents difference will be larger at the pulse onset. In most applications the relative resistance imbalance is not expected to exceed 20%, corresponding to a current imbalance of 20%, or a current division of 40% in one branch, 60% in the other. This suggests that longer pulse widths should be favoured over shorter, more intense, pulses as the current division will be closer to the 50-50 of a perfect tripole.

5.3 Instrumentation and experimental setup

5.3.1 Animal

The female frogs (*rana pipiens* and *xenopus*) were decapitated and pithed prior to dissection. The sciatic nerves on both sides were exposed, from the spinal cord to the knee (common peroneal branch). A thread was then tied at both ends to avoid losing the axoplasm. The threads were also used to handle the nerves as they should be touched as little as possible to preserve their integrity. From the start of the dissection, the nerves were kept moist with amphibian Ringer solution [5] at room temperature. The same care was taken after removal from the body. The explanted nerves were 80 to 100mm long, with a diameter of 1mm at the spinal end and about half of that below the knee. Each experiment spanned two days (one day per nerve) as frog nerves carefully handled and kept in Ringer remain excitable for up to 36 hours (see section 5.6.1.3 on page 107).

[5] In mM: $NaCl$ 111, KCl 2.5, $CaCl_2$ 1.8, $MgCl_2$ 1, HEPES 5, glucose 10, pH adjusted to 7.4 with $NaOH$ [Flores et al., 1996; Moore, 1911]

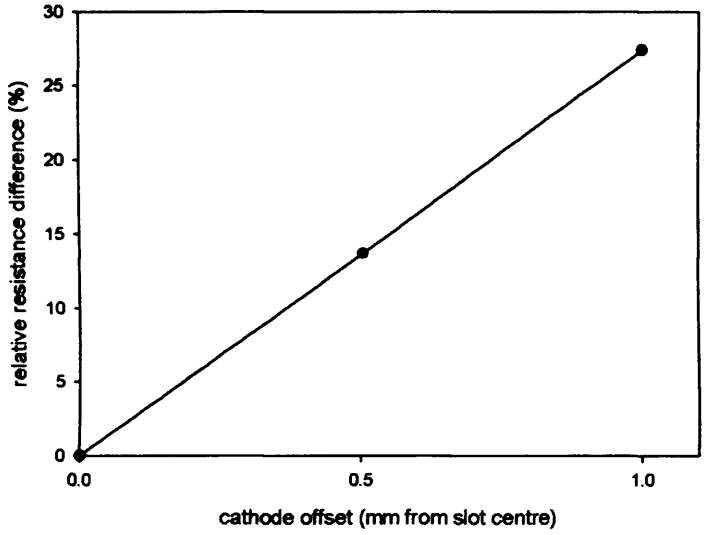

(a) Relative resistive imbalance $\left(\frac{|R_j - R_0|}{R_0}\right)$ as a function of the cathode offset, calculation not measurements.

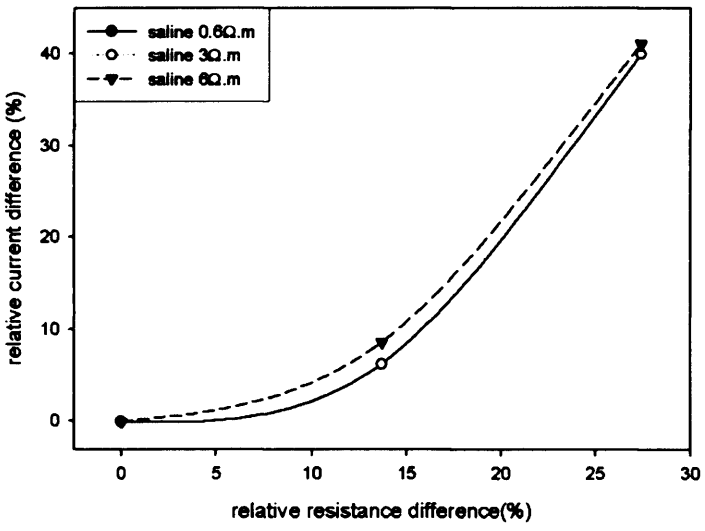

(b) Percentage of extra current measured in shorter anodal branch at pulse onset as a function of relative resistance imbalance $\left(\frac{|R_j - R_0|}{R_0}\right)$. The curves for saline resistivity $0.6\Omega.m$ and $3\Omega.m$ overlap.

Figure 5.4: Influence of book asymmetry on resistive imbalance and current distribution between the three electrodes of a LARSI book-electrode.

5.3.2 Book electrode

The book for this experiment series was also purpose-built by Finetech Medical Ltd. It is not one of those used for the preliminary experiment and has no noticeable offset. It is similar in size to those used for the LARSI, see fig. 5.5, but only has 6 separate U-shaped platinum electrodes, 0.5mm wide, independently connected to 6 wires using two Cooper cables [Donaldson, 1983]. In this way, only two of the slots contain electrodes, used as two outer anodes and one central cathode.

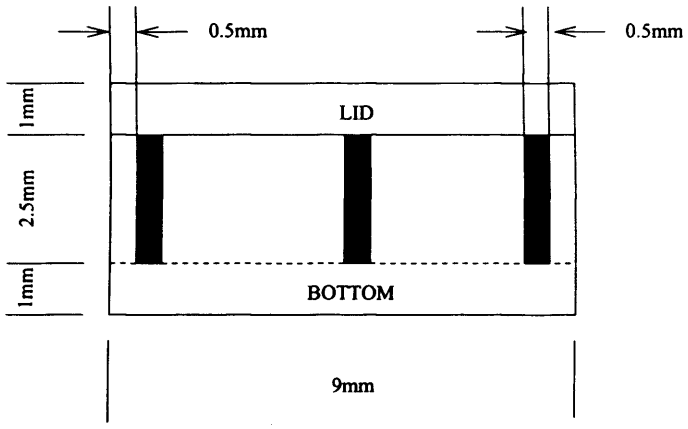

(a) Lateral view.

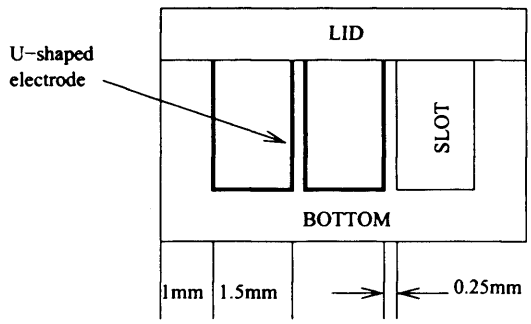

(b) Front view.

Figure 5.5: Book electrode used for the experiments.

5.3.3 Stimulator

The stimulating pulses were produced by a purpose-built stimulator described in chapter 8. Very briefly, the pulses are charge balanced, their shape is either rectangular, or rectangular with an exponential decay. Their width is adjustable up to nearly 3ms. The total current amplitude is adjustable with a potentiometer up to 10mA (maximum load: $2k\Omega$). It has two anode connections and the ratio of their current is controlled in eleven discrete steps (anode1-anode2: 100-0, 90-10, 80-20,..., 50-50, ..., 0-100).

5.3.4 Experimental bath

A two-chamber experimental bath (pictured in fig. 5.6) was built for the experiment. The chambers are separated by a metal wall which is connected to a stainless steel plate covering the floor and the back of the stimulating chamber. This metal connection can be used as a distant electrode, or connected to the oscilloscope ground to limit the artifacts and interferences (see section 8.2.6). On both ends of the bath is a clamping device used to hold the thread tied at the nerve end (as explained in section 5.3.1, the threads are used to handle and secure the nerve as it should be touched as little as possible). The clamps positions are adjusted with precision screws that allow for a fine tuning of the nerve tension [6].

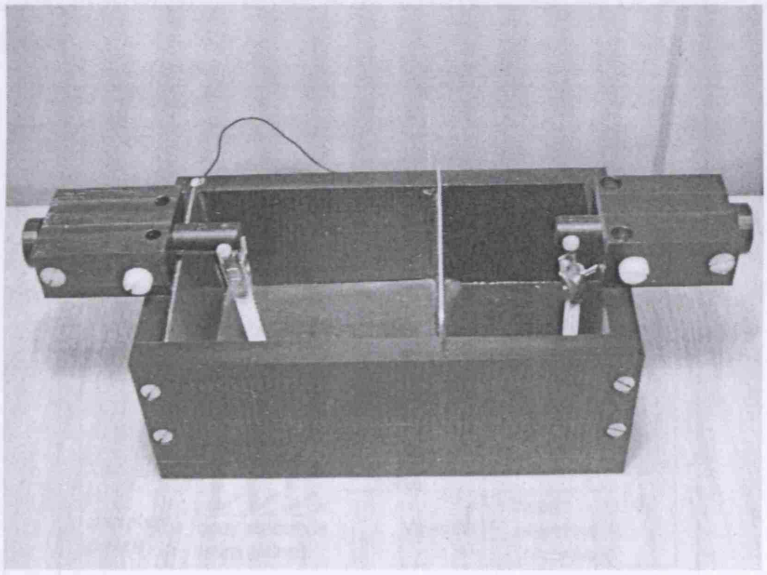

Figure 5.6: Experimental bath with stainless steel plate forming the wall and covering the bottom of the left cavity, precision adjustment screws and clamping devices visible on both sides.

5.3.5 Other apparatus

To carry the neural signals, a pair of home-made platinum hook electrodes was used. It was connected to a WorldPrecision ISO-DAM8A amplifier (see appendix ??). After amplification (variable gain, set in these experiments to 100 or 1000), the signal was displayed on an oscilloscope and recorded onto DAT tapes. The two anode signals were also recorded on the tape, and one of them was displayed on the oscilloscope screen. The current to that anode was evaluated from the oscilloscope trace, and the current to the second anode could be evaluated based on the setting of the stimulator. The cathodal current was given by the sum of both anodal currents. The DAT tapes were used afterward to review key events and acquire the data to plot the waveforms presented in this chapter.

[6] Overstretching the nerve increases its threshold. This may go unnoticed as the nerve still produces CAP, yet the results will be incorrect as the threshold has been artificially raised.

5.3.6 Setup

The nerve was mounted in the two-chamber bath as shown in fig. 5.7. Using the precision screws, the tension in the nerve was adjusted to hold it just straight (rather than bowing at the middle) without over-stretching it. On the stimulation side, it was placed in the central slot of a book (fig. 5.5) immersed in Ringer solution. On the recording side, it was resting, in the air, on the hook electrodes connected to the amplifier and the signal was displayed on an oscilloscope and recorded. It was kept moist with Ringer solution, and care was taken to avoid shorting the hooks with the formation of a drop of solution.

The current pulse was rectangular, biphasic to ensure charge balance, and the frequency fixed at 20 Hz to avoid excess fatigue of the nerve (as advised by Dr. Jarvis of Liverpool University).

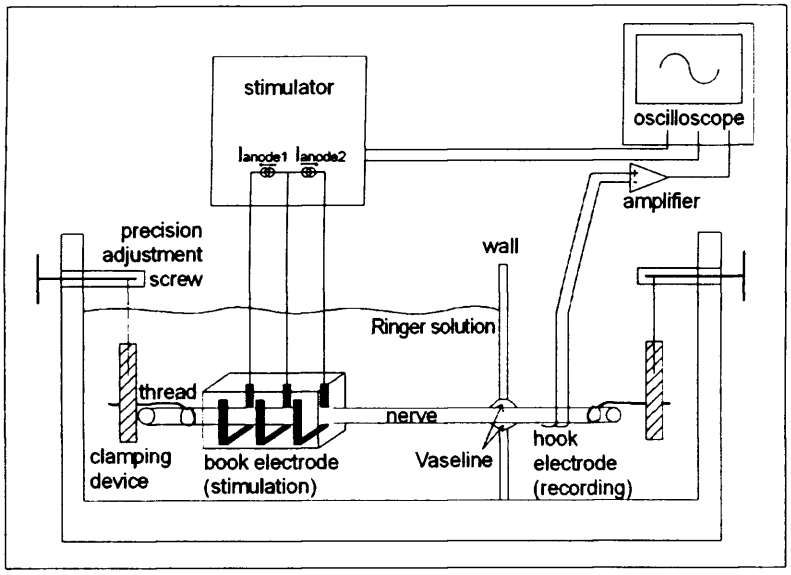

Figure 5.7: Experimental setup, for clarity only the central slot is shown and the DAT recorder is hidden.

5.4 Method

These experiments were conceived to investigate the occurrence of cross-talk and test a technique to prevent it. To give a general view of the experiments series, the basic ideas will be explained in a few lines before reviewing the methods in detail. A frog sciatic nerve was placed in the central slot of an electrode book. It was then stimulated first via the electrodes of that central slot only (SLARSI direct stimulation), then via the electrodes of the adjacent, outer, slot (SLARSI cross-talk stimulation)[7]. The CAPs were recorded, analysed separately then compared. Although the basic concept is simple, the results are numerous and the discussion at times complex. To avoid confusion the results and discussion sections have been subdivided in direct activation and

[7]LARSI situations, with all four anodes active at once were also studied, as explained in section 5.4.5.

cross-talk activation and inter-leaved. The sections following this common methods section will thus be: results for direct activation (5.5), discussion for direct activation (5.6), results for cross-talk activation (5.7) and discussion for cross-talk activation (5.8) followed by a general conclusion (5.9) and some further considerations (5.10).

5.4.1 Filtering and averaging

The amplifier (World Precision, see appendix ??) is fitted with a low pass filter of adjustable cut off frequency (0.1, 0.5, 1, 5 or $10kHz$). Yet, even with this, the signal to noise ratio of the raw action potentials was sometimes rather poor, which made threshold determination slightly subjective. Averaging, using the built in function of the oscilloscope, was introduced in such cases to confirm the threshold estimation. During the experiments, the amplified data was recorded on a DAT tape, and short sequences of interest were loaded to the pc (sampling frequency $250kHz$ default). Post processing consisted of a running average using $100\mu s$ windows and a sampling frequency of $50kHz$. More complex filter algorithms were tested and rejected as they offered little improvements while complicating noticeably the data manipulation.

5.4.2 Control of the anodal current imbalance

The slots are fitted with three independent electrodes, connected as a central cathode flanked on each side by an external anode. The stimulator is equipped with a rotary switch that provides a discrete control of the current division between the two anodes. This allows evaluation of the effect of tissue growth, geometrical asymmetries and other uncontrolled parameters altering the theoretical symmetry of the book by imposing a known current imbalance between the two halves of an active slot.

5.4.3 Stimulus: thresholds and pulse width

The threshold is the stimulus amplitude (for a fixed pulse width) at which a CAP can just be seen on the oscilloscope screen. In these experiments, it was found by increasing the amplitude manually until the trace displayed the characteristic waviness of a CAP. Once a first CAP had been triggered, its amplitude increased a little (for a constant stimulus) then stabilised. Lapicque [1926, page 79], reported the occurrence of trigger hysteresis which is probably related to this increase. Once a CAP is clearly present (muscle twitches recorded on a "myograph"), the stimulus amplitude is decreased and the value at which the CAP disappears is noted. If the stimulus amplitude is then increased, the "upward" threshold is noticeably higher than the "downward" value noted previously. In other words: there is a period of higher excitability after the firing of a CAP (called supernormality in Erlanger and Gasser [1930]; Gasser and Erlanger [1930]; Gasser and Graham [1932]; Graham [1934]; Swadlow and Waxman [1975].) This period is much longer than the refractory periods ($2ms$ [Kaufmann et al., 1996]). In the experiments presented in this chapter, the stimuli were periodic, so the nerve was kept in a high excitability state once a first CAP had been triggered. The CAP amplitude for a constant stimulus rose for a few seconds, then fatigue of the nerve

eventually supplanted this effect and the CAP decreased slowly. A variation of 25% of amplitude was not unusual for supramaximal CAPs. With hindsight, all thresholds should be recorded for the same direction of stimulus variation. This was not the case here, but the error introduced is small compared to that introduced by ambient noise pick up at threshold, and by fatigue at higher stimulation levels.
Intuitively, the thresholds for cross-talk activation are expected to increase as the tripole becomes nearly ideal (i.e. imbalance tending toward 50-50) as the current should be more contained inside the slot. Since most sets of recordings aimed at comparing direct and cross-talk stimulation, the pulse width was often set to $2.8ms$ (the longest pulse width for the stimulator) to minimise the cross-talk thresholds and record cross-talk CAPs for more imbalance positions. With such long pulses, the direct activation thresholds were sometimes very low, only two to three times the ambient noise. In such cases, the precision on the direct activation thresholds was traded for more reliable data on cross-talk activation.

5.4.4 Latencies

The action potential's latency is defined as the time delay between the onset of the stimulation pulse and the maximum of the first peak of the CAP. This peak may be positive or negative depending on the connection of the hook electrodes to the amplifier. Latencies were recorded for both direct and cross-talk stimulation, at threshold, for fixed CAP amplitude and for constant stimulus.

5.4.5 Electrodes connection: LARSI and SLARSI model

Despite the basic introduction to this method section where only the SLARSI cross-talk situation was mentioned, two configurations are in fact of interest: a SLARSI-like situation, where only the anodes in the active slot convey the current; and a LARSI-like simplified [8] situation where each anode of the central slot is paired with the corresponding anode in the adjacent, outer, slot. By working with pairs of anodes, the control of the imbalance is retained. On fig. 5.8, the switches S_1 and S_2 select the SLARSI or LARSI setup, while the multipole S_3 changes between direct and cross-talk connection by switching the current to the central or outer slot respectively. In both situations, the threshold was evaluated for every position of the imbalance rotary switch.

5.4.6 Cross-talk ratios

With the nerve in the central slot, a first series of measurements was performed to record the threshold for activation by the electrodes in the central slot (hereafter referred to as the *direct activation threshold*). To study the cross-talk threshold, current pulses were sent to the outer slot [9], and their amplitude increased until compound action potentials from the nerve (in the central slot) were recorded at the hook electrodes.

[8] Simplified situation because in the LARSI the anodes of 12 slots from four different books are connected together and may contribute to the cathodal current.

[9] With either the two anodes from the outer slot or all four anodes (central and outer slots) connected together depending on whether a LARSI or SLARSI connection scheme was tested.

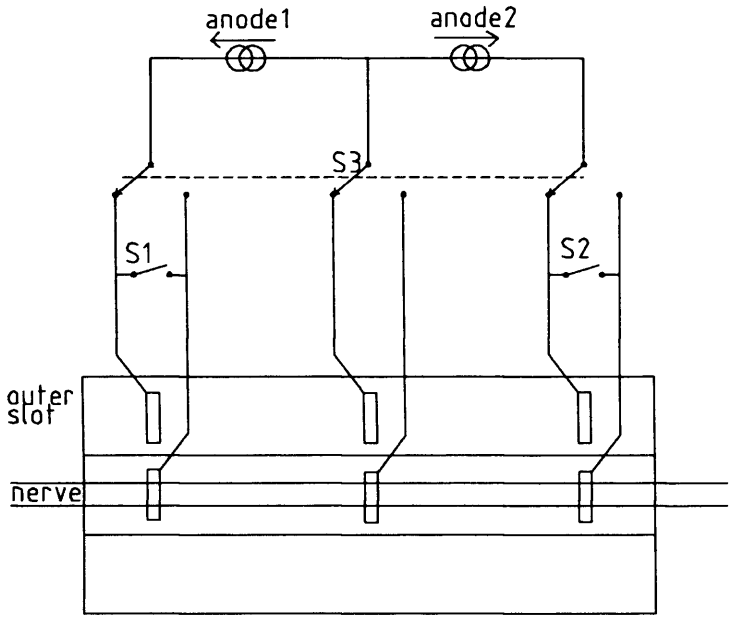

Figure 5.8: Electrode connections with the two current outputs of the stimulator. SLARSI situation: S1 and S2 open; LARSI situation: S1 and S2 closed. Direct or cross-talk stimulation selected with switch S3.

When no CAP was elicited, even at the highest amplitude (above $10mA$ at the cathode), no threshold was recorded and the imbalance was moved to the next position. These measurements were then normalised to the direct activation threshold to obtain *cross-talk ratios.*

5.4.7 Cross-talk distances

Cross-talk ratios can only be evaluated when the nerve is in a slot since the direct activation thresholds are required. Yet a nerve outside a book will also experience cross-talk activation in the vicinity of an active slot.

The nerve was setup in the bath, held by the threads as previously, but it was not laid in a slot. Instead, the book was placed alongside it, both axes parallel. The electrodes of the outer slot, which was the nearest to the nerve, were connected to the stimulator. The stimulus was maximum, i.e. $2.8ms$ pulse width and largest cathodal current (10mA). Compound action potentials so elicited were recorded using the hook electrodes and amplifier and displayed on the oscilloscope as before. For each position of the imbalance switch, the maximum distance between the book and the nerve, at which a CAP could still be elicited was recorded. These measurements were only performed for one vertical position of the book as the height adjustment was difficult. The height was that of the book's floor so that the vertical positions inside and outside the book were comparable.

After the maximum distances had been recorded for a book parallel to the nerve, a similar procedure was followed with the book's axis perpendicular to the nerve. Again, maximum activation distances were recorded for all imbalances, using the highest stim-

ulator output. With the book perpendicular, an extra experiment was performed to test the theory. Each of the three electrodes in one slot was used, in turn, as a cathode, with a large distant anode in the bath, and the threshold for stimulation was recorded.
Due to the difficulty in setting a repeatable angle between the nerve and the slot axis, the only positions studied were for the book parallel or perpendicular to the nerve. The thresholds for activation outside the slot were tested once for other angles, see below.

5.4.8 Threshold variations

The nerve contact with both the book and hook electrodes can noticeably alter the CAP recordings, hence the shape of the strength-duration curve. To limit the influence of these experimental parameters, care was taken to select sections of the nerves relatively free of connective tissue and blood vessels and to lay them in the slot in similar manner for each experiment.
Before recording the cross-talk ratios, a series of experiments was performed to evaluate the influence of the parameters described hereafter.

Local membrane conductivity and electrode contact:
Different portions of the same nerve were stimulated and the direct activation thresholds were recorded for each alternative position. As the nerve was moved, the contact with the electrode was altered. This influence cannot be dissociated from that of the local conductivity change.

Time and nerve aging:
The nerve was placed in the bath for a classic cross-talk experiment. Both direct and cross-talk activation thresholds were recorded. The setup was then left untouched for 90 minutes (the end resting in air on the hook electrodes was kept moist at all time). A second set of measurements was performed after that delay, to assess the influence of time on the thresholds and ratios. The same nerve was re-used after a night in refrigerated Ringer solution. It was re-positioned as it had been the previous day, and a third set of measurements was recorded. Here again, besides nerve degeneration, the electrode-nerve contact will influence the thresholds.

Nerve straight or bent:
The direct activation thresholds were recorded with the nerve straight inside the slot, running parallel to the walls. Then the nerve was loosened to avoid overstretching and the book rotated by 30^o (see fig. 5.9). Care was taken to maintain the same portion of the nerve inside the slot. The tension on the nerve was adjusted and the new thresholds were recorded.

Slot insulation:
Any leakage current from the slot (through gaps between the silicone walls and the lid) will influence the cross-talk ratios. To highlight the importance of an adequate closing system for the book during operation, one set of usual cross-talk experiments was run with a poorly sealed lid. The lid was then glued closed with silicone rubber and the direct and cross-talk activation thresholds were recorded for comparison. Since the

book had to be taken out of the bath to glue the lid, it was not possible to replace the nerve in exactly the same position. The parameters discussed previously will therefore have some influence on these results.

Angle between nerve and slot axis:

Cross-talk activation thresholds for the nerve running parallel to the slot, yet outside of it, were recorded. The book was then rotated by about 22.5^o, the thresholds were recorded, and the book was rotated a further 22.5^o to give a third series.

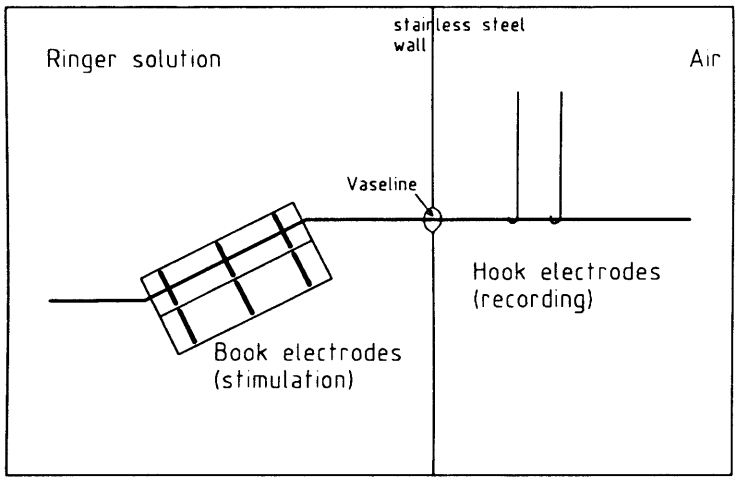

Figure 5.9: Book electrode rotated by 30^o to bend the nerve. For clarity the unused third slot is not drawn.

5.5 Results for direct activation

5.5.1 Direct thresholds

5.5.1.1 Strength-duration curves for different imbalances

Figure 5.10 shows the strength-duration curves for direct activation for the eleven different imbalances. The longest pulse width the stimulator could deliver was $2.8ms$, which was slightly too short to reach the rheobase. Since the rheobase could not be experimentally evaluated, neither could the chronaxie (which is defined as the threshold at twice the rheobasic strength, see section 2.2.1). Rather, the pulse widths were chosen to span the "usable" range, i.e. from the longest available, to the shortest for which some cross-talk results could still be recorded. On subfigure 5.10(a) all the curves for the 11 imbalances are plotted. Subfigure 5.10(b) shows the curves for imbalances 50-50 to 0-100 (i.e. when the anode furthest from the recording hook electrode, called the proximal anode, is dominant), to illustrate that the thresholds increase progressively from dipolar to tripolar stimulation [10]. Figure 5.11 illustrates the difference in thresholds for symmetrical imbalances (100-0 & 0-100, 90-10 & 10-90 and 60-40 & 40-60), the thresholds for distal [11] anode dominant are always higher. The tripolar

[10] A similar plot was obtained with the distal anode dominant curves.

[11] The distal anode is the anode closest to the recording hook electrodes.

Table 5.1: Chronaxie and rheobase for the eleven direct activation strength-duration curves, evaluated from hyperbola and exponential interpolation curves.

Imbalance	Hyperbola $i = r(1 + \frac{c}{pw})$			Exponential $i = \frac{r}{1-e^{\frac{-pw*ln2}{c}}}$		
(distal - proximal)	c (μs)	r (mA)	rms error (mA)	c (μs)	r (mA)	rms error (mA)
0 - 100	715	0.46	0.11	394	0.60	0.16
10 - 90	632	0.51	0.09	355	0.66	0.15
20 - 80	596	0.53	0.12	341	0.69	0.18
30 - 70	598	0.54	0.10	341	0.69	0.17
40 - 60	549	0.56	0.10	318	0.72	0.17
50 - 50	537	0.57	0.12	314	0.72	0.19
60 - 40	633	0.49	0.10	357	0.64	0.16
70 - 30	581	0.51	0.12	335	0.66	0.18
80 - 20	575	0.50	0.10	331	0.64	0.11
90 - 10	616	0.46	0.10	350	0.59	0.15
100 - 0	630	0.44	0.09	356	0.57	0.14

curve is added in fig. 5.11(a) for comparison. A least mean square interpolation of the data was performed using both the hyperbola and exponential equations introduced in section 2.2.1. Figure 5.12 presents three plots comparing the interpolated curves with the recordings [12], for both dipolar cases (fig. 5.12(a) and fig. 5.12(b)) and for the true tripole (fig. 5.12(c)). Table 5.1 shows, for both interpolation curves, the calculated chronaxies and rheobases (with rms error) for the 11 imbalances.

5.5.1.2 Influence of local conductivity and electrode contact, cut-off branches, position in the slot, time and nerve aging

A note on noise level:

As the aim of these experiments was to elicit cross-talk CAPs which in SLARSI mode have a very high threshold, the pulse width was set to the stimulator's maximum. To compare cross-talk thresholds with direct activation thresholds, the same pulse width was used for direct stimulation. In this case however the thresholds were so low that the noise amplitude sometimes reached 50% of the stimulus, making it difficult to evaluate the cathode current at threshold. The results presented here have been selected for their higher signal to noise ratio, yet the precision on the threshold readings is limited to ±25%.

Figure 5.13 presents 4 sets of direct activation thresholds, all measured on the same

[12]The curve joining the data points is a spline generated by the plotting software.

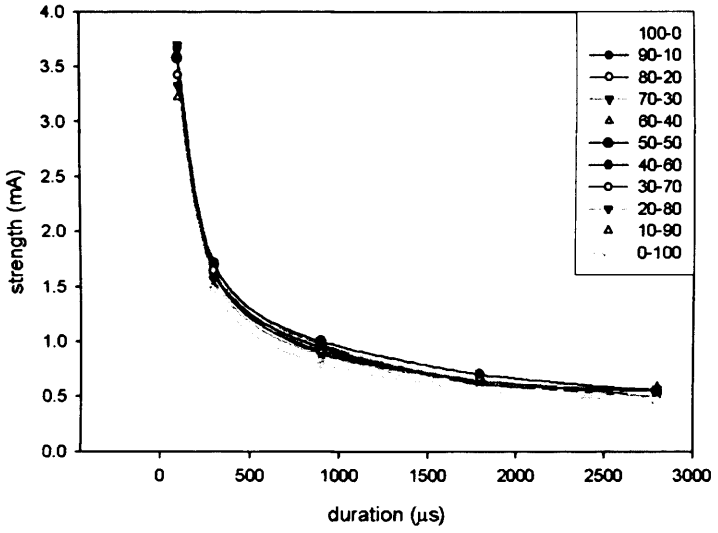

(a) Strength-duration curves for 11 imbalances.

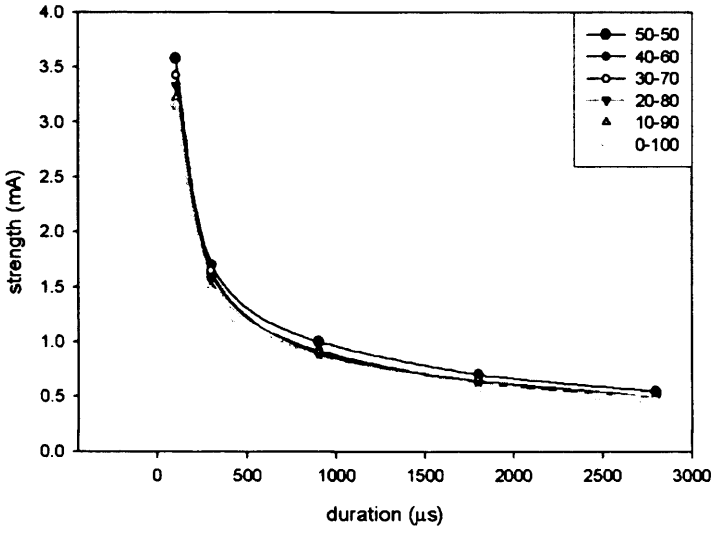

(b) Curves for imbalances 50-50 to 0-100, proximal anode dominant (furthest from the recording electrodes).

Figure 5.10: Strength-duration curves for direct activation of the xenopus sciatic nerve with a book-electrode, general overview.

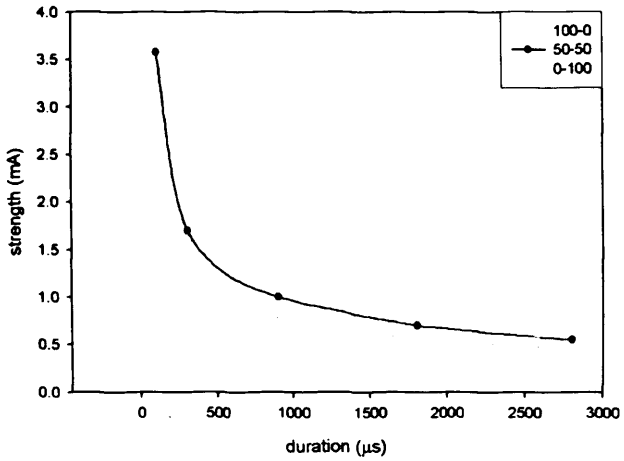

(a) Curves 50-50 (tripole), 100-0 and 0-100 (dipole) for comparison.

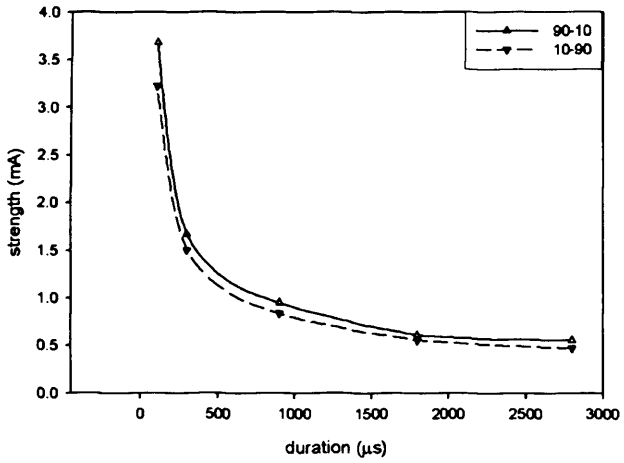

(b) Curves for symmetrical imbalances 90-10 (anode nearest to the recording electrode dominant) and 10-90 for comparison.

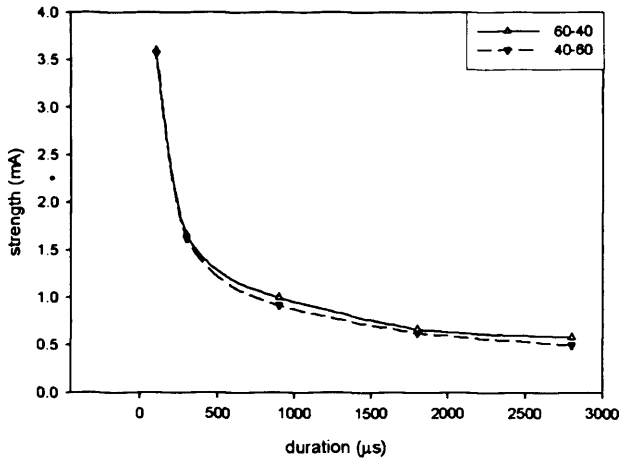

(c) Curves for symmetrical imbalances 60-40 and 40-60 for comparison.

Figure 5.11: Strength-duration curves for direct activation of the xenopus sciatic nerve with a book-electrode, comparison of symmetrical imbalances.

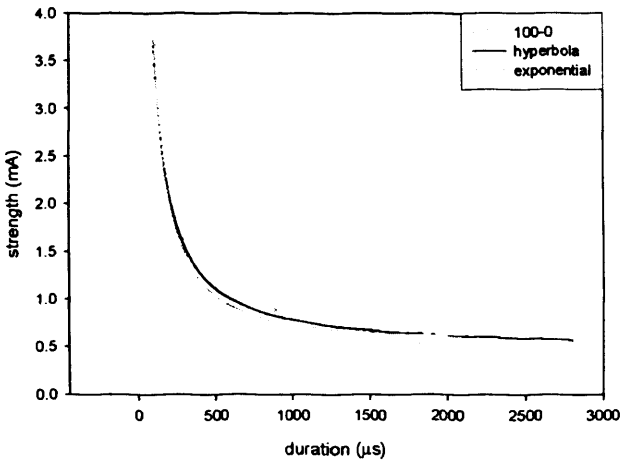

(a) Imbalance 100-0 (dipole), distal anode dominant (nearest to the recording electrodes).

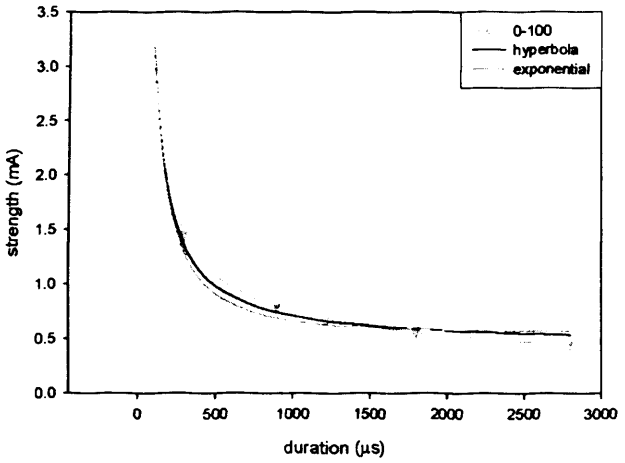

(b) Imbalance 0-100 (dipole), proximal anode dominant (furthest to the recording electrodes).

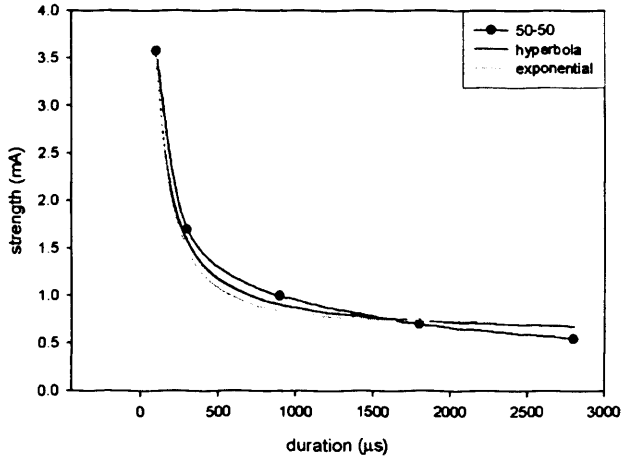

(c) Imbalance 50-50, tripole.

Figure 5.12: Strength-duration curves for direct activation of the xenopus sciatic nerve with a book-electrode, comparison with interpolated curves using either of the hyperbola or exponential equations introduced in section 2.2.1.

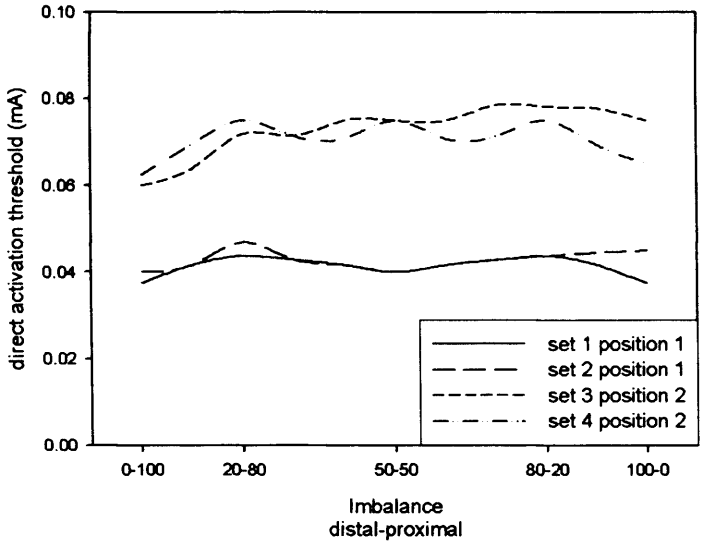

Figure 5.13: Variation of direct activation thresholds with book at two different positions along the nerve.

nerve, but with the book at two different positions. Sets 1 and 2 were recorded first (delay 45 minutes), then the book was moved $20mm$ backwards, toward the thick, spinal, end of the nerve, and sets 3 and 4 were recorded (delay 90 minutes). The nerve was fairly clear of blood vessels. The two main differences between the two positions were: nerve thickness (the nerve diameter increases from 1 to 2) and the presence of a cut-off branch [13] inside the slot in position 1. Prior to the recording of these results, the threshold was tested at a few different positions along the nerve and it was found to triple over the $50mm$ of available nerve length. It is worth noting here that moving the nerve in its slot, without changing the position, could also lead to noticeable changes in the threshold. For the curves of fig. 5.13, the change in the position happens together with a change in the contact with the electrodes.

Figure 5.14 presents thresholds for direct activation recorded on two separate occasions (with two different nerves). Both subfigures each show a selection of curves recorded using one nerve over two days of measurement (nerve kept in refrigerated Ringer solution overnight). The position of the slot (hence the contact with the electrodes) was different for each curve in the sets, both of which span about 24 hours.

5.5.1.3 Influence of nerve straightness

Figure 5.15 presents three sets of direct activation thresholds. The data for the curves labeled "straight" and "bent" were recorded without delays, while those for curve "straight early" were recorded on the same nerve, some hours earlier. The bend in the nerve was formed by rotating the book, keeping the nerve in the central slot, see

[13] There are two main cut-off branches on every nerve, one branch going to the hamstrings, the other branch is the tibial part of the nerve, cut because the peroneal end is longer and easier to dissect.

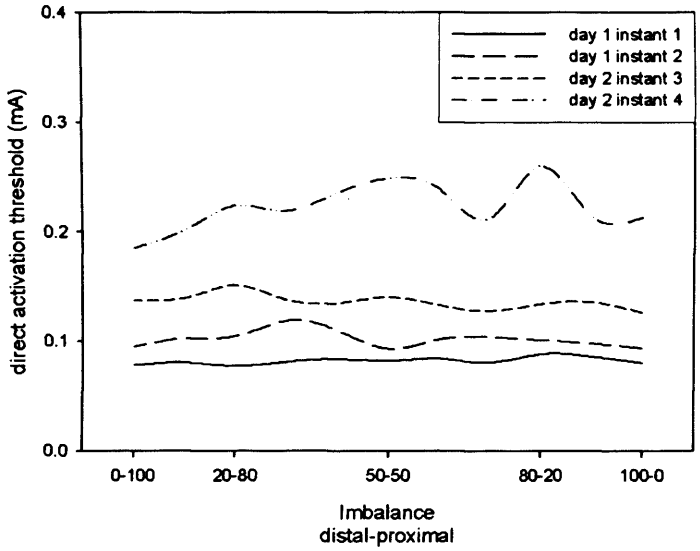

(a) Direct activation thresholds over two days, example 1.

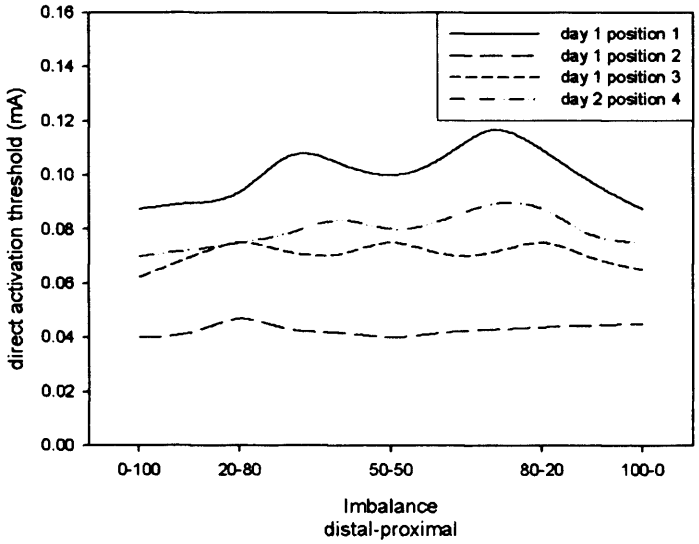

(b) Direct activation thresholds over two days, example 2.

Figure 5.14: Variation of direct activation thresholds with time, comparison of two nerves.

fig. 5.9.

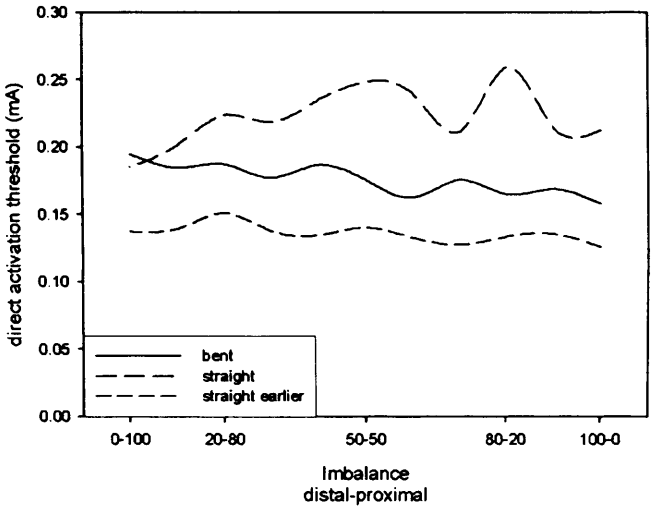

Figure 5.15: Comparison of direct activation thresholds for a nerve straight or bent.

5.5.2 Direct latencies

5.5.2.1 Effect of stimulus amplitude for a given imbalance

For all imbalances, increasing the stimulus above threshold decreases the latency. This is illustrated in fig. 5.16 for imbalances 100-0 and 0-100, the two dipolar cases. Figure 5.17 shows the same trend for a true tripole, between a CAP at threshold and a second one triggered after a 15% increase of the stimulus amplitude. Finally figure 5.18 shows the evolution of compound action potentials when the stimulus current is increased past the blocking threshold.

5.5.2.2 Effect of imbalance

At constant cathode current, increasing the contribution from the distal [14] anode increases the latency. Figure 5.19 show two sets of CAPs recorded with a constant cathodal current and different imbalance setting. In fig. 5.19(b) the CAP for setting 100-0 is just above threshold. The imbalance was then shifted to 0-100 and the CAPs were recorded, from 0-100 to 100-0. For fig. 5.19(a), which was recorded on a different day, the stimulus amplitude was increased until spanning the imbalance range led to minimal variation of the CAPs amplitude. The imbalance was then set to 0-100 and the CAPs were recorded as before. The slight decrease for increasing distal anode contribution is comparable to the variation of any CAP after a few seconds at constant imbalance and constant stimulus current. To compare the latencies, figure 5.20(a) contains only three CAPs, those for the two dipolar settings and one for the true tripole. On fig. 5.20(b), the time bases (x-axis) have been delayed to superimpose the three CAP to provide a better comparison of their shape.

[14]The distal anode is the closest to the recording hook electrodes.

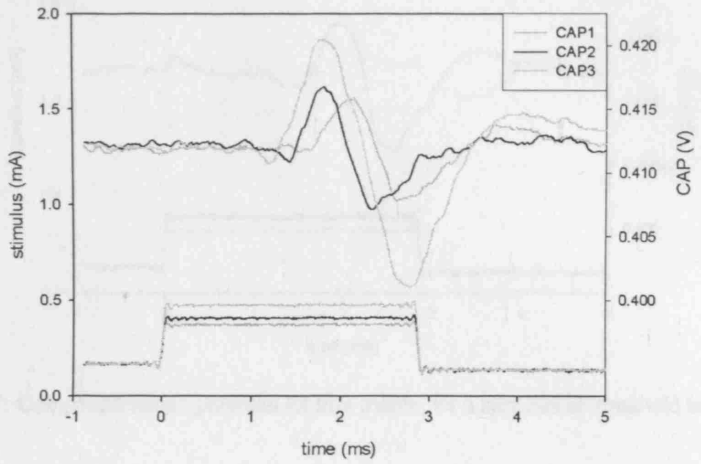

(a) Imbalance 100-0 (distal anode dominant), 10% increase in stimulus amplitude.

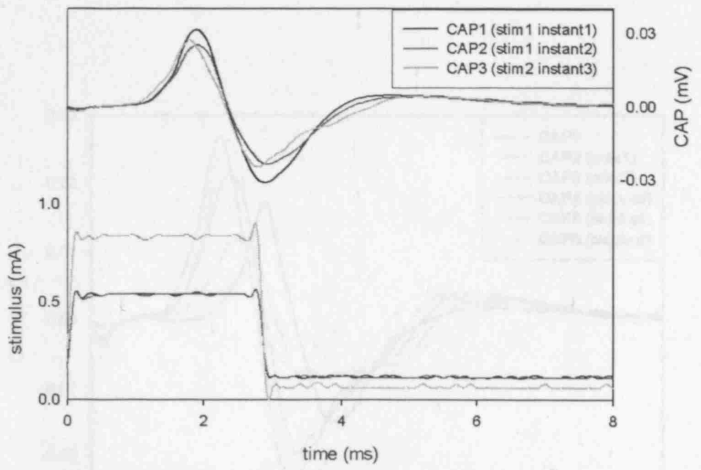

(b) Imbalance 0-100 (proximal anode dominant).

Figure 5.16: Compound action potentials for the two dipolar settings, for two stimulus amplitudes.

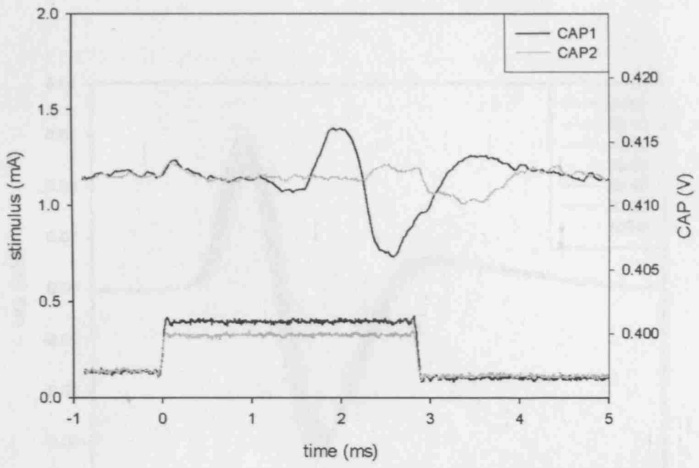

Figure 5.17: Compound action potential for true tripole, for a stimulus at threshold and one 16% larger.

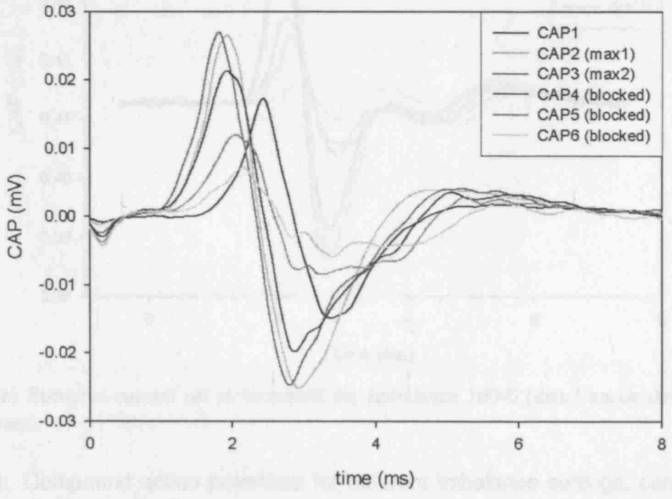

Figure 5.18: Blocking of CAP with increasing stimulus current, dipolar 0-100 setting (proximal anode dominant).

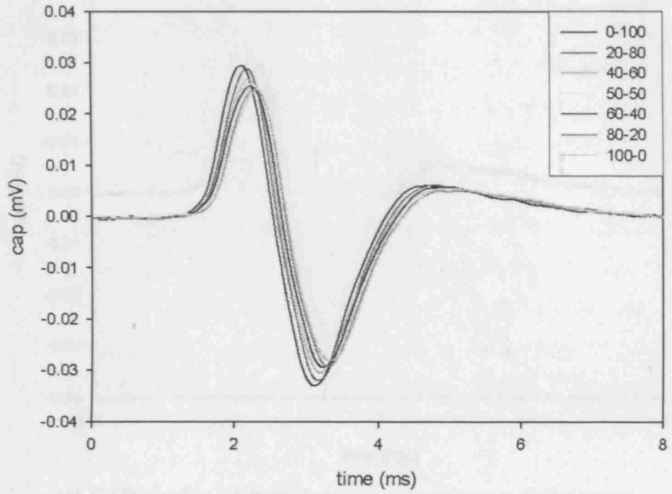

(a) Supramaximal CAPs.

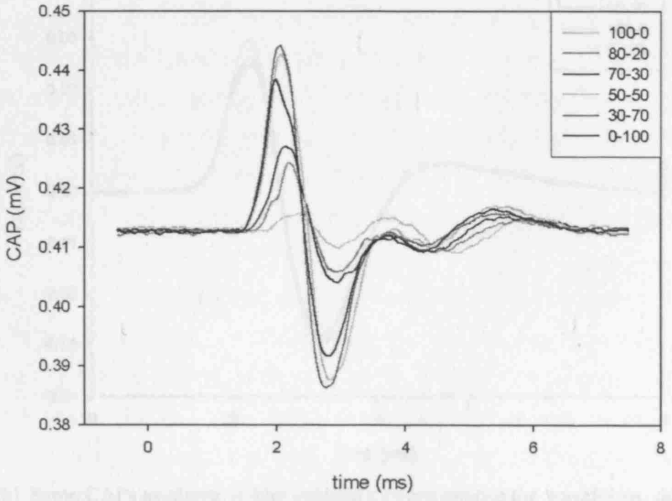

(b) Stimulus current set as threshold for imbalance 100-0 (distal anode dominant).

Figure 5.19: Compound action potentials for different imbalance settings, constant cathode stimulus current, direct activation.

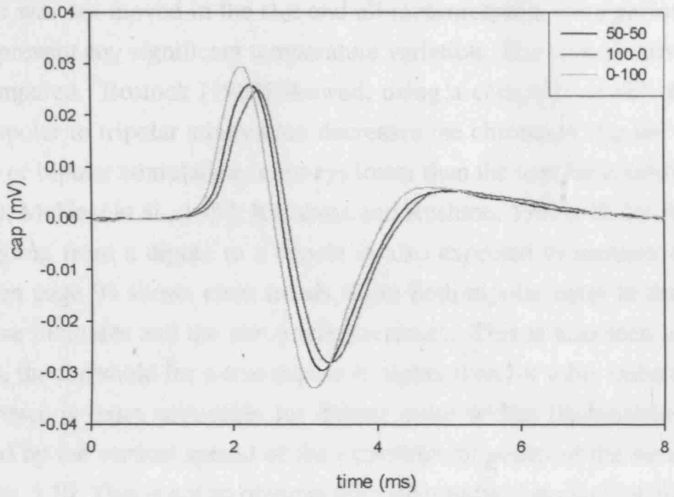

(a) CAPs for three imbalance settings at constant cathode current.

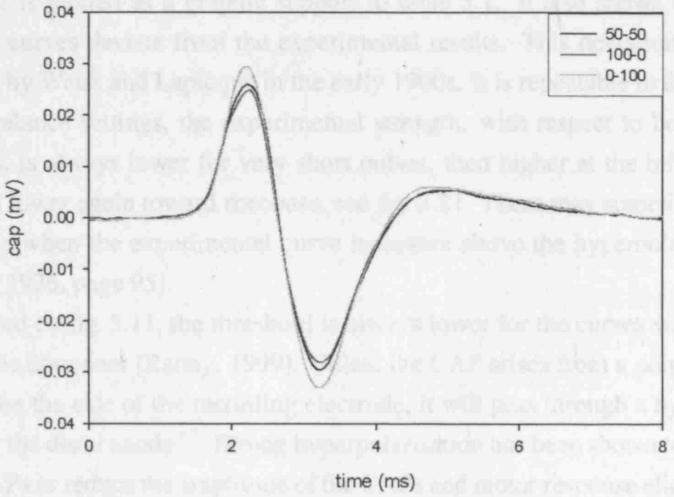

(b) Same CAPs as above, x-axis delayed to superimpose the waveforms, delay from proximal anode dipole to true tripole: $100\mu s$; delay from true tripole to distal anode dipole:$100\mu s$.

Figure 5.20: CAPs for true tripole and both dipoles with constant stimulus current. The stimulus was chosen to give the maximum CAP amplitude for the proximal anode dipole, then the imbalance was switched to true tripole and the other dipolar setting.

5.6 Discussion for direct activation

5.6.1 Direct thresholds

5.6.1.1 Strength-duration curves

The same nerve was used for all strength-duration curves (fig. 5.10, fig, 5.11 and fig. 5.12), it was not moved in the slot and all measurements were performed quickly enough to prevent any significant temperature variation. The various curves can therefore be compared. Bostock [1983] showed, using a computer model, that changing from monopolar to tripolar stimulation decreases the chronaxie. As the threshold for monopolar or bipolar stimulation is always lower than the tripolar equivalent [Deurloo et al., 2000; McNeal et al., 1987; Rashbass and Rushton, 1949a; Tarler and Mortimer, 2003] [15], going from a dipole to a tripole is also expected to increase the rheobase. Table 5.1 on page 94 shows clear trends, from both dipolar cases to the true tripole, the rheobase increases and the chronaxie decreases. This is also seen in the plots of fig. 5.10(a), the threshold for a true tripole is higher than for other imbalance settings. This difference is more noticeable for shorter pulse widths [Rubinstein et al., 2001] as indicated by the vertical spread of the experimental points of the strength-duration curves of fig. 5.10. This is not so obvious for longer pulses (as used for all other results reported in this chapter) as the increase is small and the noise level sometimes made it difficult to record threshold currents with enough precision.

Figure 5.12 is plotted as a graphic support to table 5.1. It also shows how both interpolation curves deviate from the experimental results. This deviation had already been noted by Weiss and Lapicque in the early 1900s. It is repeatable in the sense that, for all imbalance settings, the experimental strength, with respect to both interpolation curves, is always lower for very short pulses, then higher at the inflexion of the curve, then lower again toward rheobase, see fig. 5.21. There may sometimes be a last sign change when the experimental curve increases above the hyperbola at rheobase [Lapicque, 1926, page 95].

As illustrated by fig. 5.11, the threshold is always lower for the curves with the proximal [16] anode dominant [Rattay, 1999]. Unless the CAP arises from a point outside the book, and on the side of the recording electrode, it will pass through a hyperpolarised zone under the distal anode [17]. Strong hyperpolarisation has been shown to block propagating CAPs or reduce the amplitude of the CAPs and motor response elicited [Bhadra et al., 2002; Bhadra and Kilgore, 2004; Rijkhoff et al., 1994a,b; Wright and Ooyama, 1961]. It is likely that the presence of the distal anode increases the threshold for stimulation, the more so for higher potentials, hence the thresholds for imbalance 90-10 [18]

[15] Deurloo et al. [2000] uses transverse stimulation, with three electrodes forming a ring around the nerve.

[16] Reminder: the terms *distal* and *proximal* refer to the position vis-à-vis the spinal cord, or rather the spinal end in this case. As the nerves were always mounted in the bath to elicit motor impulses, i.e. with the knee end on the hook electrodes, the proximal anode is furthest from the recording hook-electrode.

[17] The anode nearest to the recording hook-electrode.

[18] The imbalance is given in the form: distal-proximal.

for example (fig. 5.11(b)) are always slightly higher than for imbalance 10-90. Taking all imbalances into account, this phenomenon was observed for about 40% of all direct thresholds recording. For all other results, the curve was symmetrical within the limits imposed by the poor precision of some direct thresholds recordings.

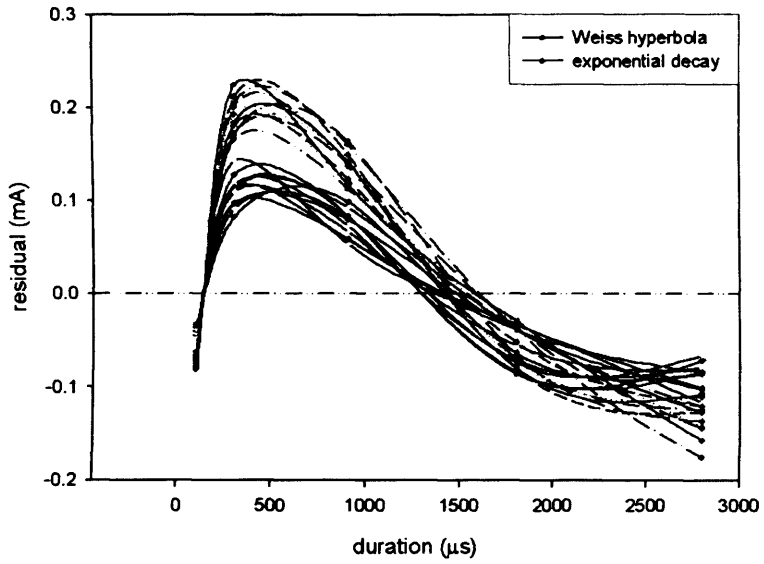

Figure 5.21: Residuals from the strength-duration curve fitting of fig. 5.12. There were two equations (hyperbola and exponential), and 11 curves (11 imbalance settings) for each equation. As only the shape of the residuals curves is relevant the imbalance ratios are not mentioned in the legend.

5.6.1.2 Influence of local tissue conductivity, position of the slot along the nerve and contact with the electrode

While the perineurium also plays a part in the resistive sheath of the frog's sciatic nerve [Krnjevic, 1954b], the epineurium is more important for these experiments as it forms a very uneven tube around the nerve. It is so loosely attached to it that it may easily be peeled off backwards [Krnjevic, 1954a; Ooyama and Wright, 1961; Rashbass and Rushton, 1949a]. This implies that the amount of connective tissue around the nerve is non-uniform and may even vary at any given position after light nerve handling. Figure 5.13 clearly illustrates these combined effects. When the nerve is left untouched, the thresholds remain nearly constant, as shown by the overlap of the two curves for each position. Yet in this case, when the position was altered, the thresholds nearly doubled. The low thresholds of position 1 are partly due to the presence of a cut off branch inside the slot, which has been shown to create a "focal zone" for stimulation in its vicinity, i.e. a zone of low excitation threshold [Rushton, 1927]. To reach position 2, the book was slid backwards, by about $20mm$. It is probable that this movement caused an accumulation of epineurium to form in the slot. This increase in connective tissue thickness, together with an unavoidable variation of the electrode-nerve contact, ex-

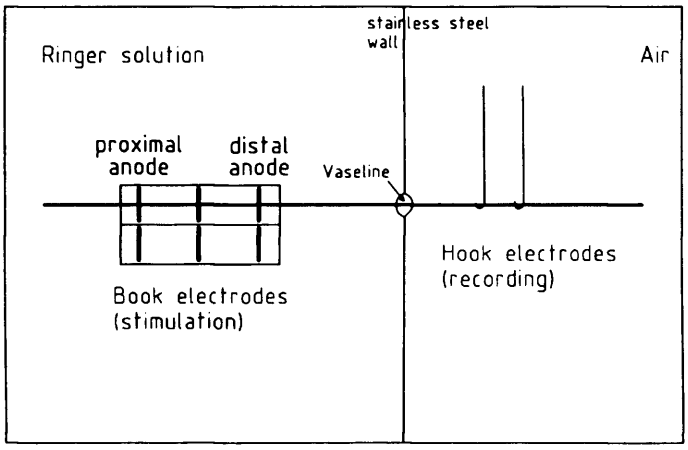

Figure 5.22: Distal and proximal anodes shown on a schematic representation of a nerve in the central slot of an electrode book, for clarity the third slot is not drawn.

plains why, the thresholds increase in the second position. A change in nerve-electrode contact by manipulating the nerve in the slot without moving it can alter the thresholds noticeably either way (tested experimentally, no curve plotted).

5.6.1.3 Influence of time and variations between nerves.

From the death of the animal onwards, the nerve degenerates slowly. Based on the data plotted in fig. 5.14(a), the thresholds seem to increase with time. This is not really conclusive as on fig.5.14(b) the first set recorded on day one has the highest threshold, the position was then altered and the threshold strongly decreased. Only the remaining three curves, recorded for different but similar positions, show an increase of threshold with time. Considering how much the direct thresholds varied with the position in fig. 5.13, the changes displayed here may be entirely accounted for by the position alteration.

The effect of time on a dissected nerve depends on the intensity of the stimulation, the handling and the storage conditions. In Parker [1933], frog sciatic nerves were transected by the illium and left in place in the body. Muscle responses to electrical stimulation distal to the cut only began to decrease after 4 to 6 days, and disappeared after 16 to 18 days. In Sollmann [1947], frog sciatic nerves were dissected with some vertebrae at the sciatic end, and parts of the gastrocnemius at the motor end (in this way the nerves were not cut). Stored in cold Ringer solution, the nerves and muscles remained responsive to electrical stimulation for 1 to 2 weeks. In Bernhart et al. [1991], *xenopus* and *rana pipiens* nerves were dissected in the usual way described in section 5.3.1 of this thesis. They were stimulated with supramaximal amplitude and a low frequency for three hours a day, for five days, and kept in Ringer solution at 3^oC between stimulation sessions. The CAP amplitude increased from day 1 to day 2, then decreased slowly to about 50% of the original value by the end of the experiment. Some days, the CAP amplitude increased noticeably at the end of the three

hours stimulation session. This might imply that more fibres were firing, yet as the stimulus was supramaximal at the beginning, this is unlikely. Rather, the protective sheath degenerated at the recording site. The nerve dries slowly as it is not immersed in Ringer, and the recording electrodes are often hooks made of small gauge metal wire, likely to cut through the sheath [19]. The impedance at the recording site decreased during the stimulation session, and the amplitude of the CAP recorded increased. This variation has little effect on thresholds determination as the appearance of the CAP is normally sharp. The conduction velocity also decreased slowly over the duration of the experiment. Theophilidis and Pavlidou [1993] continuously stimulated frog nerves in a Ringer bath (no temperature mentioned) and showed a constant CAP amplitude for 30 to 40 hours, followed by a continuous 10 hours decrease until the nerve became unreliable. Finally, Lapicque [1926, page 77], discussing a sciatic nerve and muscle preparation, writes that aging causes the chronaxie to increase and the rheobase to decrease. The chronaxie increase is in accordance with the decrease of conduction velocity reported by Bernhart et al. [1991] (inverse relationship between a fibre's chronaxie and its conduction velocity [West and Wolstencroft, 1983]) [20]. It is probable that although the rheobase decreases, the pulse width at which it is reached increases, as does the chronaxie. This might explain why the thresholds presented in section 5.5.1.2 seem to increase with time, the pulse width being slightly shorter than required for rheobase. It is nonetheless a very weak effect as, from the literature, the nerves are not expected to show noticeable signs of degeneration for the 24-32 hours of the experiments presented here.

5.6.1.4 Influence of nerve straightness

For a nerve in a uniform electric field, with its axis parallel to the current lines, a bend will create a focal zone and present a lower threshold [Rattay, 1999; Roth, 1994; Rushton, 1927, 1928a]. With tripolar stimulation, the field is not uniform along the nerve axis. If the presence of a kink lowers the threshold locally, this will only be noticeable when the bend is formed in or near the activation zone, where CAPs normally originate (it will lower the threshold or shift the activation zone toward the bend). For direct activation, the CAPs are elicited at or near the cathode (see section 5.6.2), the effect of a bend outside the nerve should therefore be negligible. In figure 5.15, the thresholds in the bent situation are comparable to those for straight nerves, even more so considering

[19] From experience, the contact with the hook electrodes becomes unreliable after half a day of recording, even when great care is taken to keep the nerve moist with Ringer throughout. Moving the hooks ahead (with respect to the CAP's propagation) of the damaged zone solved the problem, which shows that there is a localised physical alteration of the nerve.

[20] The conduction velocity is at first approximation proportional to the fibre diameter, while the threshold is invertly proportional to it [Hursh, 1939; Lussier and Rushton, 1951; Rushton, 1951; Stegeman and Weerd, 1982; Swadlow and Waxman, 1975; Tasaki, 1982]. There is thus an inverse relation between threshold and conduction velocity [21]. At equal rheobases, an increase in chronaxie is associated with an increase in threshold for all pulses shorter than the rheobasic (provided the duration at which rheobase is reached has not decreased). From this simple reasoning, an increase in chronaxie can be related to a decrease in conduction velocity.

that the position was altered by the rotation of the book. The variation in thresholds is not due to the bend, but simply to a change in local conductivity and nerve-electrode contact. A finding that was repeatedly present during the "bending" sessions is that the threshold is lower when the distal anode is dominant. Anodal hyperpolarisation, when strong enough, should cause the threshold to increase. During the straight sessions, the thresholds were either symmetrical vis-à-vis the 50-50 imbalance setting or increased slightly toward the 100-0 position, as can be seen from the various direct thresholds figures presented in this chapter. This puzzle may be understood when considering the position of the nerve inside the central slot, as shown by fig. 5.23. The nerve was slightly stretched and compressed at the distal edge of the slot as it was forced to bend. This constriction locally increased the threshold [Rushton, 1928a] and, as the CAP arises near the cathode, but on the side of the weaker anode [Rashbass and Rushton, 1949b; Rushton, 1928b, 1949], this affects the threshold for stimulation with a dominant proximal anode. Although the nerve was also bent at the other end of the slot, the situation was such that it was neither so stretched nor constricted.

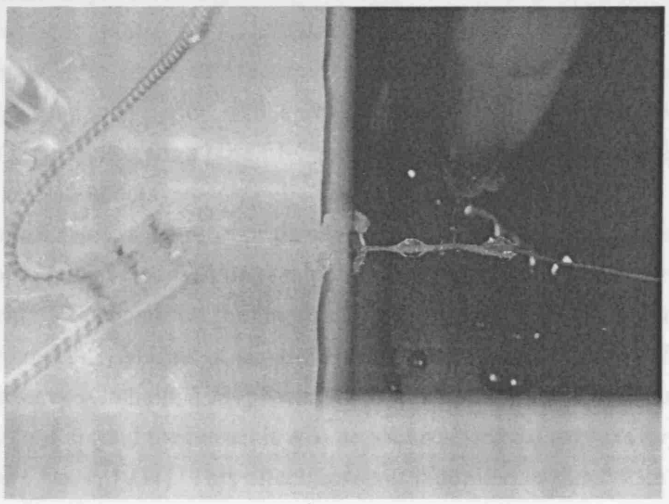

Figure 5.23: Setup to study the influence of the nerve bending at the edge of the slot.

5.6.1.5 Influence of macroscopic heterogeneity in the bath

The experimental situation is much simpler than the real case. The presence of bones and other elements in and around the spinal canal will affect the current flow outside the slot. Although no specific results were plotted, two parameters were evaluated: the presence of an insulating block in the bath and the influence of the Ringer solution level above the book.

Insulator in the bath: An insulating volume (a cylinder of about $2cm^3$) was introduced in the bath, and moved around the book. To avoid altering the position of the nerve in the slot, the insulator was not brought closer than half a centimetre from the nerve. With that limitation, no noticeable variation of the shape of the compound action

potential could be attributed to the presence of the alien volume.

Ringer solution level: For all experiments the book and nerve were immersed in Ringer solution (fig. 5.7). Decreasing the amount of liquid in the bath affects the compound action potential when there is less than one centimetre of saline above the book. All experiments reported here were performed with enough saline in the bath to consider the volume infinite for the electric field.

5.6.2 Direct latencies

5.6.2.1 Activation and propagation delays

The latency is the sum of an activation and a propagation delays.

The *activation delay* is the interval between the onset of the pulse and the rise of the action potential [Blair, 1932a; Goodall et al., 1995; Rubinstein et al., 2001]. It depends on the conditions of stimulation and expresses the need for a specific charge situation to be reached and maintained to trigger and propagate a CAP. It is probably longer for lower, just suprathreshold, stimuli [Goodall et al., 1995]. Working with a stimulus of constant amplitude, long enough to elicit an action potential, decreasing the pulse width without altering the amplitude will eventually cause the CAP to disappear. The action potential might have already risen when the stimulus was interrupted, but it needed a consolidation period which was interrupted too soon, hence no CAP propagated. This requirement for a post-trigger period makes it difficult to experimentally evaluate the activation delay.

The *propagation delay* is the ratio of the distance traveled by the action potential over the fibre's conduction velocity. The conduction velocity along a nerve fibre is not constant. Physically, it depends on the internode spacing and the fibre's diameter [Stegeman and Weerd, 1982; Veltink et al., 1989b]. Practically, it is slightly affected by the stimulation history [Graham, 1934; Swadlow and Waxman, 1975] and strongly influenced by the field around the nerve, it will be lower where the nerve is hyperpolarised [Erlanger and Gasser, 1937]. This effect however is limited in time, once the cause of the hyperpolarisation ceases to be, the conduction velocity returns to its normal value. The existence of these delays, and their variations, means that latencies can not be used to estimate where a CAP arises. CAPs rising at different sites may have a similar latency if either the activation or propagation delay is altered by the stimulation setup.

5.6.2.2 A note on amplitudes

Since the recorded CAP amplitude is strongly dependent on the recording electrodes contact with the nerve, the CAPs on different occasions (presented in the various figures of this chapter) cannot all be compared. Comparison in the following discussion was only made between CAPs recorded within a short interval, between two "Ringer wetting" (i.e. dropping some Ringer solution on the nerve to prevent it from drying) of the end of the nerve resting in air on the hook electrodes. Likewise, the stimulus amplitude required to trigger an action potential depends on the position of the nerve in the slot (amongst other parameters), the different stimulus currents, at threshold or

above, may not all be compared, there is no absolute supramaximal cathodal current.

5.6.2.3 Activation site

The latency shift between each of the three CAPs of fig. 5.20(a) (triggered by stimuli of the same amplitude) is $100\mu s$ [22] from each dipole to the tripolar arrangement (the CAP triggered when the proximal anode is dominant arrives first). The CAP for setting 80-20 or 20-80 are much closer to that triggered by a true tripole ($50\mu s$ and $10\mu s$ respectively [23]), the evolution of latencies from dipole to tripole is not linear, see fig. 5.19(a). This may a priori be due to any combination of the following factors: a different initiation site (i.e. the fibres are not all activated exactly at the cathode), a different activation delay or a different propagation delay. The three options are discussed hereafter and the reasoning is summarised in table 5.2; figure 5.22 which shows the distal and proximal anodes may be useful as a visual support throughout the following paragraph.

Since the three CAPs are similar in shape (both amplitude [24] and width, fig. 5.20(b)), it is probable that the same fibres contribute in the same manner to each of them. Hyperpolarisation (here due to the distal anode) has been shown to slow large fibres. A difference in propagation delay would result in a spread of the CAP unless all fibres are affected equally, which is unlikely. That the propagation delay may not be affected by the increasing hyperpolarisation caused by the distal anode suggests that it is the gradient of the activating function rather than the amplitude of the hyperpolarisation peak that affects the fibres (blocking or slowing down). This will be discussed further in section 5.6.2.5. The activation delay may also remain constant as the stimulus current is constant. Then the latency differences would only be due to a shift in the activation site. If it is agreed that activation takes place where depolarisation is maximal (as indicated by the activating function), then the CAP is triggered exactly under the cathode only in the case of a truly symmetrical tripole. Any current imbalance will sway the depolarisation toward the weaker anode. This alone can explain why the CAP triggered when the distal anode is dominant has a longer latency as it has to travel a longer distance than that triggered when the proximal anode is dominant. As long as the situation is somewhat tripolar, the activation site is confined between the cathode and the weaker anode (hence the relatively small latency shift from 50-50 to 90-10). In the dipolar case the depolarisation peak is not so steep as no anode increases the voltage gradient. This was already foreseen by Rashbass and Rushton [1949b]; Rushton [1928b, 1949] and is confirmed by the activating function as shown by Rattay [1999].

[22] With a conduction velocity of $36m/s$, as was measured earlier on the same nerve using two recording pairs separated by a known distance, this corresponds to a propagation difference of $3.6mm$.

[23] $50\mu s$ and $10\mu s$ correspond to displacements of $1.8mm$ and $0.36mm$ respectively.

[24] Amplitude variation over time of up to 25% of the CAP amplitude were regularly observed at constant stimulus current.

Table 5.2: Summary of discussion on activation site.

Cause	Comment or observation	Conclusion
Different initiation site	Most plausible	Activation at the cathode only for true tripole Activation site shifts towards weaker anode
Different activation delay	Unlikely with constant stimulus current	
Different propagation delay	Unlikely as the CAPs do not spread	Propagation delay not so sensitive to hyperpolarisation The blocking or slowing effect is proportional to the gradient of the activation function rather than the amplitude of the hyperpolarisation peak

5.6.2.4 Proximal anode dominant dipole

Figure 5.18 shows the effect (blocking) of stimulus amplitude for the proximal anode dominant dipole. This setting was chosen as the cathode is "in front" of the anode with respect to the action potential propagation and this should limit the influence of the anode, making the discussion simpler. Other imbalance settings, when the distal anode is active, will be discussed later (section 5.6.2.5).

From CAP1 to CAP2, the stimulus current changed from $0.42mA$ to $0.53mA$, the latency decreased noticeably, the amplitude increased yet the CAP did not spread much (only the negative peak is slightly wider). The various models of single fibre action potential presented in the literature indicate that larger, faster fibres have a lower threshold [Altman and Plonsey, 1988; Coburn, 1988; Grill, 1996; McNeal, 1976; Rattay, 1989; Rattay and Aberham, 1993; Rattay et al., 2000; Struijk, 1997]. When specifically modelling bipolar and tripolar stimulation, Shen et al. [2001] computed figure 5.24 which shows a minimum in threshold followed by an increase with larger fibre diameter[25]. Most models also predict that a fibre deeper in the nerve will have a higher threshold than a similar one closer to the electrodes. How the diameter and the fibre position in the nerve influence the threshold depends on the shape (and dimensions) of the electrodes and mount. It is possible that a slow, shallow, fibre be activated before a faster yet deeper one. This may be the case here, the CAP does not spread because even at low stimulation level both slow and fast fibres are recruited. The variation in latencies is due to a decrease of the activation delay combined with a shift in the activation site [Miller et al., 2003]. When all fibres are recruited, the CAP amplitude is maximum and a plateau is reached during which the CAP shape remains constant for increasing stimulus amplitude, see fig. 5.16(b) which shows three supramaximal CAPs. From CAP1 to CAP2 the stimulus amplitude remained constant ($0.53mA$), this illustrates the naturally occurring decrease of CAP amplitude with time (variation is 25% of CAP2). From CAP2 to CAP3 the stimulus current was increased by $0.3mA$, the amplitude changed by $0.1mV$ or 5% of CAP2 and the latency by $100\mu s$. After the plateau, blocking takes place and the CAP amplitude decreases. There is no consensus as to where the block happens [Baratta et al., 1989]. With this dipole, an hyperpolarisation peak in the activation function indicates the presence of a virtual anode between the cathode and the recording electrodes. This affects the propagation of the CAP. Some fibres are slowed down while others are blocked, hence the CAP spreads as its amplitude decreases (CAP3 to CAP6). As little is known about the activation delay it cannot be ruled out that hyperpolarisation increased it. Yet, the shift in latency can be accounted for by the blocking and slowing down of the faster fibres alone.

5.6.2.5 Distal anode dominant dipole

This setting can be related to the other dipole in the following way. When a nerve is electrically stimulated a CAP propagates in both directions (toward the recording elec-

[25] Other authors also found a mixed recruitment during experiments only [Veltink et al., 1989a].

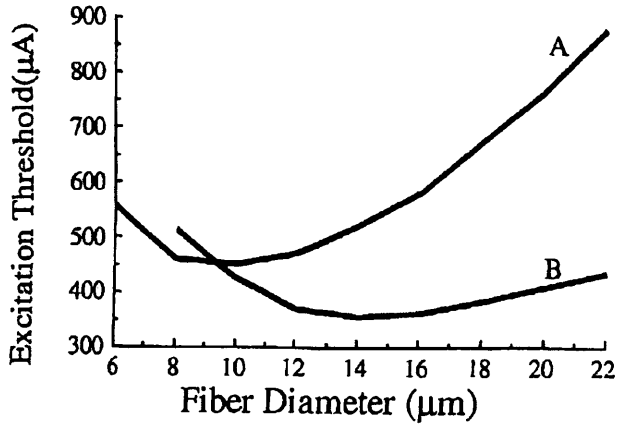

(a) Excitation thresholds with dipolar stimulation. Curve A: node of Ranvier in between the two electrodes, curve B: node of Ranvier level with the cathode.

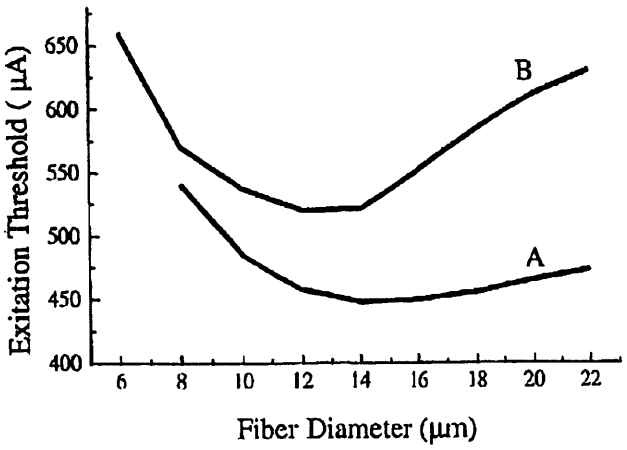

(b) Excitation thresholds with three electrodes. Curve A: true tripole, curve B: tripole with remote cathode (i.e. the sum of anodal currents is larger than the cathodal current).

Figure 5.24: Direct activation thresholds for dipolar and tripolar stimulation, reproduced from Shen et al. [2001].

trodes and toward the other end). The same fibres are therefore activated but the effect of the active anode is different whether the CAP travels away from it (proximal anode) or passes under it (distal anode). If the blocking effect discussed in section 5.6.2.4 is indeed due to the hyperpolarisation, a similar influence should be seen here but for a lower stimulus current as the anode is real, hence present from threshold. For a given submaximal stimulus, the CAP is smaller for the distal dipole (fig. 5.19(b)), indicating that some of the fibres activated near the cathode are blocked along the way, as seen on fig. 5.19(a). Yet, the CAP eventually reaches the same maximum amplitude, but at a higher stimulus current than with the proximal anode dipole. This suggests that it is not the stimulus amplitude in itself that causes the block, but rather the combination of depolarisation and hyperpolarisation. Zierhofer [2001] showed with a long mathematical development that the activating function is only representative of the reality in the first ten or less microseconds of a pulse. After the onset, a low-pass filtered version of the activating function is more suited to predict activation. The steepness of the peak of the activating function might be as, if not more, important than their amplitude. These observations are in agreement with Rattay [1999] and a review in Baratta et al. [1989] who showed (using a single fibre model) that an action potential could pass by a strong virtual anode and be blocked near the cathode (i.e. strong depolarisation is also required to cause a block). The three CAPs of fig. 5.16(a), triggered with the distal anode dipole, illustrate the various anodal effects combined. The situation is more complex than with the other dipole as the anode has an effect even at submaximal levels. From CAP1 to CAP2 the stimulus current was increased, leading to an increase in the number of fibres activated as confirmed by the proximal anode dipole results. The blocking effect increased proportionally, so that the CAP amplitude hardly changed. The CAP however shifts as the activation delay decreases. A further increase in stimulus current widens the CAP as well as increasing its amplitude (indicating that more fibres are active), see CAP3[26]. So far the results have illustrated various effects attributed to the presence of an anode (real or virtual) close to the cathode, "in the way" of the CAP. Depending not so much on the stimulus amplitude as on the gradient between depolarisation and hyperpolarisation, single fibre action potentials may be slowed down (and stretched) or completely blocked. This was perceived as a threshold increase in section 5.6.1.1. The activation delay is believed to decrease when the stimulus current increases. It may also be influenced by the presence of an anode but no conclusive evidences were found. At supramaximal stimulus amplitude, but below blocking threshold, when the

[26]The surface area of CAP3 is larger than any other which should indicate that more fibres are triggered [Accornero et al., 1977]. If the positive phases of all the single fibres action potentials at the recording electrodes are added to form the positive contribution, and all the negative phases are added to form the negative contribution, the resulting CAP will not be the succession of the positive and negative phases. Rather, its shape will depend on how much the two phases overlap. The less they do, the larger the surface area. If the hyperpolarisation slows down the regenerative process that gives rise to the action potentials, each individual action potential will be wider, and the positive and negative contribution, for a given range of conduction velocities, may not overlap so much.

CAPs are all comparable in amplitude and width, the activation delays are supposed equal and the differences in latencies are associated with a shift of the activation site.

5.6.2.6 Effect of imbalance

Figure 5.19 shows CAPs recorded with a constant stimulus current, but for different imbalance settings. It illustrates many of the effects discussed previously. From setting 100-0 to 0-100 the latency decreases as the depolarisation peak of the activating function (giving an estimate of the activation site) shifts. The CAP amplitude increases as fewer fibres are blocked when the distal anode carries a smaller fraction of the current. This is in agreement with Fitzpatrick et al. [1991], who showed, with a model of an asymmetrical tripolar cuff, that fibres are progressively blocked in the direction of the stronger anode first, then in the direction of the weaker anode. The CAP for setting 0-100 is slightly smaller than that of imbalance 30-70, showing the first signs of blocking by virtual anode. As the imbalance is reversed from 0-100 to 30-70 the virtual anode decreases and the blocking ceases, so the second CAP is a little higher.

The following reasoning was already suggested in section 5.6.2.4. For all imbalances, increasing the stimulus decreases the latency. At first approximation, the conduction velocity of a nerve fibre is proportional to its diameter [Fukushima et al., 1975; Stegeman and Weerd, 1982]. The threshold on the other hand is inversely proportional to it. It is also influenced by the position of the fibre inside the nerve. For two fibres of the same diameter, the one located deeper in the nerve will have a higher threshold. Considering whole nerve stimulation, at threshold only the larger fibres closer to the electrodes are recruited. If the stimulus is increased, smaller, slower fibres will be recruited as well as similar and larger, faster, fibres deeper in the nerve. An action potential traveling on a slower fibre will take longer to pass between the two hook electrodes. Its contribution to the nerve's compound action potential will be lower and wider (differential effect of the bipolar amplification). If the CAP amplitude increases yet does not spread, this indicates that the additional fibres recruited have a similar or faster conduction velocity at the level of the hook electrodes.

The results presented so far have been focused mainly on two imbalance settings, the two dipoles, as they are simpler yet representative of all other cases. For the dipole with proximal anode dominant, the cathode is on the recording side. At low to moderate stimulus amplitude, there is thus no hyperpolarised section of nerve between the cathode (where at first approximation the action potential originates) and the recording electrodes. At higher amplitude, the situation becomes more complex with the effect of virtual electrodes by the slot edges. In fig. 5.16(a), the two smaller CAPs are well formed yet the stimuli were kept low enough to avoid virtual electrodes. For a 16% increase of stimulus amplitude, the CAP amplitude changed by less than 1% so that the variation in latency ($330\mu s$) can only be due to a change in activation delay.

5.7 Results for cross-talk activation

5.7.1 Cross-talk activation: thresholds and ratios

5.7.1.1 General trend for SLARSI situation

As illustrated in the previous section, direct activation thresholds may vary considerably from one set of measurements to the next. The same goes for cross-talk thresholds, and the ratios do therefore cover a wide span. Figure 5.25 is a collection of cross-talk ratios computed on six different occasions (each colour indicates a different nerve), selected to show a large variation and illustrate the general trend for all cross-talk experiments.

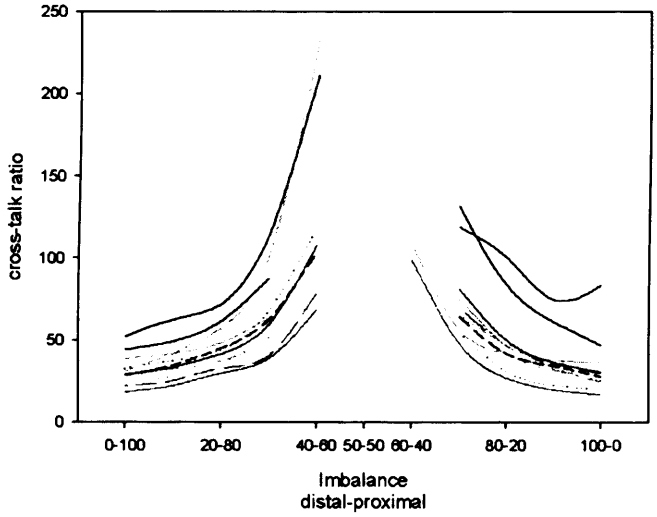

Figure 5.25: Cross-talk ratios for different anodal current imbalances in the SLARSI situation, comparison of records from six different days.

5.7.1.2 LARSI and SLARSI models

Figure 5.26 compares the cross-talk ratios computed for SLARSI-like and LARSI-like situations. The results from four different occasions have been selected for their large span of cross-talk ratios, all SLARSI curves do however display a similar shape. They are interrupted for the imbalances for which no cross-talk CAP could be triggered even at the highest intensity.

5.7.1.3 Strength-duration curves for different imbalances

On the day when the direct activation strength-duration curves were recorded, the same was done for cross-talk activation, the results are plotted in fig. 5.27. Subfigure 5.27(a) is a plot of the curves for all imbalances (for nearly true tripole there was no CAP elicited, hence no curve). Subfigure 5.27(b) compares the shape of the direct and cross-talk activation curves in the dipolar cases. The direct tripolar curve has been added to the figure for comparison. Together with the strength-duration curves, it is interesting

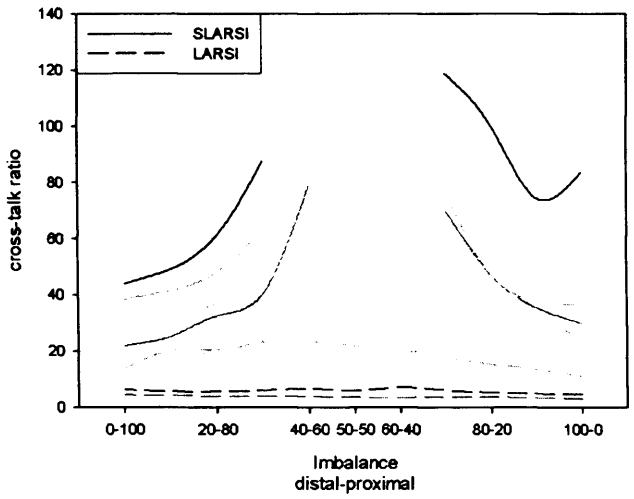

Figure 5.26: LARSI and SLARSI-like cross-talk ratios for different anodal current imbalances, comparison of results from four different sessions.

to look at figure 5.28 which shows the evolution of the cross-talk ratios with the pulse width.

5.7.2 Cross-talk stimulation threshold variations

5.7.2.1 Influence of slot insulation, local membrane connectivity and time and nerve aging on cross-talk ratios

Figure 5.29 illustrates how sensitive the thresholds measurements are to any variation in the resistance of the slot, obtained here by poorly sealing the lid using petroleum jelly. The SLARSI thresholds are plotted for a leaky and a well-glued lid. A LARSI curve, recorded once the lid had been properly sealed, has been added for comparison. These recordings were performed to "get a feel" for the effect of leakage current, no attempt was made to quantify how leaky the poorly sealed lid was.

Figure 5.30 presents curves illustrating the influence of slot displacement (including local membrane conductivity and electrode-nerve contact) on cross-talk thresholds. It is associated with the direct thresholds plotted in fig. 5.13. Likewise, fig. 5.31 corresponds to fig. 5.14(a) and fig. 5.32 to fig. 5.14(b), they illustrate the influence of time on cross-talk thresholds and cross-talk ratios. Note that the vertical scales for the cross-talk ratios have different ranges from one figure to the next.

Although this is only a qualitative observation, the following is worth noting here as it was the rule rather than the exception. For imbalance 30-70, often CAPs could not be triggered, even at the highest current level, when no CAP had been present at the previous imbalance setting. If however a CAP was triggered, say at imbalance 20-80, and the setting was then changed to 30-70, the CAP would remain, albeit much smaller. This phenomenon had been observed many times during direct stimulation (and for other settings with cross-talk stimulation), but it was never as strong as for this specific

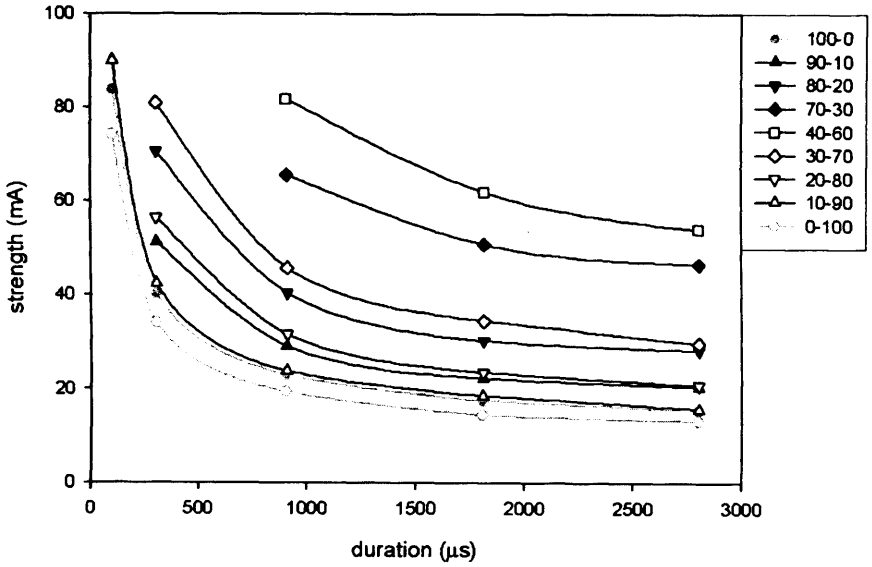

(a) Strength duration curves for cross-talk activation, imbalances 100-0 to 70-30, distal anode dominant (nearest to the recording electrodes) and imbalances 40-60 to 0-100, proximal anode dominant (furthest from the recording electrodes).

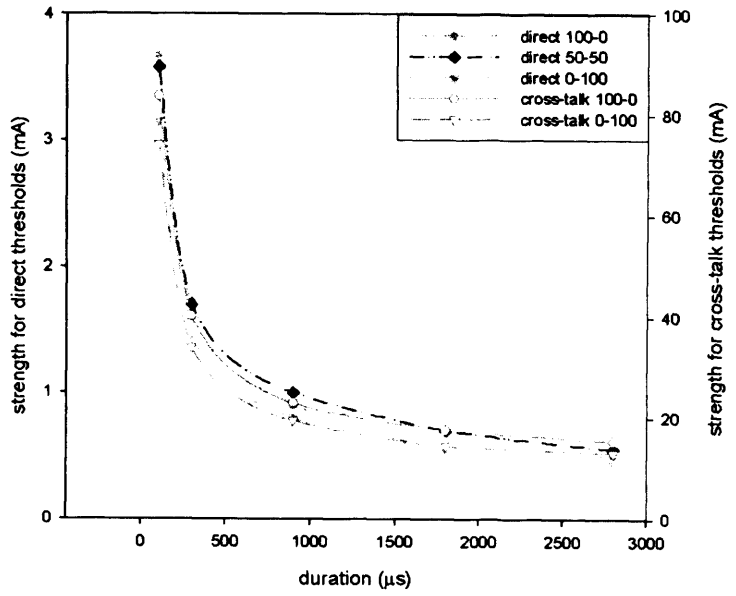

(b) Strength-duration curves for direct (left Y-axis) and cross-talk (right Y-axis) activation, for the two dipolar cases and the true tripole (direct activation only).

Figure 5.27: Strength-duration curves for cross-talk activation of the xenopus sciatic nerve with an electrode book.

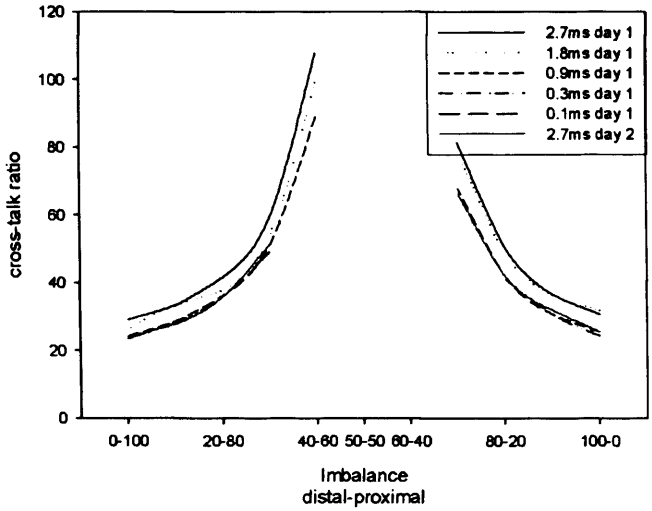

Figure 5.28: Cross-talk activation ratios for a range of pulse widths, data also presented in the strength-duration curves, fig. 5.10 and fig. 5.27.

imbalance, where currents of 10mA might fail to trigger a CAP if none pre-existed. This must be related to the phenomenon described in section 5.4.3 as "trigger hysteresis" (page 89). To eliminate this influence the cross-talk thresholds were measured twice, once from 100-0 to 0-100 and once in reversed order. Ideally the stimulus intensity should have been brought to zero between each imbalance position but this was only understood during a post-analysis session, and only done for subsequent recordings.

5.7.2.2 Influence of nerve straightness and angle between nerve and slot axis on cross-talk threshold

Figure 5.33(a) is a plot of the thresholds for activation of a nerve lying outside a slot and forming a fixed angle of 22.5° and 45° with its axis, for two different nerve-book distances. No CAP could be elicited with the nerve parallel to the slot (maximum current 12mA), even when butting against it, so there is no curve "angle 0" for comparison.

Figure 5.33(b) shows the evolution of cross-talk activation thresholds when the nerve is taken out of the electrode book. The curve labeled "parallel, in other slot" is a classic cross-talk situation, with the nerve in the external slot while the central slot is active. For the curve "parallel, distance 0", the nerve was placed alongside the book, and the external slot was active.

Figure 5.34 presents the cross-talk ratios computed with the direct thresholds plotted in fig. 5.15. Here the nerve is bent by rotating the book while the nerve is kept inside the central slot (see fig. 5.23). The curve labeled "bent" is a plot of the ratios of direct and cross-talk thresholds recorded with the nerve bent. Likewise, the

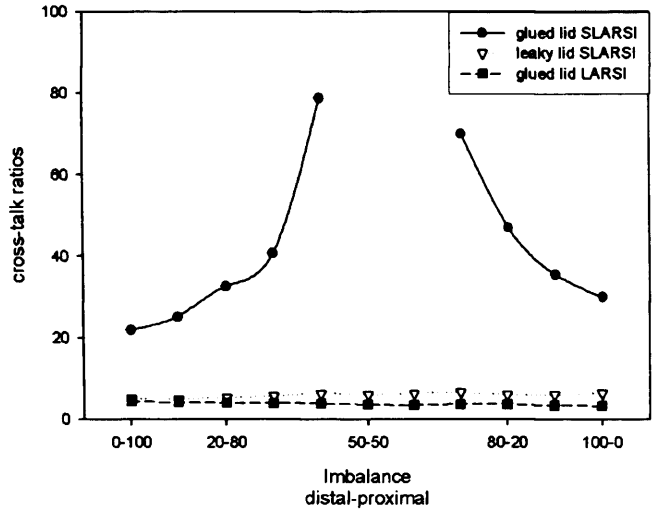

Figure 5.29: Comparison of typical cross-talk ratios with a leaky lid and a well sealed (glued) lid, see section 5.7.2.1.

curve labeled "straight earlier" was computed with both direct and cross-talk thresholds recorded with the nerve in the same position, straight in this case. The curve labeled "bent/straight" on the other hand is a plot of ratios of bent cross-talk thresholds over straight direct thresholds. This curve was included in the plot for comparison.

5.7.3 Cross-talk distances and orientation vis-à-vis the slot axis

The curves of figure 5.35 plot the maximum distance a nerve can lie away from a book and still experience cross-talk activation. To integrate the influence of orientation vis-à-vis the slot axis, the book was placed either parallel or perpendicular to the nerve. Vertically, the nerve was positioned at the same height as when it was lying inside the book, i.e. just above the level of the book's floor.

5.7.4 Cross-talk latencies

Owing to the complexity of the activation process, latencies of compound action potentials elicited by cross-talk stimulation do not bring any definitive new information. The discussion on latencies will therefore focus on direct activation, and the following cross-talk plots will be mainly used to confirm trends. Figure 5.36 shows the evolution of a CAP at different imbalance settings, the stimulus current being constant. Figure 5.37 on the other hand shows the evolution of a CAP at different current levels, the imbalance being constant.

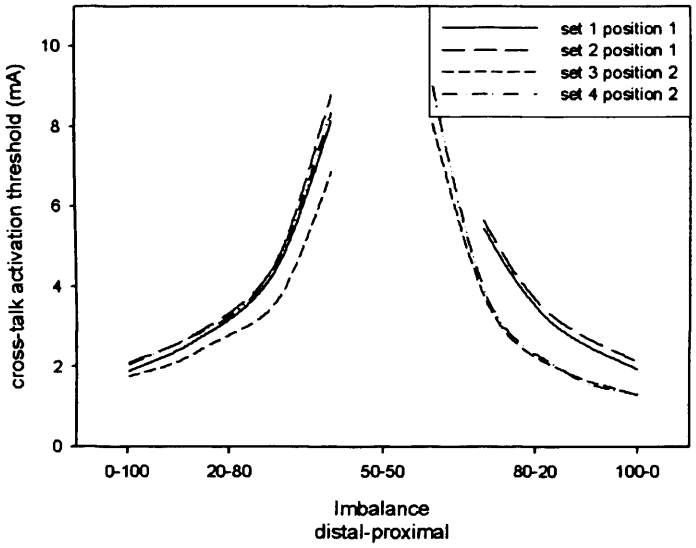

(a) Variation of cross-talk activation thresholds with the book at two different positions along the nerve.

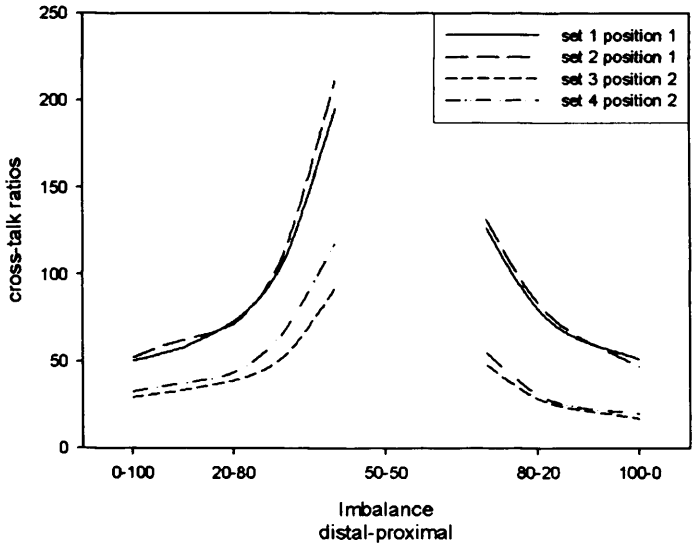

(b) Variation of cross-talk activation ratios with the book at two different positions along the nerve.

Figure 5.30: Influence of local conductivity and nerve-electrode contact on cross-talk activation thresholds and ratios (same results plotted in both subfigures). The ratios include the influence of the direct thresholds presented independently in fig. 5.13.

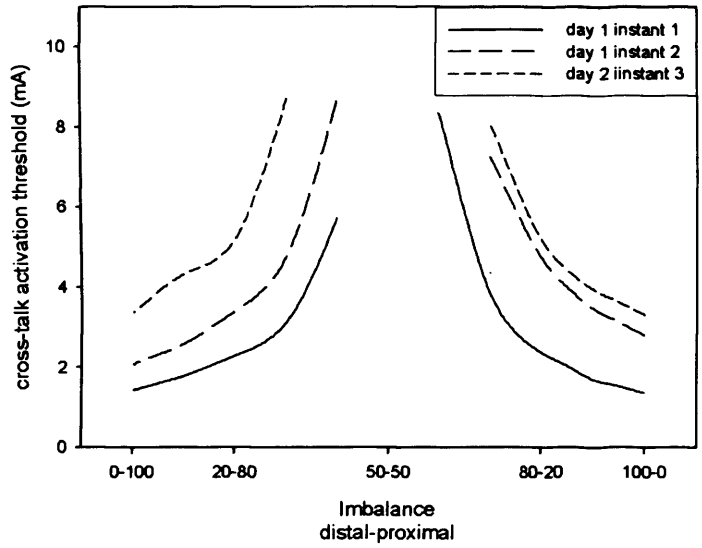

(a) Cross-talk activation thresholds over two days, example 1.

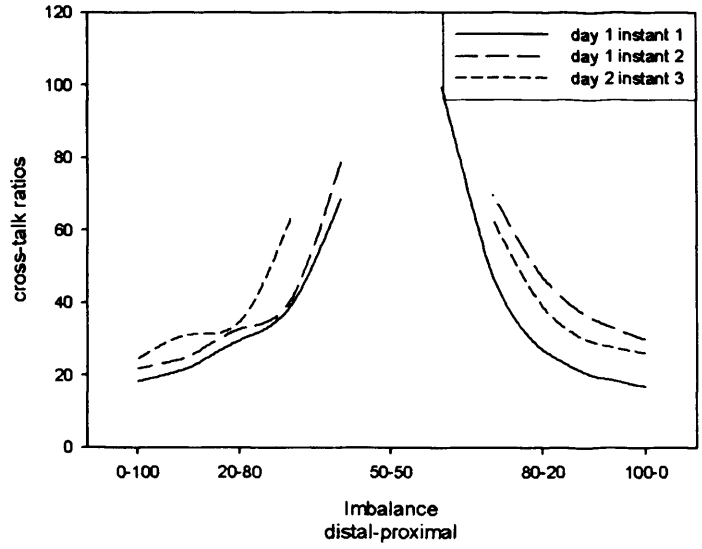

(b) Cross-talk activation ratios over two days, example 1.

Figure 5.31: Variation of cross-talk activation thresholds and ratios (same results plotted in both subfigures) with time, example 1. The ratios include the influence of the direct thresholds presented independently in fig. 5.14(a).

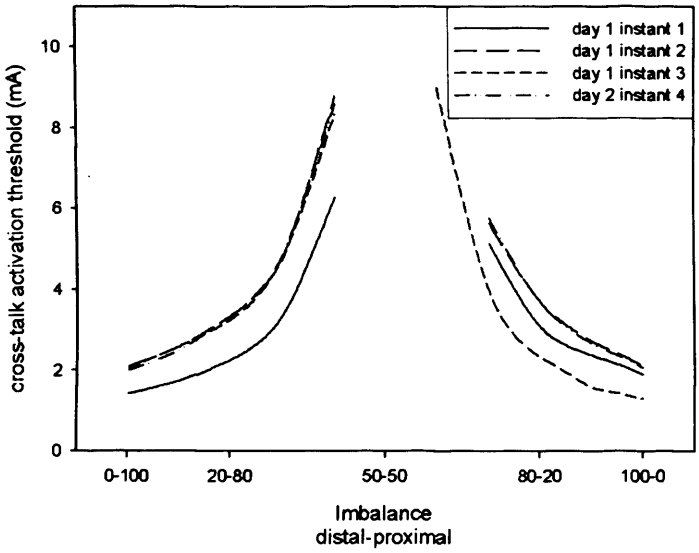

(a) Cross-talk activation thresholds over two days, example 2.

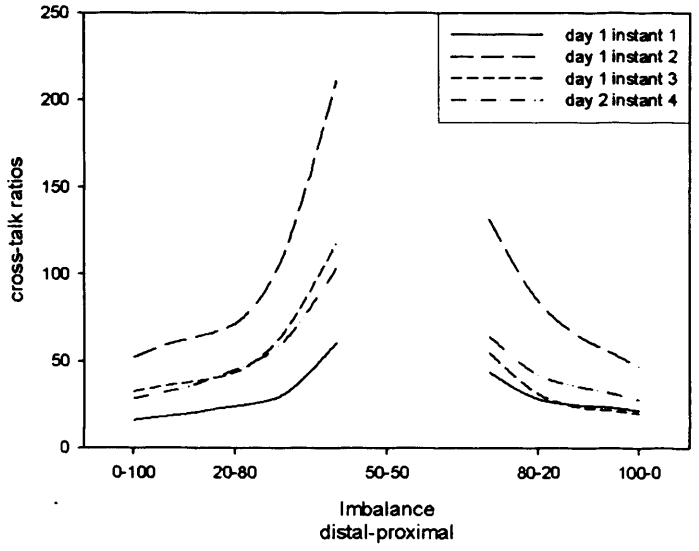

(b) Cross-talk activation ratios over two days, example 2.

Figure 5.32: Variation of cross-talk activation thresholds and ratios (same results plotted in both subfigures) with time, example 2. The ratios include the influence of the direct thresholds presented independently in fig. 5.14(b)

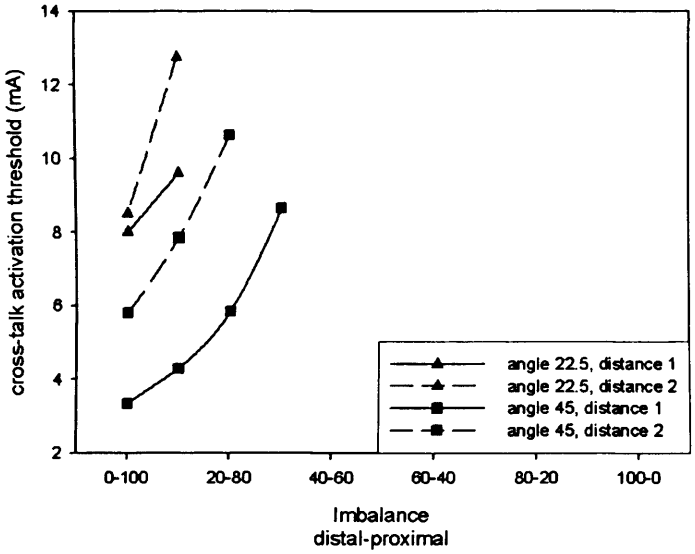

(a) Cross-talk activation thresholds with a nerve at an angle (22.5° and 45°) with the book's axis.

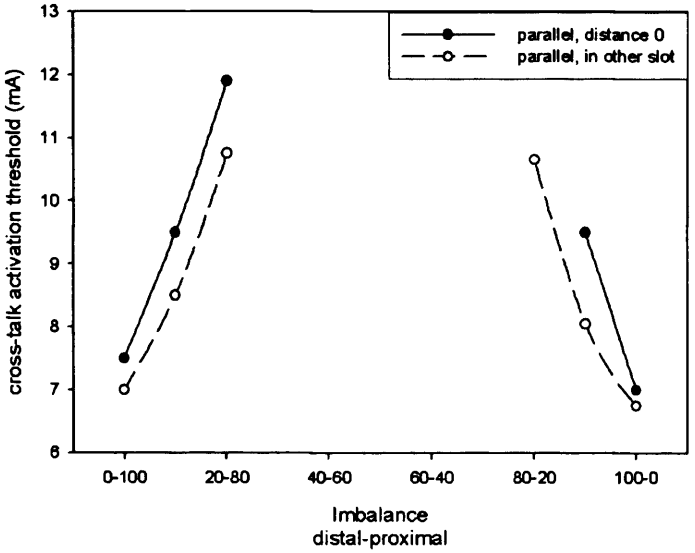

(b) Cross-talk activation thresholds with a nerve parallel with the book's axis, once inside a passive slot, once outside of the book.

Figure 5.33: Cross-talk activation thresholds for two nerves outside the book.

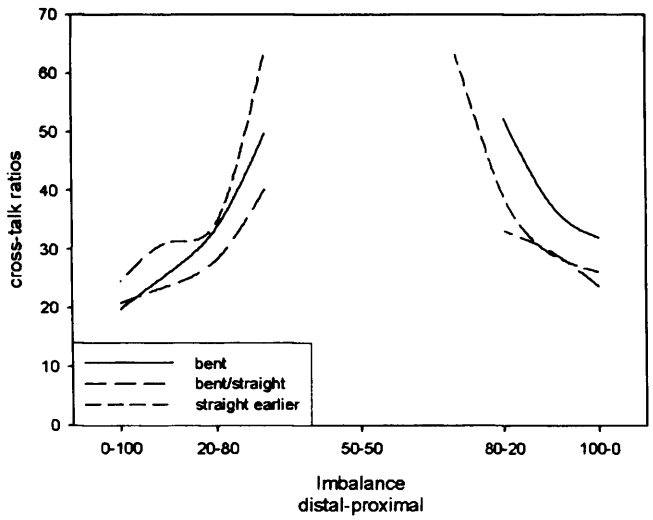

Figure 5.34: Cross-talk ratios for a nerve bending at the edges of the slot, as in fig. 5.23.

5.8 Discussion for cross-talk activation

5.8.1 Cross-talk activation: general trends

5.8.1.1 LARSI and SLARSI models

For the LARSI-like configuration (with common anodes), the ratios of the lowest curves (blue and pink on fig. 5.26) vary between 5 and 7. These values are similar to the lowest experimental cross-talk ratios given in Donaldson et al. [2003] (tables ??, ?? and ??, in appendices, page ?? and following). For the SLARSI-like curves (fig. 5.25), the trend for the cross-talk ratios at low imbalance (from 40% – 60% to 60% – 40%) is to climb above 100.

In the LARSI, the stimulation of each individual root uses a single cathode (central electrode in the slot containing the root) and all the available anodes (24 since there are 12 slots with two anodes each, section 4.1.3.3). If the cathodal current was equally shared between all anodes, the threshold for anodal excitation would be well above the functional level needed with cathode make activation (cf. section 2.1), even for the strongest responses. A more realistic division of the current shows that about 8% of the current to the cathode comes through each of the 4 inactive anodes of the book electrode [Krabbendam, 1998]. The ratio for cross-talk to direct activation should then be 4×12.5, 4 being the anodal to cathodal excitation ratio. This is nearly 12 times higher than the lowest value of 4.3 estimated in patient JH for the L3L root. This implies that contralateral responses may not be due to anodal activation of a root inside another, non-active slot. Yet, as the current converges toward the unique active cathode, it is concentrated at the slot ends which become zones of strong potential variation (giving

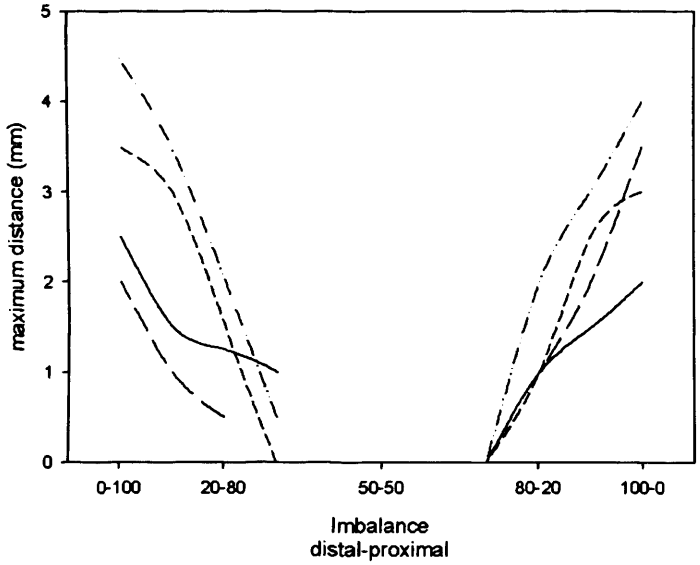

(a) Maximum distance for activation at maximum stimulator output, nerve parallel to the book axis.

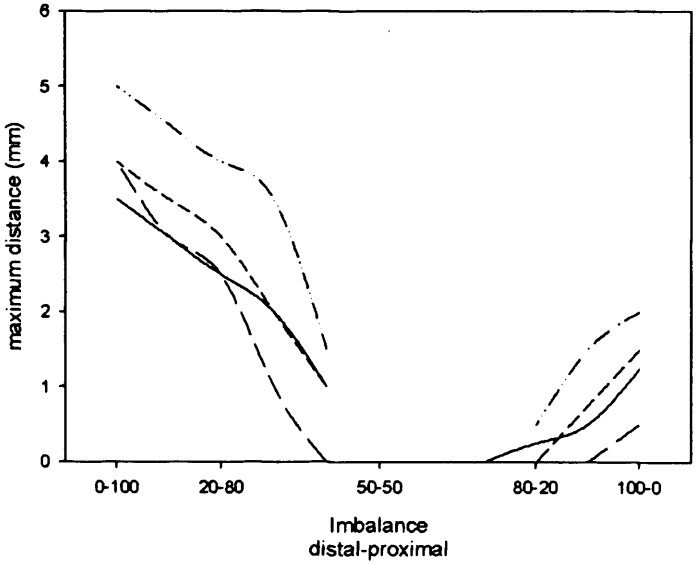

(b) Maximum distance for activation at maximum stimulator output, nerve perpendicular to the book axis, distal anode closest to the nerve.

Figure 5.35: Maximum distance for cross-talk activation for different anodal current imbalances, nerve parallel or perpendicular to the book axis, results from three different days (different nerves).

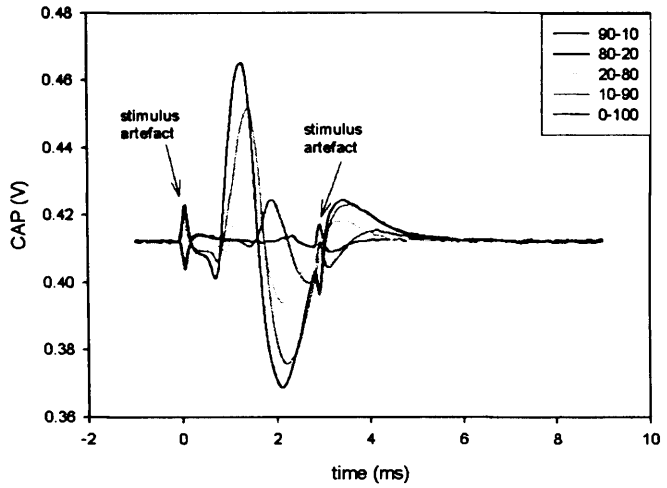

Figure 5.36: CAPs elicited by cross-talk stimulation, constant stimulus current (9.7mA at the cathode), different imbalance settings.

large peaks in the activating function)[27]. Due to the root density of the cauda equina, it is likely that other roots will be lying alongside each book. Therefore, rather than *in slot* anode-break stimulation, cross-talk activation may be caused by *virtual electrode effect* in the vicinity of the active slot. This explains why cross-talk does not necessarily cause activation of another root in the same book.

For future implant development, it is important to gain an improved understanding of those *virtual excitation zones*. Even when the effects of cross-talk are not as obvious as with the LARSI experience, they might often affect the expected stimulation patterns. Hence, the need to study cross-talk stimulation, and the extent of the virtual electrodes outside the slot. Two of the aims of these experiments were to show the occurrence of cross-talk , and to show that such activation could occur at low ratio in a LARSI-like situation. This has been demonstrated, and the remaining of this discussion is dedicated to the independent anode-pairs as this will be implemented in future implants (SLARSI, Healthy Aims, etc).

5.8.1.2 Strength-duration curves for cross-talk activation

From the comparison of the strength-duration curves in the dipolar cases (fig. 5.27(b)), the direct and cross-talk activation curves appear proportional. Other imbalances gave similar figures, with an increasing proportionality factor toward the true tripole. When the axes are adjusted to superimpose the thresholds at $900\mu s$, the cross-talk curve lies below the direct one for shorter pulses, and above it toward rheobase. This phenomenon is stronger for more symmetrical current division. The proportionality factor

[27] A first analysis of the situation, in [Donaldson et al., 2003], suggests the presence of strong virtual anodes in hemispherical regions at both ends of an active slot. This is likely to cause stimulation of any external root bending toward the end of the slot, with a threshold as low as 5.3 times the cathode made threshold.

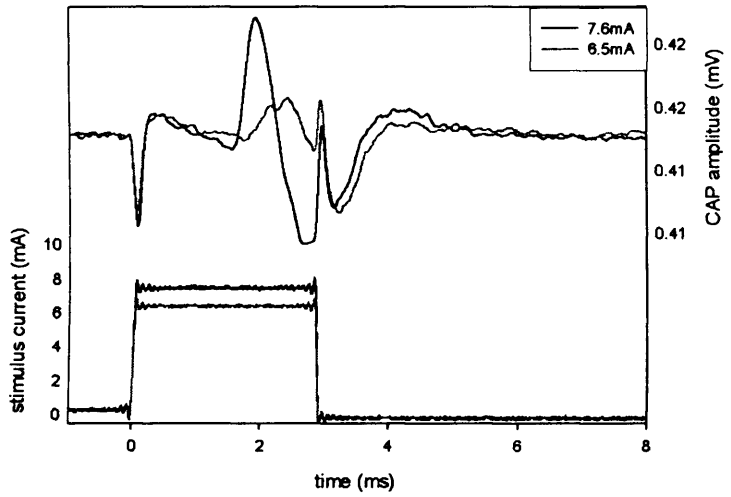

(a) Imbalance 100-0, distal anode dipole.

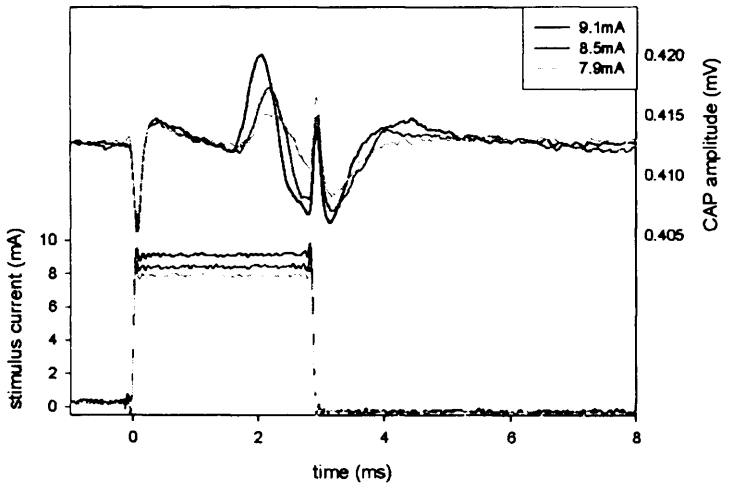

(b) Imbalance 90-10.

Figure 5.37: CAPS elicited by cross-talk stimulation with variable stimulus current.

of fig. 5.27(b) is in fact the cross-talk ratio for a given pulse width ($900\mu s$) and imbalance. When these are plotted for all pulse widths (fig. 5.28), the trend is confirmed, the cross-talk ratios increase with the pulse width, for all imbalances. Cross-talk stimulation largely increases the rheobase (factor 20 to 100), but it also decreases the chronaxie with respect to direct stimulation. From section 5.6.1.1 on direct activation, changing from a dipole to a tripole decreases the chronaxie and increases the rheobase. These trends are also observed with cross-talk stimulation, they are even stronger as the ratios all increase for more symmetrical imbalances [28], and the more so the longer the pulse width [29]. Practically, it is therefore advisable to use longer pulse width to avoid cross-talk activation, especially for dipolar stimulation, this was also suggested in McNeal et al. [1987].

5.8.2 Cross-talk activation: threshold variations

5.8.2.1 Influence of slot insulation, local membrane conductivity, time and nerve aging

The leaky lid results, plotted on fig. 5.29, show the importance of a proper seal around the active slot if cross-talk activation is to be avoided.

The electrode-nerve contact influences mainly the direct thresholds. A change in the position of the slot however may have a noticeable effect on both direct and cross-talk activation thresholds as the excitability of the nerve is non uniform (due to the loose epineurium, see section 5.5.1.2). The effect may be different on the two activation thresholds not only because of the electrode-nerve contact variation, but also because the activation zones for direct and cross-talk activation are distinct. Two opposite influences are observed on fig. 5.13 and fig. 5.30(a). While the thresholds for direct activation increase from position 1 to position 2, they decrease for cross-talk activation when the distal anode is dominant. Direct CAP arise at or near the cathode, the excitability is therefore similar for all imbalances and the threshold nearly constant (fig. 5.13). Cross-talk activation on the other hand occur outside the slot. The two activation zones (for distal and proximal anode dominant) act upon two different sections of the nerve, and the thresholds may be different (fig. 5.30(a)). The ratios in this case are separated, decreasing from position 1 to 2, yet, had the cross-talk thresholds changed the other way, the four ratio curves might have been closer together. What however can be deduced from these results is that a nerve left untouched for some hours (up to a day after explantation) shows no changes in thresholds for both direct and cross-talk activation. The measurements are repeatable provided the stimulation condition are exactly replicated, any alteration may have noticeable consequences for the thresholds (yet this may or may not be reflected by the ratios).

[28] Indicating a larger increase in the rheobase for cross-talk stimulation from dipole to tripole.

[29] The cross-talk ratios for a longer pulse width increase faster than for short pulses (i.e. the ratios span for a given imbalance increases toward true tripole). If the chronaxie from dipole to tripole varied for cross-talk activation as it does for direct, the ratios would all increase in a similar way. As the chronaxie decreases, the cross-talk thresholds for shorter pulses do not increase so fast from dipole to tripole.

Figure 5.31 and 5.32, presenting results recorded over two days on two occasions are mainly plotted for completeness as it was shown with the direct thresholds (section 5.6.1.3) that there are no noticeable trends during the first 36 hours after explantation.

5.8.2.2 Influence of nerve straightness and the angle between nerve and slot axis

Moving the nerve outside the book increases the cross-talk activation thresholds (fig. 5.33(b)). This is expected as the inner partitions of the book are thinner than the outer walls. There is thus a larger insulating volume, and the nerve electrode distance increases from "in slot" to "outside butting" (distance 0). Rotating the book around the "distal corner" [30] (while the nerve outside remains straight) demonstrates that cross-talk activation occurs on the side of the weaker anode. When the book rotates, the distal anode remains close to the nerve while the proximal anode moves away. Figure 5.33(a) shows that CAPs could only be triggered with the proximal anode dominant. Moving the book away from the nerve (without altering the angle) increases the threshold as the virtual electrode zones are concentrated by the active slot's edges. Increasing the angle decreases the threshold which is in agreement with the hypothesis that the activation zones are hemi-spherical. Sliding the book upwards also changes the threshold, but as the vertical adjustment was poor and the movements of the book altered the nerve's absolute position in the bath (as a consequence of the water displaced by the book), no results were reported.
As there is no direct activation threshold, no cross-talk ratios were computed, rather, the maximum distances for cross-talk activation are plotted as a function of the imbalance, both for a nerve parallel and perpendicular (fig. 5.35). These are discussed in the following section.

5.8.3 Cross-talk distances

Although it is of practical importance to consider how far a nerve may lie from a book and still experience cross-talk activation, the distances from fig. 5.35 do not quantitatively reflect the real situation. In the cauda equina the volume is not as homogeneous and infinite as in the bath, and the stimulator will not produce such long pulses. The field will be different, hence the virtual electrode zones. If the pulses are shorter, the threshold increases, decreasing the maximum distance to trigger a CAP. Furthermore, the results plotted in fig. 5.35 are "ideal". Often, cross-talk activation only occurred for the most dipolar settings. Of all the recordings, only the curves with a minimum of three points on each sides are plotted. These results mark therefore the "upper limit" of the maximum cross-talk distances. The two points of interest from this set of experiments stem from the comparison of the distal and proximal sides of the curve for one, and from a comparison parallel versus perpendicular for the other.

[30] The corner with the distal anode, i.e. the corner nearest to the recording electrodes.

5.8.3.1 Curve asymmetry with respect to the tripolar setting

In the perpendicular case, the distance is longer when the dominant anode is furthest from the nerve. This confirms the results discussed in the previous section (5.8.2.2) regarding the influence of the angle between the nerve and book axis. The fact that it is possible to trigger CAPs when the anode closer to the nerve is dominant could indicate that the virtual electrode zone extends, from the side of the weaker anode, to the other side and beyond, but this is unlikely. Rather, this indicates the existence of a weaker virtual activation zone beside the dominant one. The activating function has multiple peaks and valleys. Intuitively (see McNeal et al. [1987]), the spill-over current causing cross-talk activation exits the slot on the side of the dominant anode and re-enters it at the other end. There is therefore a virtual anode by the end of the real dominant anode, and a virtual cathode on the weaker anode's side (where the current is concentrated as it re-enters the slot). An anode may cause electrical stimulation, often because it creates virtual cathodes on its sides. A virtual anode may act in a similar way. As is the case with real electrodes, the threshold (or in this case the distance) for virtual cathode stimulation is 4 to 5 times lower than that for virtual anode stimulation.

In the parallel case, the trend is for a slightly longer distance when the proximal anode dominates (three curves out of four, see fig. 5.35(a)). With those imbalances, the CAP arises after the book (with respect to its direction of propagation), there is no hyperpolarised "obstacles" likely to dampen it. When the distal anode dominates, the CAP is triggered before the book. On the distal side of the book there is a weak virtual anode hyperpolarising a section of the nerve. This hyperpolarised zone will stop the weaker CAP, effectively increasing the threshold as seen by the hook-electrodes, or decreasing the maximum cross-talk distance, see also the discussion for direct activation (section 5.6.2, page 110). As the book to nerve distance is increased, the anodal effect decreases and the asymmetry becomes marginal (0.5mm difference at the most). As already discussed in section 5.6.1.2 on page 106, the excitability is non uniform along the nerve, and this accounts for the noticeably longer distance (1.5mm) with the distal anode dominant for the fourth curve of fig. 5.35(a).

5.8.4 Cross-talk latencies

The issue of the activation delay was already raised in the direct latencies discussion (section 5.6.2, page 110). The CAP does not arise at the onset of the stimulation pulse, there is an "activation delay". Little is known about this delay, except that it decreases with increasing stimulus amplitude [Goodall et al., 1995]. Besides this, the presence of an anode, real or virtual, in the way of the CAP may slow it down, increasing the propagation delay. Latency measurements are often inconsistent (from one instant to the next) as the position of the nerve in the slot (active or neighbouring) will alter the effect of the anode. Because cross-talk stimulation requires much higher currents, it was not possible to reach the supramaximal levels at which comparison of latencies might have been meaningful. Figures 5.36 and 5.37 display trends similar to those seen

with direct CAPs. At constant imbalance, increasing the stimulus amplitude increases the CAP amplitude and decreases the latency. This indicates that the activation delay decreases in a similar way for cross-talk and direct stimulation. When the imbalance is switched from 100-0 to 0-100 (distal to proximal) the latency decreases and the CAP amplitude increases (fig. 5.36). The amplitude variation indicates the presence of a virtual anode between where the CAP rises and the recording electrodes. The argument of symmetry, already advanced for direct activation[31], suggests that with cross-talk stimulation the CAP is not triggered by a virtual anode (as it passes through it), but by a virtual cathode on the side of the weaker real anode. From 0-100 to 50-50 the virtual cathode becomes weaker, so much so that no CAP can be elicited after 30-70. From 50-50 to 100-0 the virtual cathode strengthens, yet the CAPs remain smaller than their symmetrical imbalance equivalents because a virtual anode is now present "in their way" to the recording electrodes. The statement that the virtual cathode is on the side of the weaker anode is intuitive and cannot be verified using latencies as was the case with direct stimulation for the reasons explained previously, namely inconsistency of both activation and propagation delays. Two CAPs elicited at the same site could arrive at the recording electrode at two separate instants and their latencies would not give any information on the distance traveled.

5.9 Conclusion of the experiments

Cross-talk activation has now been shown to occur in nerves lying in the neighbourhood of an active slot and outside a book in its close vicinity. The highlights of the discussion are summarised hereafter.

- The cross-talk ratios in a LARSI-like situation are similar to the values reported in table ??. This confirms Donaldson's hypothesis, developed in chapter 4.1, that the lack of selectivity is due to cross-talk [Donaldson et al., 2003].
- Stimulating with only the pair of anodes of the active slot, as opposed to all available anodes as in LARSI, increases the cross-talk ratio by a minimum factor of 7 (worst case, dipolar stimulation), see fig. 5.26.
- If the imbalance is moderate, the cross-talk ratio with independent anode-pairs is expected to climb above 100 as seen in fig. 5.25, thus giving a comfortable range of amplitudes for direct stimulation without cross-talk.
- The position of the nerve inside a slot can strongly affect its threshold (section 5.6.1.2), it would be beneficial to devise a new system to insure a better, more consistent, contact between the nerve and the electrodes.

[31] The argument of symmetry states that as CAP propagates in both directions after electrical stimulation, the CAP recorded for dipole 0-100 and that recorded for dipole 0-100 were the same when they arose, but have been altered differently because they followed two different directions. The same goes for any pair of symmetrical imbalance settings. Changing the imbalance is equivalent to turning the book by 180°.

- The cross-talk ratios with independent anode-pairs in each slot are higher for longer pulse widths (fig. 5.28). A stimulator should provide both current [32] and pulse width adjustment so that lower and longer stimulus can be selected as this will further reduce the likelihood of cross-talk activation.

- Long pulses are also recommended because the resistance imbalance between the two branches of a tripole is most influential at the pulse onset (see preliminary experiment, page 84).

- The direct activation threshold increases slightly for more symmetrical situation, see figures 5.13 and 5.14.

- Direct activation takes place at the cathode only for direct stimulation with a true tripole. For all other imbalances, the activation site shifts toward the weaker anode (section 5.6.2.3).

- Cross-talk activation takes place on the side of the weaker anode (presence of a virtual cathode). For very large stimuli, activation may also occur on the side of the stronger anode, see sections 5.8.2.2 and 5.8.4.

- Current leakage, due for example to a poorly sealed lid as in fig. 5.29, strongly reduces the cross-talk ratios for independent anode-pairs. An enhanced lid that improves the slot insulation would limit the risks of cross-talk in future implants.

Electrode books remain the most suitable mounts for nerve root stimulation in the cauda equina. Provided the output stages are independent (switches at both anode and cathode connections) and the current division is reasonably tripolar, the cross-talk ratios should be high enough to prevent unwanted nerve root activation over the whole range of "useful" [33] stimulus amplitudes. Cross-talk should be expected only if the impedance imbalance between the two branches of the tripole became considerable (leading to a current division at the pulse onset of 30-70 or more). The resistive imbalance is compensated by the capacitive imbalance for longer pulses and since the latter is less likely to vary over time, long pulse widths are recommended.

5.10 Further considerations

5.10.1 Can a frog nerve model a human spinal nerve root?

As explained in the introduction to this chapter (page 77), frog sciatic nerves were used as it was not possible to experiment in vivo (in the cauda equina) on human nerve roots. This raises two questions: how does the sciatic nerve compare to the roots (and

[32] Although stimulus current and output voltages are related, it is better to develop current controlled stimulator as the load impedance is variable and a priori unknown.

[33] The "useful" amplitude range covers the lowest expected threshold up to the highest suprathreshold stimulus needed, which is evaluated as five times the highest expected threshold, see section 9.2.6 for more information.

on what basis compare the two nerves structures), and how do the experimental results translate to the case of spinal cord stimulation, are they relevant?

- Human nerve roots are myelinated with a perineurium, an epineurium and an endoneurium, so are the frog sciatic nerves [Finean, 1960]. The perineurium of the frog sciatic nerve is only loosely attached to the nerve.

- The frog sciatic nerve contains motor as well as sensory axons. Human anterior roots are mainly efferent though there are evidences that they also contain afferent fibres [Phillips et al., 2000].

- Schalow [Schalow et al., 1995] published data on human sacral roots, mainly posterior. The group conduction velocity ranges from 10m/s to 62m/s (afferent fibres) and between 10m/s and 58m/s for efferent. Single fibre diameter for anterior root S4 varies from $1.5\mu m$ to $17\mu m$ with the majority of the fibres between $2\mu m$ and $5\mu m$.

- Tasaki [Tasaki, 1982] published the conduction velocities of individual fibres of the sciatic nerves of bullfrogs. They range from 5 to $40m/s$, see fig. 5.38.

- The temperature dependence of the conduction velocity must be taken into account. Schalow's results were obtained at about $35,5^oC$, while Tasaki's graph is valid at 24^oC. Figure 5.39 shows the temperature dependence of whole nerve conduction velocity for another species of frog (*rana temporaria* L.). During the experiments reported in this chapter, the temperature of the bath was not controlled. The room temperature varied between 18^oC and 22^oC.

5.10.2 Relevance for the results presented

One aim of these experiments was to understand how the current spilling out of the active slot of the book electrode caused cross-talk activation of neighbouring roots in the cauda equina. The experimental situation can not be a true representation of the real case and these last paragraphs discuss the extent to which the experimental results may be useful for the development of spinal cord stimulation device?
The main findings on cross-talk ratios and activation distances involve no timing considerations. This limits the importance of differences in conduction velocity, hence individual fibre diameter, and temperature variation for the results analysis. It is legitimate to say that both nerves react similarly to electrical activation, i.e. they have an activation threshold, a refractory period, individual fibres spanning large conduction velocity and diameter ranges [Tasaki, 1982]. They will thus exhibit qualitatively similar reactions to electrical stimulation, i.e. to depolarisation and hyperpolarisation. To quote Altman: "Although there are quantitative differences between amphibian and mammalian nerve physiology, experimental studies suggest that qualitative responses (such as strength/duration and strength/diameter) are similar". The fact that a sciatic

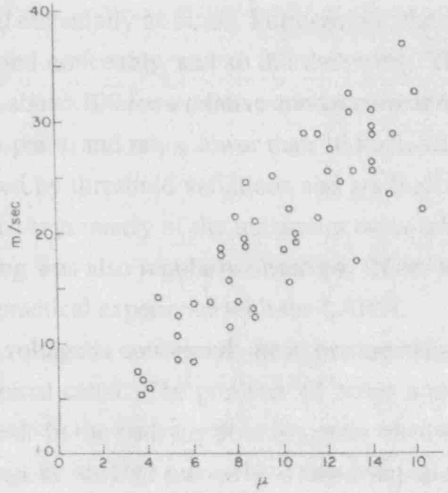

Fig. 5.14 Conduction velocity plotted against the fiber diameter. Sciatic–gastrocnemius preparations of the bullfrog were used. The outside diameters of single fibers were measured near the muscle. Temperature, 24°C. (From Tasaki et al., 1943a.)

Figure 5.38: Bullfrog sciatic nerve individual fibres conduction velocity as a function of their diameter [Tasaki, 1982].

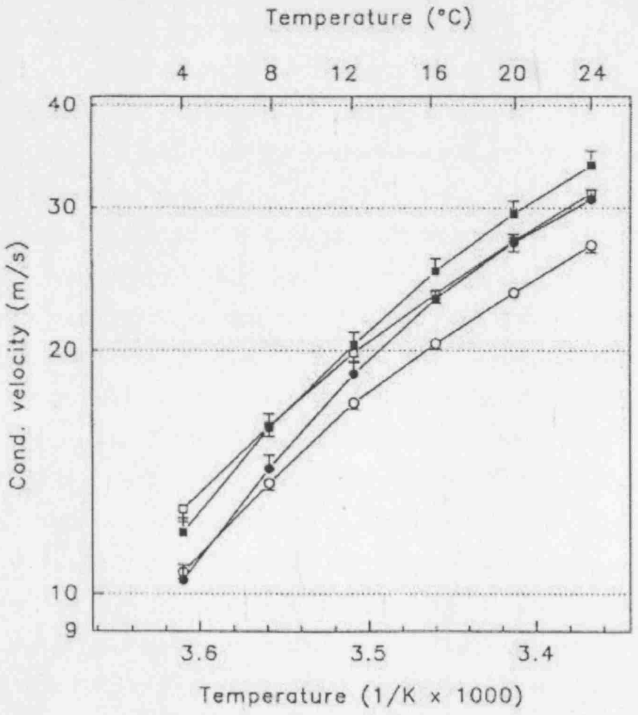

Fig. 3. Conduction velocities in the sciatic nerve of winter and summer frogs. In winter seven animals were acclimated to 4°C (○) and to 24°C (●) whereas in summer eight animals were acclimated to 4°C (□) and 24°C (■). Means are given with ± S.E.M.

Figure 5.39: Temperature dependence for whole nerve conduction velocity [Tiiska and Lagerspetz, 1999].

nerve may have a different threshold from a nerve root is of no considerable importance as the data is presented essentially as ratios. Furthermore, the direct and cross-talk activation thresholds varied noticeably, and so did the ratios. Yet they all exhibited the same trends, i.e. ratios above 100 for a relative anodal current imbalance less than 20% for independant anode-pairs, and ratios lower than 10 for LARSI-like situation. These trends were not affected by threshold variations and are therefore relevant for human nerve root stimulation. Asymmetry of the maximum cross-talk distance as a function of the imbalance setting was also regularly observed. These trends are in accordance with both theory and practical experience with the LARSI.

As far as the external voltage is concerned, the experimental setup is simpler than the real situation in the spinal canal. The presence of bones and various tissues will influence the electric field. In the bath the field is symmetrical and the heterogeneity of the spinal canal can not be studied precisely. Only some qualitative tests like those discussed in section 5.6.1.5 can be performed. Given the results, the ratios should not be very different in the bath or the spinal canal [34].

[34] As already mentioned in section 5.6.1.2, many external factors influence the results (stimulator, bath, book electrode, hook electrodes, etc). Some of these can be controlled, albeit not always precisely, like the saline level, the tension of the nerve, the lid position, etc. Yet it is not so easy to act upon the amount of connective tissue surrounding the nerve, the external interferences, the position of the nerve inside the slot, etc. The results presented in this chapter were selected from a series of experiments performed in 2003 and 2004. The thresholds did vary considerably, not only between experiments, but also throughout the 36 hours of life of a single nerve. Some sets were excluded because the recordings were too noisy, making it difficult to distinguish the onset of excitation in the background noise.

Chapter 6

Chronic nerve root entrapment

6.1 Long term use of electrode-books

6.1.1 Risks associated with implantation and stimulation

For a nerve root stimulator implant to work successfully, it is, obviously, important that the nerves and nerve roots at and below the implantation site remain intact. Great care must therefore be taken to design nerve/electrode interfaces that do not threaten the integrity of the nerve or root. The implantation technique must minimise handling and the electrode, with its mount, must be chronically safe (mechanically and biologically). Intrathecal nerve root stimulation has so far always been achieved by means of book electrodes. Other shapes of mounts have been proposed, but the book has proved the best choice because: *(i)* it minimises the root handling as they are softly lain in a slot which intrinsically remains open hence limiting the risks of squeezing and stretching; *(ii)* it optimises the use of space [1] by butting three slots next to one another and *(iii)* it was especially designed to lie harmlessly in the spinal canal amongst the roots of the cauda equina: no sharp edges and corners, a rounded "bottom", cables originating at least 1mm below the root for extra clearance. All materials used have been shown to be suitable for chronic use in human [Black, 1999; Donaldson, 1982; Helsen and Breme, 1998; Ratner and Bryant, 2004; Stieglitz, 2004; Yoda, 1998]. Implantation and biochemical risks are thus controlled. The effects of charge transmission have been extensively studied, leading to the development of rules and limits to guarantee a safe charge transfer (see chapter 7), and damages due to excessive stimulus amplitude can also be ruled out. The last kind of adverse effect to be considered is mechanical damage. This can be caused by movements of the mount after implantation, pulling and stretching the nerve, or by compression. The former is often blamed on unexpected limb movements or excessive cable tension [Brindley, 1977; Naples et al., 1990]. With the spinal placement of the book electrode, limb movements are not an issue. Nor is cable tension since the distance to the stimulator (implanted in the lower abdomen, just below the ribs) varies very little with the patient's position. If the cables are slightly loose at implantation, the risks due to cable tension can be disregarded. Further, the

[1] The space in the cauda equina is very limited, see section 1.1.2.

grommet (see fig. 4.4 on page 63) offers an extra degree of protection as it is sutured to the dura and all the cables are glued to it, making any movements of the book in the spinal cord highly unlikely [Brindley, 1981]. Therefore, the last, and most important, concern for the viability of nerve roots trapped in a book electrode is root compression.

6.1.2 Nerve root damages with sacral stimulators

Intrathecal nerve "books" have been chronically implanted in humans since the 1980s with the first Brindley sacral anterior root stimulators[2] [Brindley et al., 1982]. Yet there are no publications studying the effects of chronic intrathecal nerve root compression. This is probably because the slots for SARSI are normally much larger than the roots trapped as illustrated by fig. 6.1, see table 4.3 for standard book sizes. With these dimensions, it is assumed that the nerve root will not become compressed by the walls of the book electrode, even with post-operative swelling. Only two papers on root stimulation with book electrodes contain histological findings: Brindley [1977] and Brindley and Rushton [1990]. In the earlier, reporting on chronic implantation in baboons[3], Brindley writes :

> " The implants were designed primarily for ventral nerve roots, and the slots were made so that no ventral root was a tight fit in its slot. However, dorsal roots (which are about twice as large as ventral) were fairly often inserted into slots in which they fitted tightly. Many of these dorsal roots were found to be unexcitable, and it seems likely that they failed from ischaemia very soon after implantation."

This damage was sustained soon after implantation but not as a result of implant infection. In the same paper Brindley also describes damage to nerve roots occurring during implantation, following infection or book electrode displacement and reports that such "misfortunes" (his word) became less frequent as the operation technique improved. The issue of nerve root damage is also discussed in other papers [Brindley, 1990; Brindley et al., 1982] but there are no mention of chronic human nerve root compression. The early damage was due to the surgical manipulation. Implant infection or movement of the book caused further root degradation, often followed by complete, and effective, root regeneration after the problem was solved. All causes were reduced or eliminated by improved book design and better implantation technique. Human nerve roots (especially anterior roots) may indeed regenerate like peripheral nerves, with a delay of 8 to 12 months for full recovery [Brindley et al., 1982; Gonzalez-Darder, 1993; McCouch, 1955; Ramon y Cajal, 1991 translation][4]. Effective regeneration in baboon was demonstrated in Brindley [1977]. The anterior root (L7) of one of

[2]The first chronic implantations in baboons started in the early 1970s [Brindley, 1972, 1973].

[3]The dimensions of the books used for baboons experiments are unknown but it is reasonable to assume that they were large from the quoted text. It is probable that the book size was further altered after these experiments to be fitted to human sacral roots [Brindley, 1977].

[4]Contested in Carlstedt et al. [1995], the issue about root regeneration is that while it may regrow, it may fail to re-establish functional connections.

the implanted baboons was electrically destroyed, stimulation test after the destruction confirmed the absence of motor response. One year later the threshold had returned to its level prior to destruction, confirming the possibility of functional anterior nerve root regeneration. As far as human nerve roots are concerned, he mentioned in a SARSI follow-up paper [Brindley and Rushton, 1990] that anterior nerve roots trapped for 3.5 to 5 years (as part of implants used regularly) appeared histologically normal without further information. The LARSI experience is slightly more varied. Smaller books were used and roots had to be squeezed in their slots, which probably led to some damage during implantation, as well as later on due to excessive compression. Some recovery was observed but, as seen in the tables of appendix **??**, certain roots remain unresponsive to electrical stimulation using the implanted electrodes.

6.1.3 Book electrode improvements and future use

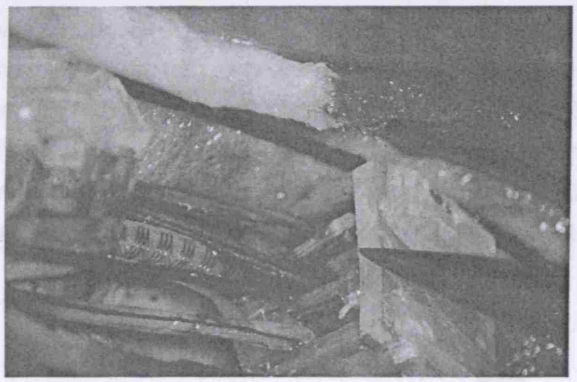

Figure 6.1: Book electrode trapping sacral nerve root in the cauda equina, photo courtesy of Dr. van der Aa.

As explained in the previous section (6.1.2), the slots of the electrode-books used with SARS implants are larger than the roots they trap, see fig. 6.1. Chapter 5 has shown the importance of nerve-electrode distance for recruitment sensitivity. Recent developments in bladder stimulators have also led to the need to record neural signals using electrode-books. To limit the chances of cross-talk stimulation even for a very imbalanced slot, to decrease the direct stimulation threshold and improve the recruitment sensitivity, and to improve the recording properties of the electrode-book, a mean of fitting the root inside the slot is needed. The shape of the book should not be altered as it has proved safe and fit for purpose over the past three decades. Rather, a simple improvement, easy to add to the existing design is sought. Given the large span of roots' cross sectional areas (see fig. 6.2 and table 6.1)[5], the rigid, one-size-fits-all SARSI slots have so far been seen as the best approach. Due to the lengthy and com-

[5]The roots are not cylindrical, and the diameter is only given as an indication, as it is felt that cross sectional areas are difficult to visualise. The diameters are calculated as that of a cylinder which would have the same cross-sectional area as the root. Large roots especially stray from the cylindrical shape as they are formed by multiples strands, or rootlets, some of which separate readily when handled [Hogan, 1996; van der Aa, 2002].

plex nature of the implantation procedure, the surgeons are unlikely to be willing to choose from a range of books of various sizes. This option would be further complicated by the fact that a book usually contains three slots, each of which traps a different root. The combination of large and thin roots and the need to allow extra room for post-operative swelling would render the selection procedure too complicated. Books where each slot is large enough to fit even the largest roots must therefore be provided.
Bearing all these limitations in mind, Prof. Craggs proposed to fit a constricting device in the slot to occupy the empty space. It should be elastic to adapt to the volume variation after operation without compressing the root excessively. This work is still in progress and the device, called the "*space limiting lid*" or "*sling*" will be briefly presented in section 6.5. So far it seems sufficient to explain that any improvement to the actual book must be shown to be safe before it may be considered for implantation. Since the only materials used for this new lid is medical grade silicone rubber, already present as the main component of the book, the bio-compatibility is guaranteed. The external shape and the implantation methods of the books are unaltered by the addition of the sling. The only safety issue is that of compression injury, which requires the determination of safe pressure limits, acute and chronic, for intradural nerve root entrapment. The previous section (6.1.2) has highlighted the scarcity of publications on the subject and the literature review that follows is an indirect attempt to fill this gap.

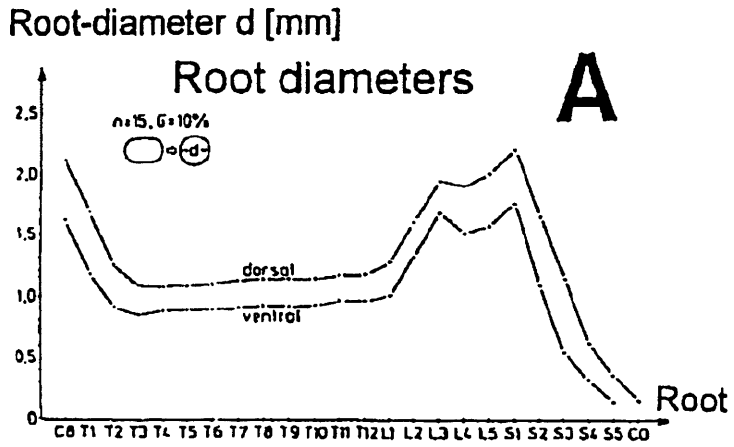

Figure 6.2: Human nerve roots diameter, reproduced from Schalow and Zach [1996].

6.2 Peripheral nerve damages by chronic cuff implantation

For more than 30 years, various types of electrodes have been implanted for peripheral nerve stimulation and recording. Applications such as phrenic nerve pacing and foot drop correction require the long term implantation of electrodes near or around peripheral nerves. There is more information available on chronic peripheral nerve entrapment than on nerve roots. Although these are morphologically different (internal

Table 6.1: Average size of human lumbosacral nerve roots to be trapped in future implants. The posterior roots would be used for recording, the anterior for motor stimulation. Roots S3 and S4 are sometimes trapped together, so their joint cross-sectional area is also tabulated. All single root diameters and standard errors from Hogan [1996]. SARSI slot cross sectional area: $7mm^2$, LARSI slot: $3.75mm^2$.

Level	area (mm^2)	σ (mm^2)	diameter average (mm)	area min[a] (mm^2)	area Max[b] (mm^2)
L3A	2.40	0.13	1.75	2.01	2.79
L3P	3.6	0.16	2.14	3.13	4.07
L4A	1.87	0.06	1.54	1.69	2.05
L4P	3.82	0.16	2.20	3.34	4.30
L5A	2.31	0.32	1.71	1.35	3.27
L5P	4.45	0.32	2.38	3.49	5.41
S1A	2.62	0.13	1.83	2.23	3.01
S1P	4.99	0.25	2.52	4.24	5.74
S2A	1.18	0.13	1.23	0.79	1.57
S2P	3.08	0.47	1.98	1.67	4.49
S3A	0.43	0.03	0.74	0.34	0.52
S3P	1.12	0.09	1.19	0.85	1.39
S4A	0.17	0.03	0.47	0.08	0.26
S4P	0.64	0.03	0.90	0.55	0.73
SA(3+4)L&R	1.2	0.12		0.84	1.56
SP(3+4)	1.76	0.26		0.98	2.54

[a] Mean area minus three standard deviation (σ), 99% confidence interval.

[b] Mean area plus three standard deviation (σ), 99% confidence interval.

structure, protective layers, elasticity, see section 1.2), the knowledge gained with the peripheral nerves forms a good basis for the study of nerve root compression injury.
Nerve damage has occasionally been reported in the literature (both on human subjects and various animals) [Carp et al., 2001; Gellman et al., 1990; Kim et al., 1983; McNeal et al., 1977; Naples et al., 1990; Potter, 1995; Stein et al., 1977; Waters et al., 1984; Yuen et al., 1984]. Although most nerve injuries were due to poor implantation technique (also damaging neighbouring tissue and vascularisation) [Brindley, 1977; Carp et al., 2001; Lundborg, 1975; Mortimer, 2000], mechanical irritation (strain induced by the lead pulling the cuff and by the rigidity of the mount)[6] [Naples et al., 1990; Rodriguez et al., 2000] or excessive stimulation charge [Agnew et al., 1990b; McCreery, 2004; McCreery et al., 1990, 1992], some reports contain indication of nerve compression injury [Bullara, 1984; Potter, 1995; Waters et al., 1984]. The damage is most often identified by a decline of the nerve conduction velocity, and confirmed by the study of histological sections when available. There is no agreement amongst authors on how much physiological or morphological changes (blood flow, state of the myelin sheath, number and diameter of fibres, composition of the connective tissue) affect electrical stimulation responses. In other words, a change in conduction velocity indicates that there is some damage along the nerve but it gives little information on the nature and extent of that damage. Some studies report clear, albeit minor, histological damages without any detectable neurological deficit [Brummer et al., 1983; Jellema and Teepen, 1995; Loeb and Peck, 1996; Romero et al., 2001; Struijk et al., 1999; Thoma et al., 1988][7].
Further, peripheral nerves have the capacity to regenerate, and this can be enhanced by the presence of a cuff around the damaged area or by electrical stimulation [Dahlin and Kanje, 1992; Daly et al., 1996; Lundborg and Dahlin, 1992; Nash et al., 1997; Zhang and Yannas, 2005][8]. Chronic cuff implantation may therefore cause limited early degeneration followed by complete regeneration. The time scale of these competing processes is not clearly established[9] and many experimental factors influence the outcome [Buti et al., 1996; Daly et al., 1996; Luff et al., 1988]. In some circumstances, the regeneration may be dominant, resulting in an extension of motor unit size leading to larger tetanic forces [Carp et al., 2001; Vleggeert-Lankamp et al., 2004].
In the USA, the Food and Drugs Administration (FDA) recommends a cuff-to-nerve

[6]Mechanical irritation occurs mainly in the weeks directly following the implantation, when the cuff is not fully encapsulated in connective tissue. Stabilisation in cats (sciatic nerve) for example takes about 3 weeks [Mortimer, 1998].

[7]Nerve conduction velocity also decreases with ageing [Larsen et al., 1998]. If an experiment spans a considerable period of the animal's life time the data must be compared with control measurements.

[8]Peripheral nerve regeneration is a large field of research, and other methods are tested to enhance functional regeneration, such as ultrasound, nerve guides or scaffolds, nerve growth factor, etc [Grill et al., 2001b; Lago et al., 2005; Navarro et al., 1994; Raso et al., 2005].

[9]In rats, regeneration was shown to occur in some fibres after 3 months of constriction while degeneration continued in others for up to 3 more months, spreading to further fibres [Mackinnon et al., 1984].

diameter ratio of 1.5, to allow for post-operative swelling of the nerve. This number has been contested [Naples et al., 1988; Stein et al., 1977] and nowadays experimental cuff electrodes fit more tightly around the nerve, often allowing it to swell by passive compliance of the cuff inner diameter (e.g. self-curling cuffs) [Agnew et al., 1990a; Bullara, 1984; Grill and Mortimer, 2000; Loeb and Peck, 1996; Mackinnon et al., 1984; McCreery et al., 1992; Mortimer, 2000; Naples et al., 1988; Romero et al., 2001; Struijk et al., 1999; Tyler and Durand, 2002; Veraart et al., 1993]. As most nerves are rather elliptical, tight circular cuffs do reshape the nerves they trap [Romero et al., 2001]. Some cuffs intentionally reshape the nerve, providing passive adaptation to swelling but mainly in a "preferred" direction [Grill and Mortimer, 1998; Krarup and Loeb, 1989; Larsen et al., 1998; Leventhal and Durand, 2004; Tyler and Durand, 2003].

6.3 Literature review

Table 6.2 summarizes the different pressure levels applied to the cauda equina by various researchers, along with the consequences on the nerve root conduction and its nutritional support.

To give some perspective, these data must be compared with normal blood pressure [10]. In a healthy young adult (20-30 years old) the mean arterial pressure lies between 100 and 120mmHg (it increases with age). It is similar in dogs [Mandel et al., 1954] and large pigs [Olmarker et al., 1989b] and lower (down to 90mmHg and 50mmHg) in mini and micropigs commonly used in scientific research [Smith et al., 1990]. Paraplegia does not have a definite influence on mean arterial pressure, it only seems to "destabilise" it. Patients may be subject to peaks of hypertension followed within a few minutes by severe hypotension.

Venular pressure is also relevant as it affects nutritional support and oedema formation. While the arterial pressure follows a cyclic pattern, the venous pressure is not consistent. It depends on the height, weight, muscular bulk and sex of the patients; it will vary with posture, level of activity, and the vein in which the pressure is measured. The closer the vein is to the heart, the lower the pressure. Venous pressure in the legs (measured from veins on the top of the foot) of healthy human subjects was between 90 and 100mmHg, with a variation of $\pm$ 65mmHg during 1 minute of treadmill walking [Kugler et al., 2001]. The pressure measured on the nerve roots of patients (when in prone position) suffering from lumbar disc herniation in Takahashi et al. [1999] ranged from 7mmHg to 256mmHg (mean$\pm SD$ is 53 $\pm$ 49mmHg). High pressures were associated with neurological deficits while at lower levels chemical irritation by nucleus

[10] Briefly, "the blood pressure is that pressure which must be applied to an artery in order to stop the pulse beyond the point of pressure" [Macpherson, 1995]. When the left ventricle contracts to expel the blood out of the heart (systole), the pressure in all arteries rises. The systole is followed by a resting phase, the diastole, associated with a lower arterial pressure (the difference between systolic and diastolic pressures is called the *pulse pressure* and is about 40mmHg in human). The *mean arterial pressure* (MAP) is by definition the diastolic pressure plus one third of the pulse pressure. The term blood pressure without any specification usually refers to the maximum systolic pressure [Sears, 1959]. Blood pressure readings are often given in pairs: the systolic and diastolic pressures.

pulposus [11] is believed to be partly responsible for the generation of pain [Takahashi et al., 2003]. The importance of mean arterial pressure (MAP) on neurological deficit during root compression was assessed in Garfin et al. [1990] and Lind et al. [1993]. Compression experiments performed on hypotensive and hypertensive pigs showed a correlation between the MAP and the onset of electrophysiological changes. These findings can be related to those of Olmarker [1991]; Olmarker et al. [1989b]; Rydevik et al. [1981]; Takahashi et al. [1993] who showed in rabbit and pig caudae equinae that the extradural pressure required to interrupt arteriolar blood flow was close to the MAP.

6.3.1 Relevance for human nerve root compression

There are no data available for chronic compression of human roots trapped in a book electrode implanted inside the cauda equina. It is therefore important to understand the limitations of other studies [12] when trying to infer a safe pressure limit for the implantation of book electrode intradurally. The relevance of any publication depends on answers to the following three questions: *(i)* What would be the influence of a spinal cord injury on the results?; *(ii)* How does the animal model compare with human nerve roots? and *(iii)* How was the pressure applied?

(i) Nerve roots do not change after injury [Schalow et al., 1995] but there may be some alteration in the overall blood pressure which could affect the nutritional supply. The consequence of compression can be studied on spinally intact animal models provided that blood pressure is explicitly monitored.

(ii) The most common animal for spinal cord and nerve root compression studies are the pig [Cornefjord et al., 1997; Olmarker et al., 1991] and the dog [Konno et al., 1995b] due to the anatomical, morphological and vascular similarities of their spinal canal with the human sacrolumbar cord. At the level of the 7th lumbar vertebrae, there are 8 to 12 pairs of roots in the cauda equina, and 2 to 3 pairs of individual, extrathecal, roots. The ratios of myelinated to non-myelinated axons are similar, as are the pia, arachnoid and dura. Other animals used less frequently are the rat, rabbit and cat.

(iii) There are different ways to apply pressure to the nervous structure. Most often the spinal cord and roots are exposed by a laminectomy of the lower lumbar, sacral or upper coccygeal vertebrae and the dura is left untouched [13]. One or two inflatable balloons are then fixed to the spine and inflated to compress the underlying nerve roots and spinal cord at a known pressure. While this defines the pressure accurately [Konno et al., 1995b; Olmarker et al., 1991], it also introduces some limitations [Konno et al., 1995a; Olmarker, 1991; Pedowitz et al., 1992]. Due to the nature of the operation, the measurements are usually acute (up to 4 hours), although a slightly different method

[11] The nucleus pulposus is the gelatinous inner core of an intervertebral disc [Macpherson, 1995].

[12] Extrathecal compression (of cauda equina and individual nerve roots) has been studied in relation to disc herniation, neuropathic pain, chronic back ache, etc. But peripheral nerves, extrathecal roots and spinal cord all react differently to constriction [Fern and Harrison, 1994b; Garfin et al., 1995; Gelfan and Tarlov, 1956; Rydevik et al., 1991].

[13] Only in Sharpless [1975] was the dura opened to compress the nerve root per se.

has been used for longer experiments [Kikuchi et al., 1996; Takahashi et al., 2003]. A cuff can also be implanted to constrict the spinal cord or individual nerve roots proximal to the dorsal root ganglion [14]. In Delamarter et al. [1990], a nylon band (like a cable-binder) has been used to constrain the spinal canal. Olmarker and coworkers used a special constrictor that shrinks slowly after implantation to increase the compression gradually. For peripheral nerves studies, various cuffs have been used, allowing for longer-term experiments [Dyck et al., 1990; Fern and Harrison, 1994a]. The balloon method only imposes a unidirectional pressure, but the level can be set and monitored accurately. The constrictors do not provide a mean of pressure monitoring, but they allow for longer term experiments with shorter compression zones. The pressure is applied radially, evenly distributed around the nerve, root or cord.

6.3.2 Morphology

Structurally, a peripheral nerve is surrounded by a thick sheath, the epineurium, and each fascicle is itself surrounded by its own protective perineurium (see section 1.1.3.3, page 7). These sheaths provide valuable mechanical strength to the nerve [15]. The spinal nerves also have some protective layers (the dura and meninges). Inside the dura, the roots and rootlets are freely moving in cerebro-spinal fluid simply surrounded by a thin pia, without any other protection [Olmarker, 1991]. In mice, the peripheral nerves and roots show a similar elasticity, but the nerves are 10 times stronger longitudinally and 5 times stiffer, i.e. less likely to deform under radial pressure [Beel et al., 1986]. Table 1.1, on page 12, summarises the properties of nerve roots and peripheral nerves, unfortunately, stress rates were not available and the comparison is therefore incomplete.

6.3.3 Nutritional support

In a peripheral nerve, small blood vessels can be found in the endoneurium, with anastomoses to larger arterioles and venules running along the perineurium and epineurium. The nutritional support of the roots is more complex with contributions from both the CSF and blood vessels [Garfin et al., 1995, 1991; Parke et al., 1981, 1999; Parke and Watanabe, 1985] [16]. As detailed in section 1.1.4, the arteries running in a root and feeding it receive blood from larger support arteries both proximally and distally; but have no connection with the extrinsic vessels running along the root [Olmarker, 1991; Parke and Watanabe, 1985; Rydevik et al., 1990]. There is therefore a supply of blood to the nerve root from both ends, but no additional interconnection radially along it. This could make it more susceptible to an interruption of the vascular network [Mao et al., 1998; Matsui et al., 1997, 1992]. On the other hand, the occurrence of neovascu-

[14] For anatomy see fig. 1.3 on page 5.

[15] Rydevik inflated a fascicle to a pressure of about 1000mmHg before bursting the perineurium. Although this is not a measure of rigidity, or resistance to external pressure, it gives an idea of the perineurium's mechanical properties [Rydevik et al., 1989].

[16] The nutrient contribution of CSF in human lumbar roots can be as high as 60 % [Parke and Watanabe, 1985].

larisation helps the root to adapt to alteration of its vascular network [Cornefjord et al., 1997; Rydevik et al., 1989].

6.4 The mechanisms of compression injury

While it is established that compression, chronic or acute, of a spinal root above a certain level is harmful, the mechanisms underlying nerve root damage are not always clearly recognised [Garfin et al., 1991]. The rate of onset of compression, the extent of the compressed area, the pressure amplitude and duration all influence the consequences of entrapment [Battista and Alban, 1983; Olmarker et al., 1990a,b, 1989a]. Compression introduces both a mechanical deformation and an alteration of the nutritional support of the root. The consequences are hypoxia or anoxia, endoneurial oedema, increased endoneurial fluid pressure, depolarisation and disruption of the physical integrity of the axons and supportive cells. These lead to cell death, demyelination and degeneration (axotomy). In the following pages different factors contributing to compression injury are analysed in an attempt to understand their individual contribution and interaction, they are eventually summarised in figure 6.3.

6.4.1 Damages of vascular origin

Compromised blood flow may cause oedema and anoxia. The pressure required to interrupt the arterial flow is directly related to the mean arterial blood pressure [Olmarker et al., 1991; Rydevik et al., 1981; Takahashi et al., 1993][17]. A milder compression might result in increased endoneurial fluid pressure and oedema formation which decrease the excitability of the nervous tissue but may recede before the occurrence of anoxia and cell death [Matsui et al., 1992]. Venular occlusion occurs at lower pressure and causes an interruption of the capillary flow at similar, slightly higher level. Yet it is less critical since the venous network has more anastomoses with outward vessels and is unlikely to be completely obstructed by local compression [Garfin et al., 1995; Matsui et al., 1992]. This may lead to a slight decrease in CAP amplitude without signs of sensory or motor deficit [Delamarter et al., 1990]. The vascular network can also adapt to localised compression by neo-vascularisation, as seen by the improvements recorded after two weeks or one month of low pressure when compared to one week [Delamarter et al., 1990; Otani et al., 2001]. This is explained by the presence of both a distal and a proximal supply to the root. Neo-vascularisation has been shown to proceed from the non occluded end to compensate for the disturbance of the other vessels but no clear time-scale can be inferred from the literature (range 1 day to 2 months) as this process competes with others. If anoxia does occur, the large myelinated axon will degenerate first [Dahlin et al., 1989; Fern and Harrison, 1991; Gelfan and Tarlov, 1956][18]. Small, non-myelinated fibres have been described in Fern and Harrison [1994b] as having a "disproportionately high resistance to ischaemia".

[17] Provided the onset of pressure is slow to avoid structural destruction

[18] This early degeneration of larger fibres is also observed in peripheral nerves [Jellema and Teepen, 1995; Struijk et al., 1999].

Table 6.2: Nerve root compression studies.

Pressure (mmHg)	Animal	Timing (compression-recovery)	Position [a]	Consequences	Reference
Sham operation	pig	1 week - none	S1L cranial to the DRG	Signs of inflammation, hyperaemia and epidural bleeding	Cornefjord et al. [1997]
5 to 10	dog	1 week - none	lumbar	Reduction in nerve conduction velocity	Kikuchi et al. [1996]
	dog	1 week - none	lumbar	Reduction in blood flow speed	Otani et al. [2001]
	dog	1 month - none	lumbar	No difference in conduction velocity	Otani et al. [1997]
	dog	1 week - none	lumbosacral [b]	Reduction in root conduction velocity	Mao et al. [1998]
	dog	1 month - none	lumbosacral [b]	Lesser reduction in root conduction velocity	Mao et al. [1998]
	pig	120 min - 90 min	sacral [b]	Significant changes in the venous blood flow of the lumbosacral nerve root	Matsui et al. [1992]
	pig	45 min - 30 min	sacral [b]	7.5mmHg: no effect on blood flow 11.5mmHg: 70% decrease within 15 minutes, recovery to 10% below normal	Baker et al. [1995]
30-40	pig	120 min - none		Blood flow interrupted in venules (30mmHg) and capillaries (40mmHg)	Olmarker [1991]
	human	30 to 90 min	carpal canal	Mild functional changes	Lundborg et al. [1982] [?]
	rat		L4 to L7 exposed [c]	Decrease in CAP amplitude	Sharpless [1975]

[a] whole cauda equina compression unless otherwise specified.

[b] Double site compression.

[c] Dura dissected, possible damage to blood supply.

[?] Paper not read, reference from abstract.

Pressure (mmHg)	Animal	Timing (compression-recovery)	Position [a]	Consequences	References
50	rabbit			Blood flow interrupted in venules (40-60mmHg)	Rydevik et al. [1981]
	pig	120 min- 20 min	coccygeal	Signs of oedema formation upon release, increase in vascular permeability, full recovery	Olmarker et al. [1989a]
	pig	120 min- 90 min	sacrococcygeal	No significant changes in efferent EMG or afferent CAP amplitude nor conduction velocity, no histological changes	Rydevik et al. [1991]
	pig	120 min - 90 min	sacrococcygeal	No significant changes in efferent EMG or afferent CAP amplitude nor conduction velocity, no histological changes	Pedowitz et al. [1992]
	dog	120 - 90	lumbosacral	No reduction in conduction velocity [d]	Otani et al. [1997]
	dog	120 - 90	lumbosacral	No reduction of conduction velocity [e]	Kikuchi et al. [1996]
60	rabbit			Blood flow interrupted in capillaries (50-70mmHg)	Rydevik et al. [1981]
		360 min - none		Functional changes, viability of nerve root jeopardized [f]	Rydevik et al. [1989]
70 - 75	rabbit			Interrupted blood flow (MAP 78mmHg)	Rydevik et al. [1981]
				No histologic damage	
	pig [g]	120 min -40 min		Threshold to cause afferent and efferent neurophysiologic changes	Rydevik et al. [1991]
				Decrease in nerve signal amplitude, full recovery	

[a] Whole cauda equina compression unless otherwise specified.

[d] Mean arterial pressure 90-150mmHg.

[e] Acute compression applied after 1 month of 10mmHg compression.

[f] Interpretation based on a study of peripheral nerve compression [Rydevik et al., 1981].

[g] Mean arterial pressure 70-100mmHg.

Pressure (mmHg)	Animal	Timing (compression-recovery)	Position [a]	Consequences	References
100		120 min - 90 min		mild endoneurial oedema, decrease in CAP amplitude, incomplete recovery	Rydevik et al. [1991]
	pig [g]	120 min -90 min		Decrease of CAP amplitude with full recovery (faster for motor fibres)	Garfin et al. [1995]
	pig [d]	240 min - 90 min		Incomplete ischaemia, moderate endoneurial oedema, decrease in roots conduction velocity more noticeable for efferent, incomplete recovery, better for efferent than afferent	Pedowitz et al. [1992]
		120 min - none		Reduction of muscle action potential amplitude	Olmarker [1991]
		45 min - none		Complete motor block	Gelfan and Tarlov [1956]
	dog	120 - 90	lumbosacral	No reduction in root conduction velocity [e]	Otani et al. [1997]
	dog	120 -90	lumbosacral	Slight reduction in root conduction velocity followed by rapid recovery [h]	Kikuchi et al. [1996]
		1 week - none		Disturbance of axonal flow of essential elements (proteins, lipids)	Kobayashi et al. [2004]
				Incomplete ischaemia, mechanical deformation more damaging to the nerve	Gelfan and Tarlov [1956]

[a] Whole cauda equina compression unless otherwise specified.

[d] Mean arterial pressure 90-150mmHg.

[e] Acute compression applied after 1 month of 10mmHg compression.

[g] Mean arterial pressure 70-100mmHg.

[h] Acute compression applied after 1 week of 10mmHg compression.

Pressure (mmHg)	Animal	Timing (compression-recovery)	Position [a]	Consequences	References
130				Blood flow interrupted in arterioles (pigs blood pressure around 130mmHg)	Olmarker [1991]
200		120 min - 90 min		Complete conduction block of afferent signals, little recovery, changes of myelin sheath, hemorrhage around nerve fibres, endoneurial oedema	Rydevik et al. [1991]
	pig [g]	240 min - 90 min		incomplete ischaemia [i], complete block for both afferent (120 min) and efferent (180 min), better recovery of efferent than afferent	Pedowitz et al. [1992]
		120 min - none		Reduction of muscle action potential amplitude	Olmarker [1991]
		120 min -90 min		Decrease of CAP amplitude with full recovery	Garfin et al. [1995]
				Incomplete ischaemia, mechanical deformation more damaging to the nerve	Gelfan and Tarlov [1956]
		60 min - none		Complete motor block	Gelfan and Tarlov [1956]
		10 - 20		Complete interruption of blood flow in intrinsic vessels, full recovery [j] no oedema formation	Olmarker et al. [1989b]
		120 -20		Idem with oedema formation	Olmarker et al. [1989b]

[a] whole cauda equina compression unless otherwise specified.

[g] Mean arterial pressure 70-100mmHg.

[i] Oxygen reached compression site either by diffusion from adjacent tissue or through the air [Pedowitz et al., 1992; Rydevik et al., 1991].

[j] Only blood flow data, no CAP monitoring.

6.4.2 Biochemical influence

Cornefjord et al. [1996] have shown that the biochemical effect of nucleus pulposus, applied for seven days around the sacral root (S1) of a pig, on dorsal nerve root conduction is comparable to that of mechanical compression by constriction of the root distal to the DRG [19]. The reduction of conduction velocity following nucleus pulposus exposure was attributed to a chemical disruption of the blood supply [20] as there was little axonal damage. The biochemical and mechanical effect did not add, when combined by trapping some nucleus pulposus on the root under an aneroid constrictor, to further decrease the conduction velocity. This highlights the fact that different mechanisms contribute to the integrity of a nerve root, and that alteration of any one of them is enough to cause noticeable disruption.

6.4.3 Damage of structural origin

A nerve root may adapt to mechanical deformation provided the compression is applied slowly (15-20s in [Pedowitz et al., 1992]) with respect to the remodeling rate and remains below a deformation limit above which direct mechanical destruction takes place. Until this limit is reached there are few alterations to the nerve root integrity and those are mainly transient (analogy with elastic and plastic deformation). The structural pressure limit for extrathecal root and cauda equina is above 200mmHg in pig and dog models and is likely to be rather high in humans too.

Faster onset rate or higher pressures will damage the nervous cells, causing demyelination and degeneration before anoxia becomes critical. This is especially important for short compression sites ($\approx 5mm$) where neo-vascularisation can compensate for occluded blood vessels [Gelfan and Tarlov, 1956]. If the compression is applied radially along a preferential axis, the nerve or root will flatten (the cross-section becomes more ellipsoidal) and, as the perimeter increases, the outer layers will stretch and suffer most damage. If, on the other hand, the nerve is wrapped within a constricting cuff, the compressed tissue will stretch lengthwise (as it is squeezed out of the cuff) to adapt to the confinement; and the displacement, as well as the pressure gradient, will be maximum at the edges of the constrictor ("Edge Effect") [Macgregor et al., 1975]. The pressure exerted on the larger fibres will be stronger because of their radius of curvature. The shear stress will cause acute structural damage to the nerve fibres and blood vessels [Rydevik et al., 1989]. The large fibres will be more deformed, hence failing at a lower pressure level than the smaller one. At extradural pressures of 100 to 150mmHg, the motor fibres of the spinal cord and roots (in dogs) were shown to be less resistant than the sensory fibres [Gelfan and Tarlov, 1956]. Likewise with cat sciatic nerves at 250mmHg, conduction in large fibres failed after 35min. At lower pressure (70mmHg), the smaller fibres failed first (56min to block). The delay was

[19] DRG: dorsal root ganglion, see fig. 1.3 on page 5

[20] The proposed mechanism of action of the nucleus pulposus is a disturbance of the nutritional blood supply causing ischaemia.

however much longer (35 vs. 56min). Myelin, which only surrounds the larger fibres, might play a role in their low pressure resistance. High pressure block is linked to earlier failure of thinner, deeper, capillaries. In Olmarker et al. [1989b], the pressure was slowly increased up to 200mmHg (on extradural roots and cauda equina) without any permanent damages as seen by the instantaneous return of blood flow without oedema formation upon pressure release.

6.4.4 Length of compression site

The length of the compression site has various influences. A short constriction will lower the pressure limit for structural damages. Surrounding the root with a silicone rubber mount, even without compressing it, limits the interaction with the CSF locally, around the entrapped area. This effect will be worse for longer mounts. Further, neo-vascularisation does not return blood flow through the compressed area, it merely reaches its periphery and is therefore more likely to prevent damage for limited compression zones. During double-level compression, the section of root between the two compression sites suffers similar, albeit less severe, symptoms than the area directly under pressure. This difference highlights the importance of CSF in providing some nutritional supply to the root (as the roots are under pressure but some CSF is still able to percolate through the compressed area to reach the intermediate zone).

6.4.5 Regeneration and the influence of time

Four hours of compression do not affect the CAP amplitude more than two[21] but the longer period alters the recovery which is slower and starts later after a longer compression [Garfin et al., 1995; Pedowitz et al., 1992]. This might be due to the presence of an intraneural oedema whose importance was correlated to the duration of compression in Olmarker [1991]. The notion of reversibility upon release of the pressure is not so relevant here as the implantation of the electrode book is permanent[22].

At 10mmHg (double site compression), Mao et al. [1998] showed a slowing down of the nerve root conduction velocity after one week of compression, followed by some recovery as the pressure was maintained for a month. Complete recovery might have occurred had the experiment lasted longer [Delamarter et al., 1990].

Cornefjord et al. [1997] placed an aneroid constrictor around a spinal nerve caudal to the dorsal root ganglion for up to 4 weeks. Its inner diameter was 3.5mm and it gradually narrowed (to 3mm after 3 weeks). The nerve root diameter was less than 3mm and the compression was due to the post operative swelling and to scar tissue growth. The conduction velocity of motor fibres decreased during the first week, then remained constant (even increased slightly but with no statistical significance). Nerve fibre damage was seen under the constrictor, distal and proximal to it, epineural damage was present on both the compressed and the contralateral control root and endoneural damage was

[21] The reduction of nervous signal amplitude may be exponential.

[22] Even when an implant fails or gets infected and has to be removed, the books are left in place unless they pose a risk to the patient, for example if they are the source of the infection.

reported mainly on the compressed side.

Delamarter et al. [1990] studied in dogs the long term effects (3 months) of cauda equina compression using a nylon cable-binder to constrict the spinal canal to 25, 50 or 75% of its original cross-sectional area. In the last case, recovery of motor and sensory functions took place during up to 2 months after the constriction had been removed. Mackinnon et al. [1984], working on rat sciatic nerves, showed that alterations could take up to four months to become noticeable while regeneration was already observed after three months.

6.4.6 Post operative swelling and connective tissue growth

Up to 50mmHg, the short term histological changes have no apparent consequences on the amplitude of the nervous signal (no mention of the conduction velocity) [Baker et al., 1995; Garfin et al., 1995; Kikuchi et al., 1996; Mao et al., 1998; Matsui et al., 1992; Olmarker et al., 1989a,b; Pedowitz et al., 1992; Rydevik et al., 1991]. Rydevik states that the cauda equina and extrathecal nerve roots can sustain a pressure of 75mmHg without significant reduction of the amplitude of the nervous signal, and no alteration of the root structure [Rydevik et al., 1991][23]. With intrathecal implantation, the portion of nerve root in the slot might receive less nutrition from the CSF, or the blood vessels if these are occluded.

Post-operative swelling, with or without oedema formation, increases the pressure on the trapped root. It may not cause ischaemia as long as the maximum pressure does not exceeds 200mmHg (complete recovery is still possible with that pressure level [Garfin et al., 1995]). The oedema, if present, will eventually disappear, and the pressure decrease consequently. There will therefore only be a transient decrease in conduction velocity. If resorption of the swelling happens at a rate comparable to that of connective tissue growth, the volume freed by one process is taken up by the other and the pressure decreases only slowly if at all[24]. Although these results relate to extradural compression, a similar process takes place within the slots of a SARSI electrode-book. The excitability of anterior nerve roots has been seen to decrease in the days after the implantation of a SARSI. It then stabilises and sometimes increase slightly for a few month to a year. The early recovery is attributed to swelling resorption. It is slow and incomplete since connective tissue growth maintains a raised pressure. Partial degeneration may therefore occur, followed by regeneration. If the oedema recedes soon after the implantation, the excess pressure due to post-operative swelling and connective tissue growth may not lead to cell death, as seen in the histological sections presented in Brindley and Rushton [1990] which appear normal, with neither signs of degeneration nor any newly-grown axons.

[23]The long term viability of a peripheral nerve is considered at risk from 60mmHg [Rydevik et al., 1989].

[24]The growth of connective tissue has been shown to cause an added pressure increase responsible for nerve fibre damage and a slowing down of the conduction velocity after a month of entrapment [Cornefjord et al., 1997].

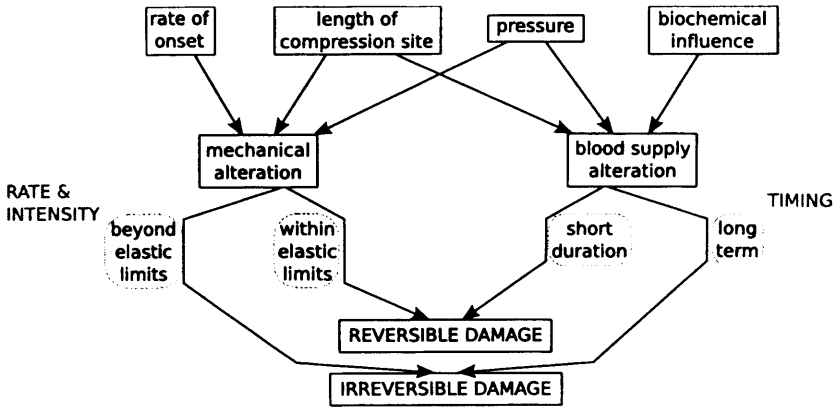

Figure 6.3: Summary of the various factors influencing nerve root function.

6.4.7 Discussion

Figure 6.3 illustrates the interaction between the various mechanisms of injury discussed above. Which consequences of nerve root compression are considered harmful for potential root stimulator patients? Without an answer to that question, no safe pressure limit can be inferred from the literature.

Some reduction in conduction velocity can be tolerated for motor roots. If recording from sensory fibres is envisaged, a decrease in afferent CAP amplitude should be avoided (reminder, afferent fibres are more resistant to pressure). Anterior nerve roots may regenerate, provided they have the room for it, which may not be the case if the compression is maintained. Degeneration should therefore be avoided. To avoid anoxia, the pressure exerted on the root should be lower than the mean arterial blood pressure of the patient. Oedema formation should also be avoided as the presence of an oedema may induce ischaemia even if the compression has ceased as it disturbs the blood flow. The pressure exerted on intradural nerve roots just after the implantation should be below 40mmHg to avoid venular stasis. This will help limit oedema formation during the first days after the operation. Swelling and connective tissue growth will cause a slow rise of pressure, which, based on table 6.2, should remain below 100mmHg to guarantee a minimal arterial blood flow. It is difficult to quantify how much a root will swell, and how thick a layer of connective tissue will form around it.

6.4.8 Conclusion

Considering the success of SARSI implantations and the lack of signs of degeneration, the large dimensions of the slot must be sufficient to accommodate for both swelling and connective tissue growth. A device that could guarantee a pressure lower than 40mmHg even for the largest root when fitted, and which would stretch to free a cross sectional area close to that of the actual SARSI slot without increasing the pressure above 100mmHg would be safe for chronic intradural implantation.

6.5 Space limiting lid

The idea of the space limiting lid was suggested by Prof. Craggs and investigated in the Implanted Devices Group at UCL. Besides solving the practical issues regarding the production and fitting of such lids, their safety was assessed. As explained earlier in this chapter, biocompatibility is guaranteed since the only material used is a medical-grade silicone rubber similar in fact to that used to form the original electrode book lid. Since this is a constraining device the main concern was the risks of nerve root compressions. The pressure exerted by the device on a nerve root, and its variation with post-operative swelling and connective tissue growth, had to be evaluated and compared to the maximum pressure that a root can withstand for long and short periods. This simple task encountered two issues: *(i)* there exist no recommendations on pressure limits for nerve roots or peripheral nerves and *(ii)* the pressure that the device exerts on a nerve root cannot be measured and monitored in vivo. The first issue was tackled with the literature review presented in the first part of this chapter, and the second was solved by the use of various models developed to estimate the pressure. As the investigation is still underway no pressure results will be presented. What follows are some pictures and extracts of a preliminary report written for a patent application requested by Prof. Craggs that was not taken forward.

6.5.1 Space limiting device for nerve or root interface

6.5.1.1 Description

Field This invention is a concept for an additional device that limits the volume surrounding a nerve or root fitted into a mount. It is particularly, but not exclusively, designed for electrical stimulation, nervous signal recording and compression injury studies. This invention also covers gauges to allow the surgeon to assess the need to fit the additional device depending on the nerve diameter and the application considered.

Statement The space limiting device will limit the available conductive space between a nerve and the mount it is trapped in. It may do so by filling in the extra space or by bringing an insulating wall (eventually a part of the mount) closer to the nerve. In either cases, the device may come in contact with the nerve which will then be trapped between the mount and the space limiting device. This must be considered when reviewing the design's safety. The main issues are biocompatibility and compression injury. While biocompatible materials for long term human implantation are nowadays readily available and indeed used to design implantable mounts, there are, so far, no guidelines on acceptable compression levels. A preliminary to any safety study therefore requires the establishment of such safe pressure limits. The risks of compression injury is further complicated by post-operative swelling which is likely to require a compliant device that is safe and efficient for a range of diameters. An extensive literature review and preliminary tests based on an implementation of the invention described hereafter have already been undertaken and gave encouraging results for the long-term safety of the

space limiting device. This invention includes a set of gauges to allow the surgeon to judge, during the implantation, whether the additional device is required depending on the diameter of the nerve and the application considered. As the mounts are designed to be operational with or without the space limiting device the surgeon is free to make a decision once the roots are exposed.

Such an invention could also be used in studies of nerve or root circular compression, whether for the development of new electrode-mounts or to advance medical understanding of compression (man-made, traumatic or slowly setting) and related neural lesions.

The invention that is presented here is an additional device that may be fitted in mounts designed to be implanted around nerves or roots. The mount must be self-standing, fully functional, without the device. Dedicated gauges are also described hereafter and considered a part of this invention.

Example An example of a potential application of the invention is described hereafter with references to the figures of the "Drawings and pictures" section.

Figure 6.5 is a schematic drawing showing the space limiting device fitted in a one-slot electrode-book.

Figure 6.4 shows schematic drawings of a three-slot electrode-book.

Figure 6.6 is a picture of an electrode-book in the spinal canal taken during a SARSI implantation.

Figure 6.7 are two frontal views of the same single slot fitted with two different space limiting devices.

The electrode-mount selected for this application is a silicone rubber electrode-book (object 1 or object 10) as used routinely for intrathecal nerve root stimulation. The book may contain one or more slots separated by inner walls (objects 2 and 3) and each slot contains three U-shaped electrodes (objects 4, 5 and 6). For simplicity only one electrode (object 4) is indicated in fig. 6.4(b) although three electrodes are present in each slot. For use, one or more nerve roots (object 7) are laid in the slots and the book is closed with a lid (object 8). The electrode-book presents many advantages: it is compact as up to four nerve roots may be trapped within a single mount (multiple slots), it has no sharp edges and the slots lay intrinsically open minimising the handling of the root and the associated risks of squeezing or stretching it. The space limiting device (object 9) is implemented as a thin sling of medical grade silicone rubber hanging U-shaped from the lid where it is fixed. Its dimensions are selected so that it runs the length of the book and does, at most, barely touch the root laid inside the slot during the operation. The sling is compliant and its thickness is controlled to insure that even with post-operative swelling there is no risks of long term compression damages to the nerve root.

This invention also relates to any system to gauge the extra space available between the nerve and the mount. Different implementations may be designed depending on the type of mount and the application envisaged. When using intrathecal electrode-books the preferred option is to prepare a set of lids adapted for different nerve root diameters. The walls of the books will be marked at different height with short cuts of suture thread. The surgeon may then judge how far up the root comes when resting at the bottom of the slot (see fig. 6.6, the sides and front edges of the wall are easy to see) and choose the lid and space limiting device accordingly.

6.5.1.2 Drawings and pictures

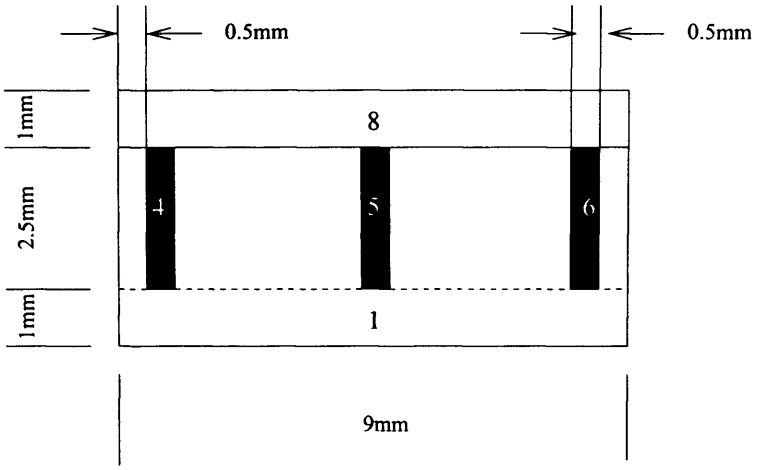

(a) Lateral cut in a tripolar electrode-book (object 1) closed with a lid (object 8), the electrodes (objects 4, 5 and 6) are U-shaped, running along both sides and the bottom of the slot.

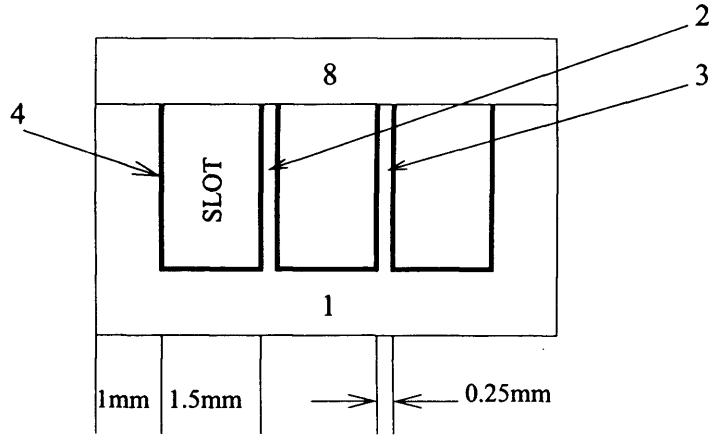

(b) Front view of a three-slot electrode book (object 1). The slots are separated by inner walls (objects 2 and 3). Each slot contains three electrodes (object 4).

Figure 6.4: LARSI electrode-book. These are schematic drawings no construction instructions, no cable is displayed for simplicity and the dimensions are given as indications.

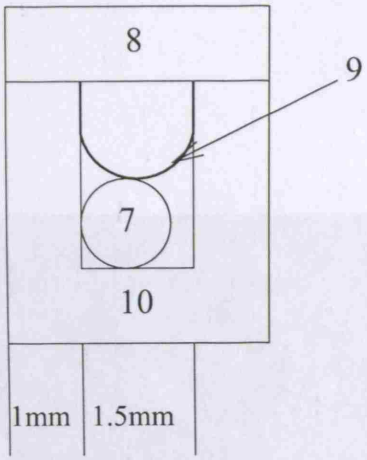

Figure 6.5: Space limiting device (object 9) fitted in a one-slot electrode-book (object 10) with a single nerve root (object 7) which will not , generally, be round. This is a schematic drawing not a construction diagram. No cable is displayed for simplicity and the dimensions are given as indications.

Figure 6.6: SARSI electrode-book during implantation, note the small size of the roots relative to the slots they are trapped in, photo courtesy of Dr. van der Aa.

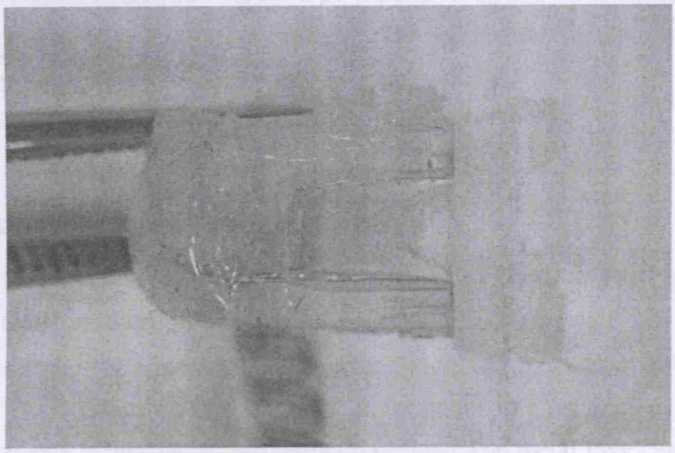

(a) Short space limiting device, 1mm depth.

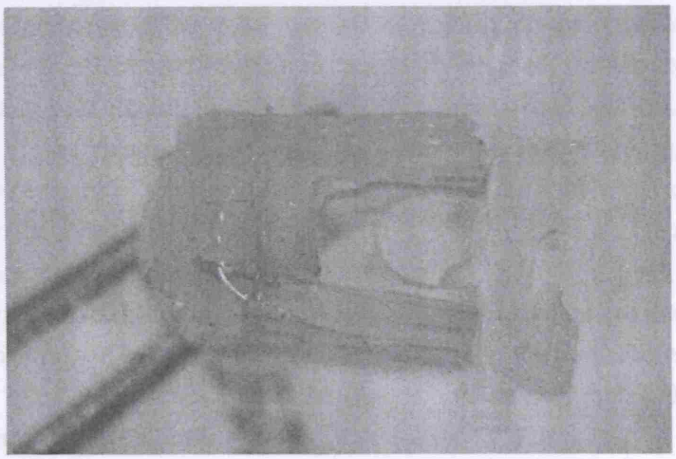

(b) Long space limiting device, 2mm depth.

Figure 6.7: SARSI single slot books fitted with space limiting lid.

Chapter 7

Electrode book: electrical equivalent circuit

7.1 Electrochemical considerations

7.1.1 Electrode-electrolyte interface without external voltage applied: the double layer interface

When a metal strip (the electrode) is immersed in a fluid (the electrolyte), charges on both sides of the interface are rearranged, with formation of a *capacitive double layer.* Three mechanisms contribute to this re-organisation. The metal may carry an excess or a penury of charge and a layer of charges of one sign appears on one side of the interface, while charges of the other sign are in majority on the opposite side. This phenomenon is transient, and equilibrium is quickly reached, leading to the appearance of a steady-state electric field E (without any external field applied). It is further enhanced by the preferential orientation of polar molecules in the fluid, and adsorption of ions on the surface of the electrode. The capacity of the double layer, by analogy with two parallel metal plates, is given by $C = \frac{q}{E}$ where q is the charge accumulated at the interface and E is the steady-state electric field.

This was first observed by Helmholtz, around 1850, who hypothesised that the surface charges are neutralised by opposite sign *counterions* in the solution. These counterions form a rigid layer, at a distance d from the surface equal to their radius. The potential across the interface varies linearly from ϕ_M to ψ_S, see fig. 7.1(a).

The second curve, subfigure 7.1(b), represent the Gouy-Chapman diffuse double layer. Gouy and Chapman independently suggested that while the charges on the metal could be represented by a rigid layer, the ions of opposite sign in the electrolyte formed a "cloud", denser towards the metal surface. In this representation, the ions are not rigidly held at the surface, they diffuse away, in a manner affected by their kinetic energy and the strength of the electric field, and the interface potential decays exponentially with distance to the phase boundary.

Both these representations fail to predict the actual charge distribution, and a third was suggested by Stern which combined both models, see fig. 7.1(c). This approach has since been refined, but it still holds for a basic understanding of the double layer con-

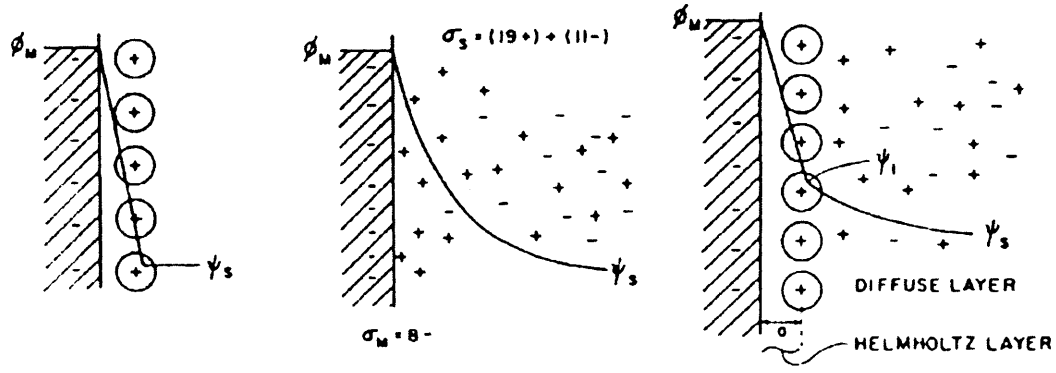

(a) Helmholtz double layer. (b) Diffuse double layer (Gouy-Chapman). (c) Stern double layer.

Figure 7.1: Double layer formation at the electrode electrolyte interface, pictures from Conway [last accessed in April 2007].

cept. Figure 7.2 is a slightly more detailed model presented by Grahame in 1947. The metal surface of the electrode is negatively charged. The solvent molecules are dipolar (mostly water molecules). They organise themselves around cations in the bulk of the electrolyte. Close to the electrode surface they are attracted by the negative charges and break their flower-like arrangement. Besides these, one adsorbed anion is shown, and a neutral molecule. In the direct vicinity of the electrode surface the polar molecules from the solvent form a tight layer, corresponding to the Helmholtz layer. With increasing distance towards the bulk of the electrolyte, they become less compact and some cations are present, as in the diffuse layer. The potential decreases at first linearly, from ψ_M to a potential on the Helmholtz plane called the ζ potential, then exponentially towards the electrolyte potential ψ_S.

The phenomenon so far explained are not the consequences of any external field, the appearance of the capacitive double layer is only due to local charge re-arrangement. Under the influence of an external voltage, the double layer is altered (charge re-organisation) but does not disappear. This alteration however implies that the capacity of the double layer varies with the applied potential, i.e. $C = \frac{dq}{dE}$ [Fisher, 2006].

7.1.2 Effect of an external voltage

When a sufficient external voltage is applied across a pair of electrodes immersed in a fluid, a current will flow. The transfer of charges at the electrode-electrolyte interface may involve either a further charge re-organisation [1] or the direct transfer of electrons [2] via reduction or oxidation reactions [Brummer and Turner, 1977b; Geddes and Baker, 1989; McCreery et al., 1987; Merrill et al., 2005]. The latter results in the production of new chemical products, some of which may be harmful if loose in the body.

[1] Also know as capacitive or non faradic charge transfer.

[2] Also known as faradic charge transfer.

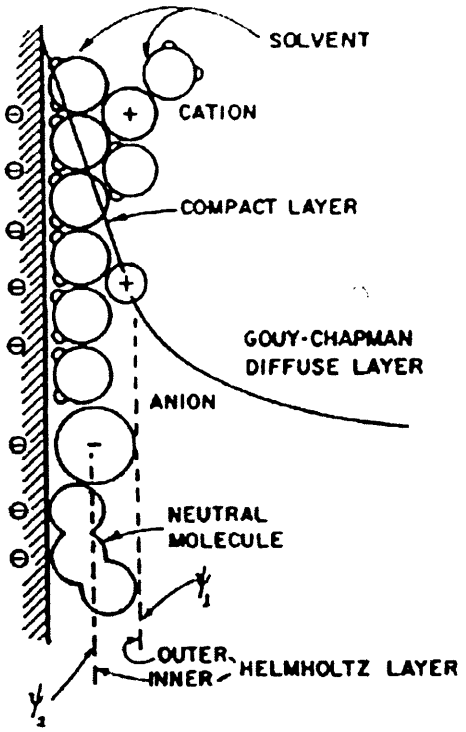

Figure 7.2: Electrode-electrolyte interface, double layer model by Grahame [Conway, last accessed in April 2007].

7.1.2.1 Reduction-Oxidation reactions

Considering only a platinum-iridium electrode in an electrolyte containing chloride (as is the case with CSF in the body), the following redox equations describe the electron transfer [McCreery et al., 1987; Merrill et al., 2005].

$$PtO + 2H^+ + 2e^- \leftrightarrow Pt + H_2O \tag{7.1}$$

$$IrO + 2H^+ + 2e^- \leftrightarrow Ir + H_2O \tag{7.2}$$

$$IrO_2 + 4H^+ + 4e^- \leftrightarrow Ir + 2H_2O \tag{7.3}$$

$$2IrO_2 + 2H^+ + 2e^- \leftrightarrow Ir_2O_3 + H_2O \tag{7.4}$$

$$Ir(OH)_{n+1} + H^+ + e^- \leftrightarrow Ir(OH)_n + H_2O \tag{7.5}$$

$$Pt + H^+ + e^- \leftrightarrow PtH \tag{7.6}$$

$$PtCl_4^{2-} + 2e^- \leftarrow Pt + 4Cl^- \tag{7.7}$$

$$PtCl_6^{2-} + 4e^- \leftarrow Pt + 6Cl^- \tag{7.8}$$

$$PtCl_4 + 2H^+ \rightarrow Pt + 4HCl \tag{7.9}$$

$$ClO^- + 2H^+ + e^- \leftarrow Cl^- + H_2O \tag{7.10}$$

$$O_2 \uparrow + 4H^+ + 4e^- \leftarrow 2H_2O \tag{7.11}$$

$$2H_2O + 2e^- \rightarrow H_2 \uparrow + 2OH^- \tag{7.12}$$

Equations 7.1 to 7.4 represent the formation and reduction of an oxide layer on the electrode. They are reversible because the products of the reactions are bound to the electrode surface. They can therefore change back to the original chemical species if the polarity of the voltage source (i.e. the direction of electron transfer) is reversed. Equation 7.5 is a reversible electron exchange, iridium changes valency (between 3 and 4) within the oxide. Equation 7.6 is also reversible as the hydrogen adsorbs at the platinum surface. This is sometimes referred to as *platinum pseudo-capacity* since the charges appeared to be "stored" at the metal interface. These reversible reactions (7.1 to 7.6) are acceptable during electrical stimulation because although some may cause a local pH variation they do not generate loose chemical reaction products that would erode the electrode and be potentially harmful in the body. The last six equations are irreversible since the products of the reaction will move away from the electrode before the inverse reaction takes place [3]. Reactions 7.7 and 7.8 (platinum corrosion) and 7.10 (chloride oxidation in electrolyte) produce harmful chemical species. Further, reactions 7.7 and 7.8 also lead to electrode dissolution, which will alter its electrical properties [4]. The reduction and oxidation of water, reactions 7.11 and 7.12, are undesirable since there is formation of a gas, and the presence of hydrogen and oxygen ions H^+ and O^- will alter the pH of the surrounding tissue [5]. Other reactions like the oxidation of glucose or other organic compounds have not been included here as they are less important and either reversible, harmless, or will be avoided if the other irreversible reactions are avoided.

7.1.2.2 Sequence

When a pulse of current is passed between a pair of electrodes in some conducting fluid, the redox equation describing the electron transfer will be one of the above, depending on the potential across the electrode-electrolyte interface. This is not directly related to the current density at the surface of the electrode, but to the charge transferred ($Q = i * t$) per units of surface area (C/mm^2). Fig. 7.3 is a plot by Brummer [Brummer and Turner, 1977c] of the potential excursion of a smooth (as opposed to sandblasted or covered with Pt-black) platinum lead [6] electrode in electrolyte under pulse condition ($100mA/cm^2$ of estimated real area). The potential on the Y-axis is measured versus a reversible hydrogen electrode (RHE) [7]. The subfigures of interest are c and d, where the

[3] The mobility of the reaction products depends to some extend on the electrolyte fluidity, which, in the case of CSF, is high enough to dissipate the newly formed chemical species quickly relative to the reaction duration.

[4] This reaction should therefore be avoided even during in vitro and terminal in vivo experiments.

[5] The buffering capacities of the body can cope with minute changes but from a safety point of view all irreversible reactions should be avoided.

[6] A *lead* electrode acts as the anode during the first phase of a biphasic pulse, then as a cathode. The opposite, acting as a cathode first, is known as a *lag* electrode.

[7] The reversible hydrogen electrode is a practical realisation of the Standard or Normal Hydrogen Electrode (SHE or NHE) which is the electrode of zero potential, to which all other electrodes are compared to establish their redox potentials. The SHE is in practice rather cumbersome to use and is often replaced by a RHE. The RHE potential versus the SHE is 0.04V.

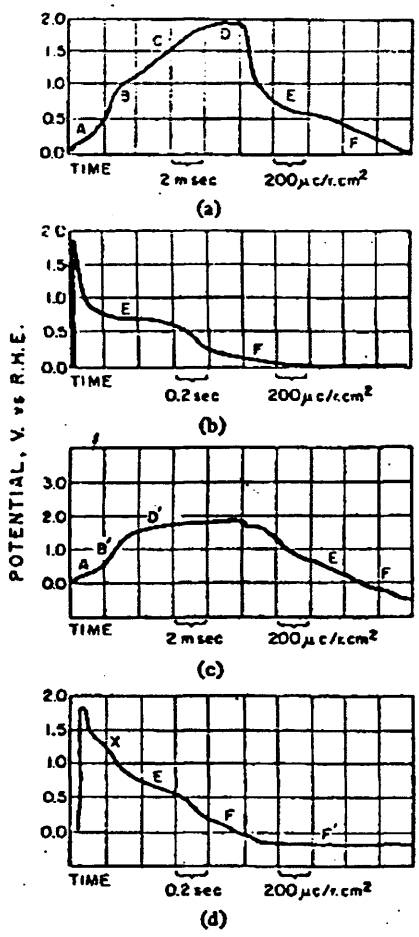

Fig. 1. Anodic charging curves at 100 mA/r.cm^2. (a) Current reversal at 100 mA/r.cm^2 in 1M $HClO_4$. (b) Current reversal at 1 mA/r.cm^2 in 1M $HClO_4$. (c) Current reversal at 100 mA/r.cm^2 in 0.13 M NaCl buffered at pH 7.3 with HCO_3^-/CO_2. (d) Current reversal at 1 mA/r.cm^2 in 0.13 M NaCl buffered at pH 7.3 with HCO_3^-/CO_2.

Figure 7.3: Potential of a platinum lead electrode versus a standard reversible hydrogen electrode reference, from Brummer and Turner [1977c]. In the original caption the units $r.cm^2$ are "real cm^2" as opposed to geometrical area, i.e. taking the roughness of the platinum in consideration.

electrolyte contains NaCl [8], and is buffered at pH 7.3. The curve is divided in slopes and plateaux each corresponding to a different dominant redox reaction.

A: Hydride oxidation, i.e. hydrogen atom plating, reaction 7.6, and double layer re-arrangement.

B (on sub-figure a only): Oxide formation and double layer re-arrangement: reaction 7.1 at the surface of the electrode, starts at 0.57V SHE; reactions 7.2 to 7.5 would occur if the electrode contained iridium.

B' (on sub-figure c only): The presence of Cl^- in the solution inhibits the surface oxidation processes. Instead, reactions 7.7, 7.8 and 7.10 are dominant. Note that the A slope is present in both subfigures, illustrating that the chlorine does not influence hydrogen adsorption.

D': Oxygen formation, reaction 7.11, starts at 0.82V SHE at pH 7. As can be seen from the equation, the oxygen evolution leads to the appearance of H^+ ions. As these cations accumulate by the electrode, the local pH decreases towards 0 and the potential of the reaction increases to 1.32V SHE. If the potential is maintained for some instants, the oxygen forms small bubbles easily seen with the naked eye.

X (on subfigure d only): Oxygen and chlorided products reduction, the oxygen reaction (7.11) is dominant. This is the reduction of the oxygen that has not moved away from the electrode. Although it is not explicitly marked, an X region can also be seen on subfigure c, after the plateau D but with a steeper slope than phase E.

E: Oxide reduction (reaction 7.1). On subfigure c and d (electrodes in saline, presence of Cl^-) phases E and X are not clearly separate. Besides the oxygen and oxide reduction there is a contribution from chloride reduction reactions.

F: Hydride formation, reaction 7.6 and double layer re-arrangement.

F': Hydrogen evolution, reaction 7.12, starts at -0.41V SHE at pH 7. Here the pH increases with the production of OH^- and the voltage for the reaction at pH 14 is -0.83V SHE.

The potentials RHE on the figure are slightly higher than the expected redox potentials given in the above explanation. Nevertheless both sets of subfigures (a & b or c & d) do show a succession of plateaux corresponding to the dominant redox equations of the system. The shift from one equation to the next takes place when there are

[8] From Brummer and Turner [1977c]: "The electrochemically significant components of extracellular fluids, such as c.s.f., are water ($\sim 55M$), NaCl ($\sim 0.13M$), HCO_3^- ($\sim 0.02M$), CO_2 ($\sim 0.05atm$), and various organic components such as glucose ($1.2 - 2.4mM$) and proteins ($200 - 400mg/l$)."

not enough reactants left to maintain the reaction (because they are too slow to reach the electrode surface, or because that surface has become covered by the products of the reaction). The maximum voltage swing, in both cases, is a little above 2V[9], it is limited by oxygen and hydrogen evolution ($1.32V + 0.83V = 2.15V$). This is called the *water window*. The voltage across the electrode-electrolyte interface does not increase further as these reactions are not rate-limited ie. the reactant are always available and the products of the reaction quickly move away by diffusion or as gas bubbles.

7.1.2.3 Influence of other parameters

In Donaldson and Donaldson [1986a]; McHardy et al. [1980]; Robblee et al. [1980] and Robblee et al. [1983], various factors influencing the rate of Pt dissolution were investigated: current density, voltage level, pulse width, frequency, electrode surface area, electrode roughness, fluid movements, presence of some components in the electrolyte, capacitive coupling of the electrodes, etc. The maximum charge that can safely pass through a specific electrode in a specific electrolyte depends on the situation in vivo, which is unknown. As summarised in Donaldson and Donaldson [1986a]:

> "The corrosion of stimulating electrodes in the body is complicated and depends on many factors. Although in principle it should be possible to measure how the rate of corrosion depends on the permutations of these factors, we believe that to do so would take up quite unjustifiable time and expense."

For this introduction it seems enough to summarise their major findings. The presence of proteins in the electrolyte [10], as will be the case in vivo, and the absence of oxygen decrease the dissolution rate. Studies of platinum electrode for stimulation have established general charge limits in vitro, in $\mu C/real\ cm^2$, and voltage ranges, or voltage maps [Craggs et al., 1986; Donaldson and Donaldson, 1986a]. The values reported for the safe injectible charge limit of Pt electrodes range from $35\mu C/real\ cm^2$ in Donaldson and Donaldson [1986b] to $300\mu C/real\ cm^2$ or $350\mu C/real\ cm^2$ in Brummer and Turner [1977b]. The larger values are obtained with the ultimate limiting factors of oxygen and hydrogen evolution. The more conservative value involves different processes including corrosion.

7.1.3 Charge balancing

Lilly and co-workers in the 1950s studied the effect of stimulation on the cortex of cats and monkeys. In Lilly et al. [1952], they established that even when heating was negligible, damage could still occur for large charge transfer. In Lilly et al. [1955], they reported no damage when a short stimulation pulse was followed, after some delay, by

[9] This is not a limit on the voltage between a pair of electrodes in saline, it is the maximum voltage across the interface of a single electrode.

[10] Obtained in vitro by addition of 10% blood serum in 0.9% NaCl saline.

another pulse of similar width but opposite current. Finally in his contribution to a book on brain stimulation [Lilly, 1961], Lilly summarised that damage may either have a thermal origin (proportional to the energy (Joule)) or electrolytic origin (proportional to the net charge, i.e. the non-balanced current). After these publications, various methods were investigated to limit the net transfer of charge [Mortimer and Kaufman, 1980]. In later studies, McCreery et al. [1992] found a link between nerve damage at low charge density and pulse shape. They claim that damage occurs at voltages below those of the harmful electrochemical reactions because of the "induced neuronal activity", i.e. an axonal hyperactivity due to the artificial nature of the stimulus.

Actively balanced pulses: the stimulator includes a circuit that produces both the stimulation pulse, and the "charge balancing" pulse. Depending on the complexity, there may be a delay, fixed or adjustable, between the two pulses. The shape of the pulses, their width and amplitude may also be adjustable, as long as the charges per phase, i.e. width times amplitude, are equal and opposite. This allows a relatively high stimulation frequency as the controlled discharge may be as fast as the discharge (the limits are imposed by the risks of anodal stimulation). Although this option seems ideal from a charge balancing point of view, the realisation of such a circuit is complex as the two pulses must be exactly matched to properly balance the charge. The stimulator may then become bulky, and less reliable, which, especially for implanted devices, are two major drawbacks.

Capacitor coupling: a capacitor is inserted in series with the electrodes. It will charge during the stimulation pulse. A passive discharge may then occur if the external capacitor and the electrodes are connected together as a loop. The capacitor and, with it, the electrodes will discharge exponentially. This option is simpler than the active charge balancing circuit and has the added advantage that the external capacitor (often called *blocking capacitor*) will limit the direct current in fault situations.

Pseudo-capacitance of polarisable electrodes: this method also uses a passive discharge phase, but instead of introducing an external capacitor, it relies upon the electrode pseudo-capacitance. As shown on page 164, the charges may be transferred via reversible redox processes. During the stimulation pulse, the potential across the electrode-electrolyte interface varies, charges are stored. They will naturally be "discharged" provided the electrode capacitor is not lossy, i.e. provided no irreversible reaction has taken place.

7.1.4 Conclusion for safe charge transfer

To summarise, both the electrolyte electrolysis and electrode corrosion should be avoided as they are irreversible, may have toxic effects and limit the longevity of the

electrode. This is achieved by providing a discharge phase after each stimulation pulse, so that no net transfer of charges occur. A key issue for any type of charge balancing scheme is that reversing the current does not guarantee that the reaction(s) occurring during the discharge is(are) the reverse of that(those) that took place during the charge. Two opposite irreversible reactions might balance the charge, leaving two types of chemical reaction products in the electrolyte. Illustrating this with simple equations, the ideal case is $A \leftrightarrow B$ while what might happen is $A \leftarrow B$ and $C \rightarrow D$. Although the electrode pseudo-capacitance, which is always present, would often be sufficient for passively balanced stimulation [11], external blocking capacitors are regularly added in the circuit to prevent passing direct current under fault conditions.

7.2 Equivalent circuit of electrodes in saline

7.2.1 Warburg impedance

The electrolysis of water and the corrosion of the metal are difficult to include in a simplified model of the contact impedance as they are non-linear and alter the working conditions as they take place [Grill and Mortimer, 1995b]. Assuming no excessive charge is passed through the electrodes, these reactions can be neglected and the following model holds.

An ideal electrode-electrolyte interface may be modelled as an access resistance R_a in series with a capacitor C_e (electrolyte pseudo-capacitance). The value of these components depends on the electrode type and area (including surface condition), the electrolyte, the frequency, and the current density. C_e increases and R_a decreases with increasing true electrode area and decreasing frequency (influences only C_e). This model is fairly simple and fails for direct current as the impedance then becomes infinite. Therefore, a leakage resistance [12] is added in parallel to the capacitance, see fig. 7.4. The interface is thus a capacitive reactance whose R and C are not constant.

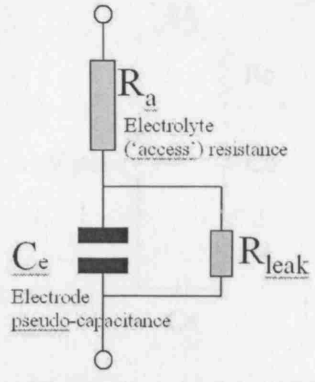

Figure 7.4: Warburg model of the electrode-electrolyte interface.

[11] Donaldson and Donaldson [1986b] reported a 99.76% discharge when passing 1mA for 20ms (60ms interval) through a spherical Pt electrode with a real area of $10mm^2$, or $200\mu C/real\ cm^2$.

[12] The term leakage resistance may be misleading and it is sometimes replaced by "faradic charge transfer resistance" R_{ct}.

7.2.2 Model for a book electrode limited to LARSI operating conditions

In the particular case of a root trapped in the slot of a book electrode (LARSI), Donaldson et al. [1998] proposed the following Thevenin equivalent for the complete output circuit (fig. 7.5). C_e is the pseudo-capacitance and R_a the access resistance from the ideal Warburg model. C_b is a blocking capacitor, physically present in the stimulator, to prevent the passage of direct current under fault conditions. R_c is the cable resistance ($\approx 90\Omega$ in LARSI[13]). Between pulses, the electrode circuit discharges through a $2.5k\Omega$ resistor (R_o) and the applied potential is 0V. During the current pulse, the potential rises to 8.33V and the charging resistor, R_o, is $1.1k\Omega$ (see table 7.1). As a fibrous capsule forms around the book and connective tissue replaces the more conductive CSF inside the slot, the access impedance varies significantly during the first months following implantation [Duan et al., 2004; Grill and Mortimer, 1995b; Thoma et al., 1988]. Donaldson et al. [1998] estimate that the access resistance between the central cathode and the two external anodes varies from 660Ω before implantation (in isotonic saline), to $1.32k\Omega$ in situ 100 days post-operation. This factor of 2 for access resistance increase post-operatively reported is not unusual.

Table 7.1: Values of the variable elements of the LARSI Thevenin equivalent circuit, from Donaldson et al. [1998].

Phase	V_{stim} (V)	R_0 ($k\Omega$)
Pulse	8.33	1.1
Discharge	0	2.5

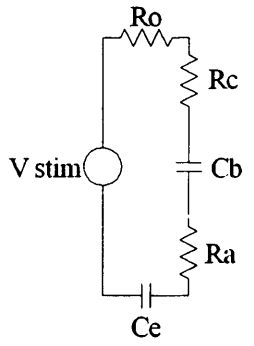

Figure 7.5: Thevenin equivalent of the electrode book in LARSI [Donaldson et al., 1998]. R_0 is the charge/discharge resistor, present in the implant, R_c is the cable resistance, C_b is a blocking capacitor, also present in the implant and R_a and C_e and the ideal Warburg components, R_{leak} assumed ∞.

[13] Cooper cable, nominal $2.2\Omega/cm$, 40cm length in LARSI.

7.2.3 Need for a general model

While the Warburg impedance is an idealised representation applicable to any type of electrode, the Thevenin equivalent circuit from Donaldson et al. [1998] has values specific to the LARSI operating conditions. If the books are to be used in different applications, there is a need for a more general model of a tripolar book slot. This need led to the in vitro study detailed hereafter. The aim was to provide a simple formula, valid for any book size, electrode dimension and implantation stage (environment conductivity). The starting model was a series of Warburg models (where R_a is the access resistance around the electrode and R_{leak} and C_e the electron transfer resistance and the electrode pseudo-capacitance) linked by R_{slot} elements representing the resistance inside the slot (connective tissue is mainly resistive [Grill and Mortimer, 1992, 1994]), see fig.7.6(a). The three electrode pads (rectangles 1, 2 and 3) are connected as follows; 1 and 3 are the anodes, connected together to a single wire, and 2 is the cathode, with it's own wire. The model may then be simplified as in fig. 7.6(b) where R_a includes the impedance of the connective tissue and CSF in the slot and R_{leak} and C_e are defined as before. Ultimately, if the formula is to be simple to use, it would be interesting to see the load as a resistor whose value vary with the book dimension and the conductivity of the environment (fig. 7.6(c)). The fact that the capacitive part of the impedance is neglected indicates that the formula will be an approximation, useful only to estimate maximum voltage drops under limited circumstances. How the capacitance is neglected, and what the limits of applicability of the formula are will be discussed at length in the following section 7.3. Five books of three sizes and with two types of electrodes (see table 7.6) were tested in salines of different conductivities. Their impedance was analysed with respect to conductivity and dimensions (of slot and electrode) to establish the respective influence of each parameters, the results are presented in the next section (7.4). Before establishing such a formula it is however relevant to discuss various factors that do influence the value of the Warburg equivalent circuit elements, making "generic impedance estimation" an uncertain task.

7.3 Parameters to consider when developing a new electrode model

The aim of the in vitro study was to develop a simple model of an electrode book in the spinal canal. To keep the equation practical, some parameters that do influence the electrode impedance had to be neglected. The reasoning that led to the simplifications is detailed hereafter in sections 7.3.1 and 7.3.2. As such these are not essential to the understanding of the model, the reader may skip them and jump to page 178 to concentrate on the model itself.

7.3.1 Influence of the current density and pulse duration

As explained in section 7.1, charges are transferred across the electrode-electrolyte interface following various redox reactions. The values of R_a, C_e and R_{leak} (fig. 7.4)

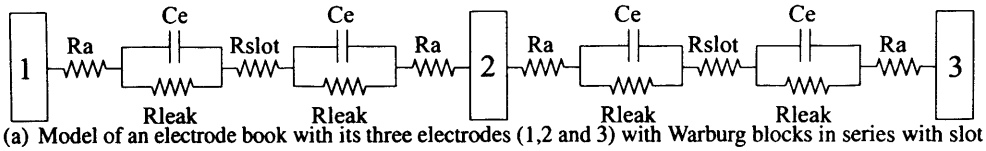

(a) Model of an electrode book with its three electrodes (1,2 and 3) with Warburg blocks in series with slot impedances (mix of connective tissue and c.s.f.) R_{slot}.

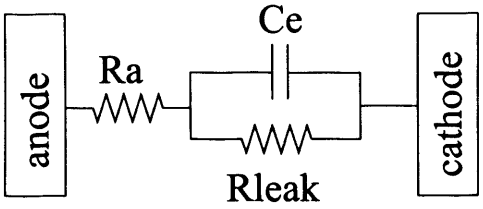

(b) Simpler model of an electrode book where the two outer electrodes (1 and 3) are connected together.

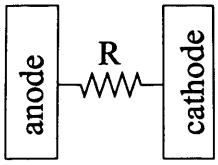

(c) Electrode book impedance idealised as a resistance function of the book dimension and environment conductivity.

Figure 7.6: Electrode book equivalent circuits at various stages of simplification.

depend on the dominant reaction which for a given electrode in a given environment varies with the current density and the duration of the current pulse (availability of the reactant). This dependency renders the Warburg model unpredictable (as its components do not have a fixed value) and impractical for implant design. Table 7.2 presents the results of a preliminary experiment performed to assess the influence of current density and pulse duration on the Warburg impedance elements. The voltage across the two anodes (outer electrodes in parallel) and the cathode (central electrode) of an electrode book immersed in saline was monitored on an oscilloscope while passing pulses of different width and amplitude. The conductivity of the saline was constant [14] and as the same slot was used for all pulses, so were the dimensions of the electrodes, and the volume conductor. R_{leak} was neglected as the error in estimating the slope on the oscilloscope screen was large [15] and with short pulses other sources of error hide that of neglecting the small voltage drop due to the leakage resistor. The influence of R_{leak} on the waveform is illustrated by figure 7.7 which shows voltage waveforms calculated for Warburg equivalent circuits (section 7.2.1) with $R_a = 600\Omega$, $C_e = 4.7\mu F$ or $2.2\mu F$ (based on results from table 7.2) and $R_{leak} = 300\Omega$, $1k\Omega$ or $5k\Omega$ in response to the same pulse of constant current I. The waveforms are analysed as follows. The instantaneous voltage variation is due to the series resistance R_a (600Ω) i.e. $V_{t1} = R_a * I$ (on fig. 7.7, $t_1 = 0$ for simplicity). A perfect capacitor of value C_e would then charge regularly during the pulse (dashed red line) giving $V_{t2} - V_{t1} = V_{C_e} = \frac{I*(t_2-t_1)}{C_e}$. The true waveform (black line) however shows a damped increase due to the leaky capacitance of the interface: $V_{t2} - V_{t1} = V_{RC}(t_2) = R_{leak} * I * (1 - e^{\frac{t_1-t_2}{R_{leak}C_e}})$. Introducing a Taylor series of the exponential function [16] and assuming that $t_1 = 0$ to simplify the notations in the equations, $V_{RC}(t) = \frac{I*t}{C_e} * (1 - \frac{t}{2R_{leak}C_e} + \frac{t^2}{6R_{leak}^2C_e^2})$. The slope of the voltage pulse at instant $t \approx 0^+$ is $\frac{I}{C_e}$ and making $R_{leak} \rightarrow \infty$ as with a perfect capacitor indeed gives $V_{RC}(t) = \frac{I*t}{C_e}$. R_a, C_e and R_{leak} may therefore be evaluated from the voltage response to a known constant current pulse. The main point of this preliminary experiment was to illustrate the variability of the value of Warburg elements. This was expected since the equivalent circuit translates the effect of complex electrochemical reactions and the value of the elements depend on the dominant reaction and the availability of the reactant amongst other factors. When specifying the output stage of a stimulator, the designer requires an upper limit for the load impedance (to estimate a maximum voltage drop). With the LARSI, the pulse width may be adjusted from a few microseconds to slightly less than a millisecond. From experience, the pulse width was rarely increased above $250\mu s$. To be practical, an equation used to estimate the load should be simple and to some extent intuitive. Trying to include variable capacitances and pulse width considerations would go against this spirit.

[14] Saline conductivity: $8.33mS$.

[15] The slope estimation error was grossly evaluated using a dummy circuit made of discrete components.

[16] $e^x = 1 + \frac{x}{1!} + \frac{x^2}{2!} + \frac{x^3}{3!} + \ldots$

Table 7.2: Values estimated for the simple Warburg equivalent circuit elements applied to an electrode book in saline.

current level mA	pulse width (μs)	R_a (Ω)	C_e (μF)
1.31	500[a]	610[b]	1.5
5.57	50	520	0.9
5.57	500	520	2
11.34	50	520	1.1
11.34	500	520	3.2

[a] At for this current level no measurement was made at $50\mu s$ as there was no noticeable slope.

[b] The resistive voltage drop was small with respect to the capacitive slope hence the poor precision on the access resistance evaluation. Higher currents gave more reliable readings as seen in the other results of this table.

Error when neglecting R_{leak}:
If the voltage difference V_{RC} is considered solely capacitive, i.e. neglecting the influence of R_{leak} and estimating $C_e^{\sim} = \frac{I*t}{V_{RC}}$, the error is:

$$\begin{aligned} C_e^{\sim} - C_e &= \frac{I*t}{V_{RC}} - \frac{I*t}{V_{RC}} * (1 - \frac{t}{2R_{leak}C_e} + \frac{t^2}{6R_{leak}^2C_e^2}) \\ &= \frac{I*t}{V_{RC}} * \frac{t}{2R_{leak}C_e} * (1 - \frac{t}{3R_{leak}C_e}). \end{aligned}$$

This error tends towards zero as $t \rightarrow 0$. More generally, to minimise the error the pulse width should be small with regards to the unknown time constant of the $R_{leak}C_e$ circuit. $C_e^{\sim}$ is always an upper approximation of the true value of the interface capacitor as shown by the simple reasoning of the following lines. If V_{C_e} is the voltage that would appear across C_e if it were a perfect capacitor i.e. $V_{C_e} = \frac{I*t}{C_e}$, while $C_e^{\sim}$ is the perfect capacitor that would charge to the measured voltage V_{RC}.

$$\begin{aligned} C_e &= \frac{I*t}{V_{C_e}} \text{ and} \\ C_e^{\sim} &= \frac{I*t}{V_{RC}} \\ \text{As } V_{RC} &\leq V_{C_e} \\ C_e^{\sim} &\geq C_e \end{aligned}$$

The question is to predict the voltage drop across the load for a given current pulse. Using $\frac{I*t}{C_e^{\sim}}$ will give the right voltage drop only if the pulse has the same width (t) as that used to evaluate $C_e^{\sim}$. The formula ($\frac{I*t}{C_e^{\sim}}$) applied to a shorter pulse will give a higher voltage drop and, conversely, with a longer pulse, a smaller drop.

7.3.2 Influence of the frequency

The load formed by any set of electrodes is a function of the frequency as seen with the capacitive Warburg impedance. This is further complicated by the fact that the components in the Warburg representation themselves will vary with the frequency and current density. As explained previously, the aim of this chapter is to provide a simple formula [17] to help with the design of future stimulators. As with pulse widths, frequency considerations should be omitted in such a tool to favour usability. It is however necessary to establish the relation between pulse width and frequency in the determination of load impedances in general to understand the influence of the measurement apparatus on the results. How can the impedance $Z(\omega)$ of a set of electrodes in saline measured with a bridge working at a given frequency (ω), be related to the impedance under normal conditions of use with square current pulses [18] evaluated by the method previously described? There is an instant t^* at which the voltage drop due to the current pulse equals that measured by the bridge, when impedance $Z(t^*) = \frac{V(t^*)}{I}$ equals $Z(\omega)$. Assuming that R_a and C_e have a constant value, and that R_{leak} is negligible:

$$\begin{aligned} V_{sine} = Z(\omega) * I &= (R_a + \frac{1}{j * \omega * C_e}) * I \\ V_{pulse} &= (R_a + \frac{t}{C_e}) * I. \end{aligned}$$

Hence $V_{sine} = V_{pulse}$ if

$$\begin{aligned} \sqrt{R_a^2 + \frac{1}{\omega^2 * C_e^2}} &= R_a + \frac{t}{C_e} \\ R_a^2 + \frac{1}{\omega^2 * C_e^2} &= R_a^2 + 2 * \frac{R_a * t}{C_e} + \frac{t^2}{C_e^2} \\ \frac{t^2}{C_e^2} + 2 * \frac{R_a * t}{C_e} - \frac{1}{\omega^2 * C_e^2} &= 0 \\ \frac{t^2}{C_e} + 2 * R_a * t - \frac{1}{\omega^2 * C_e} &= 0 \\ t &= \frac{C_e}{2}(-2 * R_a \pm 2 * \sqrt{R_a^2 + \frac{1}{\omega^2 * C_e^2}}) \\ t &= -R_a * C_e \pm \sqrt{R_a^2 * C_e^2 + \frac{1}{\omega^2}}. \end{aligned}$$

[17] A formula expressing the impedance of a slot as a function of its dimension and the conductivity of the environment.

[18] A current pulse may be described as "containing all the frequencies", large at the edges and low during the pulse.

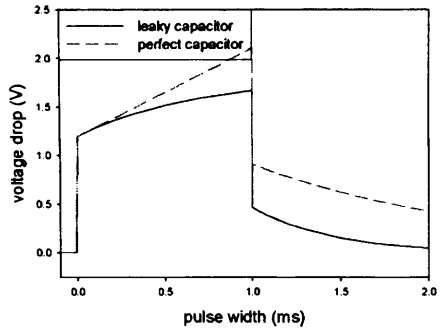

(a) $R_{leak} = 300\Omega$, $C_e = 2.2\mu F$.

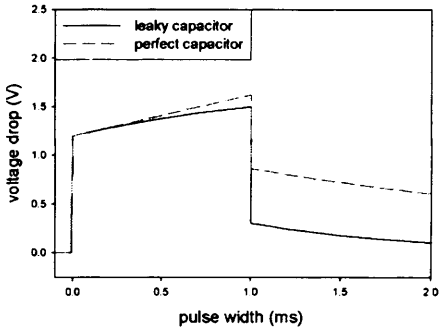

(b) $R_{leak} = 300\Omega$, $C_e = 4.7\mu F$.

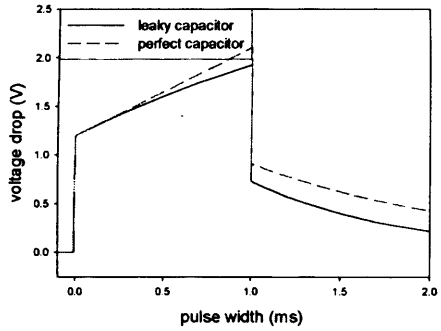

(c) $R_{leak} = 1k\Omega$, $C_e = 2.2\mu F$.

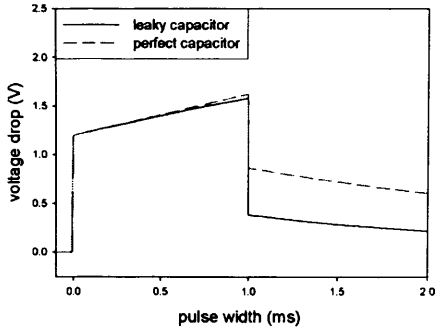

(d) $R_{leak} = 1k\Omega$, $C_e = 4.7\mu F$.

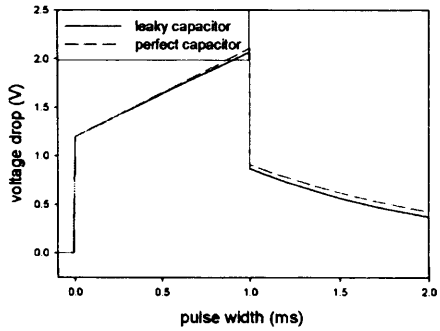

(e) $R_{leak} = 5k\Omega$, $C_e = 2.2\mu F$.

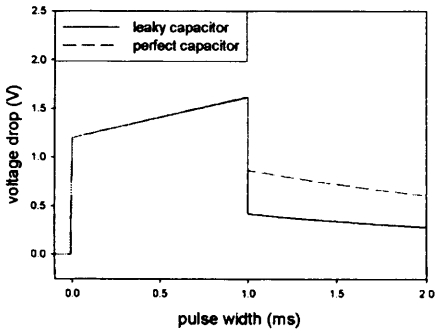

(f) $R_{leak} = 5k\Omega$, $C_e = 4.7\mu F$.

Figure 7.7: Voltage calculated across an ideal Warburg model (fig. 7.4) with perfect (dashed red line) or leaky (solid black line) capacitor. C_e is assumed completely discharged at $t = 0$. The values for the components are: $R_a = 600\Omega$, $C_e = 4.7\mu F$ or $2.2\mu F$ and variable leak resistance (300Ω, $1k\Omega$ or $5k\Omega$) as indicated.

Table 7.3: Pulse width and frequency equivalents.

Frequency (Hz)	R_a Ω	C_e μF	t ms
1000	1000	3	4.22
1000	600	3	7.02
1000	300	3	14
500	1000	3	16.8
500	600	3	27.9
500	300	3	54.6
250	1000	3	66.8
250	600	3	109
250	300	3	202
1000	1000	0.5	24.7
1000	600	0.5	39.6
1000	300	0.5	68.7
500	1000	0.5	92.7
500	600	0.5	137
500	300	0.5	202
250	1000	0.5	309
250	600	0.5	404
250	300	0.5	504

Using the above expression gives the instant t of a current pulse at which the impedance measured using a bridge at a given frequency ω equals that seen with the current pulse. That instant depends on the values of the Warburg elements. For illustration, the pulse width was evaluated at different frequencies using the formula, the results are presented in table 7.3. As explained earlier, these elements are representations of complex electrochemical reactions, and their value vary with the current density, pulse width and frequency.

7.4 In vitro study of tripolar slot for generic electrode books

Before presenting the results of the in vitro study, a note on the measurement device is required (section 7.4.1). A quick discussion on cable impedance follows (section 7.4.2)

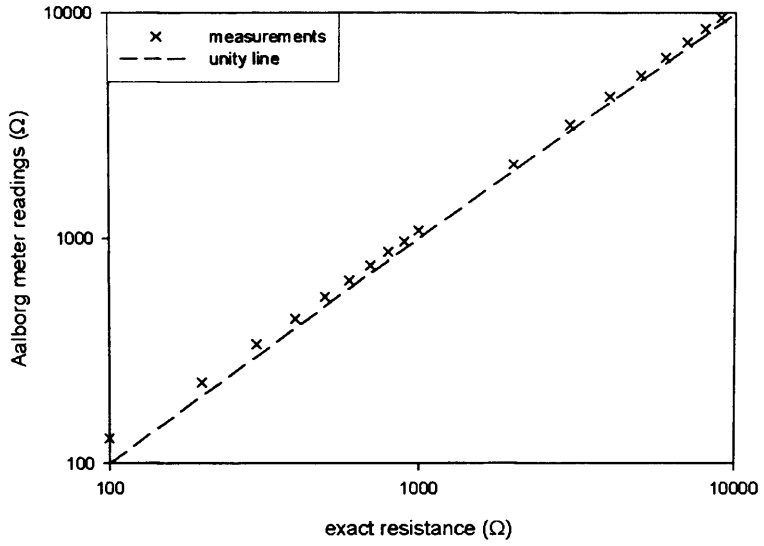

Figure 7.8: Aalborg impedance meter error.

before the results are detailed and analysed in sections 7.4.3 and 7.4.4.

7.4.1 Aalborg impedance meter

The impedances reported in this chapter were measured using a meter made at Aalborg university (DK). When tested against a set of resistors of known nominal value it exhibited a systematic error illustrated in fig. 7.8. This error can be written: $e = e_c + e_p * R$ where R is the exact resistance. To simplify the following reasoning, let us assume that the test resistors have exactly their nominal value, i.e. R in the aforementioned description of the error e. Then, any measurements will give an impedance value $Z_m = R + e_c + e_p * R$. The constants e_c and e_p can be broadly estimated graphically: when measuring low impedances, the constant part of the error, e_c will dominate over $e_p * R$; while for large values, the proportional part $e_p * R$ will dominate over e_c. In the latter case, a plot of the relative error $e_{rel} = \frac{e}{R} = e_p + \frac{e_c}{R}$ should have a constant tail (giving e_p, around 6% on fig. 7.9(b)). In the former case, a plot of the error e should be constant near the origin. On fig. 7.9(a), the smallest resistance measured is 100Ω, already too large to see a clear constant trend. A first order linear interpolation was necessary to find $e_c = 20$. The interpolation also gave a more precise value for $e_p = 5.65\%$.

The plots of figure 7.9 show the measurements together with the "error line" obtained when assuming that the Aalborg meter systematically adds 20Ω plus 5.65% of the impedance to any measurements. The correlation coefficient r^2 is 0.95.

The equation: $real\ value = reading - 20 - 0.0565 * reading$ has been applied to correct the measurements recorded with the Aalborg impedance meter. All impedances that follow have thus been corrected for this systematic error.

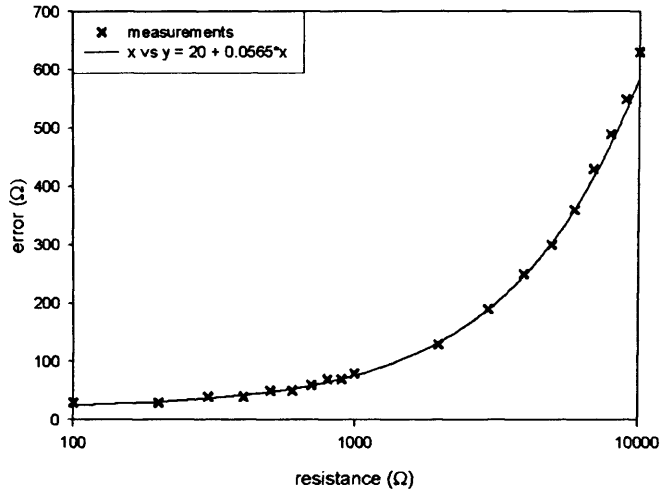

(a) Reading error.

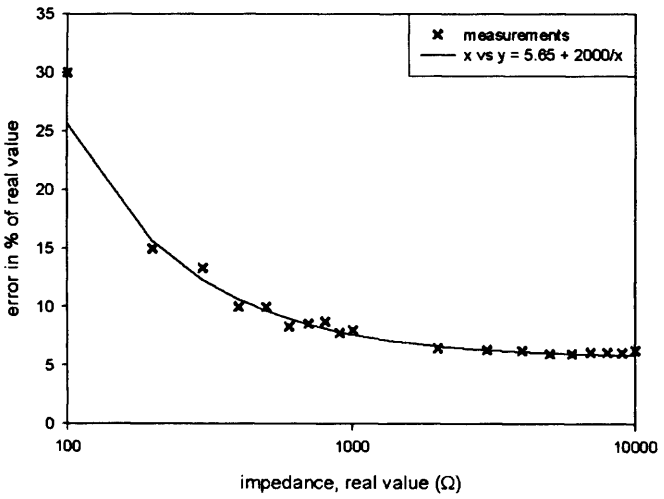

(b) Relative error.

Figure 7.9: Quantifying the error of the Aalborg impedance meter.

7.4.2 Cable impedance

Each electrode in the slot is connected to one wire of a three-strand helical Cooper cable (length 40cm), of resistance R_{wire}. At the end of this cable, the wires to the two outer electrodes (there are three electrodes in a slot, forming a tripole) are connected together, hence placing the two anodes in parallel. All impedance measurements therefore include a resistive cable contribution ($R_{cable} = R_{wire} + \frac{R_{wire}}{2}$) added to the actual slot impedance. In the results presented hereafter, this cable resistance was subtracted to analyse the slot impedance only, as would be measured across the electrodes; for the actual estimation of working conditions the cable resistance should be considered.

7.4.3 Influence of the conductivity

After implantation, the body produces a sheath of fibrous tissue [19] around the alien object. The properties of this envelope (thickness, resistivity, histology), depend on the bio-compatibility of the implanted item [Romero et al., 2001]. For connective tissue grown around a medical grade silicone rubber implant the resistivity was measured as $\rho = 627 \pm 108\Omega.cm$ or $1.6 \pm 0.25 mS/cm$, independent of the frequency, with a negligible imaginary part [Grill and Mortimer, 1992, 1994]. In mathematical models, CSF conductivity is generally set between 16.6 and $17 mS/cm$ [Coburn, 1980; Holsheimer, 1998; Sin and Coburn, 1983; Struijk et al., 1991]. This gives a range of two orders of magnitude of conductivities for the human tissues to consider for book electrodes implantation.

The impedance of the five different electrode books (closed with a silicone lid to constrain the conductor volume) was measured [20] in four solutions of different conductivity [21]. The salines conductivities were chosen to cover a range from CSF-like resistivity ($16.67 mS/cm$) to connective tissue ($1.67 mS/cm$) and below to account for any post-operative air bubbles or other less conductive tissues [22]. The dimensions of the books are presented in table 7.6 and discussed in section 7.4.4. The results are presented in table 7.4 and plotted on a bi-logarithmic graph in fig. 7.10, the measurements are indicated by symbols, the lines will be explained later. Looking at the alignment of the various symbols, there is a "power" relation between the impedance (Z) and the conductivity (σ) which may be expressed as the general equation: $Z = a * \sigma^b$ where a and b are constants. Matlab was used to evaluate the parameters a and b using a least squares approach, for values see table 7.5. Parameter b is nearly constant (with an average value $b_{average} = -0.886$) and the lines of fig. 7.10 follow the equation $log(Z) = log(a) + b_{average} * log(\sigma)$. The similarity between the symbols (representing the measurements) and these approximation lines with constant slope indicates that for all electrode and slot dimensions, the same process links conductivity and impedance.

[19] Initial tissue inflammation followed by fibrosis [Vince et al., 2005].

[20] Using an impedance meter made by Aalborg university, working at about $1 kHz$.

[21] Measured with a Jencons 4070 conductivity meter.

[22] The resistivity of connective tissue inside the human tight was estimated as $16\Omega.m$ in Reichel et al. [2002].

Table 7.4: Impedance measured (in Ω) for five electrode books in saline of different conductivities, both the systematic error from the Aalborg meter and the cable impedance have already been removed.

saline conductivity (mS/cm)	Z_{smallU} Ω	$Z_{normalU}$ Ω	$Z_{normalflat}$ Ω	Z_{largeU} Ω	$Z_{largeflat}$ Ω
0.833	6164	3420	6580	2297	5448
1.67	3145	1731	3439	1165	2825
8.33	711	410	844	268	702
16.67	390	240	504	155	419

Table 7.5: Parameters evaluated by matlab (least mean squares method).

	small U	normal U	normal flat	large U	large flat
a	5102	2802	5448	1887	4496
b	-0.921	-0.8874	-0.860	-0.901	-0.857

The second parameter, a, on the other hand, is related to the book dimensions. This dependency is the subject of the following section.

7.4.4 Influence of the book dimension

Five slots were compared, of three different sizes, see table 7.6 (the "small" dimensions are those of a LARSI book, "normal" for a SARSI book). For all of them the electrodes are made of platinum strips of equal width, therefore, the surface areas of the electrodes are in the same ratios as their length. Likewise, the distance between electrodes (along the slot axis) is the same in all books, so the volume conductor ratios follow those of the books cross-sectional areas.

In an attempt to understand the variation of the impedance with the book's dimension, it is tempting to separate the impedance due to the volume conductor from that at the electrode-tissue interface (which contributes the most to the capacitive element from Warburg's model). The total impedance could be seen as a sum of three contributions, from the cable, the electrode, and the tissue: $Z = Z_{cable} + Z_{electrode} + Z_{tissue}$. The results plotted in fig. 7.10, show that when the cable impedance is subtracted from the measurements, the remaining book impedance is proportional to the conductivity as $Z = a * \sigma^b$ (b is constant for all dimensions). The constant a must contain a term proportional to the electrode dimensions ($a_{electrode}$) and another term proportional to the volume conductor inside the slot (a_{tissue}). Expressing this in the impedance equation

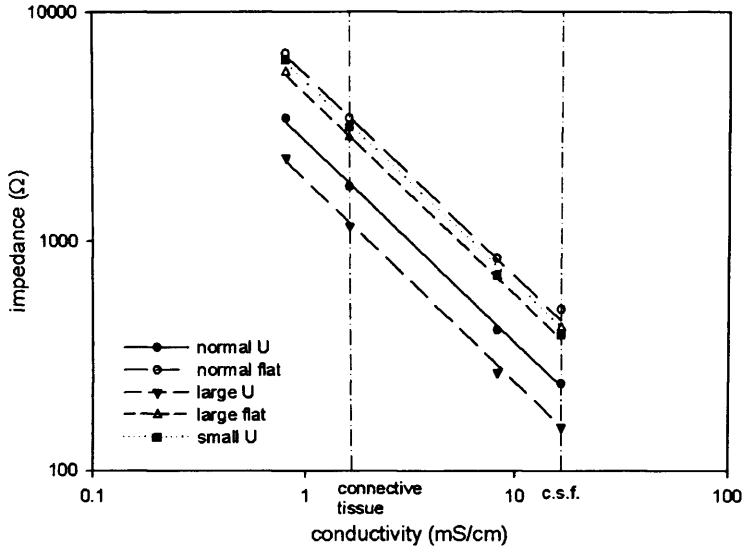

Figure 7.10: Book impedance as a function of media conductivity.

Table 7.6: Slot names and dimensions with corresponding electrode length.

name	width (mm)	height (mm)	cross sectional area (mm)	electrode length (mm)
small U	1.5	2.5	3.75	6.5
normal U	2	3.5	7	9
normal flat	2	3.5	7	2
large U	3	4	12	11
large flat	2.5	4	10	2.5

Installing Jinitiator 1.3.1.29

Introduction

The upgrade of Oracle Applications 11i to version 11.5.10.2 requires the installation of a new version of Oracle Jinitiator on each client workstation.

Multiple versions can coexist on the same machine so this install can safely be carried out in advance.

In addition, the introduction of Secure Sockets Layer for Applications 11i has required a small addition to the product delivered by Oracle. If you already have this version of Jinitiator installed from the standard source, please de-install it and use the link below to obtain the customised version. Alternatively replace the custom certificate database file as described in the additional information section below.

Installation

If you do not have software installation privileges

Please ask your system administrator to install the software on your behalf.

If you have software installation privileges

Download and run Jinitiator 1.3.1.29

Click Run.
A message that the publisher could not be verified may appear.
Click Run.
The self extractor prompt will appear with Overwrite pre-selected.
Click Start
A message that all files have been extracted will appear.
Click Ok.
A command window will open and the installer will run.
Do not change the default destination folder.
Click Next.
When the Jinitiator installation is complete.
Click OK.
If you are prompted to reboot then choose Reboot Later.
Wait until the command window indicates that the custom certificate database has been installed.
Press any key to close the command window.

The first time you log in using this version of you will be prompted to accept a digital certificate.
Click "Grant Always"

Additional Information for System Administrators

The file downloadable from this link is a self extracting zip file which runs a simple script to install the unmodified Jinitiator and then replace the certificate database with a customised version.

This is necessary because Oracle only supply a small number of root certificates by default and UCL's certificate providers are not among them.

If you wish to provide an alternative installation method, and/or to deploy the software to a location other than the default location of **%ProgramFiles%\Oracle\JInitiator 1.3.1.29** then just use the standard Jinitiator source (as included in the self-extractor) and replace the file **...\lib\security\certdb.txt** with the modified version **UCL_certdb13129.txt** (as included in the self-extractor)

Modification History

08-Oct-2007 Robert Goold First Written.

gives a formula valid for a book of any dimensions:

$$Z = Z_{cable} + (a_{electrode} + a_{tissue}) * \sigma^b$$

$$Z = Z_{cable} + \frac{k_{electrode}}{electrode\ length} * \sigma^b + \frac{k_{tissue}}{cross - sectional\ area} * \sigma^b$$

where $k_{electrode}$ and k_{tissue} are constants.
Posing, for a given conductivity σ:

$$Z^U_{electrode} = k_{electrode} * \sigma^b \quad (7.13)$$

$$Z^U_{tissue} = k_{tissue} * \sigma^b \quad (7.14)$$

gives the final equation:

$$Z = Z_{cable} + \frac{Z^U_{electrode}}{electrode\ length} + \frac{Z^U_{tissue}}{cross - sectional\ area}$$

where:

Z_{cable} is constant for all types of books, purely resistive and known;

$Z^U_{electrode}$ represents the impedance for a unitary length of electrodes (including the impedance of the metal itself and of the electrode/tissue interfaces as these cannot be separated)[23];

Z^U_{tissue} represents the impedance of a unitary volume of connective tissue[24];

$electrode\ length$ are given in table 7.6, in mm;

$cross - sectional\ area$ are given in table 7.6, in mm^2.

For the five books compared here:

$$Z_{smallU} = Z_{cable} + \frac{1}{6.5} * Z^U_{electrode} + \frac{1}{3.75} * Z^U_{tissue}$$

$$Z_{normalU} = Z_{cable} + \frac{1}{9} * Z^U_{electrode} + \frac{1}{7} * Z^U_{tissue}$$

$$Z_{normalflat} = Z_{cable} + \frac{1}{2} * Z^U_{electrode} + \frac{1}{7} * Z^U_{tissue}$$

$$Z_{largeU} = Z_{cable} + \frac{1}{11} * Z^U_{electrode} + \frac{1}{12} * Z^U_{tissue}$$

$$Z_{largeflat} = Z_{cable} + \frac{1}{2.5} * Z^U_{electrode} + \frac{1}{10} * Z^U_{tissue}.$$

[23] In the electrode book there are three electrodes of equal dimensions, $Z^U_{electrode}$ includes the contribution from these three electrodes, assuming each is of unitary length.

[24] In these experiments connective tissue growth is modelled by less conductive saline. In the body the tissue progressively replaces the CSF and Z^U_{tissue} is the impedance of a unitary volume of the mix of CSF and connective tissue that fills the electrode, which is assumed here to have an homogeneous resistivity.

Each book was immersed in saline at 4 different concentrations, giving 4 sets of 5 readings, see table 7.4. Solving this overdetermined system of equations using matlab (least-squares method) leads to 4 $Z^U_{electrode}$ and 4 Z^U_{tissue}, one pair per conductivity used for the measurements, see table 7.7. Figure 7.11 is a bi-logarithmic plot of $Z^U_{electrode}$ and Z^U_{tissue} as functions of the conductivity. As expected from equations 7.13 and 7.14, the eight points form two lines with equal slope.

Table 7.7: Unitary electrode and tissue impedances calculated for different conductivities.

conductivity (mS)	$Z^U_{electrode}$ (Ω)	Z^U_{tissue} (Ω)
0.83	8442	18030
1.66	4485	9061
8.33	1180	1969
16.66	741	1046

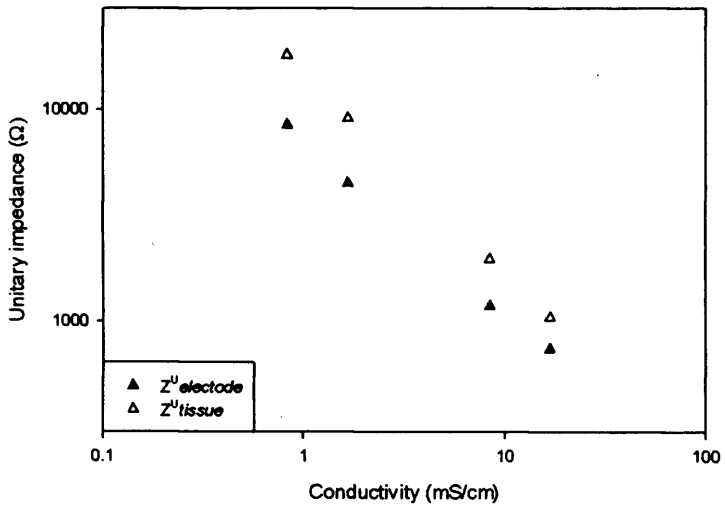

Figure 7.11: Unitary impedances as a function of the conductivity.

The graph of fig. 7.12 is a plot of the impedances measured (x-axis) versus the reconstructed impedances based on the system of equations above. It shows that the assumption of a two parts linear variation of the impedance with the book dimension is plausible since all crosses are near the equality line (45° line on plot). To quantify the interpolation errors, the differences between measured and reconstructed impedances

could be considered (fig. 7.13(a)). However, the impedance values span from about 200Ω to nearly $8k\Omega$, and a 10Ω error on the low end of the range would be more critical than a similar error at the higher values. The impedance differences can then be normalised with respect to their average value and expressed in % before being plotted, see fig. 7.13(b). These relative errors quantify how far the reconstructed impedances lie from the measurements, i.e. $-0.25\% \pm 5.75\%$ here.

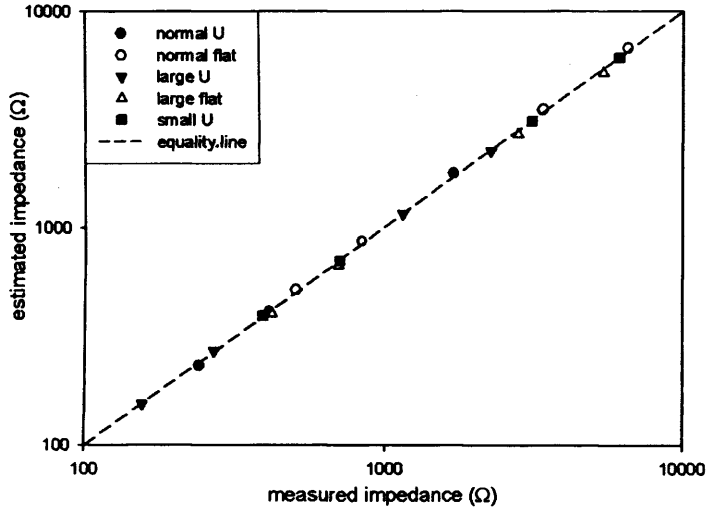

Figure 7.12: Measured vs estimated impedance.

The relative error is larger and nearly constant for the normal flat impedance (4%) and for the large flat impedance (-5%). This is probably due a difference between the real electrode length and that expected from the given slot width. The electrodes are strips of platinum cut by hand, folded then wedged in one corner of the slot. This process is not focused on precision and variation may ensue. The influence of this "dimension error" is only noticeable for the flat electrodes where the electrode impedance is the major contributor to the slot impedance. For example, with $Z_{large\ flat} = Z_{cable} + \frac{1}{2.5} * Z_{electrode} + \frac{1}{10} * Z_{tissue}$ [25], $Z_{electrode}$ is 4 times more important than Z_{tissue} ($\frac{1}{2.5}$ vs. $\frac{1}{10}$).

Further, with the U-shaped electrodes, the slot width is imposed by the rigidity of the platinum, while with the flat electrodes the vertical walls of the slot may sway slightly. The real slot width is therefore larger (or narrower) than given in table 7.6. For flat electrodes, the slot impedance (minus the cable impedance) may be written $Z_{flat\ electrode} = \frac{1}{slot\ width} * (Z^U_{electrode} + \frac{1}{slot\ height} * Z^U_{tissue})$. The small slot width variation will therefore affect equally the whole impedance. With U-shaped electrodes the slot width may be more precisely measured. Its influence is also less noticeable

[25] The cable impedance has been subtracted from all measurements involved in the error calculations.

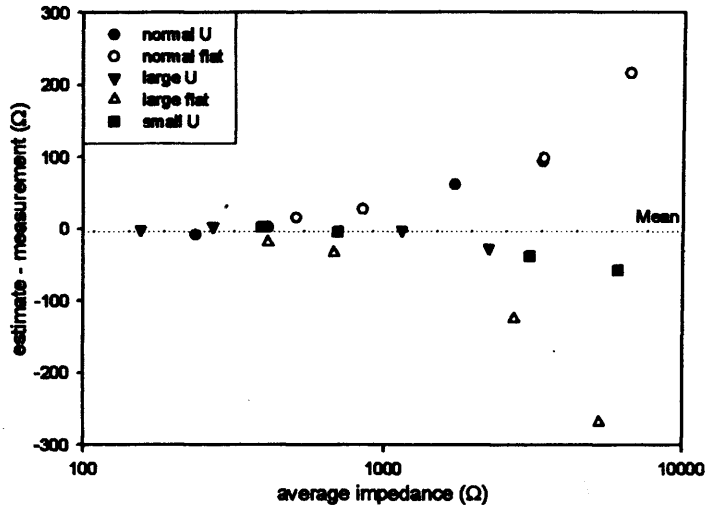

(a) Estimation error.

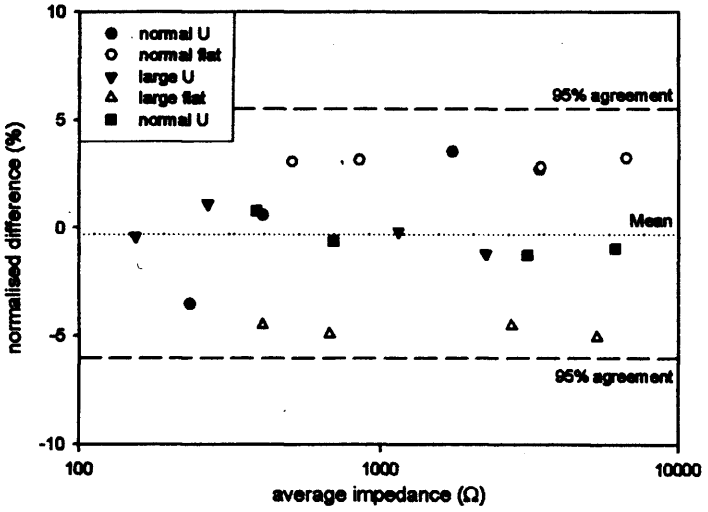

(b) Relative estimation error.

Figure 7.13: Error of mathematical impedance estimation.

since $Z^U_{electrode}$ is divided by the electrode length where the slot height dominates [26]. It does however appear as a denominator for Z^U_{tissue} as cross-sectional area is width times height. Indeed for Z_{smallU}, where the tissue impedance is the main contributor to the slot impedance, the error becomes constant as the conductivity decreases, showing the increased influence of Z_{tissue} over $Z_{electrode}$.

7.5 Conclusion: a formula to estimate the voltage drop across the electrodes of a tripolar slot

Due to the complexity of the electrochemical reactions determining the impedance of a set of electrodes in a conducting environment, there exists no formula to help the implant designer estimate the output load. A value of $1k\Omega$ is traditionally used [Perkins, 2004]. The formula developed in this chapter seeks to improve the impedance estimation while remaining practical. From the implant designer's point of view, knowing the impedance is required to estimate of the maximum voltage drop across the load for a given pulse amplitude; hence to dimension the output stage and limit the risks of saturation. For simplicity, the capacitive part of the impedance has been neglected. The assumption here is that the formula, when used in combination with a given current setting, will give the voltage drop that would be measured with a long pulse width (see section 7.3). For shorter pulse widths the voltage drop will be over-estimated. This is acceptable as this formula was developed to help with output stage dimensioning and implant design. It is by no means a reference valid for all pulse widths. It is interesting to notice the influence of the environment conductivity and how the contribution of the electrode (mostly capacitive, measured here at 1kHz) and that of the volume conductor (mostly resistive) may be separated. The slot and electrodes dimensions are explicit so the formula may be used to assess the impedance for any given book size. Table 7.8 gives values for the unitary impedances at four different conductivities, as the impedance vs. conductivity relation is linear (see fig. 7.11), the formula may be used at any implantation stage (the level of connective tissue growth alters the conductivity).

[26] $Z_{U\ electrode} = \frac{1}{slot\ width+2\times slot\ height} * (Z^U_{electrode} + \frac{1}{slot\ width\times slot\ height} * Z^U_{tissue})$

Table 7.8: Unitary electrode and tissue impedances calculated for different conductivities, copy of table 7.7.

conductivity (mS)	$Z^U_{electrode}$ (Ω)	Z^U_{tissue} (Ω)
0.83	8442	18030
1.66	4485	9061
8.33	1180	1969
16.66	741	1046

Formula:

$$Z = Z_{cable} + \frac{Z^U_{electrode}}{electrode\ length} + \frac{Z^U_{tissue}}{cross-sectional\ area}$$

where:

Z_{cable} is constant for all types of books, purely resistive and known;

$Z^U_{electrode}$ represents the impedance for a unitary length of electrodes (including the impedance of the metal itself and of the electrode/tissue interfaces as these cannot be separated)[27];

Z^U_{tissue} represents the impedance of a unitary volume of connective tissue and CSF as present in the slot;

$electrode\ length$ is expressed in mm;

$cross-sectional\ area$ is expressed in mm^2.

[27] In the electrode book there are three electrodes of equal dimensions, $Z^U_{electrode}$ includes the contribution from these three electrodes, assuming each is of unitary length.

Part III

Technical Issues

In the main part of this thesis the focus was on experimental results and literature reviews to show a need for, and demonstrate the principle of, improvements to the actual method of root stimulation. The following part takes a more "practical" tone as some technological developments are discussed. None of the experiments could have taken place without the realisation of a versatile stimulator and the many subtleties required to eliminate all possible sources of bias from the measurements will be exposed in chapter 8. The work presented so far was carried out with the aim of developing a new, improved, implant for sacro-lumbar root stimulation. The design of such a complex medical engineering device covers many areas, and the broad picture is laid in chapter 9 before a detailed explanation of the conception and testing of the demultiplexing output stage Integrated Circuit designed for the new SLARSI.

Chapter 8

A battery powered stimulator for chronic experiments

Although the Implanted Devices Group had been developing electrical stimulation systems for many years, they did not possess any experimental stimulators. As experiments like those described in chapter 5 are regularly needed to test potential improvements and demonstrate new theories, such a stimulator was required. It had to be easy to use yet versatile, with a simple architecture and no need for a PC to control it to guarantee reliability and user-friendliness; robust, portable and self-contained as experiments may take place in special procedure rooms where no extra laboratory equipment and power supplies are available. Practical issues were noise reduction and insulation as connections to measurement apparatus (usually oscilloscopes and recording equipment) should not affect the signal delivered. The design was initiated by Prof. Donaldson and E. Comi, a student from Polytechnico di Milano (Italy) who worked at UCL for four months in 2002. In this chapter the main building blocks of the IDG experimental stimulators are explained [1].

A note on the pulse shape

When deciding on the shape of the stimulation pulse, the following two phenomena, both introduced in chapter 2, must be taken into consideration: accommodation (apparent loss of excitability) and break excitation.

Accommodation occurs when the stimulus current increases more slowly than the internal processes involved in action potentials generation (K and Na ions movements essentially) [Stoney and Machne, 1969]. A sharp rising edge is therefore ideal to trigger action potentials as the steep slope limits the time for adaptation.

The second phenomenon is break stimulation. In a whole nerve, different fibre groups have different thresholds and different activation and propagation delays depending on their diameter, their position inside the nerve and relative to the electrodes. Upon stimulation, each fibre fires individually, "in its own time". All those single action potentials add up to form a compound action potential. There may be two (or more)

[1] The schematics presented in this chapter only show the most significant components, decoupling capacitors and other additional components have been left out to keep the diagrams clear and easy to read.

CAPs present for a single pulse, spread in time because of the dispersion of the single APs. Analysing the results of experiments such as those presented in chapter 5 is a complex process. It is difficult to identify whether the later CAP, when present, is due to a slower (thinner) fibre group, whether the activation and propagation delays are different or whether break excitation took place. Since anode break activation is also dependent on the rate of internal processes (the mechanisms are similar to those involved with adaptation), it may be avoided when the pulse is terminated with a slowly decreasing edge, traditionally implemented as an exponentially decaying slope.
From an experiment point of view, the ideal pulse shape is a sharp rising edge followed by a plateau and a slow, exponential, decay. As most actual stimulators produce passively balanced square pulses (they are simpler to generate, see page 168 in section 7.1.3), the experimental stimulator should also provide a square pulse shape. During an experiment it is advantageous to switch to an exponential decay to rule out break excitation. As the positive phases are equal in the two pulses [2], it is possible to switch from one to the other without altering the conditions of "make" stimulation. The comparison only affects break excitation.

8.1 Voltage waveform

The stimulator produces two types of charge-balanced current-controlled pulses: square and exponentially decaying. Internal voltage waveforms are first created, the desired shape is selected (toggle switch $Sw2$ on fig. 8.2) and a voltage to current conversion stage follows (see section 8.2.1).

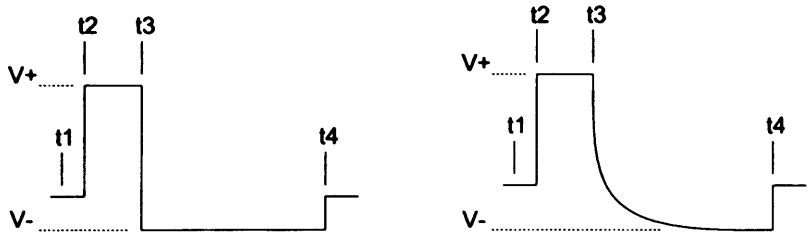

(a) Square pulse. (b) Exponentially decaying pulse.

Figure 8.1: Pulses produced by the stimulator.

The following parameters can be adjusted using potentiometers mounted on the front-panel: the positive and negative voltages, V^+ and V^- (hence the corresponding currents at the output), the slope of the exponential decay (has no effect on the square pulse), the pulse width and the frequency (this last parameter is constrained by the charge balancing condition, see section 8.1.3).
A schematic of the circuit [3] is shown in fig. 8.2, for timing indications please refer to the annotations on fig. 8.1. The circuit is divided in three logic entities following their role

[2] See figures 8.1 and 8.2: the positive phases (until instant t_3) are defined during the voltage waveform generation stage by V^+ and R_5 or V^+ and R_6 where $R_5 = R_6$.
[3] Based on the early design of E. Comi.

in the waveform generation: the clock loop, the voltage waveform generation blocks and the charge balancing circuit. Each of these will be briefly explained hereafter.

8.1.1 Timing

As seen on fig. 8.1, the pulse shape is determined by instants $t2$, $t3$ and $t4$. Instants $t1$, $t5$ and $t6$ are required for charge balancing or charging delay. Instants $t5$ and $t6$ are not indicated on fig. 8.1, their role will become clearer later in this paragraph. Monostables MONO1 and MONO2 (see schematic on fig. 8.2), marking instants $t1$, $t2$ and $t5$ provide a clock of adjustable frequency. In a simple clock loop, instant $t5$ would trigger MONO1, giving pulse $t1 - t2$ and instant $t2$ would trigger MONO2, giving pulse $t2 - t5$ and triggering MONO1 again. The frequency could be adjusted by modifying either of the two pulses width. The requirements to provide charge balanced pulses with an exponential decay option have slightly complicated this simple idea. A gate is introduced in the clock loop, for charge balancing (explained in section 8.1.3), creating instant $t6$ synchronous or later than $t5$ (its role is explained in section 8.1.3). Instant $t6$ triggers MONO1, although manual and external trigger options are available, see section 8.2.4. The frequency is adjusted, between 0.33Hz and 330Hz, by variation of the $t2-t5$ interval (potentiometer $R2$ mounted on the front panel), under the constraint of charge balancing indicated by instant $t6$. Instant $t4$ marks the end of the balancing pulse, instant $t5$ indicates the frequency required by the user and instant $t6$ the actual frequency of the stimulator: $t6 = t5$ if $t4 \leq t5$ else the charge balancing circuit lengthens the period and $t6 = t4$, see section 8.1.3.
The positive pulse width is $t2 - t3$ (not $t1 - t2$) and is controlled by monostable MONO3 ($R3$ on front panel), triggered by the falling edge of the $t1 - t2$ output of MONO1. It may be adjusted between $50\mu s$ and $2.8ms$. The role of the $t1-t2$ interval, fixed by potentiometer $R1$[4], will become clear with the explanation of the exponential waveform generation.

8.1.2 Voltage waveform generation

In this and the following sections references are made to various voltage levels. For clarity the labels used for each of these are listed in table 8.1 with a brief explanation of their role.

8.1.2.1 Exponentially decaying pulse: V_e

Between instants $t4$ and the following $t2$, V_e is grounded via switch $S3$ and between instants $t2$ and $t4$, V_e follows V_{RC}. Before instant $t1$, $V_{RC} = V^-$ as $S2$ is closed[5] and $C6$ is not charged. At $t1$, $S2$ goes open circuit and $S1$ closes, $C6$ charges through $R5$ hence $V_{RC} = V^+ - (V^+ - V^-) * (e^{-\frac{t-t1}{R5*C6}})$. $R5$ is selected to give a small time constant $R5 * C6$. The $t1 - t2$ interval is adjusted, via potentiometer $R1$ to about three times the time constant, so that $V_{RC}(t2) \approx V^+$. When $S4$ closes ($t2$), V_e is shorted to

[4] $R1$, fixing the t1-t2 interval, is not panel-mounted as this parameter does not require frequent adjustments.

[5] In this description, a closed switch is a short-circuit, an open switch is an open circuit.

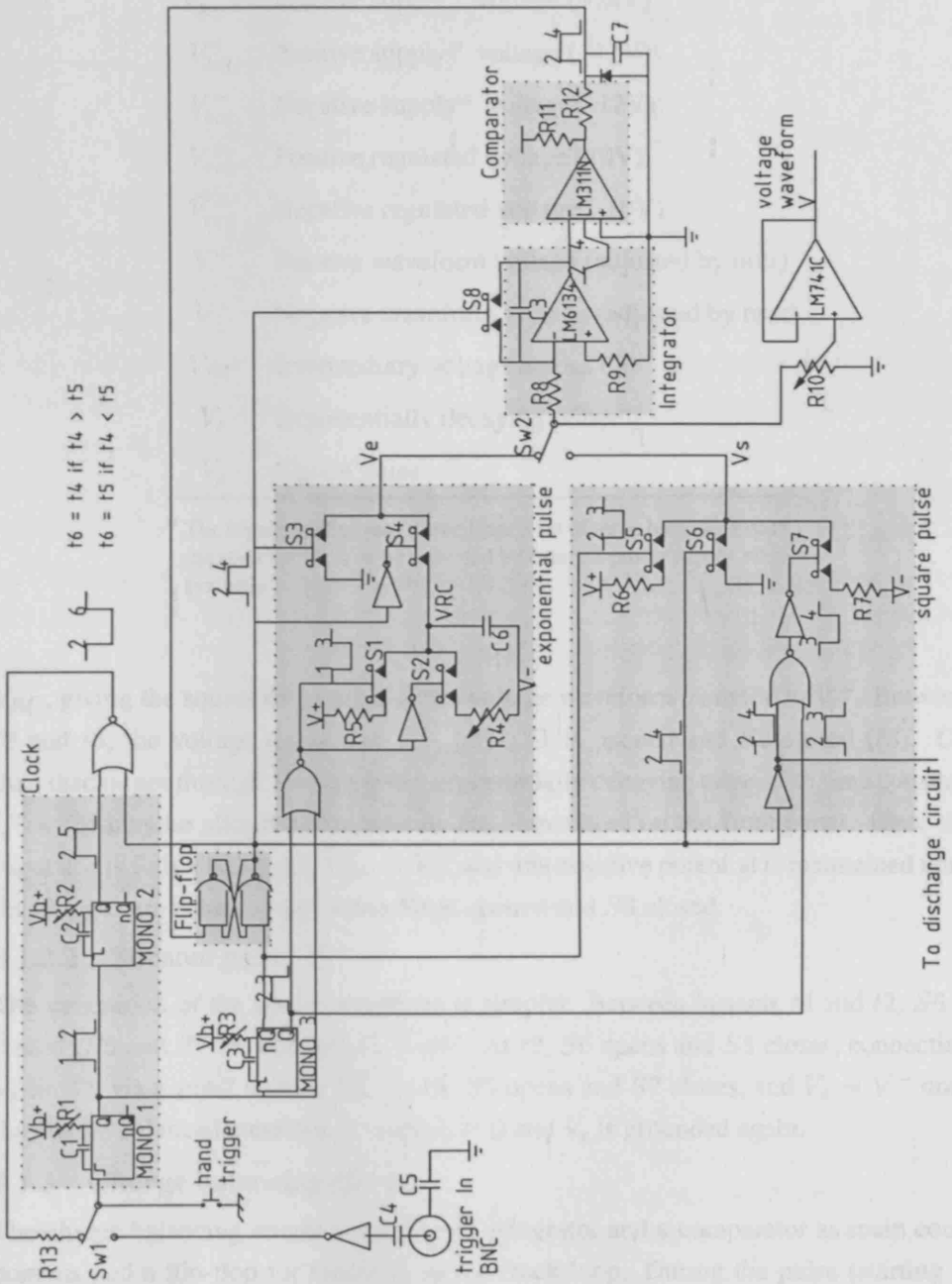

Figure 8.2: Voltage waveform generation circuit.

Table 8.1: Voltage labels and description.

Label	Description
V_{bat}^{++}	Positive supply[a] voltage (+24V)
V_{bat}^{+}	Positive supply[a] voltage (+12V)
V_{bat}^{-}	Negative supply[a] voltage (-12V)
V_{reg}^{+}	Positive regulated voltage (10V)
V_{reg}^{-}	Negative regulated voltage (-10V)
V^{+}	Positive waveform voltage (adjusted by user)
V^{-}	Negative waveform voltage (adjusted by user)
V_{RC}	Intermediary voltage across $C6$
V_e	Exponentially decaying pulse
V_s	Square pulse

[a] The supply voltage may come from a set of three batteries inside the stimulator box or be provided by external power supply when available.

V_{RC}, giving the square rising edge of the voltage waveform from 0V to V^+. Between $t2$ and $t3$, the voltage remains at V^+, until $S1$ is opened and $S2$ closed ($t3$). $C6$ then discharges through $R4$ giving the exponentially decaying edge. The time constant $C6 * R4$ may be altered by the user as $R4$ is mounted on the front panel. Once the capacitor is fully discharged, $V_{RC} = V^-$ and this negative potential is maintained until the charges are balanced ($t4$) when $S4$ is opened and $S3$ closed.

8.1.2.2 Squared pulse: V_s

The generation of the square waveform is simpler. Between instants $t4$ and $t2$, $S6$ is closed ($S5$ and $S7$ are opened) $V_s = 0V$. At $t2$, $S6$ opens and $S5$ closes, connecting V_s to V^+ via a small resistor $R6$. At $t3$, $S5$ opens and $S7$ closes, and $V_s = V^-$ until the charge balanced condition is reached ($t4$) and V_s is grounded again.

8.1.3 Charge balancing circuit.

The charge balancing circuit consist of an integrator and a comparator as main components and a flip-flop for feedback in the clock loop. During the pulse (starting at instant $t2$) the voltage waveform is integrated and the result is compared to 0. Once the integral equals zero, the output of the comparator falls, marking instant $t4$. In theory, that instant indicates that the positive and negative phases of the voltage waveform are equal. Assuming the voltage to current conversion (section 8.2.1) is perfect, the charge delivered to the output will have been exactly balanced during the negative phase. This may not always be the case as the circuit contains various offset sources and an ex-

tra discharging circuit is present to compensate for the unavoidable imperfections, see section 8.2.5. The falling edge at the comparator output ($t4$) trips the flip-flop (see fig. 8.2), resetting the integrator until the next pulse. The output of the flip-flop is also fed back into the clock loop. The NOR gate guarantees that MONO1 will only be triggered once the positive and negative phases are balanced. The period $t1 - t6$ is therefore equal to $t1 - t4$ or $t1 - t5$, whichever is the longer.

8.2 Additional circuits

8.2.1 Voltage to current conversion

The circuit of fig. 8.3 creates two anodal current pulses from, and proportional to, the voltage waveform produced by the circuit of fig. 8.2. This signal is divided in two "anodal" waveforms whose amplitudes are simultaneously controlled by the dividing resistors rotary switch (RS1). The ratio between the 2 anodal signals is adjustable in steps of 10%, from 100%−0% to 0%−100%, via 50%−50% ("pure tripole"). Both "anodal voltage signals" are fed in similar circuits: an instrumentation amplifier (INA103), a reference resistor R_{ref} (R_2 and R_7) and an operational amplifier (OPA445) to feed the reference potential ($R_{ref} * I_{out}$) back to the reference input of the INA103. The instrumentation amplifier works by adjusting the output current I_{out} so that the voltage across the sensing and reference inputs equals that across the + and − inputs times the gain:

$$R_{ref} * I_{out} = (V_{in+} - V_{in-}) * gain.$$

The voltage to current conversion follows:

$$I_{out} = \frac{V_{in+}}{R_{ref} * gain}.$$

The amplifier should deliver a maximum current of 10mA to the load. This is obtained if

$$R_{ref} * gain \leq \frac{V_{in+}}{0.01}.$$

R_{ref} being in series with the load it should be small to maximise the available output voltage (i.e. limit the saturation), but large enough so that the reference voltage fed back to the amplifier is considerably larger than the input offset estimated at about 1.85mV[6]. The value of $R4$ and $R5$ also calls for a compromise. On the one hand, the INA103 datasheets specify that the input impedance should be less than $10k\Omega$ to improve the noise performance, on the other hand $R4$ (or $R5$), in series with $R1$ and $RS1$, must be large enough to limit the current consumption of the previous stage. R_2 and R_7 are 200Ω resistors, the gain for the two INA103 ais set to one and the input voltage to the INA103 is limited to 2V by $5.1k\Omega$ resistors $R1$, $R4$ and $R5$. As the

[6]The estimation of the input offset is based on a thermal resistance of through-hole packages of $\frac{80°}{W}$, a power supply +24V-12V and a maximum output current 10mA, giving 28.8°. The datasheets indicate an offset of $30 + \frac{1200}{G}\mu V$ and a drift of $1 + \frac{20}{G}$ or a total offset of $1835\mu V$ with a unitary gain.

resistor chain used to adjust the amplitude of the two current output acts as potential dividers, the maximum voltage fed to the circuit is actually 4V. That voltage waveform is fed to the voltage to current conversion stage via an operational amplifier connected as a unity gain buffer (see fig. 8.2). As the amplitude must be limited to a maximum of $\pm 4V$ [7], it is adjusted with a large potentiometer, R_{10} on fig. 8.2.

The stimulator specification required an output current of 10mA. Given a maximum voltage of 22V (with the 24V voltage rail) at the output of the INA103, the resistance of the anode-cathode path should remain below $2.2k\Omega$ (including the internal 200Ω resistor) to avoid saturation [8]. The load of a stimulator will most often be capacitive and an external blocking capacitor is also connected in series with each output. These operating conditions make it difficult to ensure that the stimulus pulses are not saturated. Yet, in practice, the current signals may be monitored via BNC connections so saturation could be noticed.

The INA103 was selected for its wide supply range ($\pm 9V to \pm 25V$), good noise and offset performances and low voltage drop when passing up to 10mA. The feedback buffer also needed to work at similar voltages (i.e. up to 24V), hence the choice of the OPA445.

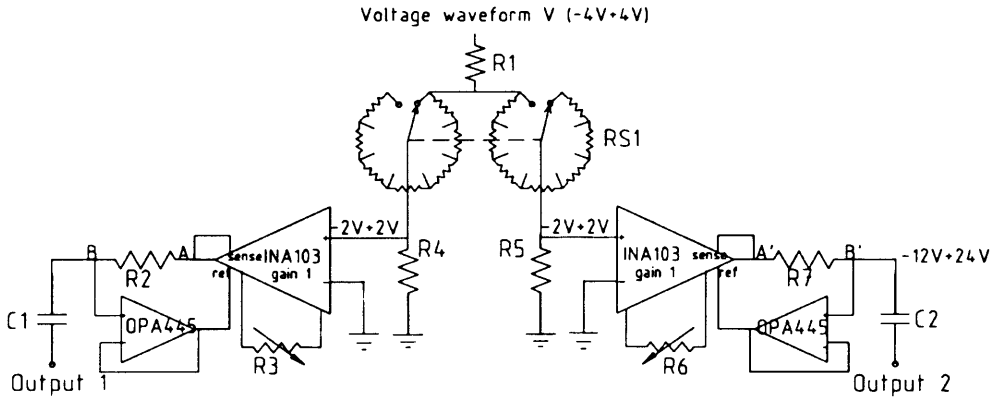

Figure 8.3: Voltage to current conversion circuit.

8.2.2 Battery regulation

In a laboratory environment the stimulator may be connected to power supplies (-12V, 0V, +12V and +24V) when available. It is otherwise powered with a set of three 12V batteries, producing four voltage levels, -12V, 0V, +12V and +24V. The highest voltage rail (+24V) is only used for the output stage to allow for a larger maximal load [9]. The voltage generation circuit uses only two batteries giving symmetrical power rails. To

[7] This amplitude of 4V is a maximum value obtained when V^+ is set to its maximum of 10V by the user. For precision on the voltage adjustement see section 8.2.3.

[8] The voltage drop across the electrodes is limited to 2V by the water window.

[9] The load impedance is unknown and depends on the experiment considered. The third 12V battery guarantees up to $10mA$ through a maximum of $2k\Omega$ (less if the load is capacitive)

account for some fluctuation of the state of charge of each batteries, two regulators are used to give stable $\pm 10V$ levels called V_{reg}^{+} and V_{reg}^{-}. These regulated power rails are further adjusted by the user to levels V^{+} and V^{-} which control the pulse amplitude as detailed in section 8.2.3.

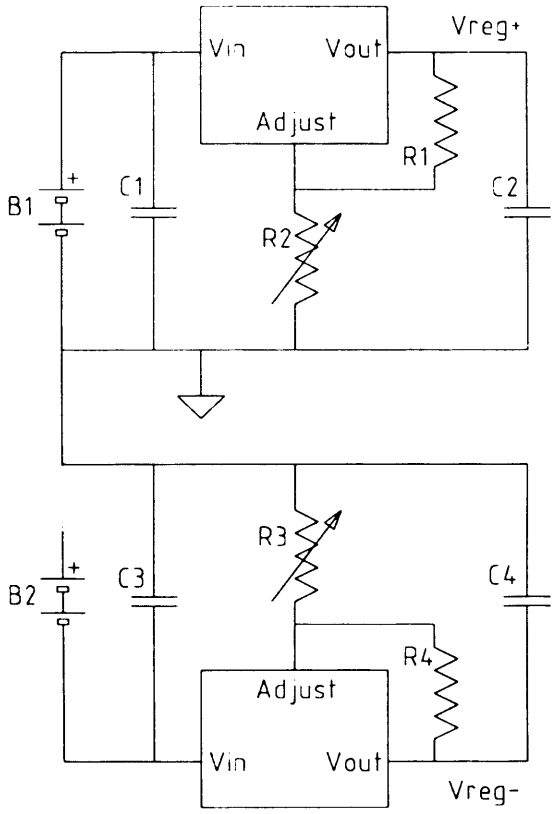

Figure 8.4: Power supply regulation.

8.2.3 Control of the pulse amplitude

The amplitude of the current pulse at the output stage is proportional to that of the voltage pulse produced by the circuit of fig. 8.2. As seen on that figure, the positive and negative phases are limited to levels V^{+} and V^{-}. These voltages may be adjusted by the user via three potentiometers mounted on the front panel, the adjustment circuit is shown on fig. 8.5. V^{+} is set (grossly) to a fraction of V_{reg}^{+} by potentiometer $R1$ and fine tuned to the desired level using $R2$. V^{-} only has a gross adjustment potentiometer, $R3$ but a toggle switch ($Sw1$) offers the added feature to set V^{-} as 10% of V^{+}. In the "tracking" position, the voltage V^{-} is set by $R5$ in series with a larger resistor ($R4$) forming a 10 to 1 resistive divider. Potentiometers $R1$ and $R5$ are on the same shaft, when the user adjusts the positive voltage using $R1$, the negative voltage automatically follows. This option is selected for experiments which do not specifically study the effects of the negative pulse. The set level (10%) is a compromise to avoid anodal stimulation while maximising the highest frequency (which is limited by the charge

balancing condition hence by the level ratio of the positive and negative phases).

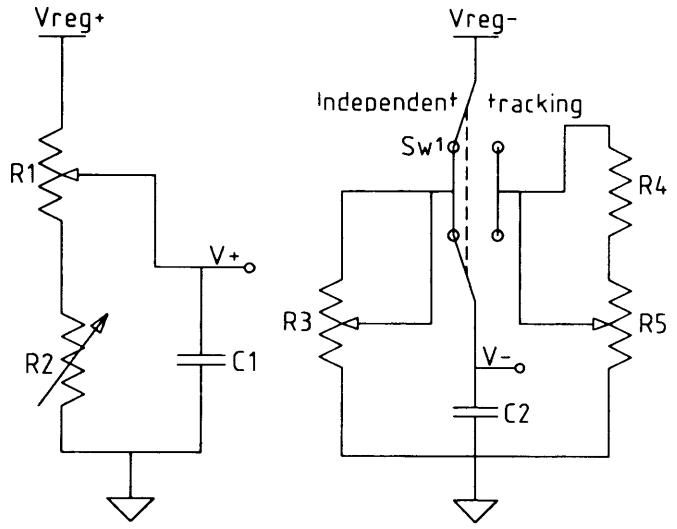

(a) Positive voltage adjustment.

(b) Negative voltage adjustment.

Figure 8.5: Circuits for the control of the pulse amplitude.

8.2.4 Triggers

A trigger circuit is included in the clock loop described in section 8.1 offering either internal or external trigger modes (toggle switch $Sw1$ in fig. 8.2). The external trigger mode was not part of the original specifications and was added later on by Dr. Schuettler. Internal triggering is caused by the rising edge defining instant $t6$ as explained before. When the stimulator is first started the clock loop may settle in a stable situation [10] and a manual trigger push button is provided to cause a first edge and trigger MONO1. In external trigger mode the clock loop is interrupted (by $Sw1$) so that the edge produced at instant $t6$ does not reach the input of MONO1. A BNC connector is provided on the front panel for the user to feed an external triggering signal. As MONO1 triggers on a rising edge while the triggering signal that this circuit was developed for was timed on falling edges, an inverting gate has been inserted between the BNC connector and $Sw1$.

8.2.5 Blocking capacitor and discharge circuit

A blocking capacitor is added in series with both anodal outputs to avoid passing direct current. It must be large so the voltage drop is small to maximise the available output voltage. The current pulses are, in theory, charge-balanced. However, the integrator and the comparator from the charge balancing circuit of fig. 8.2, as well as the instrumentation amplifier used to convert the voltage waveform to a current pulse (fig. 8.3)

[10] In the stable condition the outputs of the monostables and the flip-flop are low setting high the output of the NOR gate. Pushing the hand trigger pulls down the input to MONO1 ($R9$ is connected between the gate output and the monostable input) and causes a rising edge when it is released.

all introduce some offset. As a result, and despite careful offset adjustment, the pulses may not be exactly balanced and the voltage across the blocking capacitor may become more positive or negative with each pulse. To avoid this, a discharge circuit is included in each anodal branch, see fig. 8.6. It discharges the capacitor during the idle period between two pulses (between instants $t6$ and $t2$). There are two discharge paths as the capacitor may not only overcharge (discharge through $D1$ and $Q1$), but also over-discharge (re-charge via $D2$ and $Q2$). Branch 1 is self explanatory, when the gate is at 0V, $Q1$ (an nFET transistor) is off. At the end of the pulse, the gate goes to 5V, turning $Q1$ on and opening a discharge path for the blocking capacitor connected at node B. Similarly in branch 2, $Q2$, a pFET connected source to ground, is off while the gate is at 0V during the pulse. To turn it on the condition is $V_G < V_D$ or $V_G < 0V$ as $V_D = 0V$. This requires the use of a "negating block" to mirror the $+5V$ to $0V$ logic signal to $-5V$ to $0V$. The negating block makes use of the virtual ground at the negative input of the operational amplifier connected as shown in fig. 8.6. If the feedback resistance ($R3$) equals the input resistance ($R4$), the voltage drops will be equal, hence $V_{out} = 0V - V_{in^-}$. The diodes in both branches guarantee a unidirectional current flow. They are in germanium to minimise the voltage drop. The resistors are large to limit the current driven from the logic line (for power consumption and slew rate consideration).

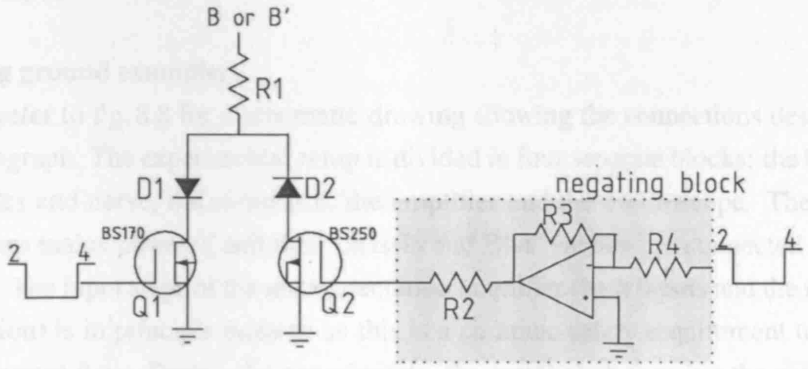

Figure 8.6: Discharge circuit for the blocking capacitor in each anodal branch.

8.2.6 Isolation amplifier

The stimulator produces thus a voltage waveform, which is converted to two anodal current pulses delivered to the electrodes via two blocking capacitors. These three signals (voltage waveform and current pulses) may need to be monitored on an oscilloscope (the potential differences across the 200Ω reference resistors R_2 and R_7 of fig. 8.3 are used as representations of the anodal current pulses). The three voltage signals are fed into isolation amplifiers (ISO124) connected to BNC connectors. Two 9V PP3 batteries are used, with the outer shield of the BNC connected to the floating 0V point, insuring that the circuit producing the current pulses is completely isolated

from the measurement apparatus. The isolation amplifier is more than a buffer that allows the observation of signals without disturbing the voltage levels and current flow, it is essential to prevent the formation of "ground-loops" during experiments. Its importance and the complex floating ground issue are better understood with an example based on the experiments detailed in chapter 5.

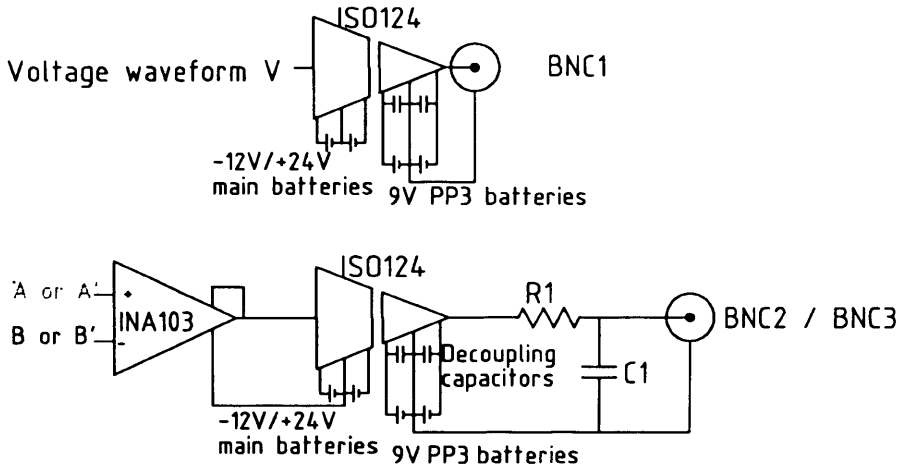

Figure 8.7: Isolation amplifier feeding the signals to the BNC connectors. There is only one pair of PP3 batteries and one set of main batteries, they are drawn twice to show the connections on both ISO124.

Floating ground example:

Please refer to fig. 8.8 for a schematic drawing showing the connections described in this paragraph. The experimental setup is divided in four separate blocks: the bath with electrodes and nerve, the stimulator, the amplifier and the oscilloscope. The last two blocks are mains powered and their chassis and BNC shields are connected to mains earth [11]. The input stage of the instrumentation amplifier (both inputs and the reference connection) is in principle isolated as this is a common safety requirement to prevent direct current flow. During the experiments, the metal plate forming the sides of the bath [12] serves as a reference to the instrumentation amplifier. This reduces the ambient interferences as they are picked up by both the reference and the recording electrodes and cancelled at the amplifier [13]. The amplified signal is expressed with reference to the amplifier's internal 0V and fed to the oscilloscope via a BNC cable where the reference is connected to the outer shield (this results in shorting the internal 0V line to mains earth). The signals produced by the stimulator are also fed to the oscilloscope using the BNC connections provided. When two or more signals are compared with an oscilloscope, all the references (the BNC shields) are shorted (and connected to mains

[11] Not all oscilloscopes have their BNC shield connections shorted to the chassis and to mains earth and the same goes for amplifier. The situation described here is based on the experiments related in chapter 5.

[12] For a description of the experimental bath see section 5.3.4, page 87.

[13] If the interferences are only present at the inputs of the amplifier, they are seen as part of the signal and amplified.

earth with this oscilloscope). If the stimulator signals (to the BNCs) are not isolated and the BNC shields are connected to the batteries 0V, this line will, via the oscilloscope be shorted to the amplifier's output reference and to mains earth. This should not be a problem provided the input stage of the amplifier is isolated and no other connection is made between the bath and the oscilloscope. Both of these conditions were breached during the cross-talk experiments. The first instrumentation amplifier used was not isolated and the input reference was the output reference, hence shorting the stainless steel wall to the oscilloscope (mains earth) and thus connecting it to the stimulator's BNCs shield. Then, after replacement with the ISO-DAM8 it happened on several occasions that the stainless steel wall was connected to the oscilloscope's 0V connector, either directly or via an extra electrode. Shorting the bath reference plate to the stimulator BNCs shield without isolation is shorting the metal plate to the stimulator's 0V line and transforming this reference in a very large distant cathode, severely affecting the true cathode's current flow. The use of the ISO124 isolation amplifier in the stimulator solved that problem but introduced an intrinsic 500kHz ripple of 20mV added at the amplifiers output. This is a known drawback, the 500kHz comes from an internal oscillator (see appendix ??) and a simple RC filter (cutoff frequency below 100kHz) in series between the amplifier output and the BNC connector is sufficient to filter it out. Other interferences can affect the signal produced by the stimulator. To limit these, the circuits are placed in a metal box which can easily be grounded. The BNCs shield are not by default connected to this box to keep the stimulator versatile. There are however two 4mm connectors on the back of the box, one connected to the chassis and the other to the BNCs shield.

8.3 Stimulator specifications

The stimulator described in this chapter was built for, and used during, the cross-talk experiments described in chapter 5. Its specifications are summarised in table 8.2.

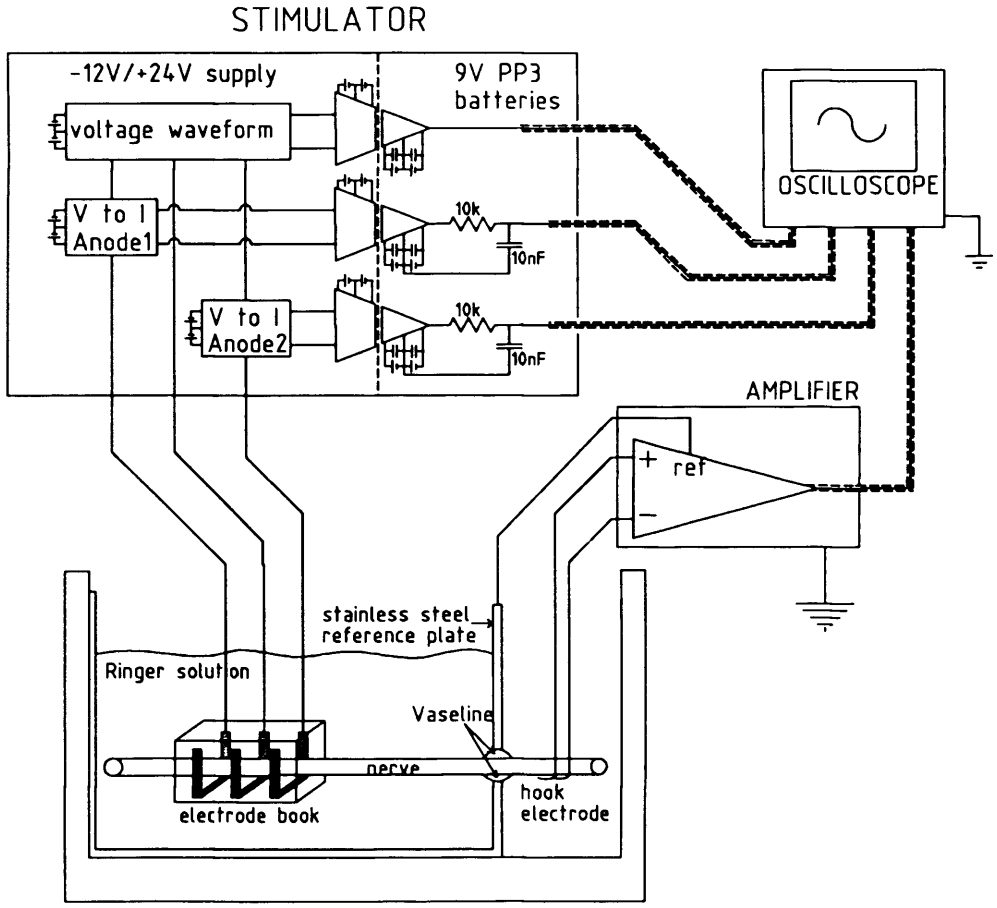

Figure 8.8: Experimental setup with earth and 0v connections. As with the previous figure, there is only one set of -12V/+24V batteries and one set of PP3 batteries, the symbol are drawn more than once to show where the various signals relate to the supply voltages.

Table 8.2: Summary of stimulator specifications.

Pulse	Frequency	0.33 to 330Hz
	Width	$50\mu s$ to 2.8ms
	Shape	Square or exponentially decaying
Output	Voltage	+ 22V to -10V
	Current	$\pm 10mA$
Supply	Voltage	+24V, +12V, 0V and -12V
	Current	50mA for the two positive supply
		70mA for the negative supply
		Battery powered (internal) or
		Power supply (4mm panel-mounted sockets)

Chapter 9

The SLARSI: the new Sacro-Lumbar Anterior Root Stimulator Implant

This new implant is designed for the intrathecal stimulation of sacral and lumbar anterior nerve roots. It aims at improving bladder and bowel functions while providing an opportunity to use functional electrical stimulation for leg exercises. It is essentially an evolution from the existing LARSI (see section 4.1, page 57) and most of the hardware derived from it remains unchanged. As demonstrated in previous chapters in this thesis, some parts required improvements, especially the charge delivery to the nerve, i.e. the book electrodes themselves and the circuitry in the stimulator responsible for delivering the current. The user interface and external control box have also been updated to improve user-friendliness. This chapter is not a design manual for the SLARSI but a brief review of the most important aspects involved in upgrading from LARSI to SLARSI as it brings together the various subjects treated in this thesis. The chapter is divided in four sections: electrodes and cables; stimulator; RF link and transmitter and external control box. These are the four conceptual building blocks of an implantable functional electrical stimulator system, each requiring a particular expertise. The issues discussed here do not cover all the areas that must be considered when designing and building an implant, they only highlight the practical implementation of the improvements.

9.1 Electrodes and cables

Conventional books (with U-shaped electrodes to reduce the access resistance) and Cooper cables will be used. Space limiting lids (see section 6.5) may be fitted if deemed necessary at the time of surgery to improve the recruitment curves and limit the power requirements. As explained in chapter 4, each channel must be electronically independent from the others to improve selectivity and avoid cross-talk stimulation. Each pair of anodes and each cathode therefore requires its own individual connection to the stimulator, giving two wires per channel. Cooper cables are available with 3,4 or 5 wires. Using one cable per electrode book there can only be two totally independent channels per book.

Table 9.1: Proposed root-channel correspondence for the SLARSI.

Channel	Root	Actions
1	L3L	hip flexion, adduction and rotation; knee extension.
2	L3R	
3	L4L	hip flexion, adduction and rotation; knee extension; foot flexion, inversion and toe extension.
4	L4R	
5	L5L	hip extension and rotation; knee flexion; foot flexion, ankle and toe movements.
6	L5R	
7	S1L	hip extension and rotation; knee flexion; foot flexion, ankle and toe movements.
8	S1R	
9	S2L - S2R	hip extension and rotation; knee flexion; foot plantar flexion, ankle inversion and toe flexion; **light gluteal stimulation and erection.**
10	S3L - S3R - S4L - S4R	knee flexion; foot plantar flexion and toe movements; **bladder and bowel emptying.**

9.1.1 Proposed root arrangement

The new implant will stimulate the anterior roots L3 to S4. Roots L3 to S1 (4 pairs) left and right separately for leg movements; roots S2, S3 and S4 for bladder and bowels (without left-right distinction). Ten completely independent channels are needed if the S3 and S4 are joined as a single channel, see table 9.1. As specified on page 61, channels are semi-abstract concepts that can be physically realised using one or more slots. Each channel is allocated one stimulation time and one set of parameters (pulse width and intensity). When more than one root belongs to the same channel, it is sometimes easier to place them in separate slots, electrically connected together to act as a single channel. This will be the case for the S2 left and right, trapped in two slots of a three-slot book to avoid stretching the roots, but stimulated as one channel.

9.1.2 Charge balanced stimuli

As explained in section 2.2.9, the net charge transfer should be close to 0 to limit electrochemical damage. The three methods presented in section 7.1.3 to deliver charge balanced stimuli are: actively balanced pulses, passive discharge with capacitor cou-

pled output stages or passive discharge of the electrode pseudo-capacitance. In theory, the third method, relying on the electrodes pseudo-capacitance, should be enough. Yet, due to inherent difficulties in calculating the "true" surface area of rough platinum, estimations of this naturally occurring capacitance are imprecise. In the SLARSI, an external blocking capacitor is included in series between the cathode and the current source on each channel. It will ensure that the charge is balanced under normal conditions (even with the large charge required for sacral root stimulation for bladder and bowel contractions) and prevent direct current passing to the electrodes under fault conditions. It was also felt that, considering the lack of clear cut safety limits, capacitor coupling would be better accepted by the reviewing body.

9.2 Stimulator

The implanted stimulator fulfils three roles, it combines a receiver circuit for the radio frequency inductive link, a gate array that interprets the signals received and produces a train of pulses for stimulation and a demultiplexor output stage which translates the trains in individual stimulation pulses for the selected channels.
When Donaldson developed the LARSI, he used a commercially available demultiplexor chip (UCN5832C) from *Sprague* with 32 current sinks with a peak current of 150mA and a maximum voltage at the sink input of 40V [Allegro MicroSystems, 1998]. Figure 9.1(a) is a block schematic of the LARSI implant. The current to the electrodes is not controlled in itself, an external regulator stabilises and limits the voltage of the positive rail, to which the common anode is connected via a $2.2k\Omega$ resistor. The cathodes are connected each to one of the 32 separate sink inputs of the demultiplexor. The UCN5832C interprets the pulse signals, and activates the current sink corresponding to the selected channel. As the anodes from all channels are connected, together, to the regulated high voltage rail (via the $2.2k\Omega$ resistor), they all contribute to the current driven by the active cathode to the current source of the UCN5832C. The channels are thus all connected together via their anodes, and this leads to cross-talk stimulation (see chapter 4).
To produce the SLARSI with independent channels, a custom integrated circuit was built to replace the following components: the UCN5832C, the voltage regulator, the $2.2k\Omega$ resistor and the discharge resistors. Figure 9.1(b) is a block schematic of the SLARSI implant. The new IC will regulate the power rail (constant 20V) to protect the switches from excessive voltage, select the channel to be activated by switching both the cathode and the anode [1], and provide a new feature by setting the current to a controlled amplitude of either 2mA, 8mA or 16mA.

[1] Strictly speaking as the stimulator uses a tripolar electrode arrangement there are two anodes but they are connected together and a channel, as a concept, only has one anode and one cathode.

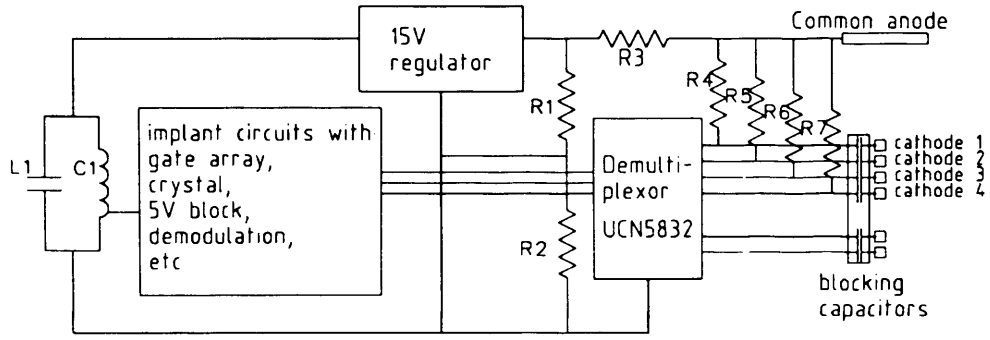

(a) Simple schematic of the LARSI implant circuit showing the components replaced by the new output stage demultiplexor IC.

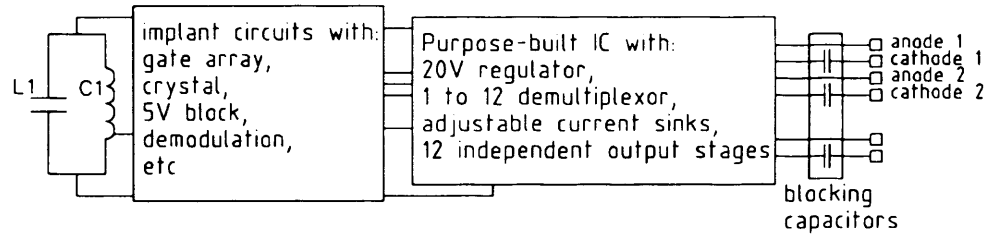

(b) Simple schematic of the SLARSI implant circuit with the new IC.

Figure 9.1: Simple schematic of LARSI and SLARSI implant circuits.

9.2.1 Stimulus frequency

In the SARSI the frequency may be set between 2 and 105Hz as lower frequencies may be required for erection and bowel programs, while sphincter fatigue may be achieved at higher frequency. In the SLARSI the frequency is set by a parameter with a default value of 20Hz. To keep setting up and usage simple, the frequency should only require adjustment for urological functions while for leg movements all channels work at the same frequency. The default of 20Hz results from a compromise to limit fatigue (needs a low frequency) while getting a smooth contraction (needs a high enough frequency to fuse muscle twitches into a tetanic contraction). Although single-channel frequency adjustment is possible for all 12 channels, this seemed unnecessarily complicated and the user interface (section 9.4.2.2) was developed with this intentional restriction.

9.2.2 Pulse shape

Charge balancing via a capacitor discharge is as good at preventing damage as an active balance output stage [Donaldson and Donaldson, 1986b,c]. Gorman and Mortimer [1983] recommend leaving a delay between the charge and discharge phases to avoid quenching late-onset action potentials which often occur in smaller fibres. In the SLARSI output stage IC, a switch on the discharge paths (see section 10.1.5) controls the opening and closing time. Using a different logic signal for the stimulation and the discharge offers the option to adjust the delay.

9.2.3 Pulse width or pulse amplitude modulation?

The stimulation level is defined by the combination of the pulse width and the stimulus current or voltage, linked by Ohm's law. A stimulator may be either designed as current-controlled (i.e. output current set to a pre-defined, controlled, value) or voltage-controlled. The parameters are then reduced to stimulation amplitude and pulse duration. Both can be adjustable, in discrete steps or in a continuous manner. There is a trade-off here between design and operation complexity, and fine tuning of stimulus (fine adjustment of muscle contraction in a motor stimulator). Although precise control is not always required (in pacemaker or bladder controller for example the stimulus only needs to be strong enough to reach a sufficient contraction), a simple ON-OFF stimulator without any adjustment of the pulse width nor the amplitude would not be of much practical use. A few crude steps are necessary to allow at least a gross adjustment of the stimulus to the patients requirements. Often only one parameter is controlled, giving either amplitude or pulse modulation (as is the case with the LARSI). While this keeps the design simpler and avoids lengthy tests and set-up sessions, it is not optimum it either lacks precision or fails to cover the full dynamic range.

9.2.4 Modulation with discrete adjustment of fixed parameter

Safety considerations and power saving issues plead for minimised charge and energy. Since Weiss and Lapicque's studies and the introduction of strength-duration curves (see section 2.2.1), it is known that amplitude and width are not inter-changeable. As summarised in Crago et al. [1974]: *"The charge required to produce comparable outputs decreases as pulse duration decreases."* It is therefore necessary to fix the amplitude above the rheobase for pulse duration modulation, or to work at or after the chronaxie for pulse width modulation. McNeal et al. [1987] recommends a few discrete steps of the "fixed" parameter with a more precise adjustment of the other parameter to optimise energy requirements and tuning precision (i.e. find the best[2] recruitment curve).

9.2.5 SLARSI modulation

In SLARSI pulse width modulation has been implemented with gross discrete adjustment of the current amplitude. The exponential pulse width adjustment is inherited from the LARSI. It is complemented by three discrete current levels: 2, 8 or 16mA for a finer stimulation setup[3]. This will allow quantification of the stimulation effect as both the pulse width and amplitude will be known. In the LARSI, neither the voltage nor the current are known which makes it difficult to evaluate the conditions of use.

[2]The ideal recruitment depend on the application envisaged, for bladder control for example it should be rather steep.

[3]Controlled current rather than controlled voltage output stages have been advocated for implanted electrodes as the current imposed between the anode and cathode is known regardless of their polarisation [Geddes, 2004; Grill and Mortimer, 1995a]. With surface electrodes, edge effects may lead to dangerously high current density, hence voltage controlled outputs are favoured.

9.2.6 Stimulation parameters with the custom-built stimulator output-stage integrated circuit.

As seen in chapters 4 and 5, cross-talk stimulation may impair selectivity, starting at very low level, unless electrically independent channels are used. In the SLARSI, these channels will be implemented with a custom-built integrated circuit that will deal with channel selection (demultiplexion), provide anode and cathode switches and include a controlled current-source and charge-balancing circuits. This IC will be detailed in chapter 10. Prior to this, some general considerations (necessary to set the IC specifications) are discussed here as part of the conceptual description of the SLARSI.

9.2.6.1 Voltage

The maximum available voltage at the output stage is limited by the technology chosen for the design of the integrated circuit, as well as by the maximum voltage of all other implants components and of course by the voltage reached across the receiver coil. Using the LARSI RF link, the voltage on the implant can vary between 71V (maximum, limited by a zener diode) and 0V when the coils are too far apart. Considering the conditions of use (thickness of the skin and fat layer between coils, movements intrinsic to the use of the implant), it seems reasonable to expect the voltage to remain at or above 25V during normal operation. The input of the IC will be preceded by a zener diode clamp to keep the voltage below a maximum set by the technology process selected, see chapter 10. To avoid the uncertainties due to a fluctuating power rail, a 20V regulator was included in the IC to control its internal voltage. All other components are protected by zener diodes with breakdown voltages lower than the components ratings (see [Donaldson, 1990a] for further information).

9.2.6.2 Pulse width

For the LARSI, Prof. Donaldson developed a complex exponential pulse width coding circuit [Donaldson, 1990a], implemented in a gate array. Despite the limited supply, this component remains unchanged for the new SLARSI. The pulse width may be discretely adjusted from $2\mu s$ to $992\mu s$, each step increasing the duration by about 6%. In future implementations of the implant, the gate-array may be replaced by FPGA [4] chips.

9.2.6.3 Current

The current levels must provide a large enough stimulation range, starting below the lowest threshold of large motor fibres and climbing up to supramaximal recruitment of the thinnest axons. The range of fibre diameters present in nerve roots and peripheral nerves was summarised in table 1.1, on page 12. As there is no information about the diameter of specific fibres in a root, the following calculations are based on peripheral nerve fibres. This is acceptable since the diameter range for a root is contained within the diameter range considered here in table 9.2. The following nerve fibres were con-

[4] Field Programable Gate Array.

sidered [Mathers, 1985]: B autonomic fibres innervating the detrusor muscle and in parts the smooth urethral muscles and sphincters and A-β motor fibres innervating the slow twitch fibers to the leg muscles. The stimulation and blocking thresholds were computed using the given diameter and formulae from Goodall et al. [1995]. They were extracted from a model of a monofascicular rabbit tibial nerve stimulated with a tripolar cuff electrode, for a $300\mu s$ pulse width. The following relationships are of interest: $I_{threshold} = 2.3 * \phi^{-1.34}$ and $I_{blocking} = 10.7 * \phi^{-1.48}$ where the current is expressed in mA and the fibre diameter ϕ is in μm. These formulas must be considered with care as they are the results of a computer simulation and have not been confirmed by any animal experiments [5]. They were chosen for although the mount is a cuff, its dimensions are somewhat close to those of a book, and, if anything else, the arrangement is tripolar with symmetrical anode contributions. The thresholds may be artificially low (cuff-electrode closely wrapped around a fascicle in saline, no connective tissue) but the diameter relationship is their major interest.

In Donaldson et al. [1998] on LARSI parameters, "working" pulse widths [6] are on average 5 times the stimulation threshold and the motor thresholds vary about a threefold from the largest to the thinnest fibres which is in gross agreement with table 9.2. With patient JH for example the thresholds ranged between 3.8 and $7.5\mu s$ for L2 to S1 (45 and $65\mu s$ for respectively S2L and S2R probably due to injury) [Donaldson et al., 2003]. The stimulation current with LARSI is fixed (set by the operating conditions, not controlled) and estimated at 3.2mA for JH and 5mA for CB. From measurements during SARSI implantations, Brindley et al. [1982] report a threshold for somatic movement ranging from 0.3 to 3mA with $100\mu s$ pulses. With similar settings, post operative measurements show a current for maximum detrusor response, evaluated as a multiple of the somatic threshold, ranging between 5 and 20mA. Other studies mention even higher amplitudes, in a clinical review of SARS implants, van Kerrebroeck [1993] mentioned a maximum cathodal current of 40mA after full growth of fibrous tissue (voltage adjustment between 0 and 40V) with a pulse width of $350\mu s$. These figures suggest a surprisingly large range, from $\sim 12nC$ ($3.8\mu s * 3.2mA$) for leg motor threshold to $\sim 14\mu C$ ($350\mu s * 40mA$) for strong bladder contractions.

Although pulse width and amplitude are not quite interchangeable, the exponential pulse width adjustment developed by Donaldson for the LARSI combined with three discrete current settings of 2mA, 8mA and 16mA should be sufficient to cover all the above mentioned data, from the lowest to the highest, for both sacral (i.e. bladder and bowel) and lumbar (i.e. lower limbs) stimulation (range: $2\mu s * 2mA = 4nC$ to $1ms * 16mA = 16\mu C$).

Ideally, the bladder should be stimulated at high level to block propagation in the mo-

[5] As remarked by the author, the fact that there was hardly any differences for a fibre in the middle or in the periphery of the fascicle shows that the equations describing the model are not sensitive enough to certain parameters like the resistivity of the different layers [Goodall et al., 1995].

[6] Pulses that give strong contractions of the desired muscles.

Table 9.2: Stimulation range computed from Goodall et al. [1995] for a $300\mu s$ pulse, nerve diameters from Mathers [1985].

fibre type	function	diameter (μm)	$I_{threshold}$ (mA)	$I_{blocking}$ (mA)
B	parasympathetic	1	2.3	10.7
	(detrusor muscles)	5	0.26	0.99
A-β	motor	7	0.17	0.60
	(skeletal muscles)	14	0.07	0.22

tor fibres and limit legs or feet movements when using the urological function of the implant. There is a slight overlap between the stimulation threshold of the largest presynaptic fibres ($0.26mA$) and the blocking threshold of the smallest motor fibres ($0.60mA$). Yet, as bladder stimulation requires a recruitment as complete as possible, it is normally done at supramaximal levels, beyond the overlap zone. Reviews of SARSI users confirm that although patients may experience mild legs or feet twitches while using the stimulator, they do not consider it a strong negative side effect, to some it may even be an indication that the device is working [Brindley, 1994; van Kerrebroeck, 1993].

Likewise, are there any risks of voiding during leg exercise (provided the S2s roots are strongly stimulated)? This has not been a problem with the LARSI patients. Voiding requires special sequences of supramaximal stimuli that contract both the sphincters and the detrusor followed by periods of relaxation when the sphincters are loose while the bladder is still contracted (because it is a slower muscle), see section 3.2, page 44. Therefore, should the strongest motor stimulation cause low level recruitment of some large autonomic fibres, this would not be likely to cause voiding [7].

9.3 RF link and transmitter

In the LARSI, the signals generated by the control box are transmitted to an implanted receiver-stimulator via a radio-frequency (RF) link [8]. A basic transmitter unit contains a coil and oscillator circuit. It is most often distinct from the control box as the transmitting coil has to be brought within centimeters of the implanted receiver coil for efficient communication (the coupling coefficient decreases with increasing distance between coils [Terman, 1943, page 67]). A small, lightweight, transmitter is easier to handle and secure in place for hour long use of the implanted stimulator. In the LARSI transmitter a feedback mechanism is also implemented to measure the coupling coefficient and adjust the transmitter's drive voltage to maintain a relatively

[7] Issues of urinal reflux and related kidney infections have also been ruled out.

[8] The terms "transmitter", "receiver" and "control box" were introduced in Part I, section 2.3, page 32.

constant implant voltage. Technical details may be found in Donaldson and Perkins [1983] and Donaldson [1990b]. The SLARSI transmitters are copies of the LARSI units as no improvements were required at this stage. They connect to the control box via purpose-built cables and shake-proof connectors.

9.3.1 A note on multiplexing

Most electrical stimulation systems are multi-channel devices: they act on more than one nerve or muscle groups, each considered as a separate channel. Conceptually, the controller produces one logic signal per channel, in sequence or independently. If there is only a small number of channels the signals may be individually transferred to their corresponding output-stage in the stimulator. This requires one link per channel, physically implemented as one set of coils with a dedicated carrier frequency. As the number of channels increases this solution becomes impractical and multiplexing is introduced. All logic signals are combined by the controller as one train of pulses and transmitted over a single link to the receiver-stimulator where they are demultiplexed. Although this increases slightly the complexity of the logic blocks, this is outweighed by the simplification of the Tx-Rx operation, assembly and overall size.

9.3.2 Communication integrity

Using an RF link for data transfer across the skin, it is difficult to maintain continuous communication. The two coils may easily get out of alignment as the patient moves (for a coil to coil separation of 25mm the maximum axial misalignment is also 25mm). Actions must be taken to avoid unexpected, uncontrolled, stimulation that could result from partial transfer of stimulation data between the external controller and the implanted stimulator.

Since the implanted stimulator is passive, and relies on the RF link to receive power, the stimulation can easily be interrupted in emergency by moving the transmitter away from the patient. Safety concerns must therefore be focused on the risks of damage from a very short, erroneous, stimulation sequence, before the user has had time to react. Considering the nature of the implant (bladder management and leg exercise), the main risk would come from unexpected interruption of stimulation on the one hand (risks of fall when the patient uses the implant to stand up and transfer), and from a supramaximal stimulation of antagonist muscles (or unselected muscles, e.g. a strong stimulation of knee extensors when the patient uses the implant for bladder management) on the other hand. Strong stimulation of only one channel at a time is not considered potentially harmful for a short duration, and is even likely to be required during regular use, especially for bladder management. Two "safety" methods are implemented in the SLARSI to prevent unexpected stimulation interruption for one, and avoid the presence of more than one stimulation pulse at once and limit the risks of mis-selection for the other.

The first method was already present in the LARSI, yet the user interaction has been improved to increase patient understanding and decrease reaction delay. The coupling

coefficient is continuously monitored by the control box (see Donaldson [1990a] for practical details). When it falls below a pre-set level, the user receives a warning (a noise is emitted, and a short explanation is displayed on the control box's LCD, advising the patient to re-adjust the transmitting coil). If the coupling falls further, the communication is properly, sequentially, interrupted, before the poor coupling renders the data transfer uncertain. A small hysteresis is introduced on the restart condition: the coupling coefficient must have reached a higher level, above the warning value, for the control box to automatically re-initiate the communication. This avoids spurious on-off-on-off sequences should the coupling be borderline.
The second method is built in the demultiplexor chip logic. An error in the stimulation pattern might cause the activation of unwanted channels, either because the selection has failed, or because the timing is faulty and two or more channels are activated at once. The error in the code may come from the RF link, but it may also arise in the circuit "translating" the received signals into stimulation pulses. The new logic block ensures that there will only be one stimulation pulse at a time, and that it will only appear on the selected channel [9]. The precise mechanism will be detailed in chapter 10.

9.4 External control box

The external control box provides the functionality to translate the patient's request into trains of pulses. To do so, it needs at the very least the following parts:

- Some simple physical means of interacting with the patient: push-buttons, simple keyboard, LCD screen, buzzer or vibrator.
- Dedicated control and transmission programs with all housekeeping routines [10].
- A means for patients and practitioners to store patient-specific information (in RAM) like threshold, maximum recommended amplitude and stimulation patterns [11]. This is either done using the small LCD display and the limited set of buttons mounted on the front panel, or, for complex information, via a connection to a PC together with the dedicated hardware and software [12].

[9] An error detection system could have been included in the receiver's design, but it would increase the conceptual and physical complexity of the implant, transmitter and controller. Even more so since the LARSI only relied on the coupling coefficient method, and no provision was made for the addition of a second safe-guard (both in the logic sequencing and in the tight layout). In keeping in line with the idea of "LARSI adaptation", the implementation of the second method should be included in a component that required a redesign anyway, i.e. the demultiplexor chip.

[10] During the development stages at least it is interesting to store most of the code in RAM where it can easily be accessed for updates. Yet, basic "bootstrap" routines must be present in a more stable memory type, like EPROM or EEPROM. Those essential routines must at least provide low level user interaction to load code in RAM and perform RAM integrity checks upon startup.

[11] Performing complex movements like cycling requires sequential activation of various muscle groups. The optimum sequences and their timing are patient dependant and also evolve with patient's fitness and training.

[12] The PC connection is only required to load the data, not to operate the device.

- An internal power supply; as the box should be portable, batteries are preferred although they add a considerable weight.

Improvements of the LARSI control box were required for the SLARSI, essentially to the following matters [13]:

1. Replacement of the bulky separate battery pack by a smaller battery integrated in the control box, see section 9.4.1.

2. Update of the internal program for increased user-friendliness and improved functionality (self explanatory, not described hereafter).

3. Re-design of the user-interface, including the physical appearance of the box and the production of dedicated software running on the pc used to store user data and allow improved practitioner interaction, see section 9.4.2.2.

9.4.1 Battery

The LARSI set of batteries was replaced by a smaller 7.2V Li-Ion battery, commercially available for video cameras. Its size is standard and there is a range of manufacturers which should guarantee availability even outside the UK and reduce the rate of obsolescence. As opposed to the LARSI which used a separate battery pack, the new battery and dedicated charging and decoupling circuits are enclosed in the control box. For safety, the battery is automatically disconnected from the control circuit (and connected to the charger) when the box is plugged in the mains. The switching mechanism is designed to ensure that the control box cannot be turned on while charging. This was devised to increase safety as the box will be used in restrooms where it may drop in water while the patient is holding the transmitter. The switching trick limits the chances of this happening while the box is connected to the mains.

9.4.2 User interface

9.4.2.1 Control box interface

Figure 9.3 shows pictures of a prototype control box. The various functions offered by the stimulator are organised in a binomial tree structure as drawn on fig. 9.2 allowing the user to browse through the menu using only two selection buttons (A and B). The third push button, "OUT", stops the program or moves back up a level. This keeps the physical user-interface fairly simple and the messages and menu are clear and easy to understand. This was deemed essential to decrease the "guinea-pig" feeling of patients taking part in the test phase of this new product.

9.4.2.2 PC interface

Using only the limited set of buttons and the small LCD display makes it difficult to define complex information and store it in the RAM. Besides the thresholds for

[13] Minor alterations of the rest of the box and its software were also necessary to adjust to the changes, these will not be described here as this would require a detailed explanation of the LARSI design which is beyond the reach of this thesis.

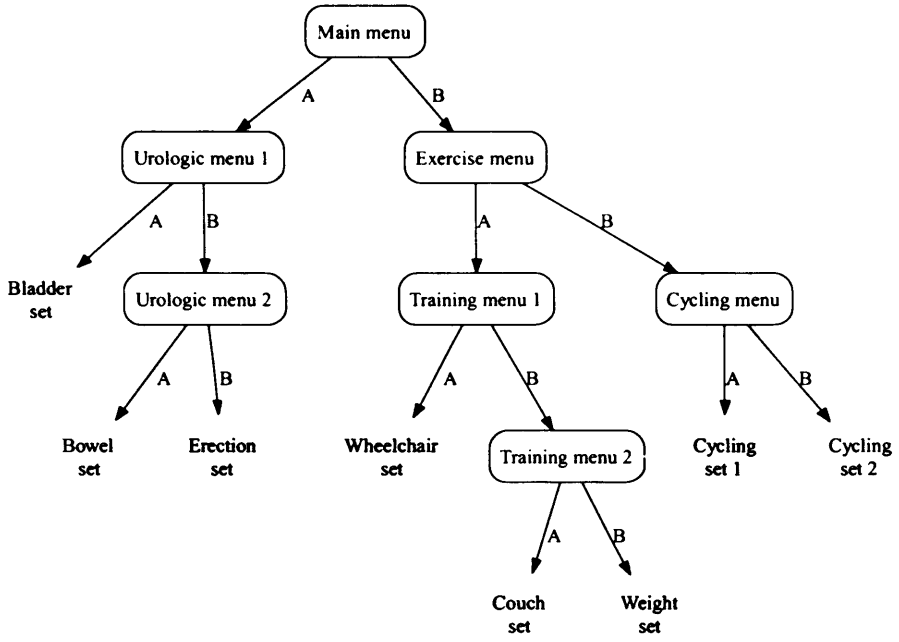

Figure 9.2: Tree structure of the control box menu.

the 10 channels, the stimulation sequences for urological and training functions need to be loaded. A cycling program even requires two sets of all parameters (minima and maxima) since the user has a control over the intensity which can be set within the limits defined by the practitioner and set in the RAM. This calls for a dedicated software to set and store the user data in a quick and reliable manner. Designing such a pc interface both user-friendly and efficient is a challenge. A first version, called LPCI, had been developed for the LARSI, but besides the fact that it did not include any urological functions, it was unintuitive and human-error prone. A new version of LPCI is now available, using intuitive GUIs to allow seamless data alterations by all SLARSI users [14].

9.5 SLARSI summary

The SLARSI is a new anterior root stimulator implant for bladder and bowel emptying and lower limb FES. It evolves from the will to combine the functions of the only two root stimulator implants available today: SARSI and LARSI, both developed by the

[14]The adaptation of the old LPCI for the new SLARSI was proposed as a rather ambitious student project. The goals were to re-write (adapt and update) the code to include the urological functions, develop user-friendly GUIs together with a clear and concise printed user-manual. The programming had to take place in parallel with the development of the internal program (running in the micro-controller of the control-box) which further complicated the task. This project was fulfilled by Simon Hearn, an intercalated student who quickly understood the drawbacks of the original LPCI and developed an easy, user-friendly, intuitive piece of software together with well documented Users and Developers manuals. Any explanation on how this program works, how it was implemented or even the specification are outside the scope of this thesis, yet Simon's most valuable contribution to the development of the SLARSI as a complete FES system, beyond the implant, had to be acknowledged in this section.

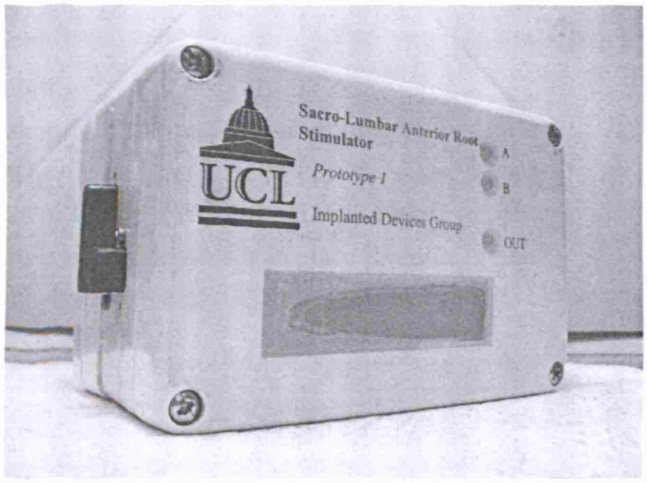

(a) Prototype of new SLARSI control box with integrated charger.

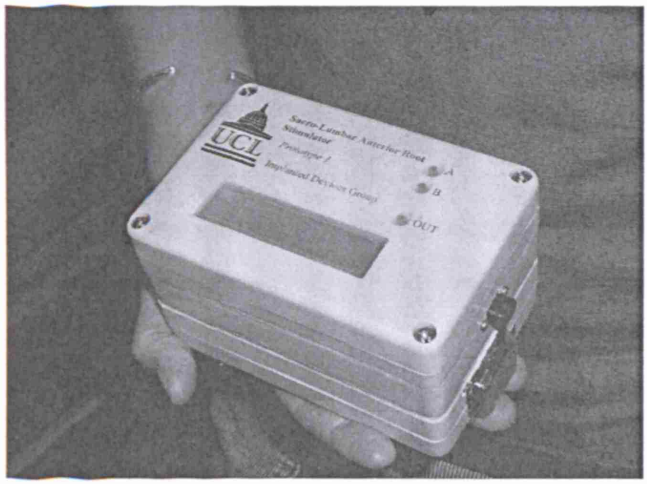

(b) The control box is easily portable as it does not require an additional battery pack.

Figure 9.3: New SLARSI control box.

Medical Research Council team now reorganised as the Implanted Devices Group of UCL. This project led to the research presented in this thesis and this chapter summarises the main improvements implemented for the SLARSI: new electrode connections with electrically independent channels; LARSI pulse-width modulation scheme now combined with discrete amplitude settings for a wider dynamic range; added resilience (in the demultiplexor logic) to erroneous stimulation patterns; smaller and lighter control-box with new battery and charging circuit; upgraded control programs, both internal (control-box) and external (pc) for better user interactions.

A note on reliability

Should the system fail, the patient will return to "pre-implant" status, requiring a catheter and\or medication as prior to the operation. Although this situation is not critical, the risks of failure should be minimised and procedures to locate the site of failure and repair it swiftly should be in place [Brindley, 1995].

Chapter 10

Purpose built integrated circuit for SLARSI

This chapter focuses on the demultiplexor with independent channels used in the new SLARSI. As explained in section 9.2, it replaces the old commercial demultiplexor as well as the voltage regulator and the current limiting resistor. Figure 10.1 shows block schematics of both the LARSI and SLARSI implants.
In 1998, Arjan Krabbendam, a masters student from the University of Twente (the Netherlands), worked for 6 months on the concept of the new IC. The early design of the present circuit was based on his notes which are quoted whenever available to emphasize the importance of his contribution. The development also owes much to the help and most valuable advice from Mike Brent.
Integrated circuits with a first version of the layout failed during the bench tests and a second batch, with an improved layout (no changes in the concept, see section 10.4), were produced. The new ICs passed all tests without failing and met the specifications (see tests section 10.3). All schematics and results presented in this chapter are for the second version.

10.1 Design

10.1.1 Concept and specifications

The circuit forms the output stage of the stimulator. It provides a maximum of 12 current-controlled independent channels, physically accessed via 12 pairs of pins. Each pair has one connection, with a switch to a high voltage rail, for the anode and one connection, with a switch to a current sink, for the cathode. Each channel also has a switched discharge path. Figure 10.2 is a general schematic of a channel, with its anode, cathode and discharge switches designed with transistors. Practically, the cathode switch and current sink may be implemented as one entity (see discussion in section 10.1.4). Each channel requires at least one control signal as shown on fig. 10.2 (turning on-off the sink and anode and cathode switches and turning off-on the discharge). In the implant [1] only three inputs signals are available: a *clock*, a *dataIn* line indicating

[1] Reminder: this IC will replace components on the existing LARSI implant. To minimise the changes only signals already available should be used.

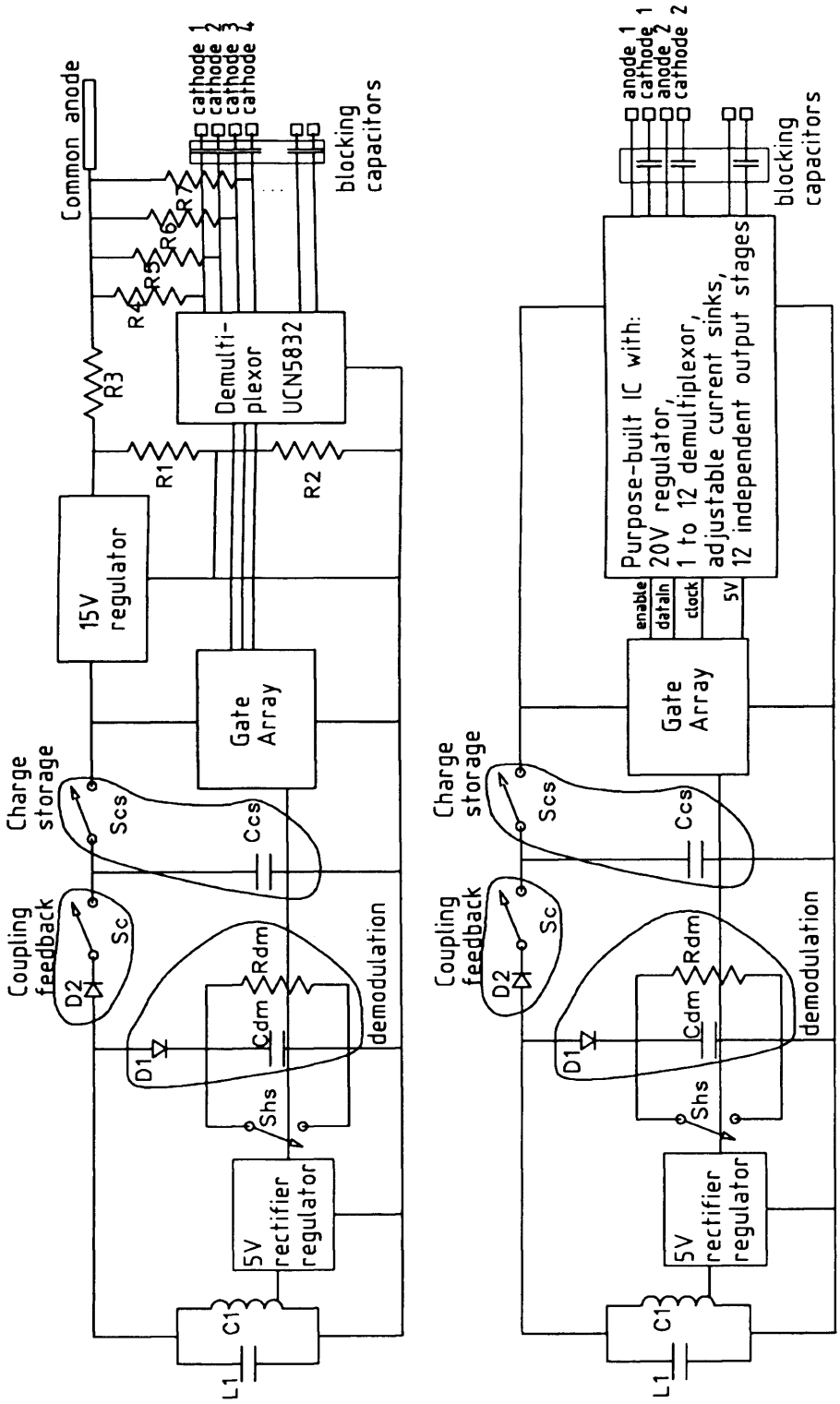

(a) LARSI schematics with 15V voltage regula- (b) SLARSI schematics with new demultiplexor.
tor and control circuit.

Figure 10.1: LARSI and SLARSI schematics.

the beginning of the stimulation on the first channel and an *enable* line multiplexing the timing pulses for the twelve channels. The IC therefore includes a 1 to 12 demultiplexing logic to translate the available signals into channel controls. It also contains some extra features to control the voltage and current levels, see section 10.1.6. The following bullet points list the most important specifications.

- 1 to 12 demultiplexor.
- Channels: 12 with anode, cathode and discharge switches.
- Inputs: *clock*, *dataIn* and *enable* lines, 5V high.
- Output constant current settings: 2mA, 8mA and 16mA (the levels are allowed a $\pm 10\%$ fluctuation).
- Maximum output voltage: 20V (this is a technological consequence, not a preliminary specification).
- Additional logic for dynamic control of the current level.

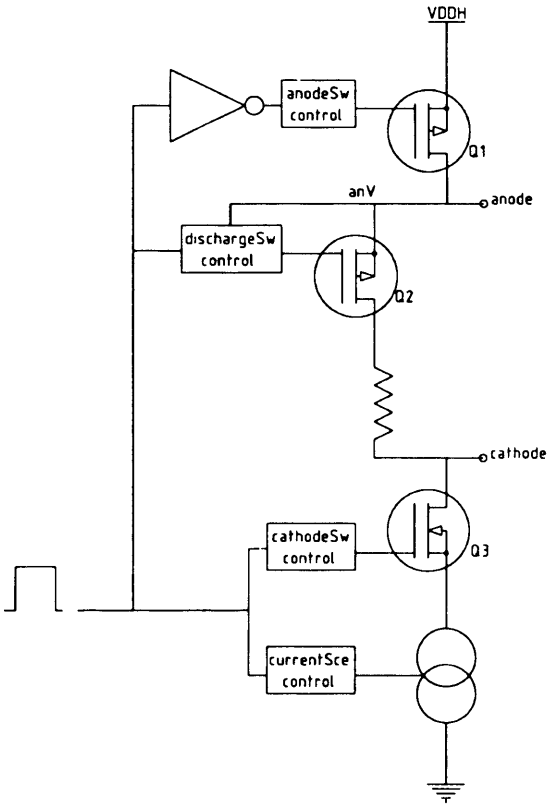

Figure 10.2: Schematic representation of a channel, with current sink and transistor switches.

10.1.2 Technology choice

The IC design tool is Cadence 4.4.5 running on a Sun machine [2]. The I.C. is designed with both an analogue part and a digital part. Due to the expected load and required current output, the process technology needed to be suitable for high voltages as well as to propose libraries for the logic control. UCL, as part of the University of London VLSI Consortium, used to be a member of Europractice [3] which offered cheaper access to certain technologies for small prototype production. The final choice was to create an ASIC using the Austria Micro Systems AMS-HV 0.8 technology, with $6mm^2$ minimum area, which would be produced by IMEC and the Franhauffer Institute Integrierte Schaltungen.

10.1.3 Voltage considerations

10.1.3.1 Voltage regulator

The operating conditions specified for the AMS-HV technology used impose limits on maximum voltages: V_{Bpsub} [4] of the pmos, the V_{Dpsub} and V_{Spsub} of the nmos all have to be less than 50V. Further restrictions exist, limiting the operating voltages of other transistors to 20V. This limits the maximum input voltage to the chip. As the power is provided to the IC (and the rest of the implant) via an RF link across the dermal layers of the patient, the coil to coil distance will vary during use and the input voltage at the receiver will change accordingly. An external zener diode at the IC input ensures no voltage higher than 50V and an internal voltage regulator stabilises the input voltage, ranging between 21V and 50V, to a steady 20V.

Functional details:

A schematic of the voltage regulator is given in figure 10.4, with details of the operational amplifier in figure 10.3. The amplifier design is based on a standard Cadence cell which has been altered to deal with higher voltages and improve current efficiency. The opamp compares, on its positive input, the voltage produced by a bandgap voltage source (box BG04 in fig. 10.4, produces a VBG of 1.2V) with, on its negative input, a fraction of the output voltage. The resistor values are adjusted so that both voltages match when the output is 20V.

The following two examples explain how the circuit works. The first illustrates an increase of the current required by the load (leading to a fall of the output voltage), the second a decrease. The first effect of a fall of the output voltage is to decrease the current in the resistor chain, leading to a diminution of the voltage at the negative opamp input. This creates a positive difference in the opamp leading to a rise of its output

[2] Cadence was installed and maintained by Mike Brent for the Medical Physics Department.

[3] EUROPRACTICE (PRomoting Access to Components, subsystems and microsystems Technologies for Industrial Competitiveness in Europe) aims to stimulate the wider application of state-of-the-art microelectronics technologies by European Industry in order to enhance European competitiveness in the global market-place and is financially supported by the European Commission (note from A. Krabbendam).

[4] Voltage between the bulk and psubstrate.

turning the two nmos transistors M5 and M6 harder on. As M5 and M6 allow more current, the voltage drop across the resistors J0 and J6 increases. The Gate-Source voltage of the two pmos transistors M0 and M4 will rise, delivering more current to the load. A maximum current of 45mA can be delivered. In contrast, a drop in the load current consumption causes a negative difference in the opamp. M5 and M6 pass less current, decreasing the Gate-Source voltage of the pmos to limit the load current.
To avoid oscillations on the output line, an external capacitor of about $5\mu F$ is required. This limits the set-up time of the *V20V* output. Figure 10.5(a) shows a Cadence simulation of the set-up when *VDDH* takes 10ns to rise to 35V, and figure 10.5(b), another Cadence simulation, the *V20V* voltage when an output current pulse of 35mA is applied for $10\mu s$.
*N*ote: a list of all labels used to describe the pads of the IC is given in section 10.2, page 244.

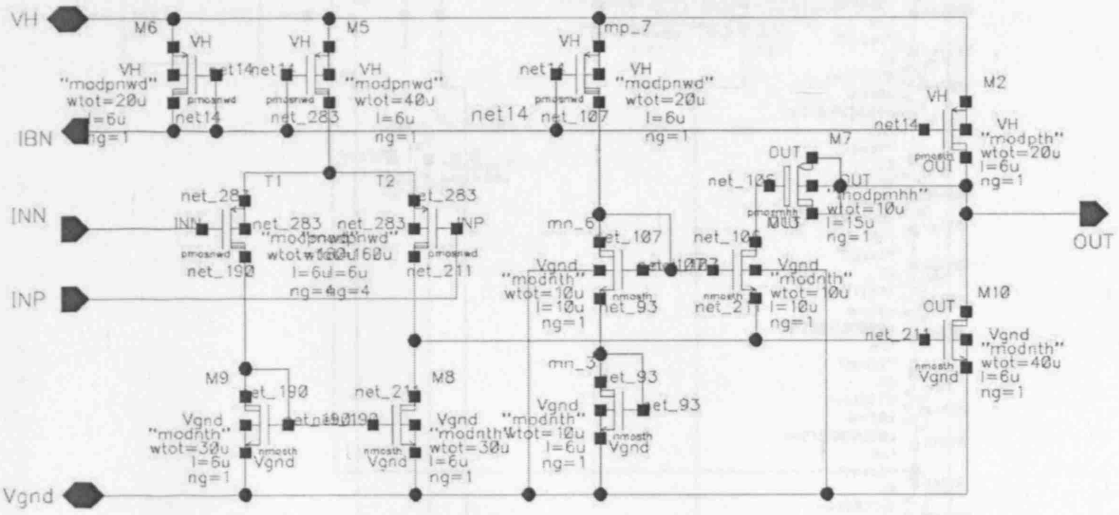

Figure 10.3: Integrated operational amplifier.

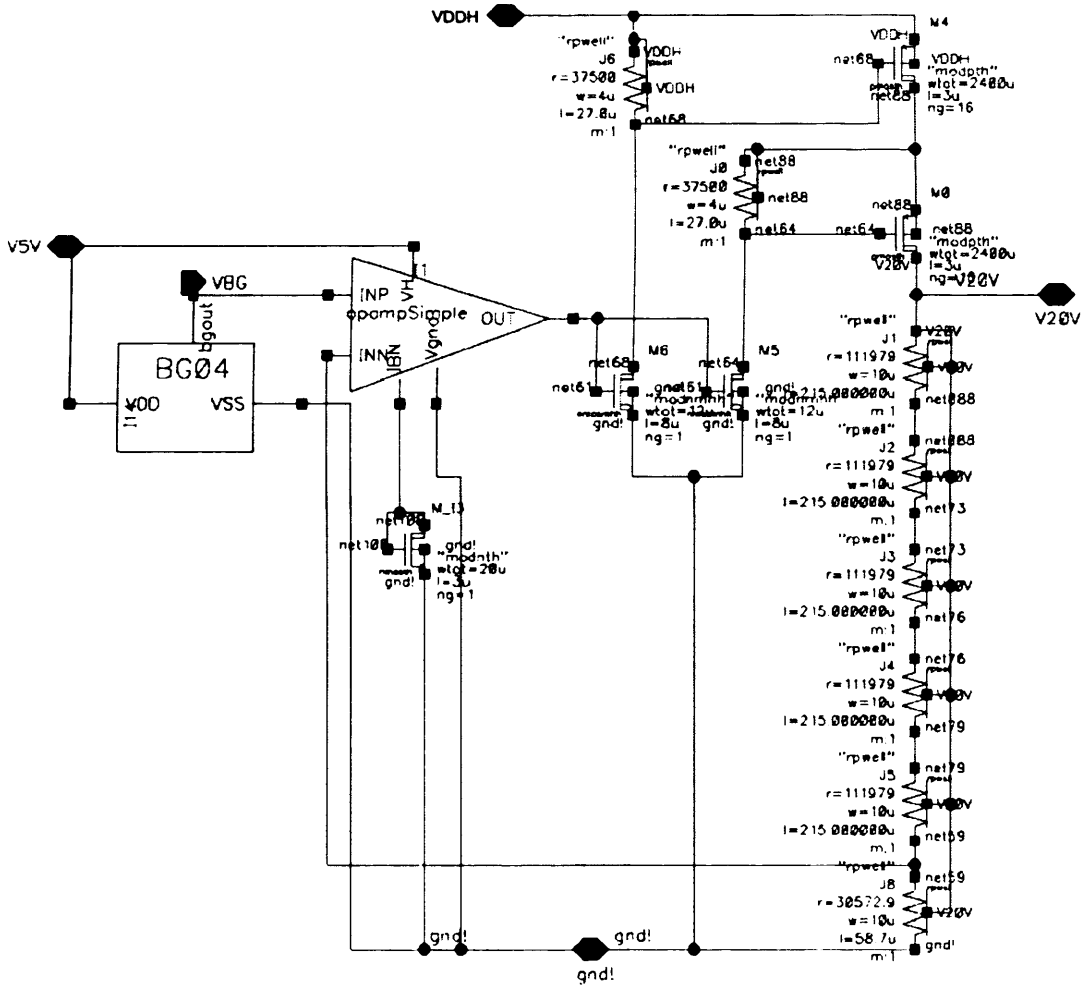

Figure 10.4: Voltage regulator.

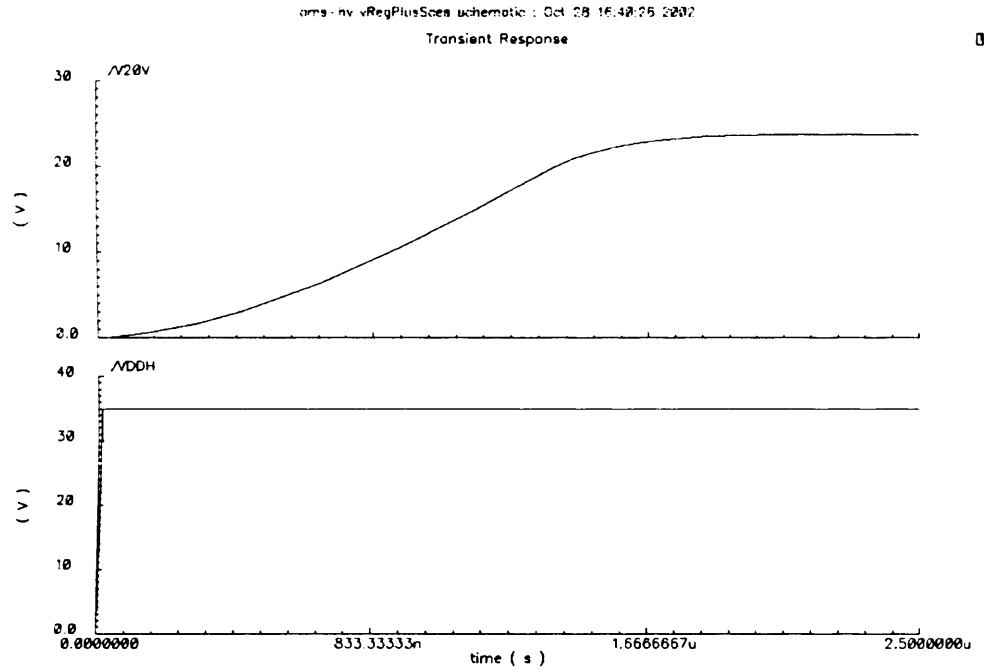

(a) Voltage regulator set up time with a 5nF capacitor, *VDDH* reaches 35V in 10ns.

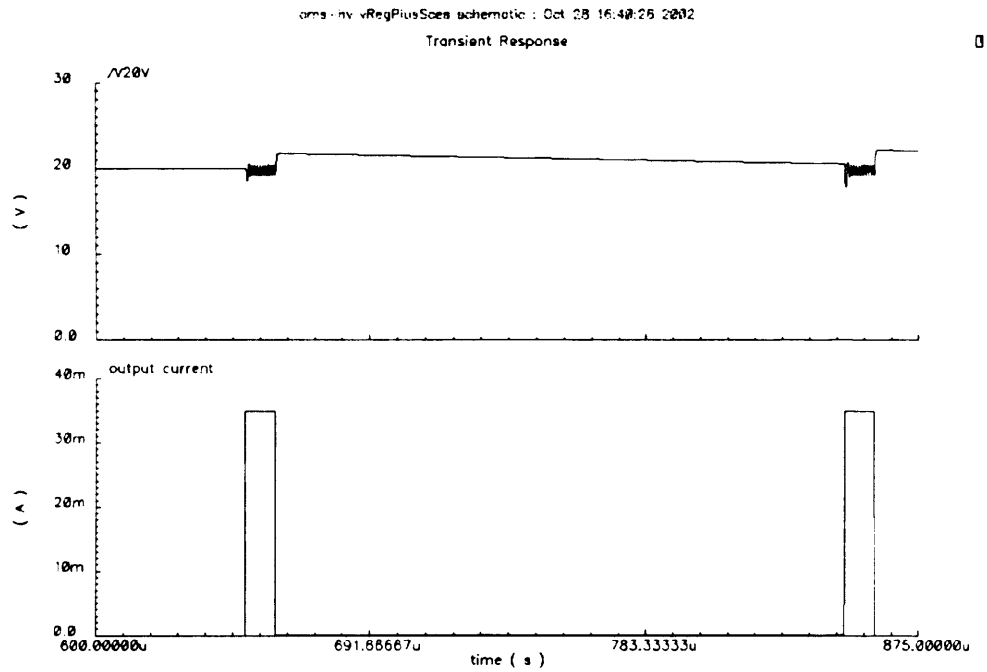

(b) *V20V* fluctuation for short ($10\mu s$) 35mA current pulses.

Figure 10.5: Voltage regulator performances.

10.1.3.2 Channel voltage drops

Knowing the maximum available voltage (20V) and the current settings (2, 8 or 16mA), the various voltage drops of the channel (across the switches and current sink) must be studied to estimate the remaining voltage available for the load. The following paragraph is quoted from A. Krabbendam's report. Although he had been advised to use the 15V regulator already available on the implant, his comments were a starting point for the voltage analysis briefly described afterwards.

> *"Voltage drop considerations.*
> Before designing the switches that are involved in stimulation, first the potentials in the channel are considered. Because one of the specifications is that it should be able to run with a supply voltage of (only) 15V, it is important to watch the voltage drop over the electrodes, switches and current source. The several voltage drops are given in fig. 10.6. When the channel is stimulated the cathode and anode switches are closed and the current source operates. The electrode impedance in series with the cable resistance is at minimum of 350Ω, in the worse case of 32mA this gives a voltage (Ve) of 11.2V. This gives 3.8V left for two switches, the current source and the capacitor. The switches should be able to drop only 500mV (Va and Vc). The current source should operate with a saturation voltage of 1V (VCS). Finally the blocking capacitor may build up a voltage of 1.8V. This is the same as the maximal voltage across the capacitor in the Mark-5 stimulator. However, now the current has a value of 32mA, so the capacitor value needs to be increased (to $> 21\mu F$)."

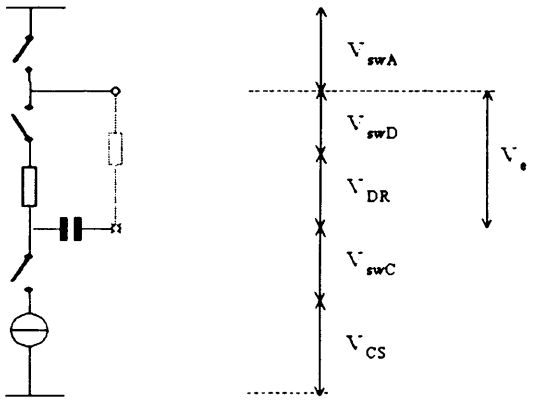

Figure 10.6: Voltage drops over several parts in a stimulation channel, reproduced from A. Krabbendam's report [Krabbendam, 1998].

Krabbendam's estimate of the electrode impedance in series with the cable resistance (350Ω) is rather low compared to the various values given in section 7. These considerations lead to a re-think of the original specifications (15V and up to 32mA). After

some early stage modelling and some research on the stimulation levels needed (see sec. 9.2), the following was decided: replacement of the 15V regulator chip with an internal regulator (20V, see section 10.1.3.1) included in the chip and current settings reduced to 2mA, 8mA and 16mA. The switches will take 1.2V together; and the current sink has about 2V at the highest current setting. These values are the result of a compromise between size and voltage drop, taking into account the intrinsic limitation of the technology, i.e. a maximum voltage of 20V across some junctions. The original proposal for the two switches to drop only 0.5V each at 32mA required very large transistors (based on symmetrical voltage drop, i.e. $R_{on} = 15.6\Omega$, the nmos $\frac{W}{L} = 837$ and the pmos $\frac{W}{L} = 1363$ with a minimum track width of $3\mu m$). This is excessive as the IC is to have twelve channels, each containing a pair of switches plus a discharge circuit. Since the maximum current had been decreased from 32 to 16mA, the size of the switches could be halved without affecting the voltage available for the load which was an improvement but still required rather large transistors. As the performances of the p and n channel transistors differ, a voltage drop of $1.2V$ for the anode and cathode switches combined was allowed. The requirement to design a current sink working with an input voltage as low as $1V$ was also seen as unrealistic, even with the lower current settings. As the internal voltage had been increased from 15V to 20V to account for the larger charge to deliver to the sacral roots, the specification for the current sink was altered to sinking a constant current of 2mA, 8mA or 16mA with a voltage drop ranging from 2 to 20V. With the updated specifications, the switches and current sink together would drop a maximum of 3.2V, leaving 16.8V for the load, including the blocking capacitor. In his analysis, Krabbendam had concluded that a capacitor of $21\mu F$ was required. As the SLARSI is an adaptation of the LARSI, the new components must fit in the space laid out in the LARSI substrate. The space available for the 12 blocking capacitors (one in each channel) is therefore restricted which limits their maximum value. To optimise this space, the two sacral channels, more likely to be used at 16mA (see table 9.2 for parasympathetic nerves), will receive larger blocking capacitors. Working with these estimates as shown in table 10.1 gives a blocking capacitor of slightly less than $5\mu F$, the "leg movements" channels will have $2.2\mu F$ capacitors and the urological channels $4.7\mu F$.

Table 10.1: Maximum voltage drops expected across the various components of a channel.

Electrodes and cable:	$550\Omega * 16mA + \frac{910\mu s * 16mA}{3\mu F^a} = 13.7V$
Switches and current sink:	1.2V + 2V = 3.2V
Voltage drop left across blocking capacitor:	20V-13.7V-3.2V = 3.1V
Minimum capacitor value of	$\frac{16mA * 910\mu s}{3.1V} = 4.7\mu F$

[a] Capacitive load, value taken from Krabbendam's report.

10.1.4 Anode and cathode switches

As for the voltage consideration, A. Krabbendam's report was used as the starting point to design the final switches. The following is a quote of his paragraphs on the cathode switch, current sink and anode switch.

> "*Cathode switch and current source*
> In the 'Design specification' the cathode switches and current sources are put in a separate box, this is not essential: the cathode switches could be designed as switched current sources. In theory the following option are available, where '-' means that the switch acts as a current source:

Cathode switch	Current source	Comment
BJT	BJT	Switching characteristics are non-linear, in current source base current effects
BJT	FET	Switching characteristics are non-linear, simple current source implementation
BJT	-	Base current effects and control lines for current setting to all channels
FET	BJT	Switching characteristics are linear, in current source base current effects
FET	FET	Switching characteristics are linear, simple current source implementation
FET	-	Control lines for current setting to all channels

Based on the comments written in the table, the FET-FET option would probably be chosen, however it should be noticed that there is a size-difference between an MOSFET and a bipolar transistor for high currents and high supply voltages. This difference is about 10 times for a current of 32mA and a saturation voltage of 0.5 V in this process. To compare the real sizes: a bipolar transistor (cell HNHP350A from library) needs $52 \times 10^3 mm^2$, the FET (FND W=10mm) $723 \times 10^3 mm^2$ and finally the round FET type (FNDR W=10mm) needs $417 \times 10^3 mm^2$. This disadvantage of the MOSFET's leads us to the solution of a BJT as switch, because the total area occupied by them is 14 times less! To design the switched current sink, three options are still available and have been sim-

> ulated. These are the FET current mirrors, with the bias voltage switched during stimulation, the bipolar mirror and the cascoded bipolar mirror.
>
> ...
>
> *Anode switch:*
>
> The same size considerations as for the cathode switches apply to the anode switches. This means that a bipolar transistor is preferable to an FET. For a low voltage drop and small switch for high currents the PNP transistor would probably be the best choice. Since a bipolar transistor is a three-terminal device, which requires a base current to turn it on, the use of a PNP version has the advantage over the NPN version, that the current through the collector, that is determined by the current source in the system, will not be affected by any base current. The use of an NPN would it make harder for the current source to keep the current on the required value, since the base current is added to the emitter current. The size of one PNP transistor in this process is $97 \times 10^{-3} mm^2$, a little larger than a NPN transistor with the same current flow. Unfortunately, the collectors of the available PNP transistors are connected to substrate, so they are not usable. The NPN transistors can't be used either, since the collector-emitter breakdown is only 10 volts. So finally the p-channel DMOST's were chosen. The voltage drop across this device will be a trade against occupied area. Given the minimum feature length of $L = 2\mu m$, a transistor with the size of $W = 500\mu m$ means a drop of 5 volts at 32mA. However, when you increase the size to a width of 1mm, the drop will be only 2.5V. To drive these anode switches an amplifier is needed to convert the 0-5 volts signal that is the output of the control logic to a signal that change from Vdd to Vss."

As explained in section 10.1.3.2, the voltage drops allowed for the switches and current sink in Krabbendam's preliminary study were unreasonable. The bipolar transistors option was dropped due to voltage considerations. Although it did save 0.5V, the proposal of combining the cathode switch with the current sink was too complex and space demanding as the three current settings must be available to each of the 12 channels. To limit the IC area and simplify the design, the alternative option of using a single sink connected to all 12 channels via individual cathode switches was evaluated and eventually selected. High voltage MOSFETs with thin to medium oxides using deep N wells for isolation from the P substrate can stand large enough voltages and were thus used as switches. In the reviewed specifications the two switch transistors (anode and cathode, see fig. 10.2) must drop only 1.2V together when passing 16mA. Practically, the anode switch is a PMOS with a width to length ratio of $\frac{1070}{3}$ (minimum dimension $3\mu m$) while the cathode switch is a slightly smaller NMOS (ratio = $\frac{999}{2}$, minimum dimension $2\mu m$). The current sink is described separately in section 10.1.6.

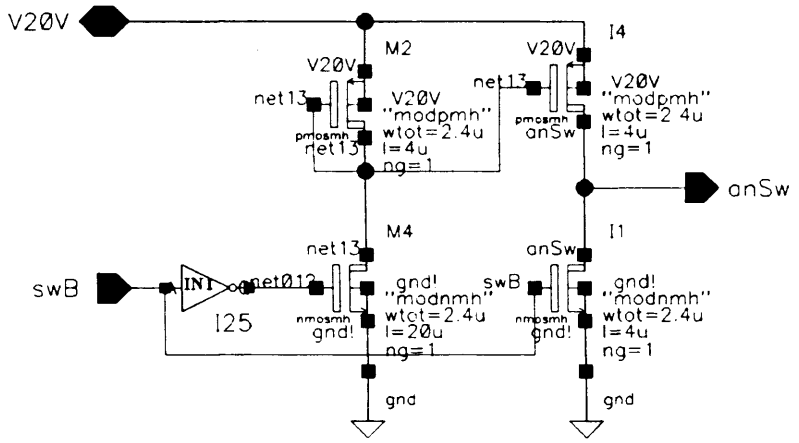

(a) Logic controlling the anode transistor.

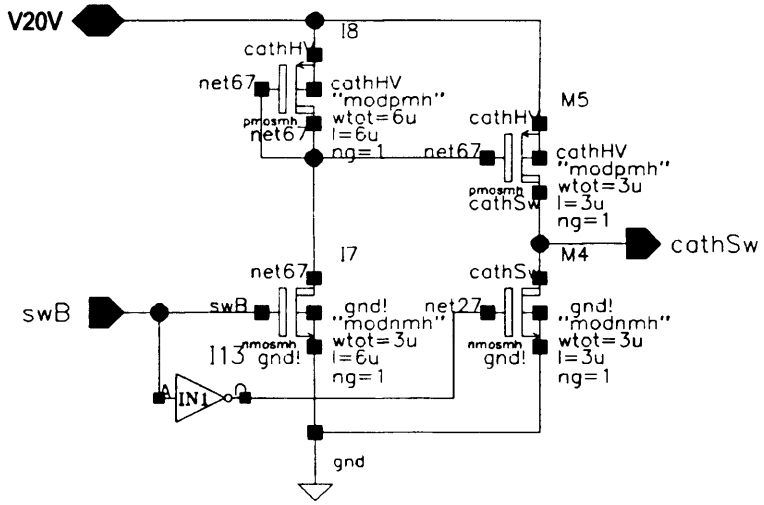

(b) Logic controlling the cathode transistor.

Figure 10.7: Anode and cathode switches

10.1.4.1 Switch control

The control of the two switches is achieved with blocks of 4 small transistors for each switch, see fig. 10.7. Each block transforms the 0-5V *swB* signal in a 0-20V logic drive for the switch according to table 10.2. The pmos Q_1 is connected gate to source, it acts as a resistor ($\frac{W}{L} = \frac{2.4}{4}$). Turning Q_3 on drives a small current through Q_1. The transistors are dimensioned to limit the current (decrease power consumption) while causing enough of a voltage drop to turn Q_2 on, Q_2 and Q_4 are symmetrical pmos and nmos. When Q_2 is turned on, Q_4 is off (0V at the gate), the output voltage is pulled up to 20V. Conversely, when swB is high (5V), Q_3 is off (inverter between swB and the gate), there is no current through Q_1, no voltage drop, Q_2 is off. Q_4 on the other hand is on and the output swings to 0V. As the output of this switch controls block

Table 10.2: Control levels for anode and cathode switches.

Gate drive voltages	anSw	dischSw[a]	cathSw
Channel off	20V	0V	0V
Channel on	0V	anV[b]	20V
timing	swB	swA	swB

[a] The discharge path must be open when the channel is on.

[b] *anV* is the voltage at the anode pin.

is connected to the gate of the large switch transistor, the $Q_2 - Q_4$ branch passes no direct current. The issues here were to minimise current consumption and minimise switching delay.

10.1.5 Discharge circuit

The discharge circuit is needed to recover the charge on the electrodes. For every channel, an external blocking capacitor is connected between the cathodal output (node *cathode* on fig. 10.2) and the actual cathode while the anode is directly connected to the anode pad. When, between pulses, the channel is idle, the discharge transistor (Q2 in fig. 10.2) is turned on, allowing the blocking capacitor to discharge through a $2k\Omega$ polysilicon resistor and balance the injected charges at the electrodes. The transistor is controlled with a block of four small transistors (fig. 10.8) as is the case for the other switches. Timing for the discharge switch is with *swA* which lasts 30ms longer than *swB*, the signal controlling the anode and cathode switches.
Here is Krabbendam's comment on the circuit:

> "*Discharge unit:*
> The discharge switch with resistor can be implemented by using a FET. Alternatively resistivity sheets are available in this process, but their value cannot be designed accurately. To remove for example 99 % of the charge from the capacitor (and electrode capacitance) through the electrode impedance and discharge resistor (FET) the later should have a value of 600Ω. This requires an area for the FET of $47 \times 10^{-3} mm^2$. As discharge resistance also pDMOST's are used, which will have an equivalent impedance of $2.5k\Omega$. Because unpredictable reverse current may flow through the discharge transistors, symmetric MOST's are used. Resistors in this process are not very accurate and also large compared with transistors, so not a nice alternative."

In the LARSI, the discharge path is passive, a $2.5k\Omega$ resistor is connected between each cathode (before the blocking capacitor) and the high voltage rail, see fig. 10.1(a).

In the SLARSI, the discharge path includes a transistor acting as a switch to disconnect the discharge resistor during stimulation. The impedance of this circuit must be high enough to limit the surge of current at the beginning of the discharge otherwise there is a risk of 'discharge stimulation' at the anode when the current is reversed. Practically, the highest stimulation level is not expected to be more than 10 times the threshold. The discharge impedance is then selected to limit the current surge to 10% of the "charging current" used during the preceeding stimulus. The impedance must also be small enough for the time constant to permit discharge of the load and external capacitor at the highest frequency. The charge may not be fully recovered for each individual pulse although the average for a complete train will be zero. The presence of a blocking capacitor allows for a small residual charge without risk of entering an unsafe working regime. If the electrodes potentials drift, the potentials will 'slide back' into the safe zone before any irreversible reaction occurs. This is a complex process, explained in Donaldson and Donaldson [1986b] and Donaldson et al. [1998].

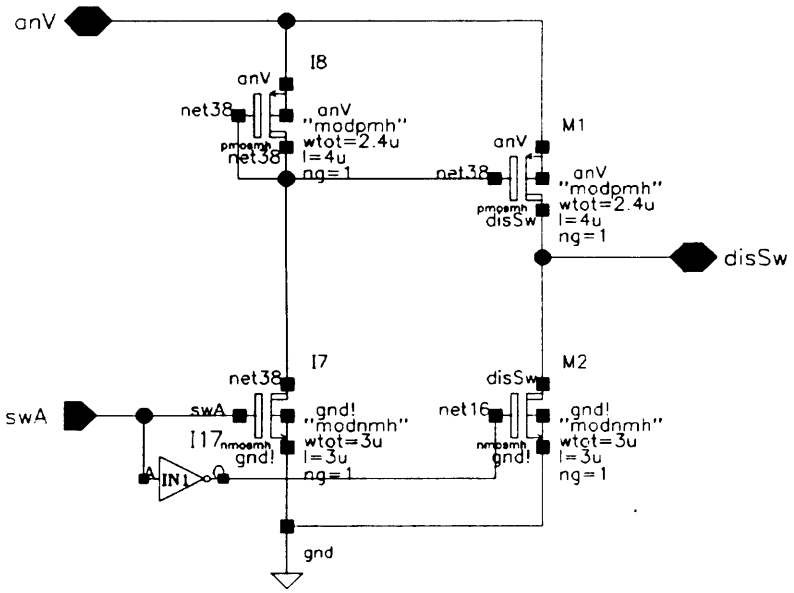

Figure 10.8: Discharge circuit.

10.1.6 Current sink with three current levels

Three designs of current mirrors using FETs were simulated: cascoded, simple and Wilson. The performances were comparable and the simple current mirror was easier to design and required less space. Figure 10.9 shows a schematic of the current sink implemented. The "original transistors", $Q1$ and $Q2$ on the left, drive a small but precise and constant current as the "mirror transistors", $Q3$, $Q4$ and $Q5$, on the right, will drive multiples of that original current. As there are three current settings, there are schematically three mirror transistors of increasing width. Practically, these are implemented as many inter-leaved gates. The gate voltage of $Q2$ sets that of the mirror

transistors, it must be well above threshold to push the transistors in saturation and have a flat drain-source voltage vs. current characteristic. The three switches $S1$, $S2$ and $S3$ are each implemented with two nFETs as shown on fig. 10.10(b). They select the current level by controlling which transistor is activated. The logic signals $curSwOn2$, $curSwOn8$ and $curSwOn16$ controlling those switches are produced by the logic block of fig. 10.11, unfortunately, the labels are a little confusing as they are different on the two figures: $q2$ is $curSwOn2$, $q8$ is $curSwOn8$ and $q32$[5] is $curSwOn16$.

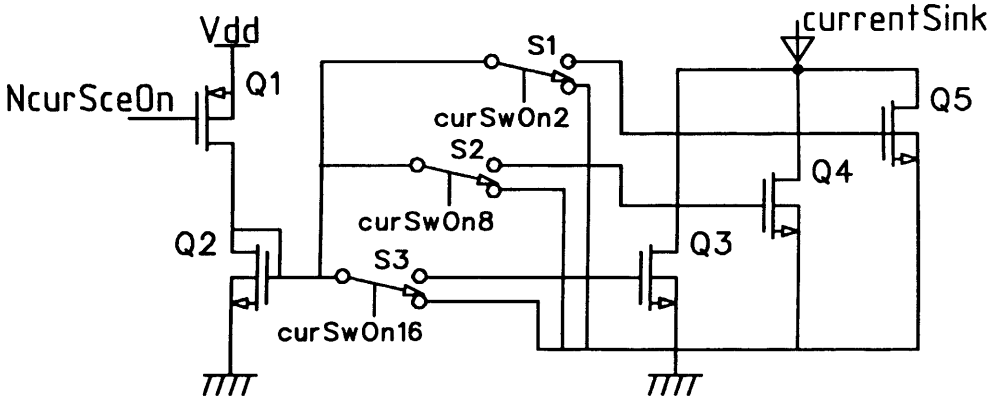

Figure 10.9: Current sink: the mirror side (transistors $Q1$ and $Q2$) is followed by 3 switches to control the three sinking transistors, $Q3$ to $Q5$.

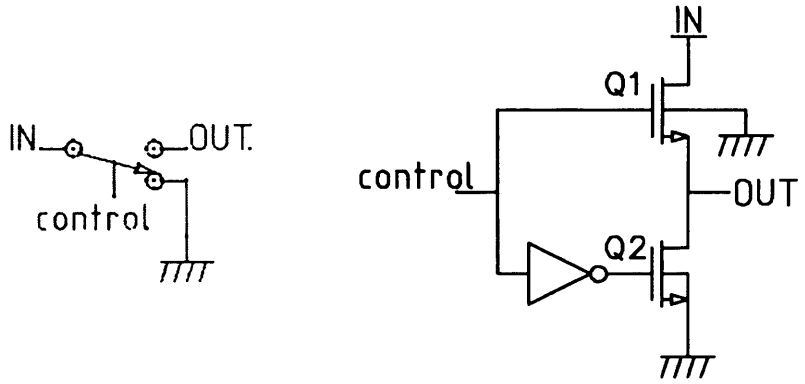

(a) Symbol.

(b) Implementation of the switch with the *control* line.

Figure 10.10: Switch controlling the current mirror, $S1$ to $S3$ in fig. 10.9.

10.1.6.1 Current level selection

The logic driving the current sink receives two kinds of signals: one to turn on the sink, the others to set the current level. The first signal, *NcurSceOn* (not current source on), is low when the sink must be turned on. It is produced by a nor gate grouping the control signals for the 12 channels, turning on any of the channels activates the current

[5] Although the current level was decreased from 32 to 16mA, the label $q32$ is a remnant from the first specification.

sink. The other signals give the current level: *curSwOn2*, *curSwOn8* and *curSwOn32*[6]. They are produced by the logic block *logicCurrent*, see fig. 10.11. The current selection works as follows. A reset level is selected with the external pad, *initial8*. If the pad is high (5V), any reset signal will set the amplitude back to 8mA; otherwise it will be 2mA. For patient safety, it is impossible to reset the current to 16mA as this is a rather high level. In use, the current amplitude can be changed from one train of pulses to an other, from low level (2mA) to intermediate (8mA), from intermediate to high (16mA) and back from high to low. This is done by using longer delays between pulse trains at the *dataIn* input to set the *swCurrentSce* signal. This signal presents a 5V pulse each time the current amplitude needs to be changed. The precise mechanism will be explained in section 10.1.9.

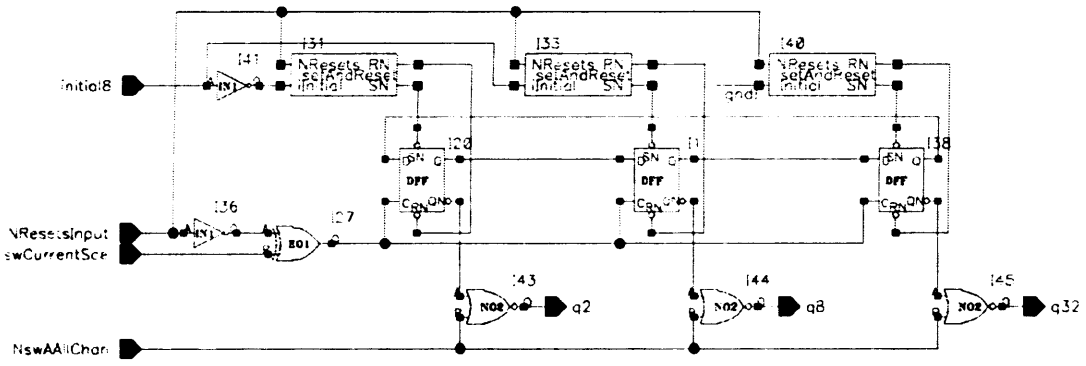

(a) Logic block for the current level control; *q2* goes to input *curSwOn2* of the current sink control, see fig. 10.19(a). Idem for *q8* and *q32* (going to *curSwOn16*).

(b) Set and Reset block., I31, I33 and I40 in (a).

Figure 10.11: Logic block for the control of the current level.

10.1.6.2 Open and short circuits

This IC offers a maximum of 12 independent outputs. Depending on the implant's application 12 or fewer channels may be required and the unused channels will be left open-circuit. Likewise, a cable failure may result in a disconnected channel, or alternatively in a short-circuit across distinct electrodes. The voltage on open-circuit electrodes will swing between 20 and 0V without causing damage to the IC or the implant circuitry. A short between two anodes will create a common anode as is the

[6]These names come from the early stage of chip development, when the specifications were for 2mA, 8mA and 32mA.

case in the LARSI. Both common anode and common cathode situations are undesirable as they will lower the cross-talk levels as explained in chapters 4.1 and 5 yet this is not dangerous. Because the current level is set by the current sink, and therefore independent of the external load (provided saturation does not occur), an undetected short circuit between anodes and cathode will not be damaging either. The implant will probably lose its functionality as the affected channel(s) cease to work but there are no risks of excessive currents.

10.1.7 Demultiplexing logic

From the pulse trains sent by the transmitter, the receiver produces 3 internal signals fed to the demultiplexor: a *clock* signal, a *dataIn* line with a 5V pulse indicating the beginning of each pulse train, and a series of *enable* pulses (a train) giving the duration of activation of each channel. As there are 12 channels, a normal pulse train will contain 12 pulses, present on the *enable* line. It is the role of the demultiplexor to associate one *enable* pulse to each of the channels without altering the pulse width as it gives the time during which the channel must remain active. The principle is simple, there is no addressing, the first pulse is for the first channel, the second pulse for the second channel and so on. To minimise the implant's current consumption, the *clock* line is only active during a train. It has a pulse for each *enable* pulse but is always at least $30\mu s$ longer. There is one extra pulse on the *clock*, called the *sync pulse*, that precedes every train, see fig. 10.12. More information on these signals, produced by the gate-array, and on their timing may be found in Donaldson [1990a].
To control the various switches (anode, cathode and discharge) of the twelve channels, two timing pulses per channel are produced: *swA* and *swB*. The *enable* line gives *swB*, while the *clock* pulses, normally $30\mu s$ wider than the *enable* ones, give *swA*, see again fig. 10.12. Signal *swA* controls the discharge switch and the current sink while *swB*, the ON signal, controls the anode and cathode switches. The delay between *swA* and *swB* will insure that the sink is fully open (and has reached its set current level) before the channel is turned on, and that the anode and cathode switches are completely closed before opening the discharge circuit. This avoids peaks of current from the high voltage rail to the sink during the few nanoseconds it takes to turn on such large transistors.
Figures 10.13 and 10.14 show the simple demultiplexing logic. It is made of 12 similar blocks, one for each channel, containing one D-flipflop for the demultiplexor, and three NOR gates. The series of d-flip-flop forms a simple shift register which is the backbone of the demultiplexor. The *dataIn* signal shifts through this register with every *clock* pulse, one at a time the Q outputs become active for the duration of the *clock* pulse. The NOR gates I29 and I30 generate *swA* and *swB*. The two pulses are timed with the inverted *clock* and *enable* signals respectively.

10.1.7.1 Multiple propagation

A third NOR gate is used after each d-flip-flop to prevent having two pulses propagating along the shift register making two channels active at once. At the start of

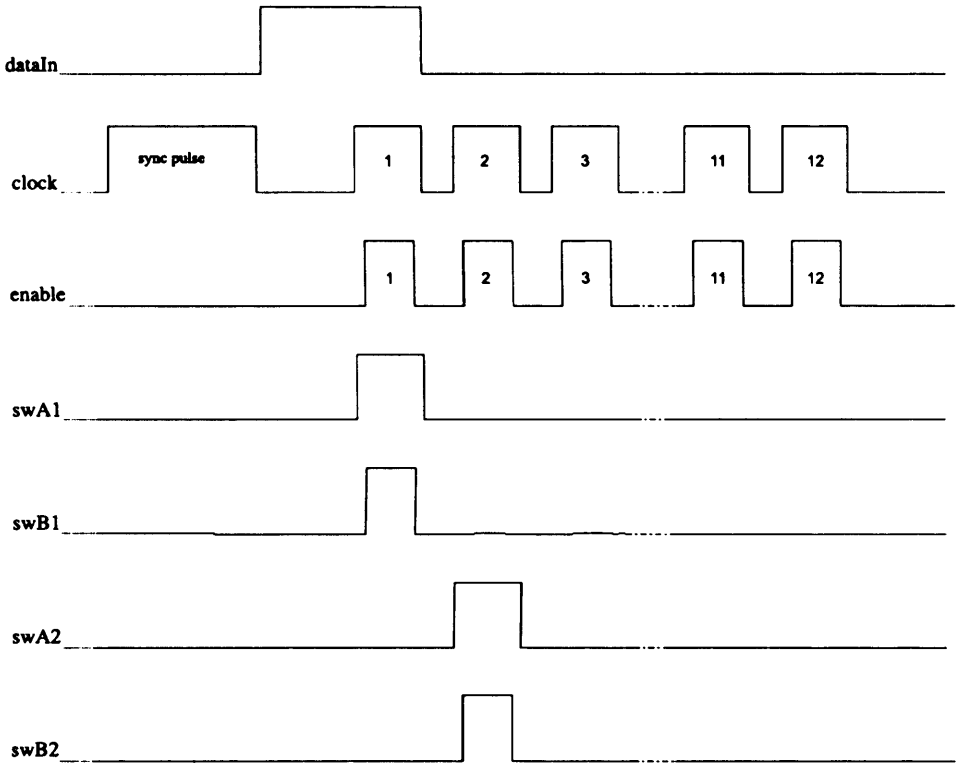

Figure 10.12: Timing signals: normal train, 12 pulses with extra sync pulse on the clock line.

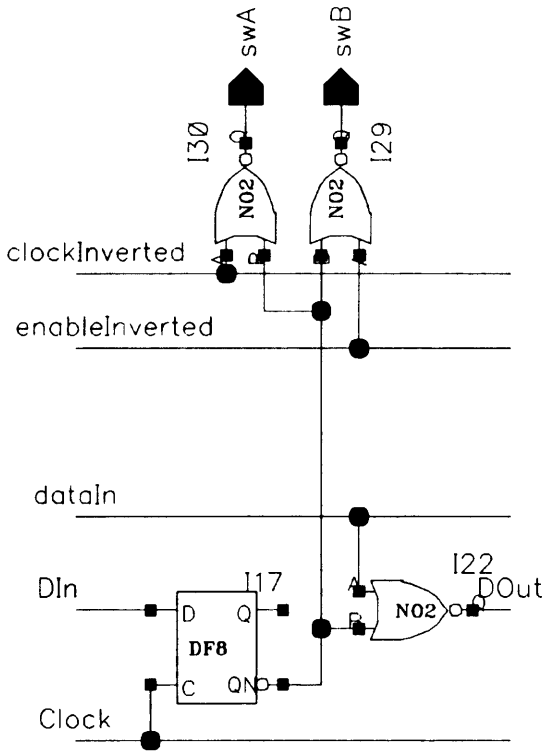

Figure 10.13: One block of the 12 block demultiplexor logic.

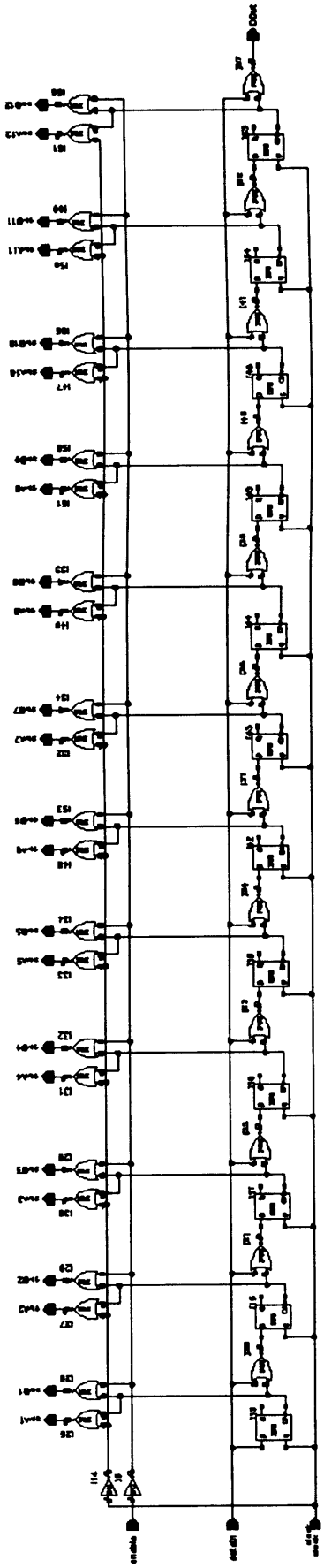

Figure 10.14: Demultiplexor logic.

each pulse train, a positive pulse is present on *dataIn* and enters the first d-flip-flop as *DIn*. It then propagates through the 12 D-flip-flops, from one *DOut* to the next *DIn*. If, following some improper operations, a second pulse appears on *dataIn* before the previous train has completed its 12-channel cycle, the *dataIn* line, common input to all anti-propagation NOR gates, will be high, stopping the propagation of the previous pulse. In this way, any new incoming pulse is bound to be the only one propagating through the demultiplexor. This improvement was already suggested by Krabbendam in the following quote.

> "To prevent the system from improper use (the second objective in the research definition), 'AND-gates' are placed between the SR-cells. As soon as data1 becomes high the inverter makes the input for all 'AND-gates' low and all SR-cells will "clock in" a low, except the first SR-cell. Therefore it will not occur that more than one channel is being stimulated. Actually, in the real design, the 'AND-gates' are replaced by 'NOR-gates', since the later are standard digital cells. This adjustment in design will be done with finally no effect in the operation of the de-multiplexer, as described above."

10.1.8 Control of the current amplitude: resets and current level switches

10.1.8.1 Reset

The reset function returns the current amplitude to a known value determined by the *initial8* input pin: 2mA if the pin is grounded, 8mA if it is high. Both a hardware and a software resets are implemented. The hard-reset, controlled with *NResetIn* pin, is used at power-on. The pin is connected to an external RC circuit between the 5V line and ground. The time constant ensures that the *NResetin* input remains low while the high voltage is settling. The soft-reset is generated while in use, at the start of every stimulation session to reset the previous settings and begin with a known level which may then be changed to the required amplitude.

10.1.8.2 Current level switch

Changing the current amplitude internally requires either a soft-reset pulse or a *swCurrentSce* (= Switch Current Source to the next current level) pulse. A pulse on the *swCurrentSce* line causes the amplitude to change to the next level: from 2mA to 8mA, from 8mA to 16mA and back from 16mA to 2mA.

10.1.9 Special pulse timing for reset and current level changes

10.1.9.1 Single letter generation

The gate array only produces three signals (*clock*, *enable* and *dataIn*), so, to limit the changes needed to build the new implant, the new IC should only use these three inputs. The two extra internal pulses previously introduced (soft reset and current source shift) must therefore be produced as the result of some specific input sequence.

As seen on fig. 10.12, the *datain* line is high with the second *clock* pulse of a train (after the sync pulse). As there are 13 *clock* pulses in a regular train, the *dataIn* line is normally high once every 13 *clock* pulses. Figure 10.15 is a schematic drawing of the logic block responsible for decoding the time delays and generating the soft-reset and *swCurrentSce* signals. The logic block producing the soft-reset and *swCurrentSce* pulses "counts" the number of *clock* pulses between two successive *dataIn* pulses and generate internal signals (*A*, *B*, *C* and *D*), see also the flow diagram of fig. 10.16. More precisely, a 14-pulses delay will cause a pulse on line *B*, 15 pulses give *C* and 16 give *D*, while line *A* is high for every gap of 13 or more pulses (i.e. for every non-aborted train). Looking at the schematic drawing of figure 10.15, the D-flip-flops (I1, I25, I0[7], I26, I27, I4, I5 and I3) act again as a shift register to count the *clock* pulses. The three logic gates I6, I7 and I8 combine signal *A* with each of three lines counting 14, 15 or 16 pulses. Any non-aborted train creates a pulse on line *A*. That pulse then propagates through the D-flip-flops and will be present at the input of gate I6 after an extra 14 pulses, gate I7 after 15 pulses and gate I8 after 16 pulses. Because of these NOR gates, to create letters *B* to *D*, the longer train must be followed by another train, long enough to cause another *A* pulse.

10.1.9.2 Code generation for reset and current level change

If a succession of long trains is sent to the demultiplexor, it will appear as a succession of letters, for example 13-15-14-13 translates through these extra logic gates as "*A-C-B-A*" where the last two letters, *B* and *A* appear together. If the last 13 pulses are not sent, there will be no pulse on line *A* hence no *B* pulse either. Two groups of three D-flip-flops: (I10, I11 and I12; and I18, I19 and I20 on fig. 10.15) register the occurrence of these letters. If the pulse-trains form *C-C-D-A*, a *swCurrentSce* pulse will be produced (this is NOT represented on the flow diagram of fig. 10.16, which was limited to the generation of individual letters). Similarly, the soft-reset is coded *B-B-D-A*, this signal is then combined in gate I22 with the hard-reset line to produce the global reset signal. The letters must be generated by successive trains since the D-flip-flops are clocked by the *A* line. Combinations like *C-nothing-C* or *C-D-C* for example will not be interpreted as two following *Cs*. This confers robustness against accidental glitches as explained in section 10.1.9.3. It is important to insist that an *A* must occur after any long train to cause a pulse on *B*, *C* or *D*. The code *C-C-D-A* represents the number of clock pulses between two successive *dataIn* pulse, it does not represent the timing of the pulses appearance (see fig. 10.17). Figure 10.17 shows a *swCurrentSce* pulse produced after a series of trains of 13, 14, 14, 15, 14 successively. This plot is the result of a simulation realised with the IC design tool Cadence, the first *dataIn* pulse is not visible since it is too close to the y axis.

[7] I25 and I0 are blocks of five D-flip-flops in series.

10.1.9.3 Why not just *A* or *B*?

To avoid unexpected resets or current amplitude changes, the codes must not be too brief or repetitive (multiple letters might occur as the result of a consistent transmission or control failure). Yet codes must remain short enough to limit the delay between the decision of changing the current and the actual change. A code length of four letters was considered a good compromise between signal complexity and time delay. For a typical stimulation frequency of 20 Hz per channel, the delay is 200ms (4*50ms), corresponding to 4 pulse-trains. This delay may be reduced by increasing the frequency. The shortest possible trains have a 3ms period (for more details on this estimate please refer to Donaldson [1990a]), giving a minimum current-change delay of 12ms.

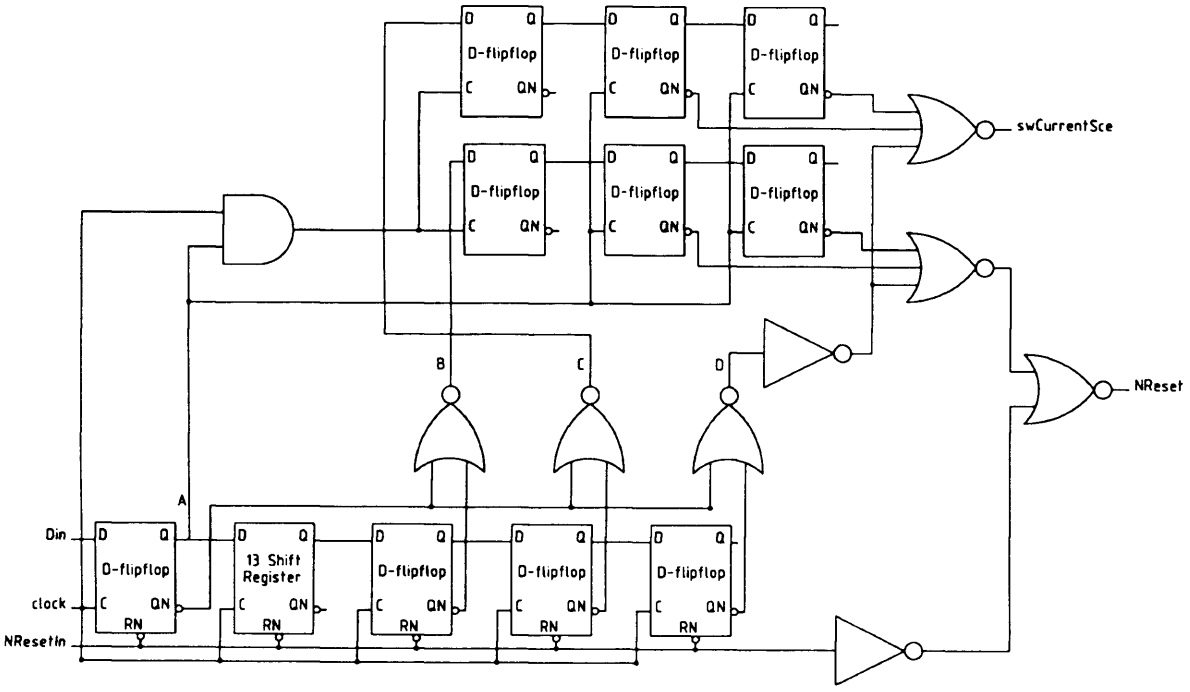

Figure 10.15: Logic block for the current level changes.

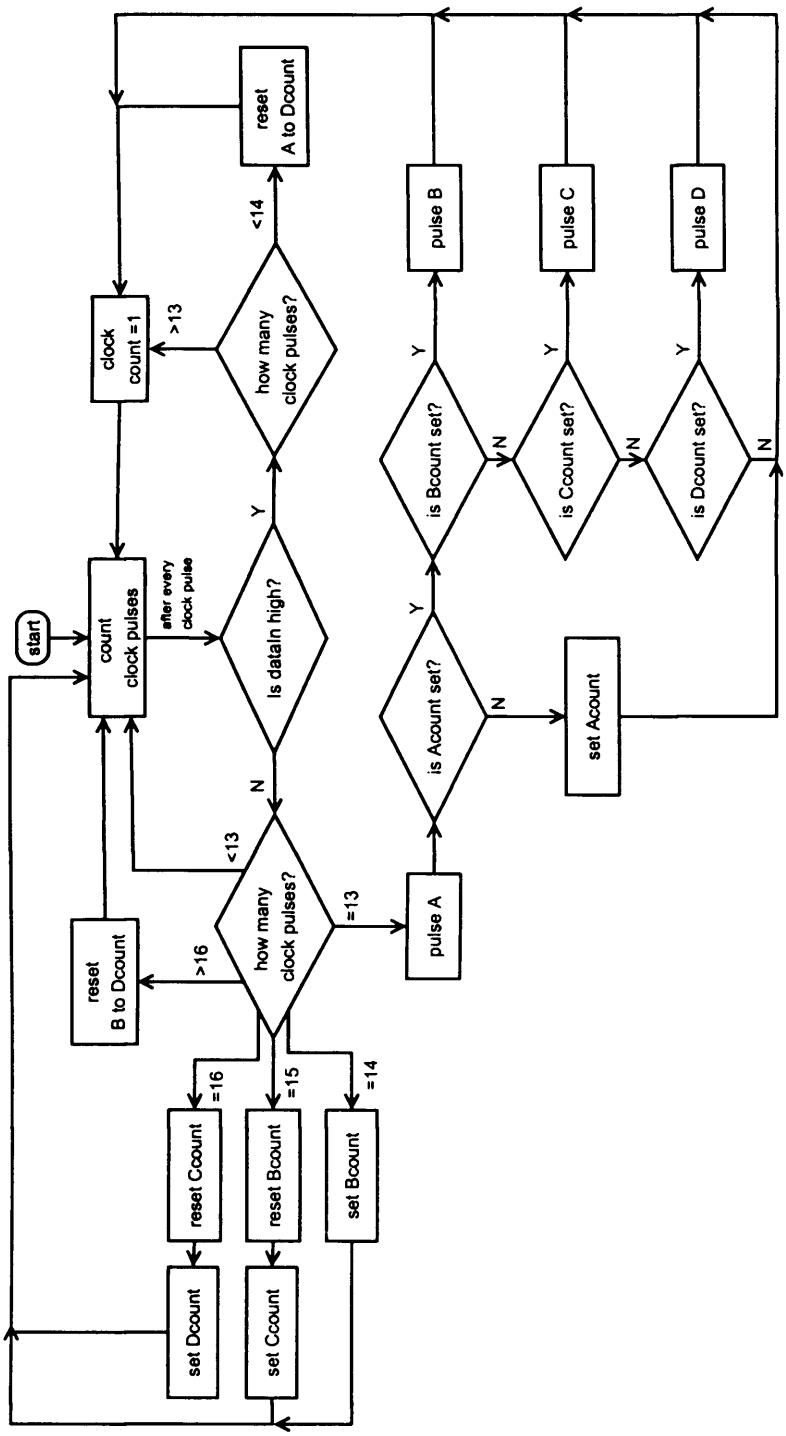

Figure 10.16: Flow diagram for the generation of internal signals *A*, *B*, *C* and *D*.

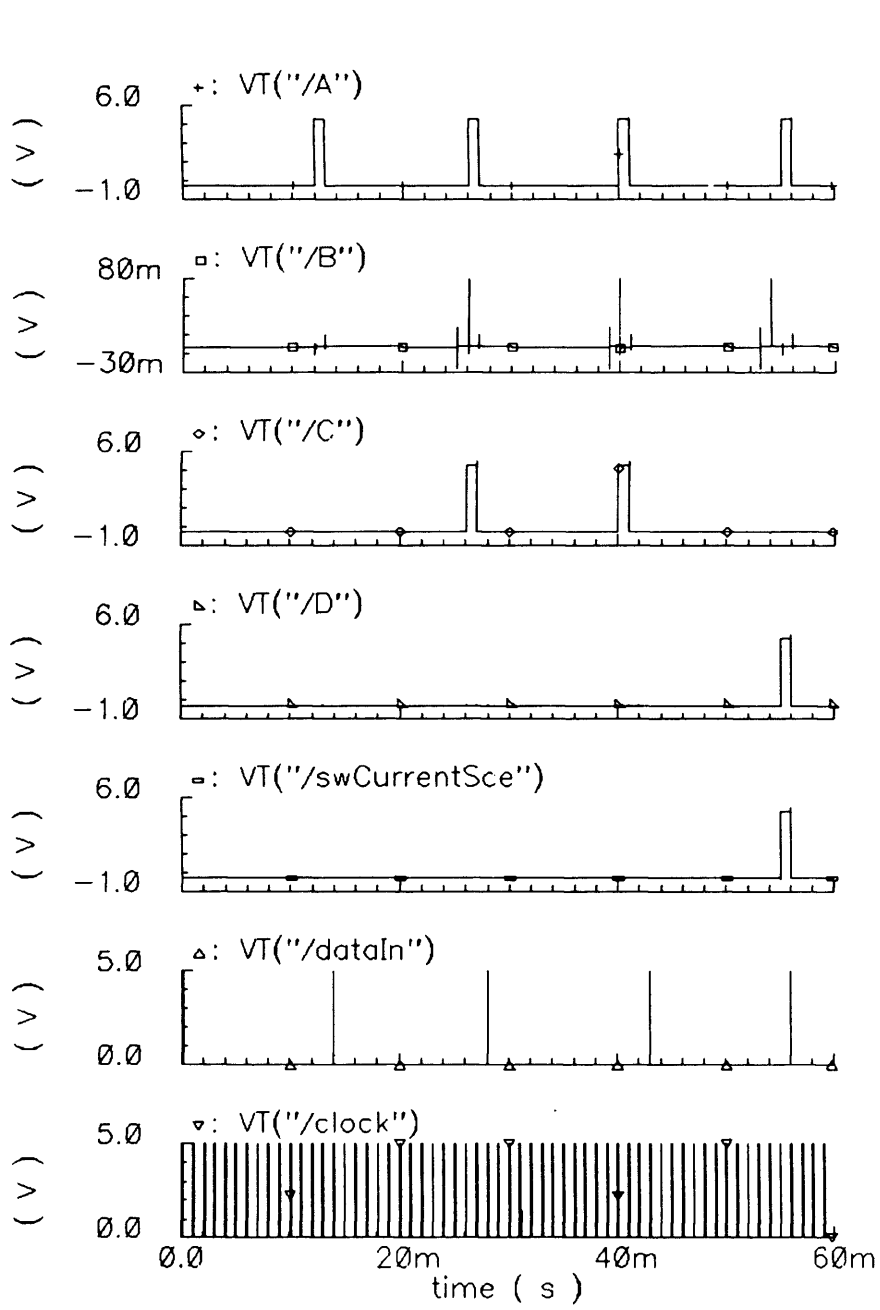

Figure 10.17: Logic lines during the production of one *swCurrentSce* pulse. Pulses on *dataIn* at the following instants, measured in clock cycles: 0, 14, 28, 43 and 56; intervals of 14, 14, 15 and 13 pulses.

10.2 Label list

Table 10.3: IC pin numbers and labels used in this section.

Category	Label	comment	pin number
Supply	gnd	digital 0V line	26
	gndA	analogue 0V line	27
	Qgnd	quiet 0V line	15
	vdd	digital high voltage, 5V	25
	VDDH	analogue high voltage (max 50V)	29
Logic input	clock	clock line	18
	dataIn	one pulse per pulse-train	17
	enable	multiplexed input	16
Logic outputs	A	represent a train of more than 12 clock cycles on *dataIn*	24
	B	train of 13 clock cycles on *dataIn*	23
	C	train of 14 clock cycles on *dataIn*	22
	D	train of 15 clock cycles on *dataIn*	21
Other	NResetIn	external reset, active low	19
	initial8	current choice, high for 9mA, low for 3mA	20
	V20V	output of regulator, should be 20 V	6
	anV	voltage at the anode connection of a channel	NA
	Icheck	connect to the current sink	34

Analogue connection	A1	anode channel 1	13
	C1	cathode channel 1	14
	A2	anode channel 2	11
	C2	cathode channel 2	12
	A3	anode channel 3	9
	C3	cathode channel 3	10
	A4	anode channel 4	8
	C4	cathode channel 4	7
	A5	anode channel 5	4
	C5	cathode channel 5	5
	A6	anode channel 6	2
	C6	cathode channel 6	3
	A7	anode channel 7	40
	C7	cathode channel 7	1
	A8	anode channel 8	39
	C8	cathode channel 8	38
	A9	anode channel 9	37
	C9	cathode channel 9	36
	A10	anode channel 10	33
	C10	cathode channel 10	35
	A11	anode channel 11	32
	C11	cathode channel 11	31
	A12	anode channel 12	30
	C12	cathode channel 12	29

10.3 Tests

The IC was first tested alone to evaluate how it met the specification, the results of these tests are presented in this section. A simple assembly program running in a Motorola M68HC11 (the micro-processor used in the LARSI control box) was written to produce the desired trains of pulses. The chip was then included in a bench version (discrete components) of the new implant and the performances of the complete system were studied. Understanding this second set of results requires a reasonable knowledge of the complete SLARSI circuit. This is beyond the scope of this thesis and the "lash up" results have not been included in this last chapter.

10.3.1 Testing the built-in voltage regulator

Connections:

- 0V to both grounds (analog and digital),
- 5V to *vdd*,
- a variable voltage source to the high voltage input *VDDH*,
- a $4.7\mu F$ capacitor between regulator output and ground unless otherwise stated.

10.3.1.1 Sweep variation of *VDDH*, from 17V to 30V

Output floating: 1MHz saw-tooth oscillations, 0.8V peak to peak, mean around 20.1V
Output with $4.7\mu F$ to ground: *V20V* steady at 19.96V for *VDDH* at 20V and above, see fig. 10.18.

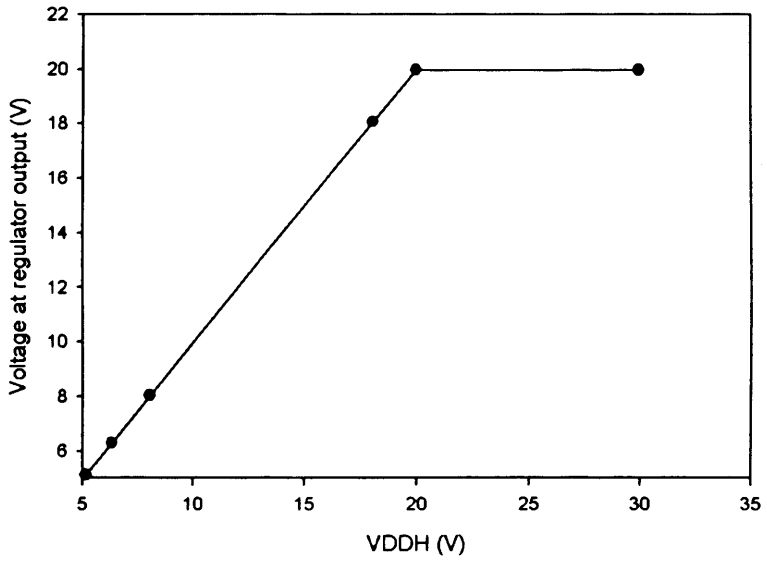

Figure 10.18: Output of the voltage regulator as a function of its input voltage.

10.3.1.2 Current driven into an external resistor, constant $VDDH$

With external $4.7\mu F$ capacitor and $VDDH = 30.2V$:

2mA : *V20V* = 19.95V

8mA : *V20V* = 19.93V

16mA : *V20V* = 19.92V

Without external capacitor and $VDDH$ at $25V$:

Output giving 3mA in an external resistor:

2MHz sinusoidal oscillations, 3V peak to peak, mean approximately 20.4V.

Output giving 8mA in an external resistor:

2.4MHz sinusoidal oscillations, 3.3V peak to peak, mean approximately 19.7V.

Output giving 16mA in an external resistor:

3MHz sinusoidal oscillations, 3.6V peak to peak, mean approximately 19.2V.

10.3.2 Testing the current sink

Connections:

- 0V to both grounds,
- 5V to *vdd* and *clock*,
- *initial8* once grounded (2mA nominal current), once at 5V (8mA nominal current),
- controlled 5V pulses on *dataIn* and *enable*.
- Either a voltage source in series with an ammeter connected to the *Icheck* pad,
- or a variable resistor connected between the anode and cathode output in series with an ammeter.

Two very similar tests were performed. In the first, an external voltage was applied at the sink input and the current was recorded. In the second test the current sink was tested in series with the channel, a variable resistor connected between the anode and cathode connection was used to simulate a load. There should be no noticeable difference whether the current flowing to the sink is supplied externally or internally. During the first experiments, the channels must not be activated, *V20V* is left floating and *VDDH* is around 20V to avoid reverse-biased voltage, only the current sink is used, sinking an external current [8]. Figure 10.19(a) shows the current taken by the sink as a function of the drain (or *Icheck*) voltage for three nominal current settings: 2mA, 8mA and 16mA. Allowing for a 10% variation of the set level, the nominal current is reached from 1.5V for settings 2 and 8mA, and from 1.9V for the higher current setting. The specifications required that the sink should be able to drive the nominal current when the available voltage was reduced down to 2V.

[8] The logic system is designed so that the current sink is only active while *clock* is high and a *dataIn* signal is present at the corresponding input to produce a *swA* signal.

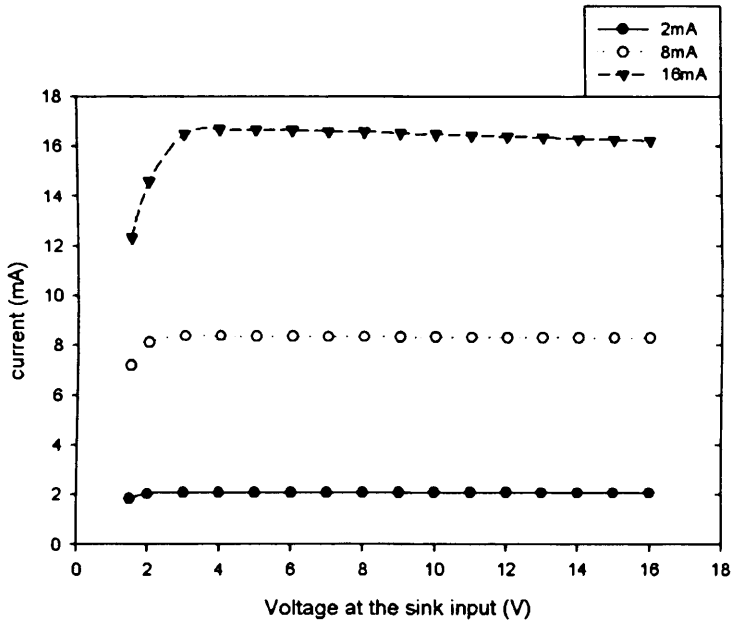

(a) External current drawn by the sink as a function of the drain voltage (voltage applied at the sink input).

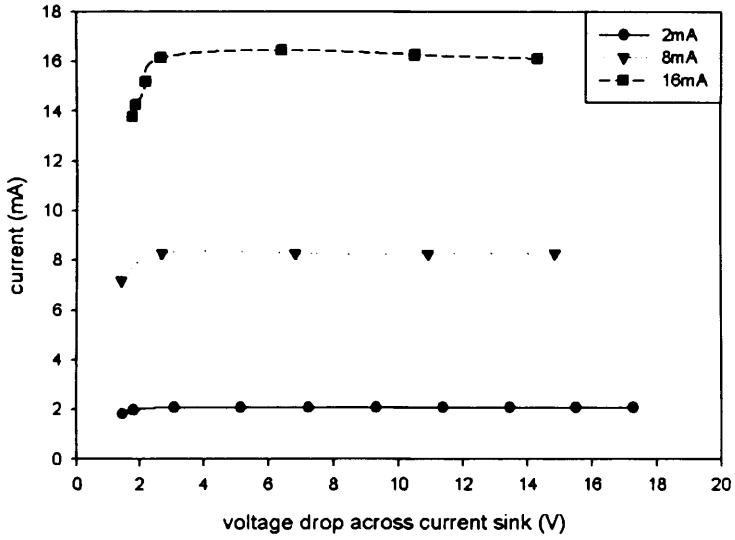

(b) Voltage drop across the sink for three current settings, current flowing through the switches of one channel and an external load resistor.

Figure 10.19: Current sink performances.

For the second test a variable resistor was connected between the anode and cathode output, and the current was monitored while the load resistance was increased until saturation. The results are plotted in fig. 10.19(b). According to the specifications the nominal current level must be set $\pm 10\%$, taking the nominal level -10% as the limit for saturation, the current sink does match the 2V limit: it delivers 1.8mA for a drop of 1.4V or more, 7.2mA for 1.5V or more and 14.4mA for 1.9V or more. As the current is set by a mirror source, all three levels depend on the voltages on the "original side" (see $Q1$ and $Q2$ in fig. 10.9). Small variations of Vdd have noticeable consequences on the current driven by the sink. Once again taking a $\pm 10\%$ variation limit for the current level, Vdd should not drop below 4.7V; the upper limit was not evaluated as it is unlikely that the voltage should rise above its normal 5V value.

10.3.3 Testing the switches

Each of the following tests were performed on at least two of the 12 channels, selected randomly. The results presented are expected to be typical of any channel.
Connections:

- 0V to both grounds,
- 5V to *vdd* and *clock*,
- *initial8* once grounded (2mA nominal current), once at 5V (8mA nominal current),
- controlled 5V pulses on *dataIn* and *enable*,
- $4.7\mu F$ at the $V20V$ line for the voltage regulator,
- a variable resistor between the anode and cathode outputs.

To test the minimum voltage drop across the switches the value of the external resistor between the cathode and anode is increased while monitoring the voltages across two switches, see fig. 10.21(a). The switches are mos transistors (see fig. 10.2), $Q1$, the anode switch, is a p-channel while $Q3$, the cathode switch is an n-channel. The discharge switch $Q2$ was open at all time. The drop allowed in the specifications is 1.2V for both switches together. The results plotted in fig. 10.20 show that the specifications are met.

10.3.4 Discharge path resistance

Connections: same settings as when testing the switches.
The resistance of the discharge path (p-channel transistor in series with a polysilicon resistor, see fig. 10.2) depends on the anode and cathode voltages as these set the gate-drain and gate-source voltages of the discharge p-channel transistor. A voltage source (Vc) was connected to either terminal via a $1M\Omega$ resistor while the anode-cathode resistance was measured, see fig. 10.21(b) showing the test circuit when the cathode voltage is set. For a cathode voltage ranging from 1 to 18V, the switch on resistance goes

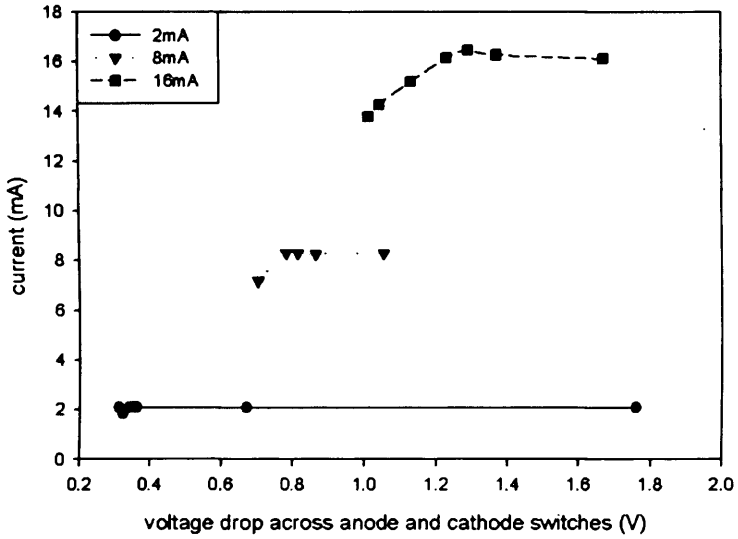

Figure 10.20: Voltage drop across the anode and cathode switches for the three current settings.

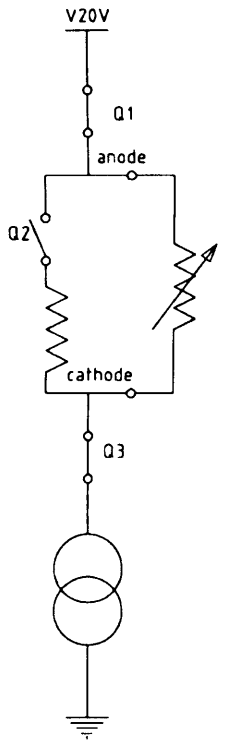

(a) Testing the anode and cathode switches with a variable resistor.

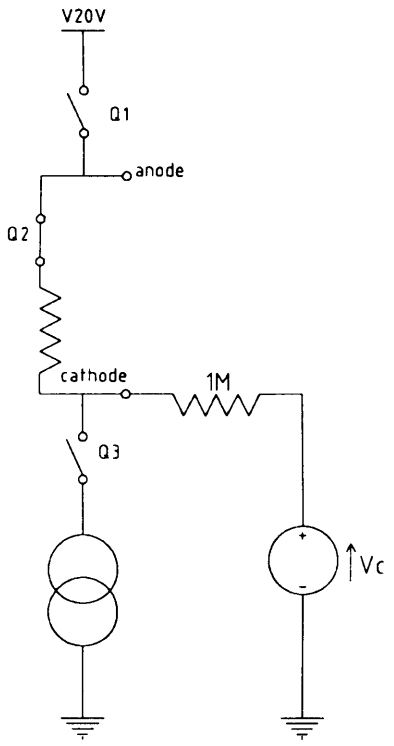

(b) Setting the cathode voltage to test the discharge switch.

Figure 10.21: Testing the switches.

from $1.5M\Omega$ down to $2.12k\Omega$. For an anodal voltage ranging from 1.55 to 18V, the resistance goes from $16.25M\Omega$ down to $2.1k\Omega$, see figure 10.22. Practically the anode and cathode voltages are undefined during the discharge phase. They are influenced by the leakage current of $Q1$ and $Q3$ as well as the voltages on other, neighbouring, electrodes. When both voltages are below 2V the discharge resistance rises above $2k\Omega$ and the charge passed during stimulation will not be exhausted during the discharge phase. The residual voltage across the external blocking capacitor will then rise, increasing the anode voltage and decreasing the discharge resistance [9].

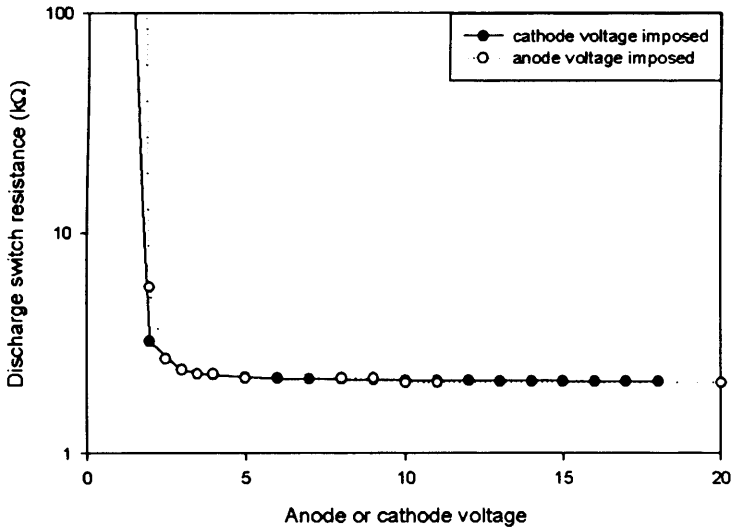

Figure 10.22: On-resistance of the discharge path as a function of the voltage applied at one terminal (via $1M\Omega$), the other left floating.

10.3.5 Testing the logic block

Connections:

- 0V to both grounds,
- 5V for *vdd*,
- *initial8* once grounded, once at 5V,
- anodes and cathodes connected in pairs using a set of 620Ω resistors.
- sets of 5V pulses for *clock*, *dataIn* [10].

Despite enclosing the discrete components test version of the implant in a metal box, the logic lines were very sensitive to interferences and glitches. Ferrite rings around the

[9] This reasoning assumes that the cathode voltage does not become negative.

[10] *dataIn* must be high on the rising edge of the reference clock pulse, counted as number one (after the sync. pulse).

cables linking the implant to the receiver solved the problem and the following results are given for de-glitched signals. To set the logic in a known state before each test, a reset was caused by pulling the reset pin down (active low).

a. trains of 12 pulses.
   1st train nothing,
   2nd train A appears from the rising edge of *clock0* until the next *clock* pulse.
b. trains of 13 pulses.
   A & B present from the rising edge of the 13th pulse until the rising edge of the *clock0* pulse.
c. trains of 14 pulses.
   A & C present from the rising edge of the 13th pulse until the rising edge of the 14th pulse.
d. trains of 15 pulses.
   A & D present from the rising edge of the 13th pulse until the rising edge of the *clock0* pulse.
e. shorter train: train of 11 pulses followed by normal 12 pulses train.
   1st train, nothing,
   2nd train, still nothing,
   3rd and following trains, A appears as in test a.
f. Normal conditions, does the shift register clear?
   Send 9 trains, some with 2 *dataIn* pulses.
   OK, no A nor B pulses produced after aborted trains.
g. *SwCurrentSce* pattern CCDA.
   Continuous operations, send 100 times a CCDA pattern,
   100 current changes counted.
h. *SoftReset* pattern BBDA.
   As in point h., 100 BBDA gave 100 resets.
i. Risks of unexpected current changes?
   Run implant for 15 minutes monitoring the logic lines *B, C* and *D*.
   No pulses.

All nine tests show the expected behaviour, the logic block of the IC meets the specifications.

10.3.6 Testing the channels

Connections:

- 0V to both grounds,
- 23V for *VDDH*,
- 5V for *vdd*,
- once grounded, once 5V for *initial8*,
- sets of pulses for *enable*, *clock* and *dataIn*,

- external capacitor of $4.7\mu F$ on *V20V*.

These tests were carried out to check the overall performances of the output stages. During experiments a and b, the voltage across the load resistor was monitored using differential scope probes to estimate the current passing through the channel and compare it with the set level.

a. Simple resistive load
   Connect one external 620Ω resistor between each pair of cathode and anode.
b. RC load
   Connect an external $4.7\mu F$ capacitor in series with the resistor.
c. RC load with common connection.
   A saline bath is used, with platinum electrodes in series with $4.7\mu F$ blocking capacitors on the cathode side.

For the resistive and capacitive values selected in these experiments the current levels were within 10% of their nominal value. This was deemed in accordance with the specifications. The experiments a. and b. were successful, no graphs were recorded as there were no particular events to report. Saturation did however occur in experiment c. at high current level as seen on fig. 10.23. As the load is capacitive the voltage across it should rise linearily during the constant current pulse. At 16mA with long 1ms pulses the voltage drop across the load as the capacitor charges become too high to allow the switches and sink to drive the full nominal current. The output stage saturates and the current decreases progressively, the maximum charge before saturation is estimated at $4\mu C$.

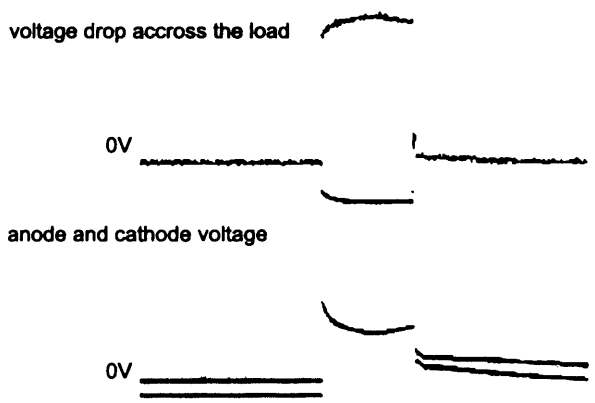

Figure 10.23: Output stage saturation: the two lower traces show the anode and cathode voltages while the top trace is the difference between them (all 5V/square), giving the voltage drop across the load (including a capacitance) and showing saturation. The 0V indications were added on the oscilloscope screen shot as the ground references for the three traces are not centered on the midline. The load voltage becomes negative after the pulse (1ms width) as the current flows from the capacitance to the discharge circuit.

10.4 Integrated Circuit failures

Four integrated circuits of a first version of the output stage failed during the tests. The failure occurred after hours of continuous use and probably following a static discharge. The first possible cause envisaged was that of the temperature, and the following experiment was performed, on a fully working IC, version 1. All schematics and test results presented throughout this chapter relate to the second version of the output stage.

10.4.0.1 Temperature as a function of power dissipation

Power: $I_{reg} * VDDH$ where I_{reg} was swept from 1 to 35mA and $VDDH$ swept between 20.9 and 30.07V.
Room temperature: $22°C$, temperature of the IC estimated using the current variation of an output diode ($I = I_0 * (e^{+\frac{eV}{kT}} - 1)$). The results are shown on fig. 10.4.0.1, for lower temperatures intervals of 3 minutes between readings allowed the temperature to settle, as the temperature did not stabilise so quickly this delay was increased to 5 then 10 minutes for the higher temperatures. The short stabilisation period of the early points may explain the non-linearity of the curve. The maximum power dissipation in use is given by the current level (max 16mA) and the input voltage to the IC which is limited by a 39V zener diode. At 624mW the temperature of the IC had just reached $35°C$ and it is unlikely that an excessive temperature alone could have been the cause of failure.

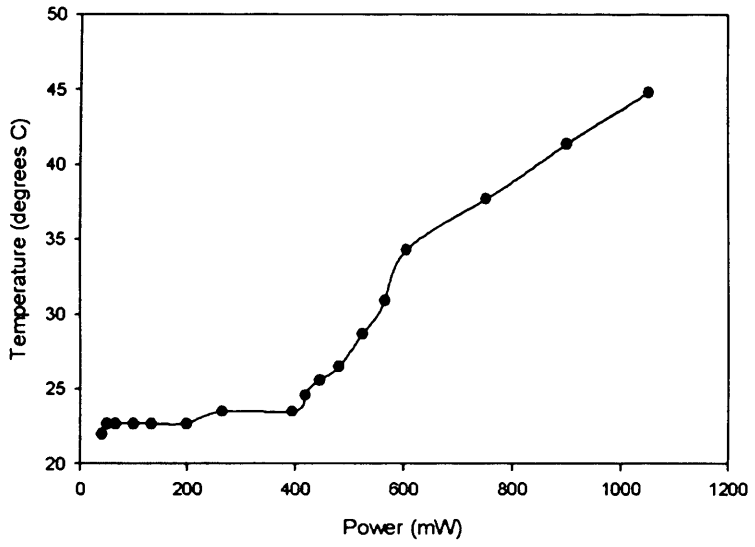

Figure 10.24: Temperature of the chip as a function of the power dissipated in the voltage regulator.

10.4.0.2 Layout weaknesses

Since excessive temperature had been ruled out as a primary cause of failure, the layout was analysed and two other possible sources of failure were identified: a long and thin (dimensions within the limits set by the foundry) track leaving the 20V regulator to the *V20V* pin and the lack of pdiffusion zones connecting the p-substrate to the quiet ground. Improving these points required a re-layout of the voltage regulator and a general review of the p-substrate.

10.4.0.3 Other alterations

Since a new integrated circuit had to be produced to implement the changes discussed above, alterations to the current source and the discharge path were included in the new layout (version 2).

Current source:

The dimensions of some of the transistors were increased to avoid working with minimum track widths, excessive length or tight ratios. This was expected, and later verified (see fig. 10.19), to give flatter current characteristics.

Discharge path:

The discharge resistor was introduced to keep the resistance of the discharge path constant when the load voltage varies. In the first version there was only a pmos transistor and the on-resistance fell below $1k\Omega$ for large load voltage, increasing the risks of stimulation by discharge overshoot (see section 10.1.5).

Minor changes:

Minor alterations of the cathode switch control (block of four transistors shown on fig. 10.7(b)) and to the pattern finding logic (fig. 10.15) were also implemented since a new integrated circuit had to be produced.

10.5 Integrated Circuit conclusion

Integrated circuits with the second version of the layout meet the specifications.

Part IV

Discussion

Chapter 11

Thesis discussion

The idea that electricity could be used to control a man's organs and muscles may be traced as far back as 1818 and Mary Shelley's Frankenstein. It took more than 100 years of research work after the publication of this pure fiction for the first realistic concept of electrical stimulation to appear on scientific scene as, in 1936, Gersuni and Volokhov presented their ideas for an hearing aid. In the years following the second world war there was a growing interest in electrical stimulation and this lead to the development of other organ controllers like the phrenic nerve stimulator and the pacemaker. These early devices were unconditional stimulators, without any sensor inputs and were therefore unresponsive to the state or activity of the patient. Much of the work then was concerned with reliability, biocompatibility and miniaturisation as they aimed to develop fully implantable stimulators and electrodes. Knowledge of material sciences and electrochemistry quickly became as important as good electronic design. In the early 1960s the emphasis was shifted towards functionality with the development of limb stimulators. Since Kantrowitz, Vudovnik and Reswick demonstrated the efficacy of their FES stimulators on paraplegic patients many researchers have followed in their steps. Apart for the hearing aid who took many years of refinement before becoming truly useful, the operations performed by organ stimulators are simple (on-off), often periodical, hence requiring only basic stimulation strategies. FES requires much more complex stimulation strategies. The user's intentions must be integrated, as well as the movements of the rest of the body (e.g. weight shifts in standing and walking applications). Selectivity is essential to elicit functional movements and a sensitive stimulation level adjustment is also critical to obtain smooth contractions adapted to the task considered. The last two points were not real issues for organ controllers. They only became critical with the advent of limb stimulators, for legs especially, and much work went into tackling them.

One question that arose during those early years and seems unlikely to ever receive a definite answer as it is so application dependent is: how to supply the electrical pulses to the nervous structures? As discussed in chapter 3, various groups followed different approaches. At first, surface electrodes were used with success, especially for applications involving a limited set of muscles, and ideally targeting patients who retained

the use of their upper limbs and hands as this made the electrode placement easier. One such application still enjoying a growing success is the dropped foot stimulator which simply targets the anterior tibial muscle, hence requiring only a single pair of electrodes on the leg. Further, the user's interaction, inherent to the concept of FES, is here provided automatically by a "heel switch" sensing when the foot is lifted off the floor, hence when the stimulation is required. The use of surface electrodes for upper limbs applications was restricted by the fact that the recipients often lacked sufficient dexterity, due to their disability, to place them properly. Carers too may find it a tedious process, or simply not be present enough to place the electrodes when needed (a permanent carer might render the stimulator less interesting for the patient to use). Further, and this is even more of an issue for leg stimulation, the number of electrodes required to gain a reasonable control of the limb is too high (typically 4 sites, i.e. 8 electrodes, on the leg) and the surface electrodes are less convenient for everyday applications. Beside the tedious placement, the wires restrain the freedom of movement of the user. This become a serious disadvantage once the patients attempts to use the system out of the laboratory environment.

The obvious solution to the placement issue is to implant the electrodes. The wires may also be implanted, solving the dangling cables problem, but this requires an implantable stimulator. If this is not possible, the wires are percutaneous, they are brought through the skin to be connected to an external stimulator. This approach is successful as far as selective and repetitive stimulation goes. Unfortunately it raises serious health issues as the skin at the wire exit points is subject to repeated infections and quick deterioration. The other alternative, a fully implanted stimulation system (with external control box for user interaction and a percutaneous RF communication link) does not suffer from such a drawback. Yet, the reliability of the cables passing across the joints (hip and knee or elbow and shoulder) and submitted to various crushing pressures (due to patient's falls, seating, resting position or other activities) is limited and failures are not easily localised and repaired. Another disadvantage of implanted peripheral nerve electrode is that muscle specificity is acquired at the cost of extensive surgery, with associated bed rest, risks of pressure sores and scar infections.

To tackle this last issue, selective electrodes have in the last few years been developed which are implanted higher on the nerve, when it still contains fascicules before they divide to innervate various muscles. This idea has been pushed even further with the development of electrodes that interact with small groups of axons for even better selectivity or for improved fatigue performance. A single electrode may then be used to activate a selection of muscles depending on the stimulus sent. While the theory is promising, there are practical problems to solve, mainly related to nerve damage. Since they aim to act on separate groups of axons (or fascicules), individual electrodes must be brought near them by reshaping, restricting or penetrating the whole nerve, and this obviously compromises its integrity. Example of such electrodes include sieve

electrodes (need to cut the nerve and have it regrow through the sieve), penetrating electrodes (arrays of pins with individual contacts at their tips which are pushed into the nerve) and reshaping electrodes (the nerve is flattened with the hope that the individual contacts then come in the vicinity of different fascicules). A lot of research work is being invested in this area as selectivity is a key to the development of the next generation of functional stimulators. Yet, so far, selective electrodes have not been tested in patients and are unlikely to be unless animal results improve.

Another option for implantable stimulators and electrodes is nerve root stimulation. It answers all but one of the issues raised above. The surgical field is limited to the cauda equina and there are no joints to cross as the stimulator may be conveniently implanted under the ribs. The method is reliable, it has been in use for more than 20 years now with the Sacral Anterior Root Stimulator Implant for bladder and bowel management. Throughout these two decades, it has shown its potential, mainly for paraplegic patients, because it is practical, realistic in terms of implant development, surgery, setup complexity, daily use and maintenance. Further, as the surgical field is limited to the cauda equina, various applications may be combined onto a single device to increase the patient's expected benefits while still requiring only one operation. Here too there has been attempts at selective stimulation using penetrating electrodes (in the spinal cord) but again, poor animal results have so far held up progress.

Despite the success of the SARSI and the potential of nerve root stimulation in general, experience acquired with the LARSI has shown that there is a limiting phenomenon which may affect all root stimulation applications (and by extension many peripheral nerve applications too): cross-talk. It is the unwanted activation of one nerve or nerve root lying in the vicinity of an active electrode. This leads to co-contraction of undesired muscles, sometimes antagonist. If cross-talk is eliminated, finer muscle selectivity should be achieved and lower limb applications will be expended, then limited only by technological development and, probably more so, by setup complexity and daily use considerations.

The main outcome of this thesis is the development of a stimulator output stage that guarantees cross-talk free stimulation up to a very high level. Globally, the work is justified, even required, by an analysis of LARSI results recorded over many years and showing the limitations, lack of selectivity, due to the occurrence of cross-talk activation of antagonist or unrequired muscle groups. The development of this integrated circuit rests on the results of in vitro experiments investigating the mechanisms behind cross-talk activation, with a focus on current spread. These experiments offer an unequivocal demonstration that the "common anode" stimulation method causes cross-talk activation at surprisingly low stimulation level. The LARSI (common anode) situation is compared to the proposed independent channels method implemented for the new output stage and the results show a clear increase (of a factor 50 or more) of the cross-talk stimulation level. Another, slightly unexpected, result was the influ-

ence of the imbalance (how unequally the current is shared between the two anodes of a tripolar electrode) on the cross-talk ratio. For a near tripolar arrangement, the ratio is expected to climb above 100. The experiments further clarify the concept of virtual stimulation and highlight the importance of current concentration for nerve stimulation.

These findings are not only relevant for electrodes placed in the cauda equina where the root density is high, they apply to any situation where a second nerve may be exposed to "stray" current from an active electrode.

The greater aim of this body of work is the development of a new complete root stimulator system combining both urological functions with leg exercises opportunities. Because the LARSI, and SARSI before it, have demonstrated the reliability of the technologies used and introduced the concept of readiness – two essential points for the successful development of an FES implant – the SLARSI is designed as an evolution from these pioneering works. The major amelioration will be the use of the purpose-built output-stage integrated-circuit, presented in the technical part of this thesis, implementing twelve independent channels controlled by setting the current at 2, 8 or 16mA. As demonstrated experimentally, these independent channels will eliminate the occurrence of cross-talk. This in turn is expected to improve selectivity and have a positive effect on implant usability, greatly simplifying post-implantation assessment and stimulation pattern generation.

Some other subjects are developed in the thesis to show that the development of a complete stimulation system involves much more that the design of its output stage or even its stimulator. Two minor research areas were investigated. The first is concerned with nerve root compression, and the second with electrodes as an output-stage load (this knowledge is necessary to set the IC's specifications). Stemming from the LARSI experience, a review of the literature on dorsal root compression is presented. Although electrodes mounts have been encasing nervous structures for many years now, there has been no direct study of post-operative compression, and resulting damage, or sustainable pressure levels. The review undertaken for this thesis is a first step in an unfortunately neglected direction and the proposed mechanisms underlying damage and recovery will undoubtedly be subject to future revisions. As the SARSI electrode book design was revisited following the compression analysis, a tentative electrode impedance formula was developed. Despite major simplifications, the study has delivered some interesting results expressed in a simple formula to calculate the output impedance of any electrode dimension at different encapsulation stages. The particularities of the formula are that the influence of the electrode area is distinct from that of the mount's cross-section, and that both are linear factors.

11.1 Conclusion

As a whole, this thesis covers a wide range of subjects (neurophysiology, electronics, electrochemistry, mechanics) as it encompasses a variety of smaller research projects (from the analysis of multi-moment-chair data to the study of nerve compression) all of which (and many more) are necessary for the development of implantable electrical stimulation devices in general, and of the SLARSI in particular. The major scientific contributions are summarised in the following list. I hope that the work undertaken will be seen as a considerable contribution to the research and development of electrical stimulation systems. It has also created or highlighted the need for further investigation and in vivo studies. The final chapter of this thesis is not concerned with detailed research anymore. It expresses my view on the context in which scientific research on such a niche subject is undertaken nowadays. Success does not only come from offering the best stimulation system from a technological point of view. Considerations such as reliability, cost-efficiency (especially when alternative options exists), usability, benefits (perceived and demonstrated) and integrability in daily living, support (not only from the manufacturers, but from the medical community as a whole), information and services are all essential. It will, I hope, become a basis for further discussions as we must not lose sight of the global interests involved in scientific research at large, and medical research in particular.

11.2 Contribution to the field

This thesis covers a wide range of subjects (neurophysiology, electronics, electrochemistry, mechanics) as it encompasses a variety of smaller research projects (from the analysis of multi-moment-chair data to the study of nerve compression) all of which (and many more) are necessary for the development of implantable electrical stimulators in general, and of the SLARSI in particular. To close this chapter, here follows a list of the key points developed in this thesis in the order in which they were introduced.

Cross-talk stimulation: in-depth analysis of force measurements have shown the occurrence of co-stimulation with nerve root stimulators (chapter 4). Simple experiments confirmed the proposed theory and validated the solution of **electrically independent channels** (chapter 5).

Anodal current imbalance: experiments have demonstrated the importance of the anodal current spread with tripolar stimulation (chapter 5): common anode connection, imperfect tripole (incl. capacitive imbalance) and virtual electrodes.

Nerve root compression: nerve roots may withstand a long-term pressure up to 40mmHg with peaks limited to 100mmHg (chapter 6) . The mechanisms of nerve and nerve root injury were detailed (section 1.1.4 and chapter 6).

Sling: Prof. Craggs' concept of space limiting lid was introduced (section 6.5) and the advantages for both stimulation and recording discussed, see also chapter 7.

The impedance of an electrode book: the voltage drop across the electrodes of a book connected as a tripole may be estimated using this formula:

$$Z = Z_{cable} + \frac{Z^U_{electrode}}{electrode\ length} + \frac{Z^U_{tissue}}{cross - sectional\ area}$$

for parameter meaning see page 184 (chapter 7).

Experimental electrical stimulator: the schematics were presented and commented and the floating ground issue was detailed (chapter 8).

SLARSI: review of improvements introduced when evolving from SARSI and LARSI to SLARSI with a focus on the issues highlighted in the thesis (chapter 9).

Independent channels demultiplexor: design and test results of the purpose-built IC providing the 12 independent channels of the new implant, chapter 10.

Chapter 12

Spinal root stimulators in context

The work presented in this thesis deals with improving the understanding and methods of nerve roots stimulation. It has been introduced in part I, detailed in parts II and III and summarised in the previous, eleventh, chapter. It will not be discussed any further. Rather, the concern of this context chapter is far more general as it reflects on the need and demand for nerve root stimulation. To develop this subject, the potential applications and beneficiaries of root stimulation as well as the alternatives, present and future, must be considered.

The nerve roots available for stimulation are those present in the cauda equina (lumbar and sacral roots). They innervate the leg muscles, the uro-genital organs, the lower bowel and anus. Although a few multiple-sclerosis patients previously received sacral stimulators [Brindley et al., 1986], implantations are now limited to spinally injured patients with a complete lesion, essentially paraplegics as the use of the implant requires a degree of functional independence. In the first stage at least, the SLARSI will be restricted to the same patient group.

12.1 Uro-genital applications and alternatives

In the targeted population, control of the bladder is often achieved by combined use of drugs to improve continence (anticholinergic, Botox) and some form of catheterisation or reflex action for voiding. Patients for which the drugs are unsuitable [1] remain incontinent and mostly rely on indwelling catheters (urethral or suprapubic) for voiding. They are then more at risk of urinary tract and kidney infections due amongst other causes to urinary reflux and autonomic dysreflexia. These methods are non-invasive (although Botox does require local injection in the detrusor muscle) and sufficiently efficient for the vast majority of the spinal cord injured community. Against this, the appeal of sacral root stimulators [2] lies in the ease of voiding and the non-reliance on

[1] Botox injections in the detrusor muscle has recently been associated with paralysis of neighbouring organs [Laet and Wyndaele, 2005; Wyndaele and Dromme, 2002]. Anticholinergic drugs are not recommended for patients treated for depression, heart rhythm problems, allergy. Drug side effects affect about one third of users and include constipation, poor sweat control, decreased visual acuity, headache

[2] SARSI is the only urological implant that will be discussed here. Alternatives have been developed but did not become so widespread, often as they failed to produce satisfactory repeatable results [Brindley, 1994; Johnston et al., 2005].

regular drug intake as well as its benefits on bowel function. Its major drawback, for potential patients, seems less the one-off surgical operation and subsequent bed-rest than the associated rhizotomy. As explained in section 3.2.2, page 46, the section of the posterior sacral roots increases compliance (decreased risks of autonomic dysreflexia, urinary tract infections and kidney failure) and provides continence (abolishes reflex contraction). During the early implantations, selective rhizotomy was only performed when pre-operative tests showed excessive bladder activity. Generalised sacral rhizotomy became popular in the late 1980s, probably under the influence of Dr. Sauerwein from Germany, to exploit the decreased detrusor tone hence improved bladder compliance, beneficial to all patients, hyperactive or not [Brindley, 1990; Kutzenberger et al., 2005].

It is probably the destructive aspect of the rhizotomy more than its actual consequences (i.e. the permanent disconnection of sensory pathways) that deter the patients. The spinal cord being completely damaged at a higher level, the posterior roots serve little purpose[3] and are indeed deleterious as they contribute to the uncontrolled reflex detrusor contractions. The consequences of rhizotomy are therefore, medically speaking, positive[4]. The key issue here is the perceived imminence of spinal cord repair techniques (see chapter 1, page 20). The situation may be summarised as follows:

- Sacral rhizotomy is beneficial to all patients but only necessary for continence amongst those with an hyperactive bladder[5].
- Functional human spinal cord regeneration is not "around the corner". When it does become available, it is probable that regenerating the sacral root neatly cut during the implantation will be a simpler task than that presented by the accidentally damaged cord. In other words, if the cord may be fixed, so can the roots[6].

One last development to consider on the subject of sacral stimulation is that of neuromodulation (section 3.2.3). Conditional stimulation of the afferent pathways (accessed in the pudendal nerve) may suppress reflex contractions of the hyperactive bladder. It may also help with voluntary voiding by preventing dyssynergia. The application of conditional neuromodulation requires a stimulator capable of monitoring the bladder

[3]The posterior roots remain useful, even necessary, for patients using reflex actions, such as voluntary reflex-triggered voiding or reflex erection.

[4]Sacral rhizotomies were performed before the appearance of the sarsi to abolish reflex contractions [Torrens, 1974, 1975; Torrens and Griffith, 1974, 1976].

[5]Sacral deafferentation may be performed extra-durally during a separate operation, although this did not become common practice during the SARSI hay-days because the benefits of rhizotomy, were so far considered, by the medical profession, to outweigh the risks associated with it. The more psychological side of the discussion, related to the destructive aspect of the rhizotomy only became prominent in the 1990s [Brindley, 1990].

[6]Hypothetically, should this not be the case, the missing roots (most likely posterior S2s, eventually S3s and S4,5s) provide sensations around the foot, see dermatome map, fig. 1.13 on page 19, they are not necessary for walking. What may be lost to the patient are uro-genital sensations like bladder fullness, sense of urine flow through urethra, sexual arousal, perception of bowel content.

for contractions (by measuring the pressure or recording neural activity) to control the onset of electrical stimulation. One-way communication implants as the one described in this thesis are not suitable for such an application, but the technology developed here may be transposed to future neuromodulating implantable stimulators.

12.2 Lower limb applications: paraplegia and exercise

The SLARSI, which is the underlying project driving this thesis, combines restoration of urologic functions with leg muscle exercises (this application does not require a rhizotomy). Mobility for a spinally injured patient is mainly achieved using a wheelchair, and the SLARSI does not aim to change this. It is an implant intended for exercise. Cardio-vascular and weight related issues are becoming increasingly prominent in most modern countries. The adverse effects of obesity are greater for the spinally injured population as they include higher risks of pulmonary emboli, reduced function below the injury level, compromised overall mobility and pain as well as chronic ailments such as diabetes and coronary artery disease. Wheelchair confinement and the difficulty to exercise are not the only factors contributing to the lower daily energy expenditure of paraplegics compared to sedentary able-bodied. Lower resting metabolic rate, reduced sympathetic nervous system activity and lower thermal effect of food are also involved. For general reference see Buchholz et al. [2003]; Buchholz and Pencharz [2004]; Jacobs and Nash [2004]; Monroe et al. [1998]; Nash and Gater [2007] which present results and literature reviews on the subject of energy expenditure of spinally-injured patients. FES induced lower limb exercise with either surface or implanted electrodes is a realistic option to increase energy expenditure of paraplegic patients. Arm-cranking and FES assisted rowing are alternatives. As the strains on the muscles, the bones and on the cardiovascular system are higher for standard submaximal upper-body exercise loads [McArdle et al., 1996, page 308], long term comparative studies are required to assess the safety and suitability of the various exercise protocols. Moving the legs also presents intrinsic advantages as it reverses the decreasing trends in bone mineral density and muscle bulk and improve joint contractures, blood flow and more [Belanger et al., 2000] (for a longer list see section 3.3.4 on page 53).

12.3 Popularity of FES exercise

With all the aforementioned benefits, why is FES exercise still mainly a research and rehabilitation concept? The answer to this question may be divided in two parts: not all suitable paraplegics are offered to join an FES training program, and only a small fraction of those who do try it go on using it as part of their everyday life. Compliance with any exercise regimen is linked to considerations of independence (does the patient require assistance?), time efficiency (what fraction of the training session is devoted to preparation?) and locality (can the patient exercise at home or locally?)[7]. Cycling

[7]Note that these factors are not independent, if for example a patient can only exercise in dedicated, distant, facilities, both the locality and time efficiency decrease. Likewise with the need for assistance

is therefore more suited than various stand up and walk processes (incl. parallel bars walking, weight supported treadmill stepping) for long term exercise programs as it is safer (low risks of falls) and may be performed at home on an ergonometer without the intervention of any other person. Compared with surface stimulation, implanted electrodes [8] considerably reduce the time pre and post exercise so that a one-hour training session takes 70 minutes rather than 150 [Newham and Donaldson, 2007]. The level of exercise, adequate assessment and reasonable expectations are also important for compliance. Cardiovascular training has little visible effects, its benefits are mainly preventive hence difficult to assess and potentially disappointing. Functional muscle training (to be able to cycle a given distance on road for example) requires longer, more intensive, daily exercise sessions [9].

Nerve root stimulators are not normally implanted before a year post-injury and only provided the patient has reached a physically and psychologically stable condition. It is therefore likely that surface stimulation will be preferred to initiate leg muscles re-training programs. Yet, while patients may comply with the tedious electrodes adjustment for the first months, their motivation will eventually decrease and implants should be available as a simpler, more efficient alternative to all patients after a first surface stimulation training period. The two techniques do not antagonise each other, on the contrary they should follow one another to optimise the patient's experience of FES.

12.4 Further considerations: information, cost, availability

Having established that root stimulators are still a potential uro-genital treatment alternative and offer an interesting approach to cardio-vascular fitness and lower limb movements, it is necessary to discuss issues of cost, availability and public information. Awareness of these FES applications should extend beyond potential patients and rehabilitation teams to everyday carers, physios, GPs, specialised media and anecdotally to the general public. Availability should also be improved, both for the equipment (implants, cycles, training stations) [10] and of qualified staff, medical and technical, for

and time efficiency or locality.

[8] Implants include anterior root stimulators as well as peripheral nerve stimulators. For a discussion of their respective advantages see table 2.2 on page 34. Bions are also implantable but as those powerful enough for lower limb functional stimulation require individual coils for power transmission, their use is therefore complex and does not decrease much the doning-doffing time.

[9] There is no consensus on the optimum exercise protocol although there is a general agreement that treatment should begin as early as possible after the injury, ideally within two to three months. While the cardiovascular benefits have not been extensively studied and compared, FES-cycling from three 30 minutes sessions a week has been shown to give better results than isotonic contractions in preventing musculo-skeletal atrophy. These statements are not the result of an extensive literature review but rather are impressions collected through discussions with various specialists within the FES field. They are supported by the following references selected amongst many other because they present both sides of the argument, have a good review quality and are easily available: Baldi et al. [1998]; Clark et al. [2007]; Dudley et al. [1999]; Eser et al. [2007]; Hettinga and Andrews [2007]; Hettinga et al. [2004]; Hicks et al. [2003]; Jones et al. [2002].

[10] CE marking, and FDA approval for the States, will be required for any equipment that is to be commercially sold rather than being treated as experimental research tools as is the case actually.

both cycle and stimulator maintenance and for questions of every day use. Issues of costs intervene at all stages of life post spinal-cord injury [Dryden et al., 2005; Priebe et al., 2007]. In the USA, SARSI has been shown to be cost-effective within five years of implantation [Creasey and Dahlberg, 2001] (there are no cost-benefits evaluations of the leg stimulator). If the patients must buy their own equipment, and if they begin with surface stimulation, this may deter them from changing to an implantable version (with all the extra costs involved) when they become ready for it. If, however, rehabilitation centers bought the surface stimulation equipment and offered to rent them to patients on demand there may be a larger market for both surface and implantable systems. This might also decrease servicing time and improve patient confidence. Liaising with local sport facilities (in hospitals as well as private gyms), cyclists communities and bicycle shops to promote recumbent tricycles is another possible alley to improve overall access to FES sport. Even a well trained FES cyclist cannot produce enough output power to enjoy an outdoor cycle ride. Tricycles fitted with motors would solve this problem and promote the more social side of cycling. Likewise, organising events during which FES-cyclists play with and compete against each other gives an extra incentive for daily training. These few ideas highlight the need for bridges between the researchers and the patients. A debate is required, involving all parties (patients, engineers, medical staff and regulatory bodies) to try to understand what limits FES cycling popularity and provide adequate remedies.

12.5 Potential beneficiaries of SLARSI and alternatives

Uro-genital applications of root stimulators as well as lower limb movements, functional or purely for exercise, have been discussed so far. The major negative points identified were the rhizotomy and the lack of awareness about FES-cycling. It is important to insist here that while SLARSI offers both lower limb and uro-genital (incl. bowel) applications in one implant, sacral deafferentation is only desirable for bladder function (especially to prevent hyperactivity). The patient may opt for an implantation without rhizotomy; the stimulation will be functional (both for the bladder and bowel, and for the lower limbs) but alternative methods of bladder management (drugs, catheters) may still be required. The beneficiaries group at first is likely to be limited to paraplegic patients with a complete spinal cord injury and meeting a restrictive list of selection criteria, a relatively small group. The alternatives are drug treatments, Botox injections, catheterisation for the uro-genital side, and physiotherapy, passive stretches, weight supported standing, parallel bars walking, wheelchair sports, surface stimulation for the lower limbs. Possible future alternatives include nerve regeneration and spinal cord repair, refined drugs and improved implants.

12.6 The future of root stimulators

The SARSI is a well established urologic treatment for neurologically impaired patients. It seems, however, to have become less popular than it was in the 1990s due to

increasing concerns over rhizotomy. The current trend in implantable nerve root stimulator research is to develop lower limb applications on the one hand, and implants with conditional neuromodulation capacities on the other hand. While both directions are justifiable in the sense that the targets are realistic and the chances of success high, the current patient groups are small (criteria may be reviewed to extend them) and the alternatives numerous. The last discussion opened in this chapter must therefore be that of the need for nerve root stimulators: can further research in this domain be justified? Academic research is not, in design, held by tight commercial imperatives. This relative freedom should, funding provided, allow the development to be driven by meaning rather than means. There is currently no cure for spinal cord injury nor any universally successful method to deal with its consequences. Nerve root stimulators are one tool amongst others available to the patients, via the medical services, to improve their quality of life. Should all research effort (hence funding) be concentrated on nerve regeneration, i.e. on a cure, rather than dispersed on palliative options? Can the condition of the current patients be set aside for future promises? After all, treatments are already available. Why not maintain a status quo in treatment and focus on a cure? The answer to these questions is mainly a matter of point of view. There will probably always be patients for whom "the cure" is not applicable. Yet, the justification for further research lies not only in the quality of life of those patients, present and future but also in the fact that work on the development of implantable stimulators does benefit a larger group than that, indeed rather limited, of potential implantee. Research advances both our knowledge of nervous communication and electrical stimulation, as shown in chapter 5, and the electronic, machining and packaging technologies, as seen in chapters 6, 7 and 10.

As more technologies become available, more applications for them will be found. Versatile stimulators with connectors fitting any electrode type and a reliable control box and software could be tuned for a specific application with little delay in response to a patient and medical team's suggestion. Reducing the time between the development of an idea and its medical trial would increase the interest in, hence the potential applications of, FES systems. To justify continuing the development efforts, the research must be, and remain, patient driven. This relies on the existence, at all levels of research, of a sustained, constructive, dialog between the engineers and the medical profession.

Part V

Appendices and references

References

Abbott N.J., Faruhana Abdullah, Mitchell G, Ward K.J., and Smith I.C.H. An electrophysiological method for measuring the potassium permeability of the nerve perineurium. *Brain Research Bulletin*, 776:204–213, 1997.

Accornero N., Bini G., Gian L., and Manfredi M. Selective activation of peripheral nerve fibre groups of different diameter by triangular shaped stimulus pulses. *Journal of Physiology*, 277:539–560, 1977.

Adams M.M. and Hicks A.L. Spasticity after spinal cord injury. *Spinal Cord.*, 43: 577–586, 2005.

Agarwal S., Triolo R.J., Kobetic R, Miller M., Bieri C., Kukke S., Rohde L., and Davis J.A. Long-term user perceptions of an implanted neuroprosthesis for exercise, standing, and transfers after spinal cord injury. *Journal of Rehabilitation Research and Development*, 40(3):241–252, 2003.

Agnew W.F. and McCreery D.B. *Neural Prostheses - Fundamental Studies*. Prentice Hall Biophysics and Bioengineering Series. Prentice Hall, Englewod Cliffs, NJ, 1990.

Agnew W.F., McCreery D.B., Bullara L.A., and Yuen T.G. Effects of prolonged electrical stimulation of peripheral nerve. In Agnew W.F. and McCreery D.B., editors, *Neural prostheses: Fundamental studies*, book chapter 9, pages 225–252. Prentice Hall, 1 edition, 1990a.

Agnew W.F., McCreery D.B., Yuen T.G., and Bullara L.A. Local anaesthetic block protects against electrically-induced damage in peripheral nerve. *J. Biomed. Eng.*, 12(4):301–308, 1990b.

Allegro MicroSystems . *5832 BiMOS II 32-BIT SERIAL-INPUT, LATCHED DRIVERS*. Allegro MicroSystems, Inc., 1998.

Allingham D., Stocks N.G., and Morse R.P. sciatic nerve of the toad xenopus laevis: integrate-and-fire and beyond. *?*, 2004.

Altman K.W. and Plonsey R. Fiber selectivity in simulated nerve bundle f.e.s. from a point source. In *IEEE Engineering in Medicine and Biology Society 10th Annual International Conference*, pages 0936–0937, 1988.

Altman K.W. and Plonsey R. Analysis of the longitudinal and radial resistivity measurements of the nerve trunk. *Ann. Biomed. Eng.*, 17(4):313–324, 1989.

Andrews B.J. and Kooi B.B.J. Localized electrical nerve blocking. *Proceedings of 18th Annual International Conference of the IEEE Engineering in Medicine and Biology Society*, 1:347–348, 1996.

Angelov D.N., Ceynowa M., Guntinas-Lichius O., Streppel M., Grosheva M., Kiryakova S.I., Skouras E., Maegele M., Irintchev A., Neiss W.F., Sinis N., Alvanou A., and Dunlop S.A. Mechanical stimulation of paralyzed vibrissal muscles following facial nerve injury in adult rat promotes full recovery of whisking. *Neurobiology of Disease*, 26:229–242, 2007.

Aspire, online , last accessed in November 2006. `http://www.aspire.org.uk/index.php?id=2`.

Bajd T., Kralj A., Stefancic M., and Lavrac N. Use of functional electrical stimulation in the lower extremities of incomplete spinal cord injured patients. *Artif. Organs*, 23 (5):403–409, 1999a.

Bajd T., Munih M., and Kralj A. Problems associated with fes-standing in paraplegia. *Technology and Health Care*, 7:301–308, 1999b.

Bajd T., Stefancic M., and Lavrac N. Fes walking after incomplete spinal cord injury. pages 275–280, 1998.

Baker A.R., Collins T.A., Porter R.W., and Kidd C. Laser doppler study of porcine cauda equina blood flow: the effect of electrical stimulation of the rootlets during single and double site, low pressure compression of the cauda equina. *spine*, 20(6): 660–664, 1995.

Balasubramaniam A.V., Bycroft J.A., Chung E.A., Middleton F., and Craggs M.D. The guardian reflex: an outcome measure for neural restoration in spinal cord injury. Generic, 2005.

Baldi J.C., Jackson R.D., Moraille R., and Mysiw W.J. Muscle atrophy is prevented in patients with acute spinal cord injury using functional electrical stimulation. *Spinal Cord.*, 36(7):463–469, 1998.

Baratta R., Ichie M., Hwang S.K., and Solomonow M. Orderly stimulation of skeletal muscle motor units with tripolar nerve cuff electrode. *IEEE Trans Biomed Eng*, 36, No. 8:836–843, 1989.

Barbeau H., Ladouceur M., Mirbagheri M.M., and Kearney R.E. The effect of locomotor training combined with functional electrical stimulation in chronic spinal cord injured subjects: walking and reflex studies. *Brain Res. Brain Res. Rev.*, 40 (1-3):274–291, 2002.

Barbeau H., Norman K., Fung J., Visitin M., and Ladouceur M. Does neurorehabilitation play a role in the recovery of walking in neurological populations? *Ann NY Acad Sci*, 860:377–392, 1998.

Battista A.F. and Alban E. Effect of graded ligature compression on nerve conduction. *Exp. Neurol.*, 80(1):186–194, 1983.

Beaudreau S.A. and Finger S. Medical electricity and madness in the 18th century. the legacies of benjamin franklin and jan ingenhousz. *Perspectives in Biology and Medicinebeaudreau*, 49(3):330–345, 2006.

Beel J.A., Stodieck L.S., and Luttges M.W. Structural properties of spinal nerve roots: biomechanics. *Exp. Neurol.*, 91(1):30–40, 1986.

Belanger M, Stein R.B., Wheeler G.D., Gordon T., and Leduc B. Electrical stimulation: Can it increase muscle strength and reverse osteopenia in spinal cord injured individuals? *Arch. Phys. Med. Rehabil.*, 81.:1090–1098, 2000.

BeMent S.L. and J. B. Ranck Jr. A model for electrical stimulation of central myelinated fibers with monopolar electrodes. *Exp. Neurol.*, 24:171–186, 1969a.

BeMent S.L. and J. B. Ranck Jr. A quantitative study of electrical stimulation of central myelinated fibers. *Exp. Neurol.*, 24(2):147–170, 1969b.

Benko H., Burger H., and Obreza P. Can fes be used as an orthotic aid in patient with SCI. In *7th Annual Conference of the International Functional Electrical Stimulation Society*, pages 26–28, 2002.

Bernhart D.M., Coogan S.M., Danielson P.D., Dannhauer A., de Majewski A., Schaaf E.R.Vander, and Zottoli S.J. Conservation in the teaching laboratory: Substitution of xenopus for rana. *BioScience*, 41(8):578–580, 1991.

Bhadra N., Grunewald V., Creasey G.H., and Mortimer J.T. Selective suppression of sphincter activation during sacral anterior nerve root stimulation. *Neurourol. Urodyn.*, 21(1):55–64, 2002.

Bhadra N., Grunewald V., Creasey G.H., and Mortimer J.T. Selective activation of the sacral anterior roots for induction of bladder voiding. *Neurourol. Urodyn.*, 2005.

Bhadra N. and Kilgore K.L. Direct current electrical conduction block of peripheral nerve. *IEEE Trans. Neural Syst. Rehabil. Eng.*, 12(3):313–324, 2004.

Bhadra N., Kilgore K.L., and Peckham P.H. Implanted stimulators for restoration of function in spinal cord injury. *Med. Eng Phys.*, 23(1):19–28, 2001.

Bhadra N. and Peckham P.H. Peripheral nerve stimulation for restoration of motor function. *J. Clin. Neurophysiol.*, 14(5):378–393, 1997.

Bijak M., Mayr W., Girsch W., Lanmuller H., Unger E., stohr H, Thoma H, and Plenk H. Functional and biological test of a 20 channel implantable stimulator in sheep in view of functional electrical stimulation walking for spinal cord injured persons. *Artif. Organs*, 25(6):467–474, 2001.

Black J. *Biological Performances of Materials.* Marcel Dekker, Incl., New York; Basel, 3rd edition, 1999.

Blair E.A. and Erlanger J. A comparison of the characteristics of axons through their individual electrical responses. *Am. J. Physiol*, 106(3):524–564, 1933.

Blair H.A. On the intensity-time relations for stimulation by electric currents. i. *The Journal of General Physiology*, 73(3):709–729, 1932a.

Blair H.A. On the intensity-time relations for stimulation by electric currents. ii. *The Journal of General Physiology*, 73(3):731–755, 1932b.

Borgens R.B. Imposed electrical fields and mammalian spinal cord regeneration. *Proceedings of the Annual International Conference of the IEEE Engineering in Medicine and Biology Society*, 13, No. 2:1001–1002, 1991.

Bostock H. The strength-duration relationship for excitation of myelinated nerve: Computed dependence on membrane parameters. *J. Physiol.*, 341:59–74, 1983.

Bowman B.R. and McNeal D.R. Response of single alpha motoneurons to high-frequency pulse trains. *Applied Neurophysiology*, 49:121–138, 1986.

Brazier M.A.B. *A History of the Electrical Activity of the Brain. The First Half-Century*. Pitman Medical Publishing Company, LTD, 1961.

Brindley G.S. Electrode array for making long-lasting electrical connections to spinal roots. *Journal of Physiology*, 222:135–135, 1972.

Brindley G.S. Emptying the bladder by stimulating sacral ventral roots. *Journal of Physiology*, 237:15P–16P, 1973.

Brindley G.S. An implant to empty the bladder or close the urethra. *J. Neurol. Neurosurg. Psychiatry*, 40:358–369, 1977.

Brindley G.S. One-way stimulation of the large fibres of spinal roots through chronically implanted electrodes. *Journal of Physiology*, 281:12P–12P, 1978.

Brindley G.S. A grommet for preventing cerebrospinal fluid from leaking along the outside of implanted tubes and cables. *Journal of Physiology*, 320:1P–1P, 1981.

Brindley G.S. Treatment of urinary and faecal incontinence by surgically implanted devices. In *Neurobiology of Incontinence*, number Symposium 151 in Ciba Foundation Symposia, pages 267–282. John Wiley and Sons, MRC Neurological Prostheses Unit, Institute of Psychiatry, London, UK, 1990.

Brindley G.S. The first 500 patients with sacral anterior root stimulator implants: general description. *Paraplegia*, 32(12):795–805, 1994.

Brindley G.S. The first 500 sacral anterior root stimulators: implant failures and their repair. *Paraplegia*, 33(1):5–9, 1995.

Brindley G.S. and Craggs M.D. A technique for anodal blocking of large nerve fibres through chronically implanted electrodes. *J. Neurol. Neurosurg. Psychiatry*, 43: 1083–1090, 1980.

Brindley G.S., Polkey C.E., and Rushton D.N. Sacral anterior root stimulators for bladder control in paraplegia. *Paraplegia*, 20(6):365–381, 1982.

Brindley G.S., Polkey C.E., Rushton D.N., and Cardozo L. Sacral anterior root stimulators for bladder control in paraplegia: the first 50 cases. *J. Neurol. Neurosurg. Psychiatry*, 49(10):1104–1114, 1986.

Brindley G.S. and Rushton D.N. Long-term follow-up of patients with sacral anterior root stimulator implants. *Paraplegia*, 28(8):469–475, 1990.

Brummer S.B. and McHardy J. Current problems in electrode development. In Hambrecht F.T. and Resnick D., editors, *Functional Electrical Stimulation*, pages 499–514. 1977.

Brummer S.B., Robblee L.S., and Hambrecht F.T. Criteria for selecting electrodes for electrical stimulation: theoretical and practical considerations. *Ann. N. Y. Acad. Sci.*, 405:159–171, 1983.

Brummer S.B. and Turner M.J. Electrical stimulation with pt electrodes: I - a method for determination of "real" electrode areas. *IEEE Trans Biomed Eng*, BME-24(5): 436–439, 1977a.

Brummer S.B. and Turner M.J. Electrical stimulation with pt electrodes: Ii - estimation of maximum surface redox (theoretical non-gassing) limits. *IEEE Trans Biomed Eng*, BME-24(5):440–443, 1977b.

Brummer S.B. and Turner M.J. Electrochemical considerations for safe electrical stimulation of the nervous system with platinum electrodes. *IEEE Trans Biomed Eng*, 1: 59–63, 1977c.

BS EN 45502-1: Active implantable medical devices part 1: General requirements for safety, marking and information to be provided by the manufacturer. Technical Report BS EN 45502-1, 1998.

Buchholz A.C., McGillivray C.F., and Pencharz P.B. Physical activity levels are low in free-living adults with chronic paraplegia. *Obes. Res.*, 11(4):563–570, 2003.

Buchholz A.C. and Pencharz P.B. Energy expenditure in chronic spinal cord injury. *Curr. Opin. Clin. Nutr. Metab Care*, 7(6):635–639, 2004.

Bullara L.A. Implantable electrode array. Patent, 1984.

Buti M., Verdu E., Labrador R.O., Vilches J.J., Fores J., and Navarro X. Influence of physical parameters of nerve chambers on peripheral nerve regeneration and reinnervation. *Exp. Neurol.*, 137(1):26–33, 1996.

Bycroft J.A., Craggs M.D., Sheriff M., Knight S., and Shah P.J. Does magnetic stimulation of sacral nerve roots cause contraction or suppression of the bladder? *Neurourol. Urodyn.*, 23(3):241–245, 2004.

Calancie B., Molano M.R., and Broton J.G. Emg for assessing the recovery of voluntary movement after acute spinal cord injury in man. *Clin. Neurophysiol.*, 115: 1748–1759, 2004.

Carlstedt T., Grane P., Hallin R.G., and Noren G. Return of function after spinal cord implantation of avulsed spinal nerve roots. *Lancet*, 346:1323–1325, 1995.

Carp J.S., Chen X.Y., Sheikh H., and Wolpaw J.R. Effects of chronic nerve cuff and intramuscular electrodes on rat triceps surae motor units. *Neurosci. Lett.*, 312(1): 1–4, 2001.

Carpenter M.B. *Carpenter's human neuroanatomy*. Williams and Wilkins, 9 edition, 1996.

Chancellor M.B. and Chartier-Kastler E.J. Principles of sacral nerve stimulation (sns) for the treatment of bladder and urethral sphincter dysfunctions. *Neuromodulation*, 3(1):15–26, 2000.

Cikalo I., Savrin R., Erzin R., Gider F., and Bajd T. Fes rehabilitative systems for re-education of walking in incomplete spinal cord injured persons. *Neuromodulation*, 3(3):167–174, 2000.

Clark J.M., Jelbart M., Rischbieth H., Strayer J., Chatterton B., Schultz C., and Marshall R. Physiological effects of lower extremity functional electrical stimulation in early spinal cord injury: lack of efficacy to prevent bone loss. *Spinal Cord*, 45: 78–85, 2007.

Clasey J.L., Janowiak A.L., and Gater D.R. Relationship between regional bone density measurements and the time since injury in adults with spinal cord injuries. *Arch. Phys. Med. Rehabil*, 85:59–64, 2004.

Coburn B. Electrical stimulation of the spinal cord: two-dimensional finite element analysis with particular reference to epidural electrodes. *Med. Biol. Eng. Comput.*, 18(5):573–584, 1980.

Coburn B. Theoretical modelling of neurostimulation. In *IEEE colloquium on Engineering Design for the Disabled*, pages 4/1–4/4, 1988.

Coggeshall R.E., AppleBaum M.L., Fazen M., Stubles T.B., and Sykes M.T. Unmyelinated axons in human ventral roots, a possible explanation for the failure of dorsal rhizotomy to relieve pain. *Brain*, 98(1):157–166, 1975.

Collado H., Bensoussan L., Viton JM., Bovis V.M.De, and Delarque A. Does fascicular neurotomy have long-lasting effects? *Journal of Rehabilitation Medicine*, 38(4): 212–217, 2006.

Conway B.E. Electrochemistry encyclopedia, last accessed in April 2007. `http://electrochem.cwru.edu/ed/encycl/`.

Cooner Wire, online , last accessed in September 2007. `http://www.coonerwire.com/Products/MIWC.html`.

Cornefjord M., Olmarker K., Rydevik B., and Nordborg C. Mechanical and biochemical injury of spinal nerve roots: a morphological and neurophysiological study. *Eur. Spine J.*, 5(3):187–192, 1996.

Cornefjord M., Sato K., Olmarker K., Rydevik B., and Nordborg C. A model for chronic nerve root compression studies: presentation of a porcine model for controlled, slow-onset compression with analyses of anatomic aspects, compression onset rate, and morphologic and neurophysiologic effects. *spine*, 22(9):946–957, 1997.

Cowan W.Maxwell. Viktor hamburger and rita levi-montalcini: The path to the discovery of nerve growth factor. *Annu. Rev. Neurosci.*, 24:551–600, 2001.

Craggs M.D., Donaldson N. de N., and Donaldson P.E.K. Performance of platinum stimulating electrodes, mapped on the limit-voltage plane. part 1: Charge injection in vivo. *Med. Biol. Eng. Comput.*, 24:424–430, 1986.

Craggs M.D. and McFarlane J. Physiological society symposium: the physiology and pathophysiology of the lower urinary tract neuromodulation of the lower urinary tract. *Exp. Physiol*, 84:149–160, 1999.

Crago P.E., Peckham P.H., Mortimer J.T., and Meulen J.P.VanDer. The choice of pulse duration for chronic electrical stimulation via surface, nerve and intramuscular electrodes. *Ann. Biomed. Eng.*, 2:252–264, 1974.

Creasey G.H. Electrical stimulation of sacral roots for micturition after spinal cord injury. *Urol. Clin. North Am.*, 20(3):505–515, 1993.

Creasey G.H. Restoration of bladder, bowel, and sexual function. *Topics in Spinal Cord Injury Rehabilitation*, 5(1):21–32, 1999.

Creasey G.H. and Dahlberg J.E. Economic consequences of an implanted neuroprosthesis for bladder and bowel management. *Arch. Phys. Med. Rehabil.*, 82(11):1520–1525, 2001.

Creasey G.H., Grill J.H., Korsten M., HS U., Betz R., Anderson R., and Walter J. An implantable neuroprosthesis for restoring bladder and bowel control to patients with spinal cord injuries: a multicenter trial. *Arch. Phys. Med. Rehabil.*, 82(11): 1512–1519, 2001.

Dahlin L.B. and Kanje M. Conditioning effect induced by chronic nerve compression. an experimental study of the sciatic and tibial nerves of rats. *Scand. J. Plast. Reconstr. Surg. Hand Surg.*, 26(1):37–41, 1992.

Dahlin L.B., Shyu B.C., Danielsen N., and Andersson S.A. Effects of nerve compression or ischaemia on conduction properties of myelinated and non-myelinated nerve fibres: an experimental study in the rabbit common peroneal nerve. *Acta Physiol Scand.*, 136(1):97–105, 1989.

Daly J.J., Marsolais E.B., Mendell L.M., Rymer W.Z., Stefanovska A., Wolpaw J.R., and Kantor C. Therapeutic neural effects of electrical stimulation. *IEEE Trans Rehabil Eng*, 4(4):218–230, 1996.

Davis H. and Forbes A. Chronaxie. *Physiological Reviews*, 6:407–441, 1936.

Davis J.A., Triolo R.J., Uhlir J.P., Bieri C., Rohde L., Lissy D., and Kukke S. Preliminary performance of a surgically implanted neuroprosthesis for standing and transfers. where do we stand? *J. Rehabil. Res. Dev.*, 38(6):609–617, 2001.

Davis R., Houdayer T., Andrews B.J., Barriskill A., and Parker S. Paraplegia: Implantable praxis24-fes system and external sensor for multi-fanctional restoration. *Proceedings of the 5th Annual Conference of the International Functional Electrical Stimulation Society*, pages 35–37, 2000.

Delamarter R.B., Bohlman H.H., Dodge L.D., and Biro C. Experimental lumbar spinal stenosis: analysis of the cortical evoked potentials, microvasculature, and histopathology. *J. Bone Joint Surg. Am.*, 72(1):110–120, 1990.

Deurloo K.E., Holsheimer J., and Bergveld P. Nerve stimulation with a multi-contact cuff electrode: validation of model predictions. *Arch. Physiol Biochem.*, 108(4): 349–359, 2000.

Dolenc V.V., Kralj A., and Bosnjak R. Biomechanical response in the ankle to stimulation of lumbosacral nerve roots with spiral cuff multielectrode. *Neurol. Med. Chir.*, 39:659–667, 1999.

Donaldson N. de N. A 24-output implantable stimulator for fes. In *Proceedings of the 2nd Vienna International Workshop on Functional Electrical Stimulation*, pages 197–200, 1986.

Donaldson N. de N. *The Electrical Design of an Implantable Stimulator to Restore Motor Control to the Paralysed.* PhD thesis, UCL, 1990a.

Donaldson N. de N. A new multiplexed stimulator for fns. *Advances in External Control of Human Extremities*, X:345–358, 1990b.

Donaldson N. de N. and Donaldson P.E.K. Performance of platinum stimulating electrodes, mapped on the limit-voltage plane. part 2: Corrosion in vitro. *Med. Biol. Eng. Comput.*, 24:431–438, 1986a.

Donaldson N. de N. and Donaldson P.E.K. When are actively balanced biphasic ('lilly') stimulating pulses necessary in a neurological prosthesis? i historical background; pt resting potential; q studies. *Med. Biol. Eng. Comput.*, 24:41–49, 1986b.

Donaldson N. de N. and Donaldson P.E.K. When are actively balanced biphasic ('lilly') stimulating pulses necessary in a neurological prosthesis? ii ph changes; noxious products; electrode corrosion; discussion. *Medical and Biological Engineering*, 24: 50–56, 1986c.

Donaldson N. de N., Munih M., Perkins T.A., and Wood D.E. Apparatus to measure simultaneously 14 isometric leg joint moments. part 1: Design and calibration of six-axis transducers for the forces and moments at the ankle. *Med. Biol. Eng. Comput.*, 37(2):137–147, 1999.

Donaldson N. de N., Munih M., Phillips G.F., and Perkins T.A. Apparatus and methods for studying artificial feedback-control of the plantarflexors in paraplegics without interference from the brain. *Med. Eng Phys.*, 19(6):525–535, 1997a.

Donaldson N. de N. and Perkins T.A. Analysis of resonant coupled coils in the design of radio frequency transcutaneous links. *Med. Biol. Eng. Comput.*, 21:612–627, 1983.

Donaldson N. de N., Perkins T.A., Fitzwater R., Wood D.E., and Middleton F. Fes cycling may promote recovery of leg function after incomplete spinal cord injury. *Spinal Cord.*, 38(11):680–682, 2000.

Donaldson N. de N., Perkins T.A., and Worley A.C. Lumbar root stimulation for restoring leg function: stimulator and measurement of muscle actions. *Artif. Organs*, 21(3):247–249, 1997b.

Donaldson N. de N., Rushton D.N., Perkins T.A., Wood D.E., Norton J., and Krabbendam A.J. Recruitment by motor nerve root stimulators: significance for implant design. *Med. Eng Phys.*, 25(7):527–537, 2003.

Donaldson N. de N., Rushton D.N., and Tromans T. Neuroprostheses for leg function after spinal-cord injury. *Lancet*, 350(9079):711, 1997c.

Donaldson N. de N. and Yu C.H. Fes standing: control by handle reactions of leg muscle stimulation (chrelms). *IEEE Trans Rehabil Eng*, 4(4):280–284, 1996.

Donaldson N. de N. and Yu C.H. A strategy used by paraplegics to stand up using fes. *IEEE Trans Rehabil Eng*, 6(2):162–167, 1998.

Donaldson P.E.K. The underwater life of joints between some adherend and adhesive materials useful in neurological prosthesis-making. In *BES Int Conf Biomedical Polymers*, pages 143–151, Jul 1982.

Donaldson P.E.K. The cooper cable: An implantable multiconnector cable for neurological prostheses. *Med. Biol. Eng. Comput.*, 21:371–374, 1983.

Donaldson P.E.K. The craggs connector: a termination for cooper cable. *Med. Biol. Eng. Comput.*, 23:195–196, 1985.

Donaldson P.E.K. Twenty years of neurological prosthesis-making. *J. Biomed. Eng.*, 9(October):291–298, 1987.

Donaldson P.E.K. Aspects of silicone rubber as an encapsulant for neurological prostheses - part 1: Osmosis. *Med. Biol. Eng. Comput.*, 29:34–39, 1991.

Donaldson P.E.K. Hydrothermal stability of joints, using a silicone rubber adhesive, for a range of adherends of interest to makers of surgically-implanted microelectronic devices. *Int. J. Adhesion and Adhesives*, 14(2):103–107, 1994.

Donaldson P.E.K. The essential role played by adhesion in the technology of neurological prostheses. *International Journal of Adhesion and Adhesives*, 16(2):105–107, 1996.

Donaldson P.E.K., Donaldson N. de N., Rushton D.N., and Perkins T.A. Estimated electrode operating conditions of the first london mk v implanted stimulator. *Journal of Medical Engineering and Technology*, 22(5):216–219, 1998.

Dryden D.M., Saunders L.D., Jacobs P., Schopflocher D.P., Rowe B.H., May L.A., Yiannakoulias N., Svenson L.W., and Voaklander D.C. Direct health care costs after traumatic spinal cord injury. *J. Trauma*, 59(2):443–449, 2005.

Duan Y.Y., Clark G.M., and Cowan R.S.C. A study of intra-cochlear electrodes and tissue interface by electrochemical impedance methods in vivo. *Biomaterials*, 25 (17):3813–3828, 2004.

Dudley G.A., Castro M.J., Rogers S., and Apple D.F.Jr. A simple means of increasing muscle size after spinal cord injury: a pilot study. *Eur J Appl Physiol*, 80:394–396, 1999.

Dyck P.J., Lais A.C., Giannini C., and Engelstad J.K. Structural alterations of nerve during cuff compression. *Proc. Natl. Acad. Sci. U. S. A*, 87(24):9828–9832, 1990.

ECG library, online . A (not so) brief history of electrocardiography., last accessed in May 2006. `www.ecglibrary.com/ecghist.html`.

Edgerton V.R. and Roy R.R. Paralysis recovery in humans and model systems. *Current Opinion in Neurobiology*, 12:658–667, 2002.

Encarta . *World English Dictionary*. Bloomsbury Publishing Plc, 1st edition, 1999.

Erlanger J. and Gasser H.S. The action potential in fibres of slow conduction in spinal roots and somatic nerves. *Am. J. Physiol*, 92(1):43–82, 1930.

Erlanger J. and Gasser H.S. *Electrical Signs of Nervous Activity*. University of Pennsylvania Press, Philadelphia, 1937.

Eser P., de Bruin E.D., Telley I., Lechner H.E., Knecht H., and Stussi E. Effect of electrical stimulation-induced cycling on bone mineral density in spinal cord-injured patients. *European Journal of Clinical Investigation*, 33:412–419, 2007.

Fang Z.P. and Mortimer J.T. A method to effect physiological recruitment order in electrically activated muscle. *IEEE Trans Biomed Eng*, 38,No.2:175–179, 1991a.

Fang Z.P. and Mortimer J.T. Selective activation of small motor axous by quasitrapezoidal current pulses. *IEEE Trans Biomed Eng*, 38,No.2:168–174, 1991b.

Fenik V., Fenik P., and Kubin L. A simple cuff electrode for nerve recording and stimulation in acute experiments on small animals. *J. Neurosci. Methods*, 106(2): 147–151, 2001.

Fern R. and Harrison P.J. The effects of compression upon conduction in myelinated axons of the isolated frog sciatic nerve. *J. Physiol.*, 432:111–122, 1991.

Fern R. and Harrison P.J. The contribution of ischaemia and deformation to the conduction block generated by compression of the cat sciatic nerve. *Exp. Physiol*, 79 (4):583–592, 1994a.

Fern R. and Harrison P.J. The relationship between ischaemic conduction failure and conduction velocity in cat myelinated axons. *Exp. Physiol*, 79(4):571–581, 1994b.

Ferrante S., Pedrocchi A., Ianno M., Momi E.De, Ferrarin M., and Ferrigno G. Functional electrical stimulation controlled by artificial neural networks: pilot experiments with simple movements are promising for rehabilitation applications. *Funct. Neurol.*, 19(4):243–252, 2004.

Finean J.B. Electron microscope and x-ray diffraction studies of the effects of dehydratation on the structure of nerve myelin. i peripheral nerve. *The Journal of Biophysical and Biochemical Citology*, 8:13–29, 1960.

Finger S. Benjamin franklin, electricity, and the palsies: On the 300th anniversary of his birth. *Neurology*, 66(1556):1563, 2006.

Fisher A.C. *Electrode Dynamics*. Oxford Chemistry Primers. Oxford University Press, 5 edition, 2006.

FitzGerald M.J.T. *Neuroanatomy Basic and Clinical*. W.B. Saunders Company Ltd., 3rd edition, 1996.

FitzGerald M.J.T. and Folan-Curran J. Peripheral nerves. In *Clinical neuroanatomy and related neuroscience*, book chapter 7, pages 65–71. W.B. Saunders, 4th edition, 2002.

Fitzpatrick D.M., Struijk J.J., and Andrews B.J. A nerve cuff design for the selective activation and blocking of myelinated nerve fibres. *Proceedings of the Annual International Conference of the IEEE Engineering in Medicine and Biology Society*, 13, No. 2:906–907, 1991.

Flores A., Leon-Olea M., Vega R., and Soto E. Histochemistry and role of nitric oxide synthase in the amphibian (ambystoma tigrinum) inner ear. *Neuroscience letters*, 205:131–134, 1996.

Frankenhaeuser B. and Huxley A.F. The action potential in the myelinated nerve fibre of xenopus laevis as computed on the basis of voltage clamp data. *Journal of Physiology*, 171:302–315, 1964.

Frankenhaeuser B. and Schneider D. Some electrophysiological observations on isolated single myelinated nerve fibres (saltatory conduction). *J. Physiol.*, 115:177–184, 1951.

Fredericq H. Chronaxie: Testing excitability by means of a time factor. *Physiological Reviews*, pages 501–544, 1928.

Frijns H.M., Mooij J., and Kate J.H.Ten. A quantitative approach to modeling mammalian myelinated nerve fibers for electrical prosthesis design. *IEEE Trans Biomed Eng*, 41(6):556–566, 1994.

Fukushima K., Yahara O., and Kato M. Differential blocking of motor nerve fibers by direct current. *Pflgers. Arch.*, 358:235–242, 1975.

Garfin S.R., Cohen M.S., Massie J.B., Abitbol J.J., Swenson M.R., Myers R.R., and Rydevik B.L. Nerve-roots of the cauda equina: the effect of hypotension and acute graded compression on function. *J. Bone Joint Surg. Am.*, 72(8):1185–1192, 1990.

Garfin S.R., Rydevik B., Lind B., and Massie J. Spinal nerve root compression. *spine*, 20(16):1810–1820, 1995.

Garfin S.R., Rydevik B.L., and Brown R.A. Compressive neuropathy of spinal nerve roots: a mechanical or biological problem? *spine*, 16(2):162–166, 1991.

Garshick E., Kelley A., Cohen S.A., Garrison A., Tun C.G., Gagnon D., and Brown R. A prospective assessment of mortality in chronic spinal cord injury. *Spinal Cord*, 43:408–416, 2005.

Gasser H.S. and Erlanger J. The ending of the axon action potential and its relation to other events in nerve activity. *Am. J. Physiol*, 94(2):247–277, 1930.

Gasser H.S. and Graham H.T. The end of the spike potential of nerve and its relation to the beginning of the after-potential. *Am. J. Physiol*, 101(2):316–330, 1932.

Geddes L.A. Accuracy limitations of chronaxie values. *IEEE Trans Biomed Eng*, 51 (1):176–181, 2004.

Geddes L.A. and Baker L.A. Electrodes. In *Principles of Applied Biomedical Instrumentation*, book chapter 9, pages 315–452. Wiley-Interscience, 3rd edition, 1989.

Geddes L.A. and Bourland J.D. The strength-duration curve. *IEEE Trans Biomed Eng*, BME-32(NO. 6):458–459, 1985.

Gelfan S. and Tarlov I.M. Physiology of spinal cord, nerve root and peripheral nerve compression. *Am. J. Physiol*, 185(1):217–229, 1956.

Gellman H, Waters R.L., Lewonowski K., McNeal D.R., Govindarajan S., and Kanel G. histologic comparison of chronic implantation of nerve cuff and epineural electrodes. *Advances in External Control of Human Extremities*, pages 403–409, 1990.

Gonzalez-Darder J.M. Experimental microsurgical repair of spinal roots. *Neurosurgery*, 33(6):1083–1087, 1993.

Goodall E.V., Kostermann L.M., Holsheimer J., and Struijk J.J. Modeling study of activation and propagation delays during stimulation of peripheral nerve fibers with a tripolar cuff electrode. *IEEE Trans Rehabil Eng*, 3(3):272–282, 1995.

Gorman P.H. and Mortimer J.T. The effect of stimulus parameters on the recruitment characteristics of direct nerve stimulation. *IEEE Trans Biomed Eng*, Vol. BME-30 (No. 7):407–414, 1983.

Graham H.T. Supernormality, a modification of the recovery process in nerve. *Am. J. Physiol*, 110:225–242, 1934.

Grandjean P.A. and Mortimer J.T. Recruitment properties of monopolar and bipolar epimysial electrodes. *Ann. Biomed. Eng.*, 14:53–66, 1986.

Grant L. Functional electrical stimulation. *IEE review*, 34(11):443–445, 1988.

Graupe D. An overview of the state of the art of non invasive fes for independent ambulation by thoracic level paraplegics. *Neurological Research*, 24:431–442, 2002.

Grill W.M. The effect of stimulus pulse duration on selectivity of neural stimulation. *IEEE Trans Biomed Eng*, 43(2):161–166, 1996.

Grill W.M., Craggs M.D., Foreman R.D., Ludlow C.L., and Buller J.L. Emerging clinical applications of electrical stimulation: Opportunities for restoration of function. *J. Rehabil. Res. Dev.*, 38(6):641–653, 2001a.

Grill W.M., McDonald J.W., Peckham P.H., Heetderks W.J., Kocsis J., and Weinrich M. At the interface: Convergence of neural regeneration and neural prostheses for restoration of function. *J. Rehabil. Res. Dev.*, 38(6):641–653, 2001b.

Grill W.M. and Mortimer J.T. Electrical impedance of electrode encapsulation tissue. *IEEE*, pages 1376–1377, 1992.

Grill W.M. and Mortimer J.T. Electrical properties of implant encapsulation tissue. *Ann. Biomed. Eng.*, 22:23–33, 1994.

Grill W.M. and Mortimer J.T. Stimulation waveforms for selective neural stimulation. *IEEE Engineering in Medicine and Biology*, (July/August):375–385, 1995a.

Grill W.M. and Mortimer J.T. Temporal stability of nerve cuff electrode recruitment properties. *IEEE-EMBC and CMBEC*, 1995b.

Grill W.M. and Mortimer J.T. Inversion of the current-distance relationship by transient depolarization. *IEEE Trans Biomed Eng*, 44(1):1–9, 1997.

Grill W.M. and Mortimer J.T. Stability of the input-output properties of chronically implanted multiple contact nerve cuff stimulating electrodes. *IEEE Trans Rehabil Eng*, 6(4):364–373, 1998.

Grill W.M. and Mortimer J.T. Neural and connective tissue response to long-term implantation of multiple contact nerve cuff electrodes. *J. Biomed. Mater. Res.*, 50 (2):215–226, 2000.

Grill W.M., Richardson A.G., and McIntyre C.C. Influence of the myelin sheath on excitation properties of nerve fibers. In *Proceedings of the 22nd Annual International Conference of the IEEE Engineering in Medicine and Biology Society*, 2000.

Gruner J.A., Glaser R., Feinberg S.D., Collins S.R., and Nussbaum N.S. A system for evaluation and exercise-conditioning of paralyzed leg muscles. *Journal of Rehabilitation Research and Development*, 20(1):21–30, 1983.

Guckenheimer J and Oliva R.A. Chaos in the hodgkin-huxley model. *Siam J. Applied Dynamical Systems*, 1(1):105–114, 2002.

Guest RosalindS., Klose K.J., Needham-Shropshire BelindaM., and Jacobs PatrickL. Evaluation of a training program for persons with SCI paraplegia using the parastep(r)1 ambulation system: Part 4. effect on physical self-concept and depression,. *Archives. of Physical. Medicine and Rehabilitation*, 78(8):804–807, 1997.

Guiraud D., Pacetti A., Meola E., and Rabischong P. One year implantated patients follow up: Suaw project first results. *Proceedings of the 6th Annual Conference of the International Functional Electrical Stimulation Society*, pages 55–57, 2001.

Guiraud D., Taroni G., Denis B., Couderc P., and Stieglitz T. Description of a sixteen-channel fes implantable system. *Proceedings of the 5th Annual Conference of the International Functional Electrical Stimulation Society*, pages 292–294, 2000.

Hatakeyama K., Shimada Y., Sato K, Matsunaga T., Sato M., Misawa A., Ando S., Takashi M., Chida S., and Iizuka K. Clinical appication of the hybrid fes in a t4 completely parapletic patient. *Proceedings of the 5th Annual Conference of the International Functional Electrical Stimulation Society*, pages 77–79, 2000.

Haugland M., Childs C., Ladouceur M., Haase J., and Sinkjaer T. An implantable foot drop stimulator. *Proceedings of the 5th Annual Conference of the International Functional Electrical Stimulation Society*, pages 59–63, 2000.

Helsen J.A. and Breme H.J. *Metals as Biomaterials*. John Wiley and Sons, Chichester, 1st edition, 1998.

Hettinga D.M. and Andrews B.J. The feasability of functional electrical stimulation indoor rowing for high-energy training and sport. *Neuromodulation: technology at the neural interface*, 10(3):291–297, 2007.

Hettinga D.M., Andrews B.J., Wheeler G.D., Jeon J.Y., Verellen J., Laskin J.J., Olenik L.M., Lederer R., Burnham R., and Steadward R.D. Fes-rowing for persons with

spinal cord injury. In *Proceedings of the 9th Annual Conference of the International Functional Electrical Stimulation Society*, Sep 2004.

Hicks A.L., Martin K.A., Ditor D.S., Latimer A.E., Craven C., Bugaresti J., and McCartney N. Long-term exercise training in persons with spinal cord injury: effects on strength, arm ergometry performance and psychological well-being. *Spinal Cord*, 41:34–42, 2003.

Hill A.V. Excitation and accommodation in nerve. *Proceeding of the Royal Society of London, Series B, Biological Sciences*, 119(814):305–355, 1936.

Hodgkin A.L. Saltatory conduction in myelinated nerve. In *The conduction of the nerve impulse*, book chapter 4, pages 47–54. Liverpool University Press, 4 edition, 1971.

Hodgkin A.L. and Huxley A.F. A quantitative description of membrane current and its application to conduction and excitation in nerve. *J. Physiol.*, 117:500–544, 1952.

Hogan Q. Size of human lower thoracic and lumbosacral nerve roots. *Anesthesiology*, 85:37–42, 1996.

Holle J., Frey M, Gruber H., Kern H., stohr H, and Thoma H. Functional electrostimulation of paraplegics. experimental investigations and first clinical experience with an implantable stimulation device. *Orthopedics*, 7(7):1145–1155, 1984.

Holsheimer J. Computer modelling of spinal cord stimulation and its contribution to therapeutic efficacy. *Spinal Cord*, 36(8):531–540, 1998.

Holsheimer J. and Struijk J.J. Electrode combination and specificity in spinal cord stimulation. *Advances in External Control of Human Extremities*, pages 393–404, 1987.

Hook M.A., Liu G.T., Washburn S.N., Ferguson A.R., Bopp A.C., Huie J.R., and Grau J.W. The impact of morphine after a spinal cord injury. *Behav. Brain Res.*, 2007.

Hsu K.H. and Durand D. Prediction of neural excitation during magnetic stimulation using passive cable models. *IEEE Trans Biomed Eng*, 47(4):463–471, 2000.

Hu Y, Ming D., Wang Y.Z., Wong Y.W., Wan B.K., Luk K.D.K., and Leong J.C.Y. Three-dimensional dynamical measurement of upper limb support during paraplegic walking. In *Engineering in Medicine and Biology Society, 2004. EMBC 2004. Conference Proceedings.*, volume 2, pages 4944–4947, 2004.

Hunt K.J., Munih M., and Donaldson N. de N. Feedback control of unsupported standing in paraplegia. i. optimal control approach. *IEEE Trans Rehabil Eng*, 5(4):331–340, 1997.

Hursh J.B. Conduction velocity and diameter of nerve fibers. *Am. J. Physiol*, 127: 131–139, 1939.

IEEE, online . Ieee virtual museum, last accessed in May 2006. `www.ieee-virtual-museum.org`.

Irnich W. The chronaxie time and its practical importance. *PACE*, 3(3):292–301, 1980.

Jacobs P.L. and Nash M.S. Exercise recommendations for individuals with spinal cord injury. *Sports Med.*, 34(11):727–751, 2004.

Jaeger R.J., Yarkony G.M., Roth E.J., and Lovell L. Estimating the user population of a simple electrical stimulation system for standing. *Paraplegia*, 28(8):505–511, 1990.

Jaeger R.J., Yarkony G.M., and Smith R.M. Standing the spinal cord injured patient by electrical stimulation: refinement of a protocol for clinical use. *IEEE Trans Biomed Eng*, 36(7):720–728, 1989.

Jellema T. and Teepen J.L.J.M. A miniaturized cuff electrode for electrical stimulation of peripheral nerves in the freely moving rat. *Brain Research Bulletin*, 37(5):551–554, 1995.

Jezernik S., Craggs M.D., Grill W.M., Creasey G., and Rijkhoff N.J.M. Electrical stimulation for the treatment of bladder dysfunction: current status and future possiblities. *Neurological Research*, 24(5):413–430, 2002.

Johnston T.E., Betz R.R., Smith B.T., Benda B.J., Mulcahey M.J., Davis R., Houdayer T.P., Pontari M.A., Barriskill A., and Creasey G.H. Implantable fes system for upright mobility and bladder and bowel function for individuals with spinal cord injury. *Spinal Cord*, 2005.

Johnston T.E., Finson R.L., McCarthy J.J., Smith B.T., Betz R.R., and Mulcahey M.J. Use of functional electrical stimulation to augment traditional orthopaedic surgery in children with cerebral palsy. *J. Pediatr. Orthop.*, 24(3):283–291, 2004.

Jones D.G., Anderson E.R., and Galvin K.A. Spinal cord regeneration: moving tentatively towards new perspectives. *NeuroRehabilitation.*, 18(4):339–351, 2003.

Jones L.M., Legge M., and Goulding A. Intensive exercise may preserve bone mass of the upper limbs in spinal cord injured males but does not retard demineralisation of the lower body. *Spinal Cord.*, 40(5):230–235, 2002.

Kao C.C., Bunge R.P., and Reier P.J., editors. *Spinal cord reconstruction.* Raven Press, New-York, 1982.

Kaufmann P., MacNeil J.M., and Lei O.C. The compound action potential of the frog sciatic nerve. Technical report, 1996.

Keynes R.D. and Aidley D.J. Cable theory and saltatory conduction. In *Nerve and muscle*, Studies in Biology, book chapter 6, pages 73–85. Cambridge university press, 3rd edition, 2001.

Kikuchi S., Konno S., Kayama S., Sato K., and Olmarker K. Increased resistance to acute compression injury in chronically compressed spinal nerve roots: an experimental study. *spine*, 21(22):2544–2550, 1996.

Kilgore K., Scherer M., Bobblitt R., Dettloff J., Dombrowski D.M., Godbold N., Jatich J.W., Morris R., Penko J.S., Schremp E.S., and Cash L.A. Neuroprosthesis consumers' forum: Consumer priorities for research directions. *J. Rehabil. Res. Dev.*, 38(6):655–660, 2001.

Kim J.H., Manuelidis E.E., Glenn W.W.L., Fukuda Y., Cole D.S., and Hogan J.F. Light and electron microscopic studies of phrenic nerves after long-term electrical stimulation. *J. Neurosurg.*, 58:84–91, 1983.

Kingsley R.E. *Concise text of neuroscience.* 2nd edition, 2000.

Kingsley R.E., Messenger K.K., and Seall R.H. Long-term survival of peripheral axons that have reinnervated the spinal cord. *Exp. Neurol.*, 84:347–357, 1983.

Kirkham A.P.S., Knight S.L., Craggs M.D., Casey A.T.M., and Shah P.J.R. Neuromodulation through sacral nerve roots 2 to 4 with a finetech-brindley sacral posterior and anterior root stimulator. *Spinal Cord*, 40:272–281, 2002.

Kobayashi S., Yoshizawa H., and Yamada S. Pathology of lumbar nerve root compression part 2: morphological and immunohistochemical changes of dorsal root ganglion. *J. Orthop. Res.*, 22(1):180–188, 2004.

Kobetic R, Marsolais E.B., and Samame P. The next step: artificial walking. In Rose JamesG.G.Jessica, editor, *Inman's human walking*, pages 225–252. Williams and Wilkins, 2nd edition, 1994.

Kobetic R., Triolo R.J., Uhlir J.P., Bieri C., Wibowo M., Polando G., Marsolais E.B., Davis J.A.J., Fergusson K.A., and Sharma M. Implanted functional electrical stimulation system for mobility in paraplegia: A follow-up case report. *IEEE Trans Rehabil Eng*, 7(4):390–398, 1999.

Konno S., Olmarker K., Byrod G., Rydevik B., and Kikuchi S. Intermittent cauda equina compression: an experimental study of the porcine cauda equina with analyses of nerve impulse conduction properties. *spine*, 20(11):1223–1226, 1995a.

Konno S., Yabuki S., Sato K., Olmarker K., and Kikuchi S. A model for acute, chronic, and delayed graded compression of the dog cauda equina: presentation of the gross, microscopic, and vascular anatomy of the dog cauda equina and accuracy in pressure transmission of the compression model. *spine*, 20(24):2758–2764, 1995b.

Krabbendam A.J. Design of a de-multiplexer ic for larsi stimulator. Technical report, 1998.

Kralj A. and Bajd T. *Functional electrical stimulation: standing and walking after spinal cord injury.* 1989.

Kralj A., Bajd T., and Turk M.D. Enhancement of gait restoration in spinal injured patients by functional electrical stimulation. *Clinical Orthopaedics and Related Research*, 233(Aug):34–43, 1988.

Kralj A., Bajd T., and Turk R. Electrical stimulation providing functional use of paraplegic patient muscles. *Med. Progr. Technol.*, 7:3–9, 1980.

Kralj A., Bajd T., Turk R., and Benko H. Results of fes application to 71 SCI patients. In *RESNA 10th Annual Conference*, pages 645–647, 1987.

Kralj A. and Grobelnik S. Functional electrical stimulation - a new hope for paraplegic patients? *Bulletin on Prosthetics Research*, (Fall):75–102, 1973.

Krarup C. and Loeb G.E. Conduction studies in peripheral cat nerves using implanted electrodes: Iii. the effect of prolonged contriction on the distal nerve segment. *Muscle and Nerve*, 12(11):915–928, 1989.

Krnjevic K. The connective tissue of the frog sciatic nerve. *Q J Exp Physiol Cogn Med Sci.*, 39(1):55–72, 1954a.

Krnjevic K. Some observations on perfused frog sciatic nerves. *J. Physiol.*, 123:338–356, 1954b.

Kuffler S.W. and Williams E.M.Vaughan. Small-nerve junctional potentials, the distribution of small motor nerves to frog skeletal muscle, and the membrane characteristics of the fibres they innervate. *J. Physiol*, 121:289–317, 1953.

Kugler C., Strunk M., and Rudofsky G. Venous pressure dynamics of the healthy human leg. role of muscle activity, joint mobility and anthropometric factors. *J. Vasc. Res.*, 38(1):20–29, 2001.

Kuhfeld A. The retrospectroscope. medical electricity i: Electrostatics. *IEEE Engineering in Medicine and Biology*, pages 101–102, 1995.

Kutzenberger J., Domurath B., and Sauerwein D. Spastic bladder and spinal cord injury: seventeen years of experience with sacral deafferentation and implantation of an anterior root stimulator. *Artif. Organs*, 29(3):239–241, 2005.

Laet K.De and Wyndaele J.J. Adverse events after botulinum a toxin injection for neurogenic voiding disorders. *Spinal Cord*, 43:397–399, 2005.

Lago N., Ceballos D., Rodriguez F.J., Stieglitz T., and Navarro X. Long term assessment of axonal regeneration through polyimide regenerative electrodes to interface the peripheral nerve. *Biomaterials*, 36:2021–2031, 2005.

Lancet editorial . Phrenic nerve pacing in quadraplegia. *Lancet*, 2(I):88–90, 1990.

Langzam E., Isakov E., Nemirovsky Y., and Mizrahi J. Muscle force augmentation by low-intensity electrical stimulation. In *Proceedings of the 27th Annual International Conference of the IEEE Engineering in Medicine and Biology Society*, pages 5808–5811, 2005.

Lapicque L. *L'excitabilité en fonction du temps: la chronaxie, sa signification et sa mesure.* 1926.

Lapicque L. *La machine nerveuse.* 1943.

Larsen J.O., Thomsen M., Haugland M., and Sinkjaer T. Degeneration and regeneration in rabbit peripheral nerve with long-term nerve cuff electrode implant: A stereological study of myelinated and unmyelinated axons. *Acta Neuropathol.*, 96: 365–378, 1998.

Lee I.S., Whang C.N., Choi K., Choo M.S., and Lee Y.H. Characterization of iridium film as a stimulating neural electrode. *Biomaterials*, 23:2375–2380, 2001.

Leventhal D.K. and Durand D. Subfascicle stimulation selectivity with the flat interface nerve electrode. *Ann. Biomed. Eng.*, 31:643–652, 2003.

Leventhal D.K. and Durand D.M. Chronic measurement of the stimulation selectivity of the flat interface nerve electrode. *IEEE Trans. Biomed. Eng*, 51(9):1649–1658, 2004.

Lilly J.C. Injury and excitation by electric currents. a. the balanced pulse-pair waveform. In D.E.Sheer , editor, *Electrical Stimulation of the Brain*, book chapter 6 (A), pages 60–64. Texas Univ. Press, 1961.

Lilly J.C., Austin G.M., and Chambers W.W. Threshold movements produced by excitation of cerebral cortex and efferent fibers with some parametric regions of rectangular current pulses (cats and monkeys). *Journal of Neurophysiology*, 15(4):319–341, 1952.

Lilly J.C., Hughes J.R., Alvord E.C., and Galkin T.W. Brief, noninjurious electric waveform for stimulation of the brain. *Science.*, 121:468–469, 1955.

Lim P.A. and Tow A.M. Recovery and regeneration after spinal cord injury: a review and summary of recent literature. *Ann. Acad. Med. Singapore*, 36(1):49–57, 2007.

Lind B., Massie J.B., Lincoln T., Myers R.R., Swenson M.R., and Garfin S.R. The effects of induced hypertension and acute graded compression on impulse propagation in the spinal nerve roots of the pig. *spine*, 18(11):1550–1555, 1993.

Lindwall . *Nature*, 2006.

Livshits A., Catz A., Folman Y., Witz M., Livshits V., Baskov A., and Gepstein R. Reinnervation of the neurogenic bladder in the late period of the spinal cord trauma. *Spinal Cord.*, 42(4):211–217, 2004.

Livshitz L.M., Einziger P.D., and Mizrahi J. Current distribution in skeletal muscle activated by functional electrical stimulation: Image-series formulation and isometric recruitment curve. *Ann. Biomed. Eng.*, 28:1218–1228, 2000.

Loeb G.E. and Peck R.A. Cuff electrodes for chronic stimulation and recording of peripheral nerve activity. *J. Neurosci. Methods*, 64:95–103, 1996.

Loeb G.E., Peck R.A., Moore W.H., and Hood K. Bion system for distributed neural prosthetic interfaces. *Med. Eng Phys.*, 23(1):9–18, 2001.

Luff A.R., Hatcher D.D., and Torkko K. Enlarged motor units resulting from partial denervation of cat hindlimb muscles. *J. Neurophysiol.*, 59(5):1377–1394, 1988.

Lundborg G. Structure and function of the intraneural microvessels as related to trauma, edema formation, and nerve function. *J. Bone Joint Surg. Am.*, 57(7):938–948, 1975.

Lundborg G. and Dahlin L.B. The pathophysiology of nerve compression. *Hand Clin.*, 8(2):215–227, 1992.

Lundborg G., Gelberman R.H., Minteer-Convery M., Lee Y.F., and Hargens A.R. Median nerve compression in the carpal tunnel: functional response to experimentally induced controlled pressure. *J. Hand Surg. [Am.]*, 7(3):252–259, 1982.

Lundborg G., Myers R., and Powell H. Nerve compression injury and increased endoneurial fluid pressure: a "miniature compartment syndrome". *J. Neurol. Neurosurg. Psychiatry*, 46(12):1119–1124, 1983.

Lussier J.J. and Rushton W.A.H. The relation between the space constant and conduction velocity in nerve fibres of the a group from the frog's sciatic. *J. Physiol.*, 114 (3):399–409, 1951.

Macgregor R.J., Sharpless S.K., and Luttges M.W. A pressure vessel model for nerve compression. *J. Neurol. Sci.*, 24(3):299–304, 1975.

Mackinnon S.E., Dellon A.L., Hudson A.R., and Hunter D.A. Chronic nerve compression - an experimental model in the rat. *Annals of Plastic Surgery*, 13(2):112–120, 1984.

Macpherson G., editor. *Black's Medical Dictionary*. A and C Black, London, 38 edition, 1995.

Maghribi M., Hamilton J., Polla D., Rose K., Wilson T., and Krulevitch P. Stretchable micro-electrode array. *Processdings of the 2nd Annual International IEEE-EMBS Special Topic Conference on Microtechnology in Medicine and Biology*, pages 80–83, 2002.

Mandel M.J., Greene R.W., Sapirstein L.A., and Ogden E. Reduction of mean arterial pressure in dogs with chronic hypertension by pentobarbital. *Am. J. Physiol*, 176(2): 352–354, 1954.

Mao G.P., Konno S., Arai I., Olmarker K., and Kikuchi S. Chronic double-level cauda equina compression: an experimental study on the dog cauda equina with analyses of nerve conduction velocity. *spine*, 23(15):1641–1644, 1998.

Marsolais E.B. and Kobetic R. Functional walking in paralyzed patients by means of electrical stimulation. *Clinical Orthopaedics and Related Research*, No. 175:30–36, 1983.

Marsolais E.B. and Kobetic R. Implantation techniques and experiences with percutaneous intramuscular electrodes in the lower extremities. Technical Report MSL4 (V.2), 1986.

Marsolais E.B. and Kobetic R. Functional electrical stimulation for walking in paraplegia. *Journal of Bone and Joint Surgery - American*, 69-A(5):728–733, 1987.

Marsolais E.B. and Kobetic R. Development of a practical electrical stimulation system for restoring gait in the paralyzed patient. *Clinical Orthopaedics and Related Research*, 233:64–74, 1988.

Mathers L.H. *The Peripheral Nervous System: Structure, Function and Clinical Correlations*. Addison-Wesley, 1985.

Matjacic Z., Hunt K., Gollee H., and Sinkjaer T. Control of posture with fes systems. *Med. Eng Phys.*, 25(1):51–62, 2003.

Matsui H., Kanamori M., Kawaguchi Y., Kitagawa H., Nakamura H., and Tsuji H. Clinical and electrophysiologic characteristics of compressed lumbar nerve roots. *spine*, 22(18):2100–2105, 1997.

Matsui H., Olmarker K., Cornefjord M., Takahashi K., and Rydevik B. Local electrophysiologic stimulation in experimental double level cauda equina compression. *spine*, 17(9):1075–1078, 1992.

Mayr W., Bijak M., Rafolt D., Sauermann S., Unger E., and Lanmuller H. Basic design and construction of the vienna fes implants: existing solutions and prospects for new generations of implants. *Med. Eng Phys.*, 23(1):53–60, 2001.

McArdle W.D., Katch F.I., and Katch V.I. *Exercise physiology: energy, nutrition, and human performance*. Williams and Wilkins, 4th edition, 1996.

McCouch G.P. Comments on regeneration of functional connections. In Windle W.F., editor, *Regeneration in the central nervous system*, book chapter XVI, pages 171–180. 1955.

McCreery D.B. Tissue reactions to electrodes: the problem of safe and effective stimulation of neural tissue. In Horch K.W. and Dhillon G.S., editors, *Neuroprosthetics, theory and practice*, Bioengineering and Biomedical Engineering - Vol 2, book chapter 3.4, pages 592–607. World Scientific Publishing Co. Pte. Ltd., 1 edition, 2004.

McCreery D.B., Agnew W.F., and Hardy J.Mc. Electrical characteristics of chronically implanted platinum- iridium electrodes. *IEEE Trans Biomed Eng*, 34, No. 9:664–668, 1987.

McCreery D.B., Agnew W.F., Yuen T.G., and Bullara L.A. Charge density and charge per phase as cofactors in neural injury induced by electrical stimulation. *IEEE Trans Biomed Eng*, 37(10):996–1001, 1990.

McCreery D.B., Agnew W.F., Yuen T.G., and Bullara L.A. Damage in peripheral nerve from continuous electrical stimulation: Comparison of two stimulus waveforms. *Med. Biol. Eng. Comput.*, 30:109–114, 1992.

McCreery D.B., Pikov V., Lossinsky A.S., Bullara L.A., and Agnew W.F. Arrays for chronic functional microstimulation of the lumbosacral spinal cord. *IEEE Trans. Neural Syst. Rehabil. Eng.*, 12(2):195–207, 2004.

McDonald J.W., Becker D., Sadowsky C.L., J. A. Jane Sr., Conturo T.E., and Schultz L.M. Late recovery following spinal cord injury. case report and review of the literature. *J. Neurosurgery (spine)*, 97(2):252–265, 2002.

McDonald J.W. and Sadowsky C. Spinal-cord injury. *Lancet*, 359(9304):417–425, 2002.

McHardy J., Robblee L.S., Marston J.M., and Brummer S.B. Electrical stimulation with pt electrodes. iv - factors influencing pt dissolution in inorganic saline. *Biomaterials*, 1(July):129–134, 1980.

McIntyre C.C., Richardson A.G., and Grill W.M. Modeling the excitability of mammalian nerve fibers: influence of afterpotentials on the recovery cycle. *J. Neurophysiol.*, 87(2):995–1006, 2002.

McKinley W.O., Seel R.T., Gadi R.K., and Tewksbury M.A. Nontraumatic vs. traumatic spinal cord injury: a rehabilitation outcome comparison. *Am. J. Phys. Med. Rehab.*, 80:693–699, 2001.

McNeal D.R. Analysis of a model for excitation of myelinated nerve. *IEEE Trans Biomed Eng*, Vol. BME-23(No. 4):329–337, 1976.

McNeal D.R. and Apkarian A.V. Analytical design of a cuff electrode. *Advances in External Control of Human Extremities*, pages 45–54, 1978.

McNeal D.R., Baker L.L., and Symons J. recruitment characteristics of nerve cuff electrodes and their implications for stimulator design. *Advances in External Control of Human Extremities*, IX:15–25, 1987.

McNeal D.R. and Bowmann B.R. Selective activation of muscles using peripheral nerve electrodes. *Med. Biol. Eng. Comput.*, 23:249–253, 1985.

McNeal D.R., Waters R., and Reswick J. Experience with implanted electrodes. *Neurosurgery*, 1(2):228–229, 1977.

Merrill D.R., Bikson M., and Jefferys J.G.R. Electrical stimulatio of excitable tissue: design of efficacious and safe protocols. *J. Neurosci. Methods*, 141:171–198, 2005.

Mettler F.A. and Liss H. Functional recovery in primates after large subtotal spinal cord lesions. *journal of neuropathology and experimental neurology*, 18:509–516, 1959.

Miller C.A., Abbas P.J., Nourski K.V., Hu N., and Robinson B.K. Electrode configuration influences action potential initiation site and ensemble stochastic response properties. *Hear. Res.*, 175(1-2):200–214, 2003.

Mino H. and Grill W.M. Modeling of mammalian myelinated nerve with stochastic sodium ionic channels. In *Proceedings of the 22nd Annual International Conference of the IEEE Engineering in Medicine and Biology Society*, pages 915–917, 2000.

Moffitt M.A., McIntyre C.C., and Grill W.M. Prediction of myelinated nerve fibre stimulation thesholds: Limitations of linear models. *IEEE Trans Biomed Eng*, 51 (2):229–236, 2004.

Monroe M.B., Tataranni P.A., Pratley R., Manore M.M., Skinner J.S., and Ravussin E. Lower daily energy expenditure as measured by a respiratory chamber in subjects with spinal cord injury compared with control subjects. *Am. J. Clin. Nutr.*, 68(6): 1223–1227, 1998.

Moore B. In memory of sidney ringer [1835-1910]. *Biochemical Journal*, 5(6-7): i.b3–xix, 1911.

Mortimer J.T. Electrical excitation of nerve. In Agnew W.F. and McCreery D.B., editors, *Neural Prostheses: Fundamental Studies*, book chapter 3, pages 68–83. 1990.

Mortimer J.T. Electrodes for functional electrical stimulation. Technical Report 8, 1998.

Mortimer J.T. Electrodes for functional electrical stimulation. Technical Report NO1-NS-6-2346, 2000.

Mortimer J.T. and Kaufman J. Intramuscular electrical stimulation: tissue damage. *Ann. Biomed. Eng.*, 8:235–244, 1980.

Mortimer J.T. and Peckham P.H. Intramuscular electrical stimulation. 1990.

Moynahan M., Mullin C., Cohn J., Burns C.A., Halden E.E., Triolo R.J., and Betz R.R. Home use of a functional electrical stimulation system for standing and mobility in adolescents with spinal cord injury. *Archives. of Physical. Medicine and Rehabilitation*, 77(10):1005–1013, 1996.

Mushawar V.K. and Horch K.W. Selective activation of muscle groups in the feline hindlimb through electrical microstimulation of the ventral lumbo-sacral spinal cord. *IEEE Trans Rehabil Eng*, 8(1):11–21, 2000.

Naples G.G., Mortimer J.T., Scheiner A., and Sweeney J.D. A spiral nerve cuff electrode for peripheral nerve stimulation. *IEEE Trans Biomed Eng*, 35(11):905–916, 1988.

Naples G.G., Mortimer J.T., and Yuen T.G. Overview of peripheral nerve electrode design and implementation. In Agnew W.F. and McCreery D.B., editors, *Neural Prostheses*, book chapter 5, pages 107–146. Prentice-Hall, 1 edition, 1990.

Nash M.S. and Gater D.R. Exercise to reduce obesity in SCI. *Topics in Spinal Cord Injury Rehabilitation*, 12(4):76–93, 2007.

Nash M.S., Jacobs PatrickL., Montalvo B.M., Klose K.J., Guest RosalindS., and Needham-Shropshire BelindaM. Evaluation of a training program for persons with SCI paraplegia using the parastep1 ambulation system: Part 5. lower extremity blood flow and hyperemic responses to occlusion are augmented by ambulation training,. *Arch. Phys. Med. Rehabil.*, 78(8):808–814, 1997.

Navarro X., Verdu E., and Buti M. Comparison of regenerative and reinnervating capabilities of different functional types of nerve fibers. *Exp. Neurol.*, 129(2):217–224, 1994.

Newham D.J. and Donaldson N. d. N. Fes cycling. *Acta Neurochir. Suppl*, 97(1): 395–402, 2007.

Noback C.R., Strominger N.L., Demarest R.J., and Ruggiero D.A. *The Human Nervous System Structure and Function*. Humana Press, 6th edition, 2005.

Norton J., Donaldson N. de N., Day B.L., Dekker L., Perkins T.A., Wood D.E., McFadden C., and Tromans A.M. The determinants of posture in paraplegics standing using lumbar anterior root stimulation. In *Proceedings of the 5th Annual Conference of the International Functional Electrical Stimulation Society*, pages 478–481, 2000.

O'Connor P.J. Forecasting of spinal cord injury annual case numbers in australia. *Arch. Phys. Med. Rehabil.*, 86(Jan):48–51, 2005a.

O'Connor P.J. Survival after spinal cord injury in australia. *Arch. Phys. Med. Rehabil.*, 86(Jan):37–47, 2005b.

Olmarker K. Spinal nerve root compression: nutrition and function of the porcine cauda equina compressed in vivo. *Acta Orthop. Scand. Suppl*, 242:1–27, 1991.

Olmarker K., Holm S., Rosenqvist A.L., and Rydevik B. Experimental nerve root compression: a model of acute, graded compression of the porcine cauda equina and an analysis of neural and vascular anatomy. *spine*, 16(1):61–69, 1991.

Olmarker K., Holm S., and Rydevik B. Importance of compression onset rate for the degree of impairment of impulse propagation in experimental compression injury of the porcine cauda equina. *spine*, 15(5):416–419, 1990a.

Olmarker K., Rydevik B., Hansson T., and Holm S. Compression-induced changes of the nutritional supply to the porcine cauda equina. *J. Spinal Disord.*, 3(1):25–29, 1990b.

Olmarker K., Rydevik B., and Holm S. Edema formation in spinal nerve roots induced by experimental, graded compression: an experimental study on the pig cauda equina with special reference to differences in effects between rapid and slow onset of compression. *spine*, 14(6):569–573, 1989a.

Olmarker K., Rydevik B., Holm S., and Bagge U. Effects of experimental graded compression on blood flow in spinal nerve roots: a vital microscopic study on the porcine cauda equina. *J. Orthop. Res.*, 7(6):817–823, 1989b.

Ooyama H. and Wright E.B. Anode break excitation on single ranvier node of frog nerve. *Am. J. Physiol*, 200:209–218, 1961.

Oozeer M., Veraart C., Legat V., and Delbeke J. A model of the mammalian optic nerve fibre based on experimental data. *Vision Research*, 46:2513–2524, 2006.

Otani K., Kayama S., Mao G.P., Konno S., Sato K., Olmarker K., and Kikuchi S. Tolerance to acute compression injury and recovery of nerve function in chronically compressed spinal nerve roots: Experimental study. *J. Orthop. Sci.*, 2(4):266–270, 1997.

Otani K., Kikuchi S., Konno S., and Olmarker K. Blood flow measurement in experimental chronic cauda equina compression in dogs: changes in blood flow at various conditions. *J. Spinal Disord.*, 14(4):343–346, 2001.

Pacemaker Club, online . Frequently asked question page, last accessed in 2007. `http://www.pacemakerclub.com`.

Parent A. *Human neuroanatomy*. 9th edition, 1995.

Parke W.W., Gammell K., and Rothman R.H. Arterial vascularization of the cauda equina. *J. Bone Joint Surg. Am.*, 63(1):53–62, 1981.

Parke W.W., Settles H.E., Bunger P.C., Whalen J.L., and Said S. Lumbosacral anterolateral spinal arteries and brief review of "accessory" longitudinal arteries of the spinal cord. *Clin. Anat.*, 12(3):171–178, 1999.

Parke W.W. and Watanabe R. The intrinsic vasculature of the lumbosacral spinal nerve roots. *spine*, 10(6):508–515, 1985.

Parker G.H. The progressive degeneration of frog nerve. *Am. J. Physiol*, 106:398–403, 1933.

Peckham P.H. Principles of electrical stimulation. *Topics in Spinal Cord Injury Rehabilitation*, 5(1):1–5, 1999.

Pedowitz R.A., Garfin S.R., Massie J.B., Hargens A.R., Swenson M.R., Myers R.R., and Rydevik B.L. Effects of magnitude and duration of compression on spinal nerve root conduction. *spine*, 17(2):194–199, 1992.

Perkins T.A. Versatile three-channel stimulation controller for restoration of bladder function in paraplegia. *J. Biomed. Eng.*, 8(3):268–271, 1986.

Perkins T.A. Impedance of common surface stimulation electrodes. In *Proceedings of the 9th Annual Conference of the International Functional Electrical Stimulation Society*, pages 419–421, Sept 2004.

Perkins T.A., Donaldson N. de N., Dunkerley A.L., Hatcher N.A.C., Tromans A.M., and Wood D.E. Development of paraplegic leg powered cycling with the lumbosacral anterior root stimulator implant. *Proceedings of the 4th Annual Conference of the International Functional Electrical Stimulation Society*, pages 139–142, 2002a.

Perkins T.A., Donaldson N. de N., Fitzwater R., Phillips G.F., and Wood D.E. Leg powered paraplegic cycling system using surface functional electrical stimulation. In *Proceedings of the 7th Vienna International Workshop on Functional Electrical Stimulation*, 2001.

Perkins T.A., Hatcher N.A., Swain I.D., and Wood D.E. Control of leg-powered paraplegic cycling using stimulation of the lumbo-sacral anterior spinal nerve roots. *IEEE Trans. Neural Syst. Rehabil. Eng.*, 10(3):158–164, 2002b.

Peters K.M., Feber K.M., and Bennett R.C. Sacral versus pudendal nerve stimulation for voiding dysfunction: A prospective, single-blinded, randomized, crossover trial. *Neurourology and Urodynamics*, 24:643–647, 2005.

Petrofsky J.S. Sequential motor unit stimulation through peripheral motor nerves in the cat. *Med. Biol. Eng. Comput.*, 17:87–93, 1979.

Petrofsky J.S. and Phillips C.A. Impact of recruitment order on electrode design for neural prosthetics of skeletal muscle. *Am. J. Phys. Med.*, 60, No.5:243–253, 1981.

Phillips L.H., Park T.S., Shaffrey M.E., and Shaffrey C.L. Electrophysiological evidence for afferent nerve fibers in human ventral roots. *Muscle Nerve*, 23(3):410–415, 2000.

Pickett W., Simpson K., Walker J., and Brison R. Traumatic spinal cord injury in Ontario, Canada. *The journal of Trauma, Injury, Infection and Critical Care*, 55(6): 1070–1076, 2003.

Pollack G.H. *Cells, Gels and the engines of life*. Ebner and Sons, 2001.

Popovic D., Radulovic M., Schwirtlich L., and Jaukovic N. Automatic vs hand-controlled walking of paraplegics. *Medical Engineering and Physics*, (25):63–73, 2003.

Popovic D.B., Stein R.B., Jovanovic K.L., Dai R., Kostov A., and Armstrong W.W. Sensory nerve recording for closed-loop control to restore motor functions. *IEEE Trans Biomed Eng*, 40(10):1024–1031, 1993.

Potter D. Neuroprosthesis for ventilatory support. In Brindley G.S. and Rushton D.N., editors, *Neuroprostheses*, number 1 vol 4 in Bailliere's Clinical Neurology, book chapter 6, pages 77–94. 1995.

Previnaire J.G., Soler J.M., Perrigot M., Boileau G., Delahaye H., Schumacker P., Vanvelcenaher J., and Vanhee J.L. Short-term effect of pudendal nerve electrical stimulation on detrusor hyperreflexia in spinal cord injury patients: importance of current strength. *Paraplegia*, 34(2):95–99, 1996.

Priebe M.M., Chiodo A.E., Scelza W.M., Kirshblum S.C., Wuermser L.A., and Ho C.H. Spinal cord injury medicine. 6. economic and societal issues in spinal cord injury. *Arch. Phys. Med. Rehabil.*, 88(3 Suppl 1):S84–S88, 2007.

Ramon y Cajal . *Cajal's degeneration and regeneration of the nervous system. Translated by R.M.May*. 1991 translation.

Rashbass C. and Rushton W.A.H. The relation of structure to the spread of excitation in the frog's sciatic trunk. *J. Physiol.*, 110(1-2):110–135, 1949a.

Rashbass C. and Rushton W.A.H. Space distribution of excitability in the frog's sciatic nerve stimulated by slot electrodes. *Journal of Physiology*, 109:327–342, 1949b.

Raso V.V.Monte, Barbieri C.H., Mazzer N., and Fasan V.S. Can therapeutic ultrasound influence the regeneration of peripheral nerves? *J. Neurosci. Methods*, 142:185–192, 2005.

Ratner B.D. and Bryant S.J. Biomaterials: where we have been going and where we are going. *Annual Review of Biomedical Engineering*, 6:41–75, 2004.

Rattay F. Analysis of models for external stimulation of axons. *IEEE Trans Biomed Eng*, 33(10):974–977, 1986.

Rattay F. Analysis of models for extracellular fiber stimulation. *IEEE Trans Biomed Eng*, 36(7):676–682, 1989.

Rattay F. Analysis of the electrical excitation of cns neurons. *IEEE Trans Biomed Eng*, 45(6):766–772, 1998.

Rattay F. The basic mechanism for the electrical stimulation of the nervous system. *Neuroscience*, 89(2):335–346, 1999.

Rattay F. and Aberham M. Modeling axon membranes for functional electrical stimulation. *IEEE Trans Biomed Eng*, 40(12):1201–1209, 1993.

Rattay F., Minassian K., and Dimitrijevic M.R. Epidural electrical stimulation of posterior structures of the human lumbosacral cord: 2. quantitative analysis by computer modeling. *Spinal Cord*, 38(8):473–489, 2000.

Rattay F. and Resatz S. Effective electrode configuration for selective stimulation with inner eye prostheses. *IEEE Trans Biomed Eng*, 51(9):1659–1664, 2004.

RDS, online . Understanding animal research in medicine: Spinal cord injury, last accessed in November 2006. `http://www.rds-online.org.uk/pages/page.asp?i_PageID=145&i_ToolbarID=3`.

Reichel M., Breyer T., Mayr W., and Rattay F. Simulation of the three-dimensional electrical field in the course of functional electrical stimulation. *Artif. Organs*, 26 (3):252–255, 2002.

Rijkhoff N.J.M., Holsheimer J., Koldewijn E.L., Struijk J.J., van Kerrebroeck P.E.V., Debruyne F.M.J., and Wijkstra H. Selective stimulation of sacral nerve roots for bladder control: A study by computer modeling. *IEEE Trans Biomed Eng*, 41(5): 413–424, 1994a.

Rijkhoff N.J.M., Koldewijn E.L., van Kerrebroeck P.E.V., Debruyne F.M.J., and Wijkstra H. Acute animal studies on the use of an anodal block to reduce urethral resistance in sacral root stimulation. *IEEE Trans Rehabil Eng*, 2(2):92–99, 1994b.

Rijkhoff N.J.M. and Sinkjaer T. Orderly recruitment of motorneurons in an acute rabbit model. *Proceedings of the 21th Annual International Conference of the IEEE Engineering in Medicine and Biology Society*, 20(5):2564–2565, 1998.

Robblee L.S., McHardy J., Agnew W.F., and Bullara L.A. Electrical simulation with pt electrodes. vii. dissolution of pt electrodes during electrical stimulation of the cat celebral cortex. *J. Neurosci. Methods*, 9:301–308, 1983.

Robblee L.S., McHardy J., Marston J.M., and Brummer S.B. Electrical stimulation with pt electrodes. v - the effect of protein on pt dissolution. *Biomaterials*, 1:135–139, 1980.

Rodriguez F.J., Ceballos D., Schuettler M., Valderrama E., Stieglitz T., and Navarro X. Polyimide cuff electrodes for peripheral nerve stimulation. *J. Neurosci. Methods*, 98:105–118, 2000.

Romero E., Denef J.F., Delbeke J., Robert A., and Veraart C. Neural morphological effects of long-term implantation of the self-sizing spiral cuff nerve electrode. *Med. Biol. Eng. Comput.*, 39(1):90–100, 2001.

Roth B.J. Mechanisms for electrical stimulation of excitable tissue. *Crit. Rev. Biomed. Eng.*, 22(3/4):253–305, 1994.

Rozman J. and Trlep M. Multielectrode spiral cuff for selective stimulation of nerve fibres. *Journal of Medical Engineering and Technology*, 16(5):194–203, 1992.

Rubinstein J.T., Miller C.A., Mino H., and Abbas P.J. Analysis of monophasic and biphasic electrical stimulation of nerve. *IEEE Trans Biomed Eng*, 48(10):1065–1070, 2001.

Rushton D.N. Choice of nerve routes for multichannel leg controler implant. *Advances in External Control of Human Extremities*, pages 99–108, 1990.

Rushton D.N. Functional electrical stimulation. *Physiol Meas.*, 18(4):241–275, 1997.

Rushton D.N. Functional electrical stimulation and rehabilitation–an hypothesis. *Med. Eng Phys.*, 25(1):75–78, 2003.

Rushton D.N., Barr F.M., Donaldson N. de N., Harper V.J., Perkins T.A., Taylor P.N., and Tromans A.M. Selecting candidates for a lower limb stimulator implant programme: a patient-centred method. *Spinal Cord.*, 36(5):303–309, 1998.

Rushton W.A.H. The effect upon the threshold for nervous excitation of the length of nerve exposed and the angle between current and nerve. *Journal of Physiology*, 67: 357–377, 1927.

Rushton W.A.H. Excitation of bent nerve. *J. Physiol.*, 65(2):173–190, 1928a.

Rushton W.A.H. Nerve excitation by multipolar electrodes. *J. Physiol.*, 66(3):217–230, 1928b.

Rushton W.A.H. Lapicque's canonical strength duration curve. *J. Physiol.*, 74(4): 424–440, 1932.

Rushton W.A.H. The site of excitation in the nerve trunk of the frog. *Journal of Physiology*, 109:314–326, 1949.

Rushton W.A.H. A theory of the effects of fibre size in medullated nerve. *J. Physiol.*, 115(1):101–122, 1951.

Rydevik B., Holm S., Brown M.D., and Lundborg G. Diffusion from the cerebrospinal fluid as a nutritional pathway for spinal nerve roots. *Acta Physiol Scand.*, 138(2): 247–248, 1990.

Rydevik B., Lundborg G., and Bagge U. Effects of graded compression on intraneural blood flow: an in vivo study on rabbit tibial nerve. *J. Hand Surg. [Am.]*, 6(1):3–12, 1981.

Rydevik B., Pedowitz R., Hargens A., Swenson M.R., Myers R.R., and Garfin S.R. Effects of acute, graded compression on spinal nerve root function and structure. an experimental study of the pig cauda equina. *spine*, 16(5):487–493, 1991.

Rydevik B.L., Lundborg G., and Skalak R. Biomechanics of peripheral nerves. In Nordin M. and Frankel V.H., editors, *Basic biomechanics of the musculoskeletal system*, book chapter 4, pages 75–87. Lea and Febiger, second edition, 1989.

Sabah N.H. Aspects of nerve conduction. *IEEE Eng Med. Biol. Mag.*, 19(6):111–118, 2000.

Sadowsky C., Volshteyn O., Schultz L., and McDonald J.W. Spinal cord injury. *Disabil. Rehabil.*, 24(13):680–687, 2002.

Sassen M. and Zimmermann M. Differential blocking of myelinated nerve fibres by transient depolarization. *Pflgers. Arch.*, 341:179–195, 1973.

Sauerwein D., Ingunza W., Fischer J., Madersbacher H., Polkey C.E., Brindley G.S., Colombel P., and Teddy P. Extradural implantation of sacral anterior root stimulators. *Jounal of Neurology, Neurosurgery and Psychiatry*, 53:681–684, 1990.

Schalow G. Impulse pattern, innervation density and two point discrimination of skin and mucosal afferents in humans. considerations for a sensory reinnervation of urinary bladder and anal canal in spinal cord lessions. iv (iv). *Electromyography and clinical neurophysiology*, 32:259–285, 1992.

Schalow G. and Zach G.A. *Spinal Locomotion: a New Approach to HUman Neurophysiology and Treatment in Spinal Cord Lesion Original research based on new human measurements with basic methods.* General Physiological Biophysics, supplement, 15. 1996.

Schalow G., Zach G.A., and Warzok R. Classification of human peripheral nerve fibre groups by conduction velocity and nerve diameters is preserved following spinal cord lesion. *Journal of the Autonomic Nervous System*, 52:125–150, 1995.

Schuettler M. Grundlagen der nervenelektrode. In *Dreidimensionale Formgebung von planaren Mikroelectroden zur Optimierung der Signalableitung und Stimulation am peripheren Nerven*, book chapter 4, pages 24–34. Fraunhofer IRB Verlag, 2002.

Schuettler M., Stieglitz T., Gross M., Altpeter D., Staiger A., and Katzenberg F. Reducing stiffness and electrical losses of high channel hybrid nerve cuff electrodes. *Proceedings of the 23th Annual International Conference of the IEEE Engineering in Medicine and Biology Society*, 2001.

Schwab M.E. Repairing the injured spinal cord. *Science.*, 295(5557):1029–1031, 2002.

Schwarz J.R. *Pflgers. Arch.*, 430:283–292, 1995.

Scremin E.A.M., Kurta Lyvia, Gentili Amilcare, Wiseman Barbara, Perell Karen, Kunkel Charles, and Scremin OscarU. Increasing muscle mass in spinal cord injured persons with a functional electrical stimulation exercise program. *Archives. of Physical. Medicine and Rehabilitation*, 80(12):1531–1536, 1999.

Sears W.G. The circulatory system. In *Anatomy and physiology for nurses*, book chapter 5, pages 114–151. Edward Arnold, 3 edition, 1959.

Seif C., Braun P.M., Bross S., Scheepe J.R., Wei J, Schumacher S., Zendler S., Alken P., and Jnemann K.P. Selective block of urethral sphincter contraction using a mocified brindley electrode in sacral anterior root stimulation of the dog. *Neurourology and Urodynamics*, 21:502–510, 2002.

Seil F.J. *Nerve, Organ, and Tissue Regeneration: Research Perespectives.* New-York, 1983.

Shaker H.S., Tu L.M., Robin S., Arabi K., Hassouna M., Sawan M., and Elhilali M.M. Reduction of bladder outlet resistance by selective sacral root stimulation using high-frequency blockade in dogs: an acute study. *Journal of Urology*, 160(3 Pt 1):901–907, 1998.

Sharma M., Marsolais E.B., Polando G., Triolo R.J., Davis J.A.J., and Uhlir J.P. Implantation of a 16-channel functional electrical stimulation walking system. *Clinical Orthopaedics and Related Research*, 1(347):236–242, 1998.

Sharpless S.K. Susceptibility of spinal roots to compression block. *The Research Status of Spinal Manipulative Therapy.*, NINCDS monograph 15:155–161, 1975.

Shen Q., Jiang D., and Tai C. Selective stimulation of smaller nerve fibers using biphasic rectangular pulses. *Front Med. Biol. Eng*, 10(4):319–335, 2001.

Sin W.K. and Coburn B. Electrical stimulation of the spinal cord: a further analysis relating to anatomical factors and tissue properties. *Med. Biol. Eng. Comput.*, 21(3): 264–269, 1983.

Sinkjaer T., Haugland M., Inmann A, Hansen M., and Nielsen K.D. Biopotentials as command and feedback signals in functional electrical stimulation systems. *Medical Engineering and Physics*, (25):29–40, 2003.

Smit J.P.A., Rutten W.L.C., and Boom H.B.K. Endoneural selective stimulating using wire-microelectrode arrays. *IEEE Trans Rehabil. Eng*, 7(4):399–412, 1999.

Smith A.C., Spinale F.G., and Swindle M.M. Cardiac function and morphology of hanford miniature swine and yucatan miniature and micro swine. *Lab Anim Sci.*, 40 (1):47–50, 1990.

Solandt D.Y. The measurement of "accommodation" in nerve. *Proceeding of the Royal Society of London, Series B, Biological Sciences*, 119(814):355–379, 1936.

Sollmann T. Survival of excitability of frog muscle, nerve and reflexes after somatic death. *Am. J. Physiol*, 148(2):299–301, 1947.

Solomonow M. Fatigue optimal selective electroblock parameters in the linear control of paralyzed muscle force. *Advances in External Control of Human Extremities*, 7: 139–144, 1981.

Solomonow M., Eldred E., Lyman J., and Foster J. A new technique for functional neuromuscular stimulation. *Advances in External Control of Human Extremities*, 6: 47–62, 1978.

Solomonow M., Shoji H., King A., and D'Ambrosia R. Synthetic proprioceptive feedback of recruitment forces in the electrically stimulated muscle. *Advances in External Control of Human Extremities*, 8:391–401, 1984.

Spinal Injuries Association, online . What is SCI?, last accessed in April 2007. `www.spinal.co.uk`.

Stampfli R. Saltatory conduction in nerve. *Physiological Reviews*, 34:101–112, 1954.

Stanic U. History of functional electrical stimulation. *Proceedings of the 3rd Annual Conference of the International Functional Electrical Stimulation Society*, CD ROM, 1998.

Steeves J.D. and Wolfram T. Engines, accelerators, and brakes on functional spinal cord repair. *Ann NY Acad Sci*, 860:412–424, 1998.

Stefanovska A., Vodovnik L., Gros N., Rebersek S., and Acimoviz-Janezic R. Fes and spasticity. *IEEE Trans Biomed Eng*, 36(7):738–745, 1989.

Stegeman D.F. and Weerd J.P.C.De. Modelling compound action potentials of peripheral nerves in situ. i.model description; evidence for a non-linear relation between fibre diameter and velocity. *Electroencephalogr. Clin. Neurophysiol.*, 54:436–448, 1982.

Stein R.B., Nichols T.R., Jhamandas J., Davis L., and Charles D. Stable long-term recordings from cat peripheral nerves. *Brain Res.*, 128:21–38, 1977.

Stieglitz T. Considerations on surface and structural biocompatibility as prerequisite for long-term stability of neural prostheses. *Journal of Nanoscience and Nanotechnology*, 4(5):469–503, 2004.

Stieglitz T., Schumacher S., Seif C., Bross S., Junemann K.P., and Meyer J.U. Selective activation of the bladder with quasi-trapezoidal pulses in sacral anterior root stimulation in the dog. *Biomed Tech. (Berl.)*, 42 Suppl:492-3:492–493, 1997.

Stone R.J. and Stone J.A. *Atlas of the skeletal muscles*. Wm. C. Brown Publishers, 1990.

Stoney S.D. and Machne X. Mechanisms of accommodation in different types of frog neurons. *J. Gen. Physiol*, 53(2):248–262, 1969.

Struijk J.J. The extracellular potential of a myelinated nerve fiber in an unbounded medium and in nerve cuff models. *Biophys. J.*, 72(6):2457–2469, 1997.

Struijk J.J., Holsheimer H., Veen B.K.Van, and Boom H.B.K. Epidural spinal cord stimulation: Calculation of field potential with special reference to dorsal column nerve fibers. *IEEE Trans Biomed Eng*, 38(1):104–110, 1991.

Struijk J.J., Holsheimer J., and Boom H.B. Excitation of dorsal root fibers in spinal cord stimulation: a theoretical study. *IEEE Trans Biomed Eng*, 40(7):632–639, 1993.

Struijk J.J., Holsheimer J., Spincemaille GH, Gielen F.L., and Hoekema R. Theoretical performance and clinical evaluation of transverse tripolar spinal cord stimulation. *IEEE Trans Rehabil Eng*, 6(3):277–285, 1998.

Struijk J.J., Thomsen M., Larsen J.O., and Sinkjaer T. Cuff electrodes for long-term recording of natural sensory information. *IEEE Engineering in Medicine and Biology*, (May/June):91–98, 1999.

Swadlow H.A. and Waxman S.G. Observations on impulse conduction along central axons. *Proc Natl Acad Sci U S A.*, 72(12):5156–5159, 1975.

Sweeney J.D., Deng K., Warman E., and Mortimer J.T. Modeling of electric field effect on the excitability of myelinated motor nerve. *IEEE Engineering in Medicine and Biology Society 11th Annual International Conference*, pages 1281–1282, 1989.

Sweeney J.D., Mortimer J.T., and Durand D. Modeling of mammalian myelinated nerve for functional neuromuscular stimulation. *Proceedings of the 9th Annual International Conference of the IEEE Engineering in Medicine and Biology Society*, 1987.

Tai C. and Jiang D. Selective stimulation of smaller fibers in a compound nerve trunk with single cathode by rectangular current pulses. *IEEE Trans Biomed Eng*, 41(3): 286–291, 1994.

Takahashi K., Olmarker K., Holm S., Porter R.W., and Rydevik B. Double-level cauda equina compression: an experimental study with continuous monitoring of intraneural blood flow in the porcine cauda equina. *J. Orthop. Res.*, 11(1):104–109, 1993.

Takahashi K., Shima I., and Porter R.W. Nerve root pressure in lumbar disc herniation. *spine*, 24(19):2003–2006, 1999.

Takahashi N., Yabuki S., Aoki Y., and Kikuchi S. Pathomechanisms of nerve root injury caused by disc herniation: an experimental study of mechanical compression and chemical irritation. *spine*, 28(5):435–441, 2003.

Tarler M.D. and Mortimer J.T. Comparison of joint torque evoked with monopolar and tripolar-cuff electrodes. *IEEE Trans. Neural Syst. Rehabil. Eng.*, 11(3):227–235, 2003.

Tasaki I. *Physiology and Electrochemistry of Nerve Fibers*, volume 3. 1982.

Tator C.H. and Koyanagi I. Vascular mechanisms in the pathophysiology of human spinal cord injury. *J. Neurosurg.*, 2006.

Teeter J.O'Malley. Learning about electrical stimulation: Access to information for the spinal cord injury treatment team. *Topics in Spinal Cord Injury Rehabilitation*, 5(1):66–77, 1999.

Terman F.E. *Radio Engineers Handbook*. McGraw-Hill Book Company, Inc, New York, 1st edition, 1943.

Testerman R.L. Comments on "accuracy limitations of chronaxie values". *IEEE Trans Biomed Eng*, 52(4):750–750, 2005.

Theophilidis G. and Pavlidou P. The vitality of the sciatic nerve of the frog and rat in a chamber which allows maintained in vivo recordings of the compound action potential. *Muscle Nerve*, 16:113–114, 1993.

Thoma H, Frey M, Holle J., Losert U, Rosenkranz D, and stohr H. Experiments on the electrode nerve connection. *Advances in External Control of Human Extremities*, pages 121–135, 1988.

Tiiska A.J. and Lagerspetz K.Y.H. Effects of thermal acclimation on nervous conduction and muscle contraction in the frog rana temporaria. *Comparativa Biochemistry and Physiology*, 124(Part A):335–342, 1999.

Torrens M.J. The effect of selective sacral nerve blocks on vesical and urethral function. *J. Urol.*, 112(2):204–205, 1974.

Torrens M.J. Urodynamic analysis of differential sacral nerve blocks and sacral neurectomy. *Urol. int.*, 30(1):85–91, 1975.

Torrens M.J. and Griffith H.B. The control of the uninhibited bladder by selective sacral neurectomy. *Br. J. Urol.*, 46(6):639–644, 1974.

Torrens M.J. and Griffith H.B. Management of the uninhibited bladder by selective sacral neurectomy. *J. Neurosurg.*, 44(2):176–185, 1976.

Triolo R.J. and Bogie K. Lower extremity applications of functional neuromuscular stimulation after spinal cord injury. *Topics in Spinal Cord Injury Rehabilitation*, 5 (1):44–65, 1999.

Troyk P.R. and Donaldson N. de N. Implantable fes stimulation systems: What is needed? *Neuromodulation*, 4(4):196–204, 2001.

Tyler D.J. and Durand D.M. Interfascicular electrical stimulation for selective activating of axons. *IEEE Eng Med. Biol. Mag.*, pages 575–583, 1994.

Tyler D.J. and Durand D.M. Functionnally selective peripheral nerve stimulation with a flat interface nerve electrode. *IEEE Trans. Neural Syst. Rehabil. Eng.*, 10(4):294–303, 2002.

Tyler D.J. and Durand D.M. Chronic response of the rat sciatic nerve to the flat interface nerve electrode. *Ann. Biomed. Eng.*, 31:633–642, 2003.

Uranga A. and Rijkhoff N.J.M. A modified pulseshape for selective stimulation using anodal block. *Proceedings of the 6th Annual Conference of the International Functional Electrical Stimulation Society*, CD ROM, 2001.

van Balken M.R., Vergunst H., and Bemelmans B.L. The use of electrical devices for the treatment of bladder dysfunction: a review of methods. *J. Urol.*, 172(3): 846–851, 2004.

van Bolhuis A.I., Holsheimer J., and Savelberg H.H. A nerve stimulation method to selectively recruit smaller motor-units in rat skeletal muscle. *J. Neurosci. Methods*, 107(1-2):87–92, 2001.

Van Den Honert C. and Mortimer J.T. Generation of unidirectionally propagated action potentials in a peripheral nerve by brief stimuli. *Science.*, 206:1311–1312, 1979.

Van Den Honert C. and Mortimer J.T. A technique for collision block of peripheral nerve: Frequency dependence. *IEEE Trans Biomed Eng*, 28(5):379–382, 1981a.

Van Den Honert C. and Mortimer J.T. A technique for collision block of peripheral nerve: Single stimulus analysis. *IEEE Trans Biomed Eng*, 28(5):373–378, 1981b.

van der Aa H.E. SARSI operation, Twente Hospital. Personal Communication, 2002.

van der Aa H.E., Bultstra G., Verloop A.J., Kenney L., Holsheimer J., Nene A., Hermens H.J., Zilvold G., and Buschman H.P. Application of a dual channel peroneal nerve stimulator in a patient with a "central" drop foot. *Acta Neurochir. Suppl*, 79: 105–107, 2002.

van Kerrebroeck E.V., Scheepens W.A., de Bie R.A., and Weil E.H. European experience with bilateral sacral neuromodulation in patients with chronic lower urinary tract dysfunction. *Urol. Clin. North Am.*, 32(1):51–57, 2005.

van Kerrebroeck P.E.V. *Clinical and Experimental Aspects of Bladder Stimulation in Spinal Cord Injury*. Ph.d., Katholieke Universiteit Nijmegen, 1993.

Vastenholt J.M., Snoek G.J., Buschman H.P., van der Aa H.E., Alleman E.R., and Ijzerman M.J. A 7-year follow-up of sacral anterior root stimulation for bladder control in patients with a spinal cord injury: quality of life and users' experiences. *Spinal Cord*, 41(7):397–402, 2003.

Veltink P.H. and Donaldson N. de N. A perspective on the control of fes-supported standing. *IEEE Trans Rehabil Eng*, 6(2):109–112, 1998.

Veltink P.H., van Alste J.A., and Boom H.B.K. Influences of stimulation conditions on recruitment of myelinated nerve fibres: a model study. *IEEE Trans Biomed Eng*, 35 (20):917–924, 1988.

Veltink P.H., van Alste J.A., and Boom H.B.K. Multielectrode intrafascicular and extraneural stimulation. *Med. Biol. Eng. Comput.*, 27:19–24, 1989a.

Veltink P.H., Veen B.K.Van, Struijk J.J., Holsheimer J., and Boom H.B.K. A modeling study of nerve fascicle stimulation. *IEEE Trans Biomed Eng*, Vol. 36(No. 7):683–691, 1989b.

Veraart C., Delbeke J., Wanet-Defalque M.C., Vanlierde A., Michaux G., Parrini S., Glineur O., Verleysen M., Trullemanns C., and Mortimer J.T. Selective stimulation of the human optic nerve. *Proceedings of the 4th Annual Conference of the International Functional Electrical Stimulation Society*, pages 57–59, 1999.

Veraart C., Grill W.M., and Mortimer J.T. Selective control of muscle activation with a multipolar nerve cuff electrode. *IEEE Trans Biomed Eng*, 40(7):640–653, 1993.

Verma P and Fawcett J. Spinal cord regeneration poonam verma james fawcett ( ). *Adv. Biochem. Eng Biotechnol.*, 94:43–66, 2005.

Vesper J., Klostermann F., Stockhammer F., Funk T., and Brock M. Results of chronic subthalamic nucleus stimulation for parkinson's disease: A 1-year follow-up study. *Surgical Neurology*, 57:306–313, 2002.

Vince V., Thil M.A., Gerard A.C., Veraart C., Delbeke J, and Colin I.M. Cuff electrode implantation around the sciatic nerve is associated with an upregulation of tnf-a and tgf-b1. *Journal of Neuroimmunology*, 159:75–86, 2005.

Vleggeert-Lankamp C.L.A.M., van den Berg R.J., Feirabend H.K.P., Lakke E.A.J.F., Malessy M.J.A., and Thomeer R.T.W.M. Electrophysiology and morphometry of the aa- and ab-fiber populations in the normal and regenerating rat sciatic nerve. *Exp. Neurol.*, 187:337–349, 2004.

von Wild K., Rabischong P., Brunelli G., Benichou M., and Krishnan K. Computer added locomotion by implanted electrical stimulation in paraplegic patients (suaw). *Acta Neurochir. Suppl*, 79:99–104, 2001.

Vuckovic A. and Rijkhoff N.J.M. A new pulse shape to optain selectibe small fibre acitivation by anodal blocking. *Proceedings of the 23th Annual International Conference of the IEEE Engineering in Medicine and Biology Society*, CD-ROM: 773–775, 2001.

Vuckovic A., Rijkhoff N.J.M., and Struijk J.J. Different pulse shapes to obtain small fiber selective activation by anodal blocking–a simulation study. *IEEE Trans Biomed Eng*, 51(5):698–706, 2004.

Waters R., McNeal D.R., Clifford B., and Faloon W. Long term follow up of peroneal nma patients. In *Proceedings of the 8th International Symposium on ECHE*, pages 471–478, 1984.

West D.C. and Wolstencroft J.H. Strength-duration characteristics of myelinated and non-myelinated bulbospinal axons in the cat spinal cord. *J. Physiol.*, 337:37–50, 1983.

Whitwam J.G. Classification of peripheral nerve fibres. an historical perspective. *Anaesthesia*, 31(4):494–503, 1976.

Wikipedia . The free encyclopedia, last accessed in 2007. `http://en.wikipedia.org/wiki/Action_potential`.

Williamson R.P. and Andrews B.J. Localized electrical nerve blocking. *IEEE Trans Biomed Eng*, 52(3):362–370, 2005.

Wood D.E., Donaldson N. de N., and Perkins T.A. Apparatus to measure simultaneously 14 isometric leg joint moments. part 2: Multi-moment chair system. *Med. Biol. Eng. Comput.*, 37(2):148–154, 1999.

Wright E.B. and Ooyama H. Anode break excitation and pfluger's law. *Am. J. Physiol*, 200:219–222, 1961.

Wyndaele J.J. and Dromme S.A.Van. Muscular weakness as side eect of botulinum toxin injection for neurogenic detrusor overactivity. *Spinal Cord*, 40:599–600, 2002.

Yarkony G.M., Jaeger R.J., Roth E., Kralj A.R., and Quintern J. Functional neuromuscular stimulation for standing after spinal cord injury. *Arch. Phys. Med. Rehabil*, 71 (3):201–206, 1990.

Yarkony G.M., Roth E.J., Heinemann A.W., Wu Y., Katz R.T., and Lovell L. Benefits of rehabilitation for traumatic spinal cord injury. *Archives of Neurology*, 44(Jan): 93–96, 1987.

Yoda R. Elastomers for biomedical application. *J Biomat Sci Polymer Edn*, 9(6): 561–626, 1998.

Yuen T.G., Agnew W.F., and Bullara L.A. Histopathological evaluation of dog sacral nerve after chronic electrical stimulation for micturition. *Neurosurgery*, 14:449–455, 1984.

Zhang M. and Yannas I.V. Peripheral nerve regeneration. *Adv. Biochem. Eng Biotechnol.*, 94:67–89, 2005.

Ziaie B., Arx J.Von, and Najafi K. A micro-fabricated planar high-current irox stimulating microelectrode. *Proceedings of 18th Annual International Conference of the IEEE Engineering in Medicine and Biology Society*, 18, 1996.

Zierhofer C.M. Analysis of a linear model for electrical stimulation of axons - critical remarks on the "activating function concept". *IEEE Trans Biomed Eng*, 48(2):173–184, 2001.

Zimmermann M. Selective activation of c-fibers. *Pflgers. Arch.*, 301:329–333, 1968.